THE UNIVERSITY
of EDINBURGH

SCHOOL OF CHEMISTRY

THE UNIVERSITY OF EDINBURGH

Synthesis and characterisation of novel phthalocyanine-based porous materials

Thesis submitted for the degree of Doctor of Philosophy by:

Alexander Stiven

Supervisor: Neil B. McKeown **2021**

Declaration

Statement 1

This work has not been submitted in substance for any other degree or award at this or any other university or place of learning, nor is it being submitted concurrently in candidature for any degree or other award.

Signed Alexander Stiven……

Date 30/11/21……

Statement 2

This thesis is being submitted in partial fulfilment of the requirements for the degree of Doctor of Philosophy.

Signed Alexander Stiven ……

Date 30/11/21……

Statement 3

This thesis is the result of my own independent work/investigation, except where otherwise stated. Other sources are acknowledged by explicit references. Any views expressed are my own.

Signed Alexander Stiven ……

Date 30/11/21……

Statement 4

I hereby give consent for my thesis, if accepted, to be available for photocopying and for inter-library loan, and for the title and summary to be made available to outside organisations.

Signed Alexander Stiven ……

Date 30/11/21……

Acknowledgements

I would like first of all to thank my supervisor, Professor Neil McKeown, for giving me the chance to undertake the project and for all his help and guidance during the past few years, as well as my second supervisor, Dr Claire Hobday, for her advice in numerous areas of the project. I also owe huge thanks to all of my colleagues in the McKeown group: post-docs Grazia, Rich, Bibiana and John and fellow PhD students Rich, Hannah, Panos, Jie, ChunChun, Sarah, Travis, Emily, Khairul, Emily and Kimia for their support with research and also for making the group a great place to work. Thanks are also due to the CRITICAT CDT for funding the project, and for organising useful and enjoyable training events.

A special thanks go to the undergraduate students who I had the pleasure of supervising: 4P students Bella Chen, Jinling Wang, Lucinda Wilson, Scarlett Brown, Igor Zamorski, Charlie Nason, Toria Twiddy and Iona Ivalo as well as Amy Zhang and Igor Zamorski as individual students. They have been instrumental in establishing the background to the final chapter of the thesis and have also made important contributions to the experimental work described.

I would also like to thank all of the technical staff in the School of Chemistry especially in NMR, mass spectrometry and crystallography for their help in gathering data throughout the project.

Abstract

Phthalocyanines are planar aromatic macrocycles whose unique properties give them a wide variety of potential applications, particularly as pigments and dyes, but also in solar cells, photodynamic therapy and as catalysts. The latter in particular is of interest given the ability of phthalocyanines to complex all metal atoms, and so the further development of materials to allow the use of phthalocyanines in heterogeneous catalysis is an important field.

To this end, this work describes the efforts which we have undertaken to incorporate different phthalocyanine ligands into novel materials, with a view to achieving sufficient porosity to allow catalytic applications. In seeking to develop phthalocyanine-based Metal Organic Frameworks (MOFs), we have employed both novel and previously reported ligands in MOF syntheses, and have obtained crystalline structures, though full structural elucidation remains elusive. Relatively low internal porosities have also been measured, likely due to the inherent aggregation tendencies of phthalocyanines.

We also demonstrate the use of the tetraimidophthalocyanine functionality in the synthesis of a series of network polymers, using the tetracyclomerisation step for polymerisation. Whilst several examples are entirely non-porous as a result of dense packing of the phthalocyanine rings, we also report two novel polymers containing bulky functionalities to overcome this restraint, which do show greater internal surface areas.

Finally, new molecular crystals are described, showcasing the incorporation of numerous tetraphenylporphyrin (TPP) ligands into a phthalocyanine molecular crystal system widely studied within the group. Extensive spectroscopic studies of the resulting interactions have been carried out, and these are compared to crystallographic data to give significant insight into the effect of variation of the metal centre and by substitution of different functionalities in the TPP.

Lay Summary

Phthalocyanines (Pcs) are large, planar, multi-ringed molecules in which the electrons are extensively delocalised. Due to this, and their very high stability, phthalocyanines possess several useful properties. In particular, their intense absorbance means that they are very widely used as pigments and dyes but due to their ability to complex a very wide variety of metals, they have also been employed in catalysis, organic solar cells and photodynamic therapy.

It is therefore desirable to include the phthalocyanine functionality within porous materials and the work in this thesis describes various means of doing this. The incorporation of Pcs into Metal Organic Frameworks (MOFs), consisting of organic linkers coordinated to metal clusters, was an area of particular interest. New phthalocyanine-based polymers have also been developed, and previous work within the research group on porous Pc crystals has been extended by studying their interactions with the similar tetraphenylporphyrin molecule.

Abbreviations

Abbreviation	Definition
Å	Ångstrom
BDC	Benzenedicarboxylic acid
BTC	Benzenetricarboxylic acid
BET	Brunauer-Emmett-Teller
Bpy	4,4-bipyridine
COF	Covalent Organic Framework
DBU	1,8-Diazabicyclo[5.4.0]undec-7-en
DCM	Dichloromethane
DEF	Diethylformamide
DMF	Dimethylformamide
DMSO	Dimethylsulfoxide
EA	Ethanoanthracene
EI	Electron ionisation
ESI	Electrospray ionisation
G	Gram
Hr	Hour
Hz	Hertz
ICP	Inductively Coupled Plasma
IR	Infrared
J	Coupling constant
K	Kelvin
LDI	Laser desorption/ionisation
MALDI	Matrix-assisted laser desorption/ionisation
MMPF	Metal MetalloPorphyrin Framework
MOF	Metal Organic Framework
Mp	Melting Point
MS	Mass Spectrometry
NMR	Nuclear Magnetic Resonance

OCPc	Octacarboxyphthalocyanine
OES	Optical Emission Spectrometry
Pc	Phthalocyanine
$(dipPhO)_8Pc$	2,3,9,10,16,17,23,24-octa(2',6'-di-iso-propylphenoxy)phthalocyanine
PCN	Porous Coordination Network
PIZA	Porphyrinic Illinois Zeolite Analogue
PPF	Pillared Porphyrinic Framework
SA	Surface Area
SBU	Secondary Building Unit
TCIPc	Tetracarboxyimidophthalocyanine
TGA	Thermogravimetric analysis
THF	Tetrahydrofuran
TLC	Thin layer chromatography
TPP	Tetraphenylporphyrin
TTSBI	5,5',6,6'-tetrahydroxy-3,3,3',3'-tetramethyl-1,1'-spirobisindane
UV	Ultraviolet
UV-Vis	Ultraviolet-visible spectroscopy
XRD	X-ray Diffraction
ZnPO MOF	Zinc Porphyrin Octa-oxygen Metal Organic Framework

Contents

1 Introduction

1.1 Phthalocyanine

Phthalocyanine (Pc), or tetrabenzotetraazaporphyrin, is a highly stable, planar macrocycle consisting of four isoindole units linked by nitrogen atoms. Whilst phthalocyanines are purely synthetic, they are structurally related to the naturally occurring porphyrin functionality, as shown in **Figure 1.1**. The phthalocyanine ring system is aromatic, with 18 π electrons and this extensive delocalisation gives it interesting molecular properties, including its intense adsorption of visible light. This accounts for by far the most significant use of phthalocyanines, as dyes and pigments, as well as their use in photoelectronic applications.[1]

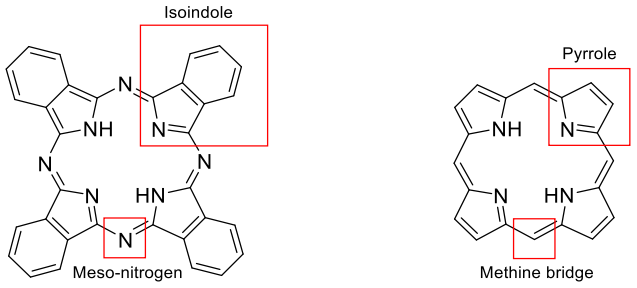

Figure 1.1: The basic structure of phthalocyanines and porphyrins.

Due to their industrial applications, the relationship between the structure and the optical properties of phthalocyanines has been extensively investigated. As extended aromatic systems, a series of molecular orbitals exist between which the 18 π electrons are spread, with the most relevant to electronic transitions, and therefore optical absorption, being the HOMO and LUMO orbitals, shown in **Figure 1.2**. As a result of the D_{4h} symmetry of metallated phthalocyanines, there are one HOMO and two degenerate LUMO orbitals.[2] These orbitals have even been directly imaged using scanning tunnelling microscopy.[3]

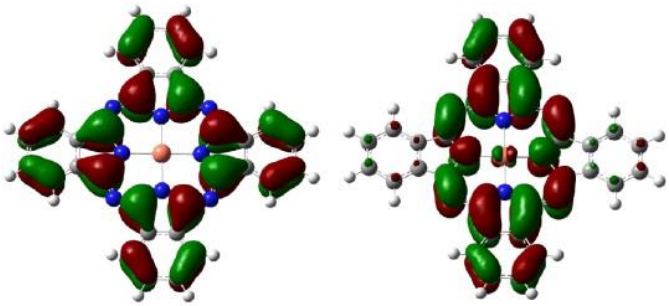

Figure 1.2: The form of a HOMO (left) and LUMO (right) orbital of copper metallated phthalocyanine ligand, showing red and green as different phases of the molecular orbitals overlaid on the molecular structure. Adapted from ref. 2.

The energy of orbital transitions in phthalocyanines can be probed using a variety of techniques such as magnetic circular dichromism,[4] fluorescence spectroscopy,[5] and chemiluminescence,[6] but by far the most widely employed is absorption spectroscopy in the UV-visible light range.[7] The vast majority of phthalocyanines exhibit two distinct areas of absorbance in this range; one at 300-400 nm, referred to as the B- or Soret band, and another at 650-800 nm, referred to as the Q-band, as seen in the spectrum in **Figure 1.3**. Metallated phthalocyanines show a single Q-band peak, but as a result of their lower D_{2h} symmetry, metal-free phthalocyanines show two separate peaks in this region. However, as the peaks are due to electronic transitions within the ligand, the identity of the metal ion that is coordinated to a phthalocyanine ligand generally has only a slight influence on the spectrum.[7]

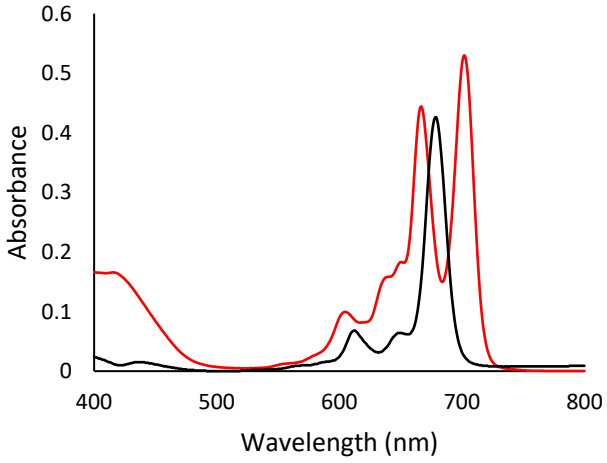

Figure 1.3: The typical optical absorbance spectra of a metal free (red) and metallated (black) phthalocyanine.

Additional variants of the phthalocyanine structure also exist, differing in the presence or absence of nitrogen atoms within the macrocycle. As shown in **Figure 1.4**, benzoporphyrins are macrocycles with a methine bridge instead of the meso-nitrogen found in phthalocyanines, and while sharing the same size and symmetry as phthalocyanines are in fact, as suggested by the name, formally porphyrin

derivatives. Pyrazinoporphyrazines, or azaphthalocyanines, have a pyrazine ring in place of the benzo unit normally found in phthalocyanines, but again have the rigid, planar structure expected in such macrocycles. Previous studies have shown that significantly different electronic properties result from these variations.[8, 9]

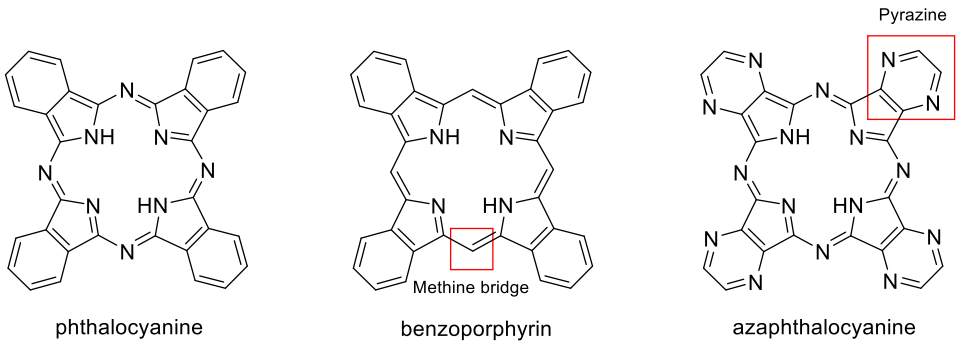

Figure 1.4: The structures of phthalocyanine, compared to benzopoprhyrin and azaphthalocyanine.

The optical absorption spectra of these macrocycles are nonetheless generally similar to those of phthalocyanines. Those of benzoporphyrins, as may be expected, are also influenced by their porphyrin-like structure, with proportionally larger Soret bands and red-shifted absorbances.[10] Contrastingly, azaphthalocyanines exhibit Q and Soret bands of similar intensity to phthalocyanines, but the maximum absorbances are generally blue-shifted as a result of the altered electronic environment.[11]

Numerous routes exist for the synthesis of phthalocyanines (**Fig. 1.5**). The most common is from 1,2-dicyanobenzene (phthalonitrile), which can be converted to a metallated phthalocyanine by heating in a high boiling point solvent along with a suitable metal salt. The same methodology can also be used with diiminoisoindole. Phthalocyanines can also be synthesised directly from phthalimides and phthalic anhydrides. Again, high temperatures and a suitable metal source are used, along with a nitrogen source such as formamide or urea.

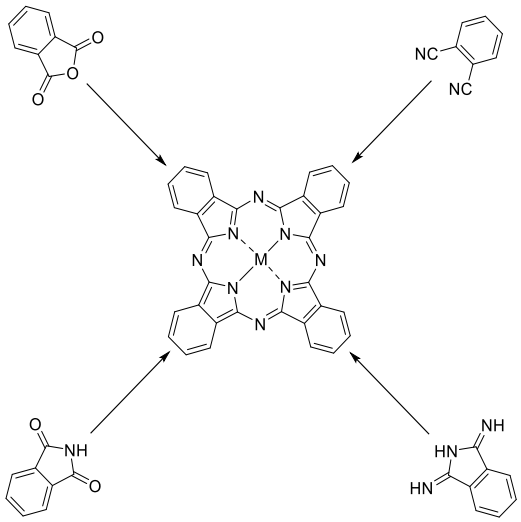

Figure 1.5: Common synthetic precursors to metal phthalocyanines.

Metal-free phthalocyanines can also be produced by reacting a phthalonitrile with an alkali metal and a primary alcohol in order to initially form a phthalocyanine around the metal template. Due to the relatively weak binding of the alkali metal ions to the phthalocyanine, they can then be removed under acidic conditions.

Beyond the core functionality, substitution of the phthalocyanine ring is of great importance in determining their properties. Substitution can either be in the peripheral or non-peripheral sites (R and R_1 respectively in **Figure 1.6**), and has a very significant effect on the electronic nature of the phthalocyanine.[12] Use of large bulky substituents can also have a steric affect, preventing the otherwise favoured π-stacking of phthalocyanines and therefore significantly increasing their solubility.[13]

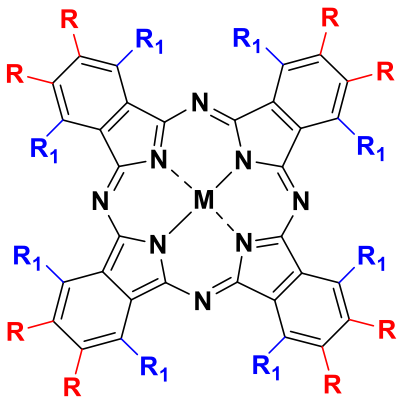

Figure 1.6: Substitution sites on phthalocyanines.

1.1.1 Homogeneous phthalocyanine catalysis

Since phthalocyanines, like porphyrins, are capable of complexing a very wide variety of metals, building on the natural catalytic ability of porphyrins in metalloenzymes much work has been carried out on the development of phthalocyanine as catalysts. Oxidative catalysis has seen by far the largest number of results and phthalocyanines have been found to show excellent activity in numerous reactions including the epoxidation of terminal alkenes[14] and alkanes.[15] These can be carried out with molecular oxygen as oxidant and importantly the catalysts can generally be easily recovered by simple removal of the solvent and reused with no appreciable reduction in performance. In an example of large-scale use of phthalocyanines in industry, the oxidation of thiols via the Merox process, which generally employs cobalt(II) phthalocyanines, is important in removing sulphur containing contaminants during petroleum refining.[16]

Beyond oxidation, phthalocyanines have also been shown to catalyse reactions such as allylic C-H aminations reactions[17] significantly more effectively than porphyrins or other metal-containing macrocycles. This has been assumed to be due to the more electron-withdrawing nature of phthalocyanine ligands relative to porphyrins which results in a more electrophilic metal centre. They have also been found to be effective in the degradation of environmental contaminants, especially in water. This is a result of the fact that certain phthalocyanines are able to photocatalytically produce highly reactive singlet oxygen species upon excitation with visible or UV light, which in turn can react with and degrade numerous potential contaminants. Specific examples have demonstrated their ability to degrade 4-chlorophenol, a characteristic trace pollutant[18] as well as more complicated natural toxins.[19]

The promising results observed with phthalocyanine complexes in homogeneous catalysis have been extended to incorporate advantages of heterogeneous catalysis by supporting or encapsulating the catalysts on a solid support. Examples of this include the encapsulation of Cu, Co and Fe phthalocyanines within zeolite structures which have been shown to catalyse the oxidation of methane to methanol and formaldehyde.[20] Phthalocyanines anchored to the porous silicate material MCM-41[21] have also been shown to heterogeneously catalyse the degradation of contaminants.

1.2 Porosity

As highlighted by the example of phthalocyanine encapsulation in zeolites and mesoporous silicates, the production of materials with a very high surface-area-to-volume-ratio afforded by an internal network of pores is of great interest. As the usefulness of these materials in a wide variety of applications is highly dependent on the exact degree of their internal porosity, several techniques have been developed to quantify it. These generally consider the simplest case of gas adsorption, with one of the more basic being the Langmuir adsorption model,[22] which assumes that only one gas molecule can be adsorbed per site, with a monolayer covering the adsorbent. However, while generally the adsorption of the first layer is the most important, in many cases the presence of multiple layers of gas molecules is significant and must be considered, which has led to the development of Brunauer–Emmett–Teller (BET) theory.[23] Building on the Langmuir model, BET theory applies all of its assumptions to each individual layer of adsorbed molecules, but also assumes that the gas molecules are adsorbed physically onto the surface in indefinite layers which do not interact with each other.

By examining the isotherms obtained when carrying out such surface area measurements, differences can be observed between the adsorption properties of different materials. This has allowed 6 main categories of adsorbent materials to be defined by IUPAC, with additional subcategories, as shown in **Figure 1.7**.[24] In microporous materials, those with a pore diameter of less than 2 nm, a type I isotherm is generally seen, with high gas uptake at low partial pressure but the final quantity limited by accessible pore volume. This is in contrast to macroporous materials with pore diameters of more than 50 nm, which generally display type II isotherms, where the final quantity of gas adsorbed is unrestricted. The intermediate class of mesoporous materials most commonly show type IV isotherms.

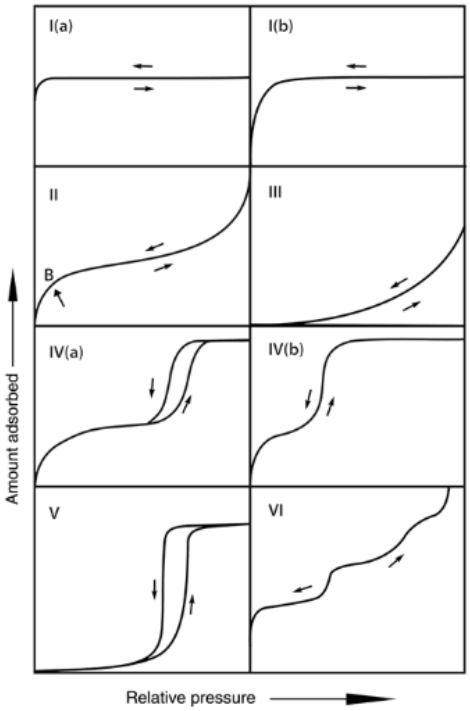

Figure 1.7: The different types of adsorption isotherms, as defined by IUPAC. Type I generally refers to microporous materials with relatively small external surface areas, with Type I(a) being seen in materials with narrow micropores and Type I(b) in those with a wider range of pore sizes. Type II and III isotherms are generally observed with non-porous or macroporous materials, with Type II corresponding to those in which complete monolayer coverage is observed, and Type III those in which adsorbance is clustered around a few favourable sites. Type IV isotherms are seen with mesoporous materials, either with hysteresis (Type IV(a)) or without (Type IV(b)). Type V isotherms are seen when adsorbent-adsorbate interactions are particularly weak and Type VI with adsorbance on a uniform non-porous surface. Adapted from ref. 24.

1.3 Microporous materials

Of the different classes of porous materials, the very small diameter of the pores in microporous materials means that they have come to play an ever more prominent role in materials science. Their pore size is close to the scale of adsorbate molecules and consequently such materials, summarised in **Figure 1.8**[25] have been extensively studied and have been developed for a wide range of applications.

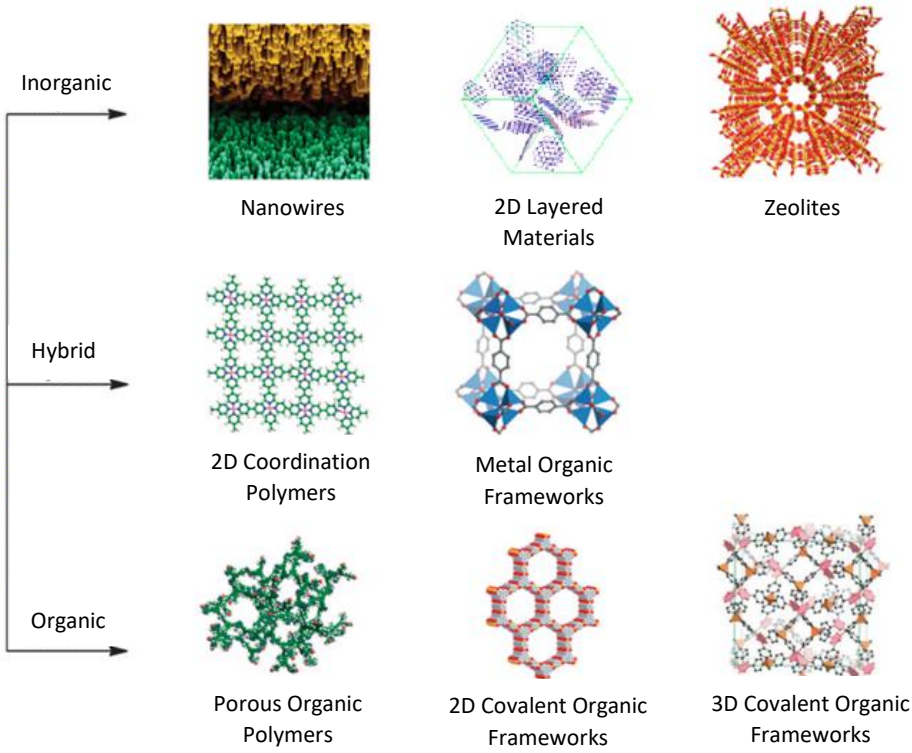

Figure 1.8: An overview of different types of potentially microporous materials. Adapted from ref. 25.

Zeolites are the most industrially significant example of such microporous materials. They are inorganic aluminosilicate minerals with regular crystalline structure, containing a large number of pores. Zeolite materials possess high surface areas of up to 940 m^2/g,[26] and have porous structures that are maintained even after pore evacuation. Zeolites are also very stable and can be heated to hundreds of degrees without decomposition. At present, several hundred different zeolite structures have been identified, with many natural examples having been discovered in mineral deposits. Synthetic zeolites have also been produced, both with entirely novel structures and as adaptions of naturally occurring examples. The importance of zeolites comes from their very widespread use as heterogeneous catalysts, for example they are of vital importance in hydrocarbon cracking in the petrochemical industry.[27] Purely inorganic amorphous structures, such as boron nitride, have also been investigated, and have been shown to have BET surface areas in excess of 1000 m^2/g.[28] Whilst applications are yet to be conclusively proved, they have been suggested for use in drug delivery.[29]

1.4 Organic Microporous Materials

As with zeolites, the study of purely organic materials with a highly porous structure was also rooted initially in those derived from nature. There are an incredible number of such naturally occurring porous materials, including structures such as honeycombs and sponges, but the most important

example would arguably be activated carbon, in the form of charcoal. This has been used for millennia as an adsorbent material, and often has a surface area in excess of 500 m^2/g.[30]

1.4.1 Microporous polymers

With the burgeoning of synthetic organic chemistry in the last century, it is unsurprising that much work has been undertaken to create synthetic porous materials, given the obvious advantage of the much greater structural control this can afford. In recent years, the use of polymers as highly porous materials has received particularly significant attention. This requires careful choice of both the monomer and the polymerisation methodology but can yield highly stable materials with exceptional porosities. For example, a tetraphenylmethane based polymer has been found to have a BET surface area of almost 6000 m^2/g.[31] Such materials have therefore naturally been studied for their potential uses in gas storage.[32]

By the incorporation of metal centres within the polymer structure, applications of porous polymers can be extended to heterogeneous catalysis. One example is the Iridium-containing CMP-CpIr-3,[33] shown in **Figure 1.9,** which has a specific surface area of 469 m^2/g and is able to catalyse a number of reductive amination reactions. In an example of the use of larger macrocycles in such porous organic polymers, FeP-CMP has been synthesised from a tetrabrominated porphyrin via a Suzuki cross-coupling reaction with an aromatic boronic acid.[34] The resulting polymer, also shown in **Figure 1.9**, exhibits a BET surface area of up to 1270 m^2/g, and is capable of efficiently catalysing the epoxidation of a variety of different substrates.

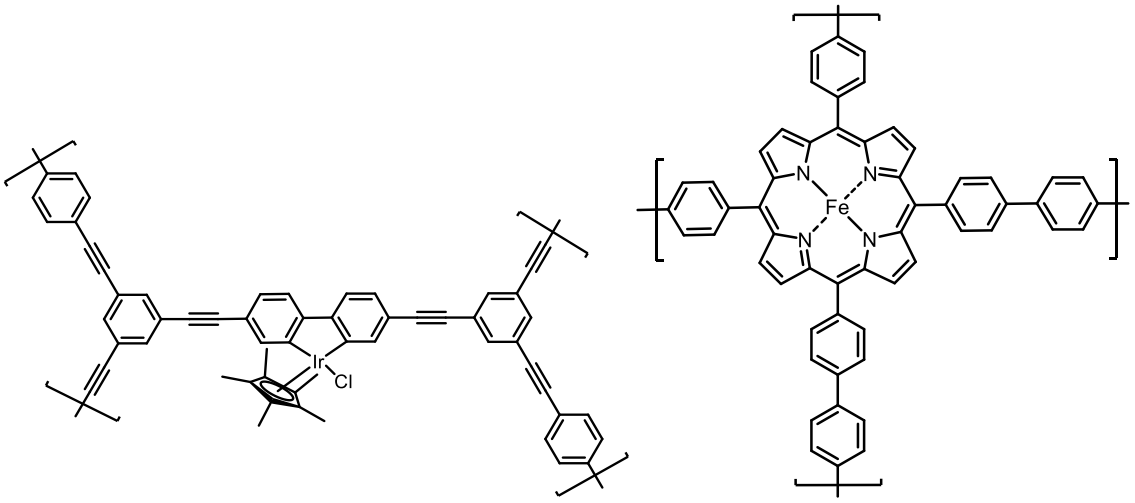

Fig 1.9: The structures of CMP-CpIr-3 (left) FeP-CMP (right).

Like these examples, most porous polymers have a 3-D network of covalent bonds, however much work in our research group has explored the use of Polymers of Intrinsic Microporosity (PIMs) as an alternative. In PIMs the rigidity and contortion inherent in their structure means that they pack space inefficiently, providing high free volume which corresponds to micropores. The importance of PIMs comes from the fact that their microporosity comes only from their chain structure and is not dependent on the formation of a 3-D network.[35] This means that it is possible for them to dissolve in common solvents, and so they are far easier to process. They can, for example, be cast as freestanding films and coated onto surfaces.[36,37]

The first example of a PIM, named PIM-1, was formed from the dibenzodioxin-forming polymerisation reaction between 2,3,5,6-tetrafluoroterephthalonitrile and 5,5',6,6'-tetrahydroxy-3,3,3',3'-tetramethyl-1,1'-spirobisindane.[35] The non-network PIM-1 has been shown to be highly microporous, with an apparent BET surface area of 850 m^2/g due to the fact that it contains no single bonds about which rotation can take place, consisting instead of a semi-ladder structure, and that the presence of the spiro-centre causes it to adopt a contorted shape. As previously mentioned, this results in inefficient packing of the polymer chains, leading to microporosity.

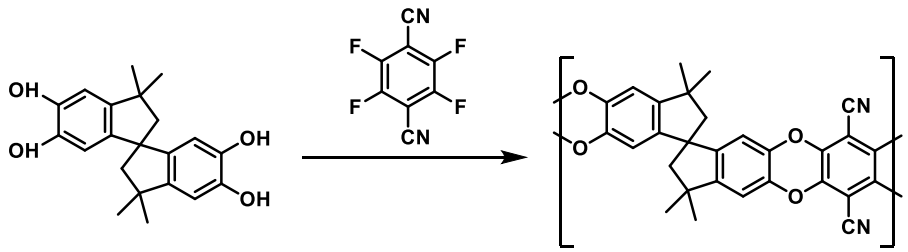

Scheme 1.2: Synthesis of PIM-1.

Further development of PIMs has involved the use of polyimides, as shown in **Figure 1.10**, known to form high molecular weight polymers.[38] These have been shown to have an apparent BET surface area of 600 m^2/g, which has allowed them to show promise as a material for membrane gas separation.[39] Highly performing PIMs have also been synthesised containing the Tröger's Base functionality; a rigid chiral structure containing two tertiary amines. These have demonstrated the highest apparent BET surface area of any solution processable microporous material, at 1028 m^2/g.[40] In this case, the high surface area is due to both the high internal molecular free volume of the ethanoanthracene group, and the rigid, ladder structure of the Tröger's Base functionality.

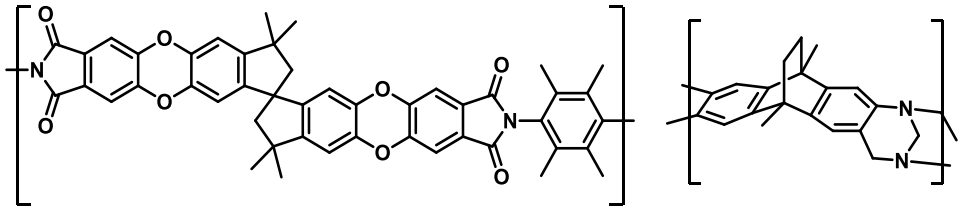

Figure 1.10: Examples of polyimide (left) and Tröger's Base (right) PIMs.

1.4.1.1 Phthalocyanine network polymers

Given the examples of porphyrins being used as building blocks in microporous polymers, phthalocyanines have unsurprisingly been seen as an attractive possibility in such materials. Compared with previously described examples of heterogeneous phthalocyanine-containing materials, such polymers offer advantages including greater control over the structure of the material and higher loading of the active metal centres.

Early phthalocyanine polymeric materials were generally obtained through fairly crude syntheses, starting for example, from pyromellitic dianhydride.[41] The structures of such materials could not be fully characterised, and they were generally of interest due to their interesting electronic and magnetic properties afforded by the extended conjugation and interaction with the metal centres. Where attention was given to the adsorption properties of such polymers, for example by Wohrle, the surface areas of the materials were found to be very low, on the order of 1 m^2/g.[42] More recently, more synthetically complex metallophthalocyanine polymers have been reported, such as the electrochemically polymerised polythiophene-metallophthalocyanine shown in **Scheme 1.3**.[43] Again however, interest was directed at the electrochemical properties of the polymer, and its porosity was not examined.

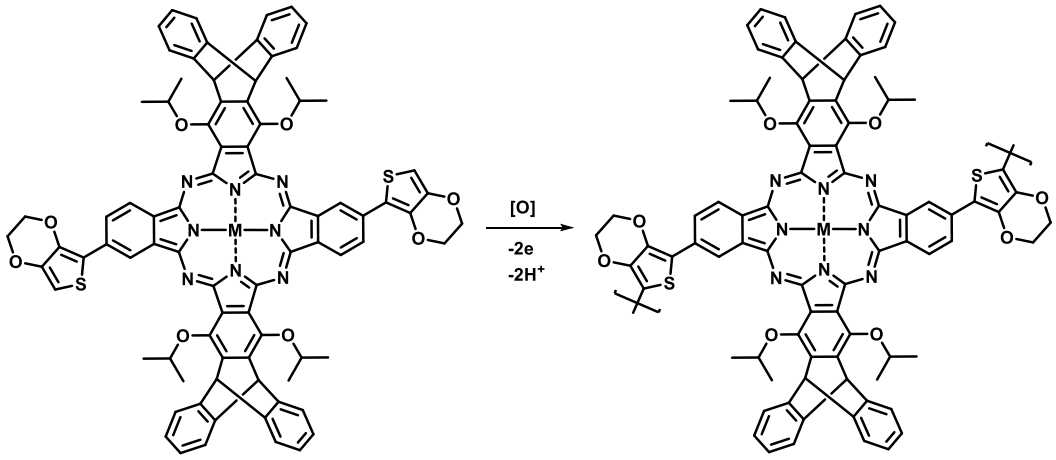

Scheme 1.3: The electrochemical synthesis of the polythiophene-metallophthalocyanine polymer.

The incorporation of phthalocyanines into polymer structures specifically designed for their high porosity has however been an area of great interest within our own research group. By building spirobisindane units into the polymer network, polymers containing cobalt phthalocyanines were successfully developed (**Figure 1.11**). This was possible due to the formation of a rigid and non-planar structure, leading to the formation of void space into which substrates could diffuse and also preventing π-stacking between phthalocyanine units.[44] As a result the material showed a BET surface area of up to 950 m^2/g. Initially the synthetic route involved the formation of the phthalocyanine macrocycle during the polymerisation reaction but it was later determined that a similar polymer could be synthesised by the polymerisation of pre-formed phthalocyanine units. In both cases the materials have been shown to be catalytically active for alkene oxidation.[45] Yields of the catalysed reaction were significantly greater than those achieved with a heterogeneous low molecular weight CoPc catalyst, since π-stacking of phthalocyanine faces in the latter significantly reduced the number of available catalytic sites.

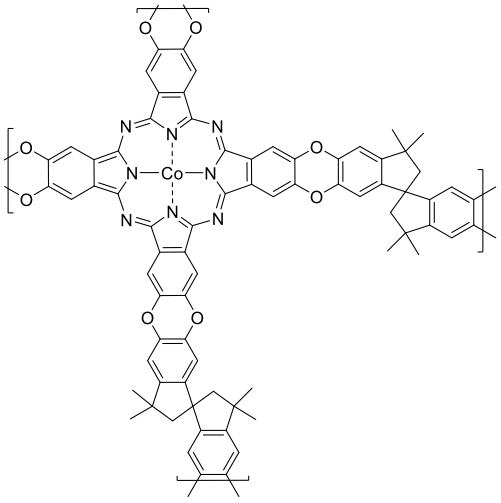

Figure 1.11: Amorphous microporous phthalocyanine polymer CoPc-PIM-A.

A variety of more recent phthalocyanine polymers have also demonstrated catalytic ability, with structures shown in **Figure 1.12**. β-ZnPc-CMP, a benzabisoxazole polymer incorporating zinc phthalocyanines,[46] was found to be highly effective for the photocatalytic degradation of organic dye pollutants despite having a relatively low BET surface area of 292 m^2/g. Even more recently, Yoon *et al* described a chromium phthalocyanine polymer termed POP-Pc'Cr, formed via a Friedel-Crafts polymerisation reaction.[47] A highly porous structure with a BET surface area of 725 m^2/g was obtained,

which was post-synthetically treated to obtain the final material, a selective catalyst for the mono-carbonylation of epoxides to lactones.

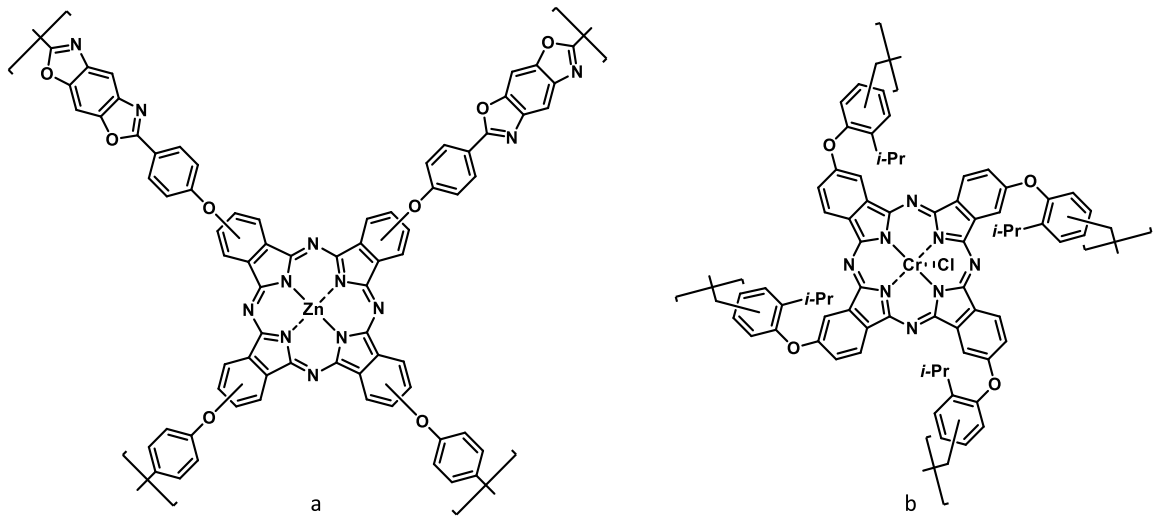

Figure 1.12: The structures of the catalytically active phthalocyanine microporous polymers; a) β-ZnPc-CMP; and b) POP-Pc'Cr.

Whilst there are numerous reports of phthalocyanine-containing network polymers, descriptions of polymers incorporating other structurally similar macrocycles such as the previously described pyrazinoporphyrazine, or azaphthalocyanine, are far more limited. As shown in **Figure 1.13** however, there are a handful of examples such as a pyrene-linked azaphthalocyanine network polymer with several different metals incorporated.[48] However, the polymer has only been investigated for its electronic and magnetic properties. A similar truly porous polymer, with BET surface areas of up to 466 m^2/g, depending on the metal ion, has also been described.[49] It was also shown to catalyse the oxidation of thiols to disulphides using atmospheric oxygen. In this case however, the polymer structure contained dihydopyrazine rings rather than pyrazine, so its description as a true azaphthalocyanine is debatable.

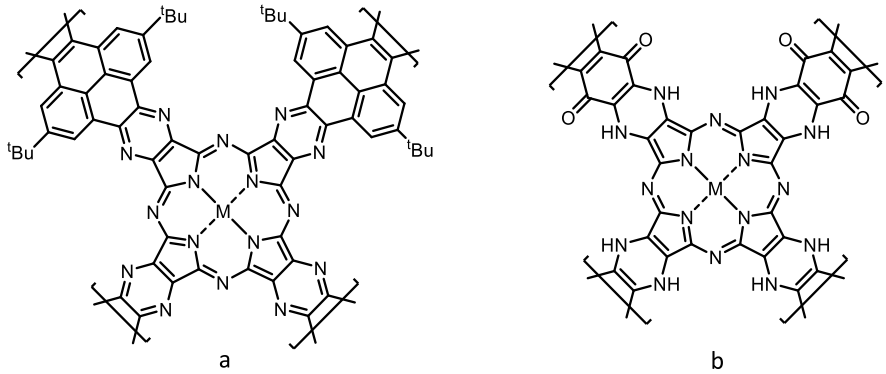

Figure 1.13: The structures of a) the true azaphthalocyanine pyrene-linked polymer and b) the dihydopyrazine-containing catalytically active porous polymer.

1.4.2 Covalent Organic Frameworks (COFs)

Whilst numerous examples of porous organic materials with entirely amorphous structures have been reported, the synthesis of ordered, crystalline organic materials linked by covalent bonds had remained largely unstudied until Yaghi *et al* described, in 2005, regularly arranged 2D sheets of hexagonal aryl-boronates.[50] Crystallinity was achieved by carrying out the synthesis in a sealed tube in order to avoid loss of water released in the condensation reaction, and therefore ensure reversible bond formation. This in turn allowed the elimination of defects and the eventual emergence of the highly ordered framework, as shown in **Figure 1.14**. 3D COFs have subsequently also been reported, for example from the condensation of a tetrahedral tetramine and terephthalaldehyde. The resulting material is highly crystalline and porous, with a BET surface area of 1360 m^2/g.[51]

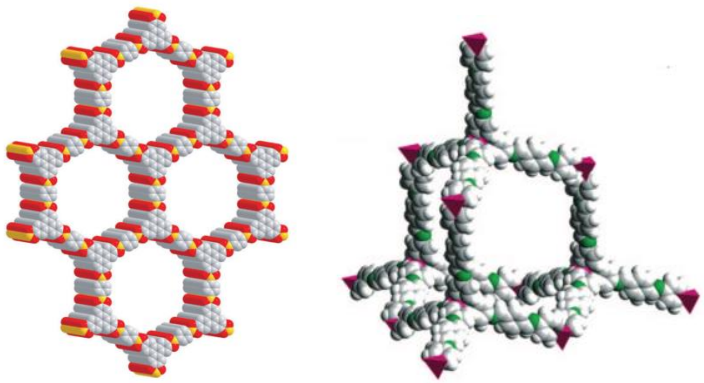

Figure 1.14: The molecular structure and packing arrangements of a) 2D COF-5 (grey = C, red = B, orange = C) and b) 3D COF-300 (grey and pink = C, green = N, white = H). Adapted from refs 50 - 51.

Since COFs generally lack metal centres, their application in catalysis has been limited, though specific catalytically active examples have been synthesised by coupling metal ions to ligands to produce a material capable of efficiently catalysing a variety of Suzuki-Miyaura coupling reactions.[52] A similar methodology has also opened the possibility of chiral catalysis using COFs, for example by using chiral COF produced from enantiopure diamines.[53]

The advantages of incorporating porphyrins into functional materials has also spurred the development of COFs containing the moiety. An early example was 2D COF formed from the condensation reaction of a tetraboronic acid porphyrin[54] with a surface area of 1742 m^2/g. However, the layered stacking of the porphyrin units, whilst potentially advantageous in applications such as electronics, meant that bound metal centres were unable to be accessed for catalysis. This has

subsequently been overcome by the synthesis of 3D porphyrin COFs which have been found to be highly microporous and also capable of acting as catalysts for the production of singlet oxygen[55] and the reduction of carbon dioxide.[56]

Building on work done with porphyrin-containing COFs, examples incorporating phthalocyanines have also been developed, featuring 2D stacked sheets formed from acetonide-protected phthalocyanine catechols linked by boronate-ester connections, as shown in **Figure 1.15**.[57] The layers are non-intercalating, giving a highly porous structure with a Langmuir surface area calculated at 506 m^2/g. As of yet however, the different geometry of phthalocyanines compared to porphyrins has hindered their incorporation into imine-based and 3D COFs.

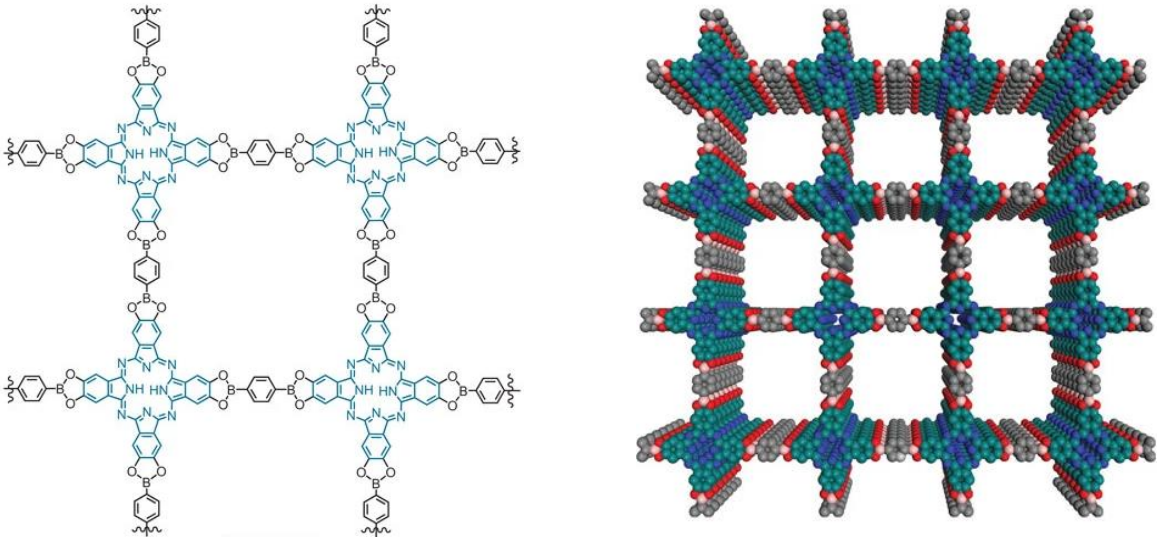

Figure 1.15: The molecular structure and 3D stacking arrangement of phthalocyanine-based Pc-PBBA COF (turquoise and grey = C, blue = N, red = O, pink = B). Adapted from ref. 57.

1.5 Metal Organic Frameworks (MOFs)

As well as the purely organic materials already outlined, a great deal of interest has arisen in recent years in the potential of hybrid organic/inorganic microporous materials such as Metal Organic Frameworks (MOFs).[58] MOFs can fundamentally be described as organic struts or linkers coordinated by metal centres or clusters, termed Secondary Building Units (SBUs). They are of great current interest due to their potential applications in a number of fields, including gas storage and separation, and are also being investigated for use in membranes, thin-film devices and biomedical imaging.[59]

Simple three dimensional MOFs generally consist of networks of metal ions coordinated by simple bidentate ligands as shown in **Figure 1.16**, for example an early structure reported by Yaghi and co-

workers in 1995 in which Cu(I) centres were linked by 4,4-bipyridyl ligands to form an extended framework.[60] Later work expanded the SBUs from single metal ions to clusters of atoms linked by the coordinating ligand. A seminal example was MOF-5, also synthesised by Yaghi, in 1999.[61] This contained Zn_4O clusters, each coordinated to six benzenedicarboxylic acid (BDC) ligands. It proved possible to remove all guest molecules from the pores of the MOF under vacuum. In addition, sorption isotherm studies showed a total pore volume comparable with the best zeolites. Another important milestone in the development of MOFs was HKUST-1, which contains Cu(II) centres coordinated to 4 benzenetricarboxylic acid (BTC) linkers.[62]

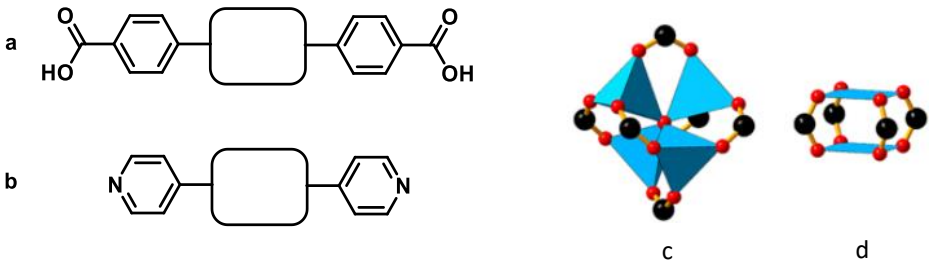

Figure 1.16: Common ligand types and SBUs employed in MOFs; a) carboxylic acid, b) pyridine, c) $Zn_4O(CO_2)_6$, d) $Cu_2(CO_2)_4$.

This extensive development has led to great potential for the use of MOFs as catalysts. Due to their construction from metal clusters and organic linkers, MOFs offer almost unlimited opportunities for modifications with the aim of tuning the selectivity of catalysis, which has frequently been a pitfall of other types of heterogeneous catalyst. Difficulties have however been experienced in the development of effective MOF catalysts.[63] Their propensity to lose their porous structures and their often-exhibited instability to moisture have limited their use and the metal centres which form the most obvious site for catalysis are often inaccessible due to coordinative saturation from bonding to the ligands. Despite these pitfalls however, a wide range of catalysis has been shown to be performed by MOFs, and this has been covered in several reviews, for example by Hupp[64] and Yaghi.[63]

1.5.1 Porphyrin MOFs

The porphyrin moiety, widely employed in nature, has presented an obvious target for incorporation into MOFs, due to its previously outlined catalytic ability, high stability and planar rigidity and a significant number of porphyrin MOFs are indeed reported in literature. Particularly noteworthy examples include the PIZA (Porphyrinic Illinois Zeolite Analogue) structures, based on the original

example, PIZA-1, which was synthesised from tetra(4-carboxyphenyl)porphyrin coordinated to trinuclear Co(II) clusters (**Figure 1.17**).[65] In addition to displaying permanent porosity, PIZA-1 is also able to selectively uptake certain molecules into its pores.

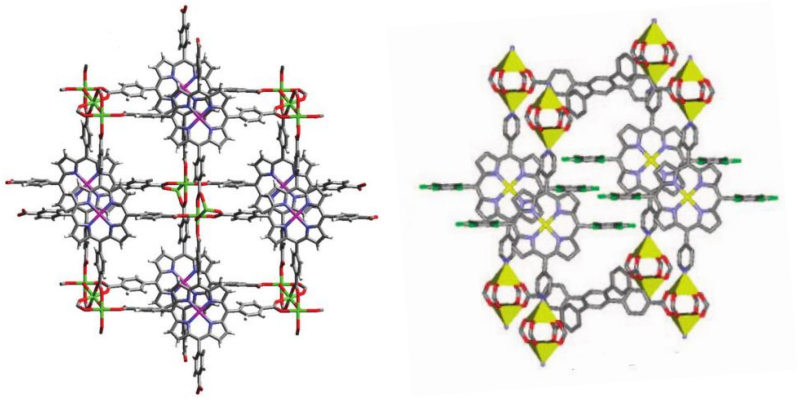

a b

Figure 1.17: The structures of a) PIZA-1 (grey = C, blue = N, red = O, purple and green = Co) and b) ZnPO-MOF (grey = C, blue = N, red = O, green = F, yellow = Zn). Adapted from refs 65-66.

ZnPO-MOF, reported by Hupp, was a further significant development, in which bipyridyl zinc porphyrin ligands were used to axially coordinate Zn paddlewheel SBUs, in turn linked equatorially by tetracarboxylate ligands (**Figure 1.17**).[66] The framework proved to be an effective acyl transfer catalyst.

Oxidative catalysis has also been extensively demonstrated in porphyrin MOFs. One example, built from porphyrin ligands containing 8 carboxylate groups, forms a 3-D framework structure containing two distinct secondary building units, one dinuclear and one trinuclear.[67] Intriguingly, a reduction in catalytic activity is observed when cadmium is used instead of manganese in the SBUs, suggesting that they can play a role in catalysis alongside the metal centres. The MMPFs (Metal MetalloPorphyrin Frameworks), consisting of a 3-D network of porphyrin-encapsulated polyhedral 'cages' are another significant group of catalytic porphyrin MOFs.[68] A prominent example is MMPF-3,[69] which is synthesised from a novel tetracarboxylate porphyrin ligand coordinated to Co_2 paddlewheel SBUs and demonstrates efficient ability as a catalyst for epoxidation reactions, with significantly improved performance compared to homogeneous analogues, as summarised in **Figure 1.18**.

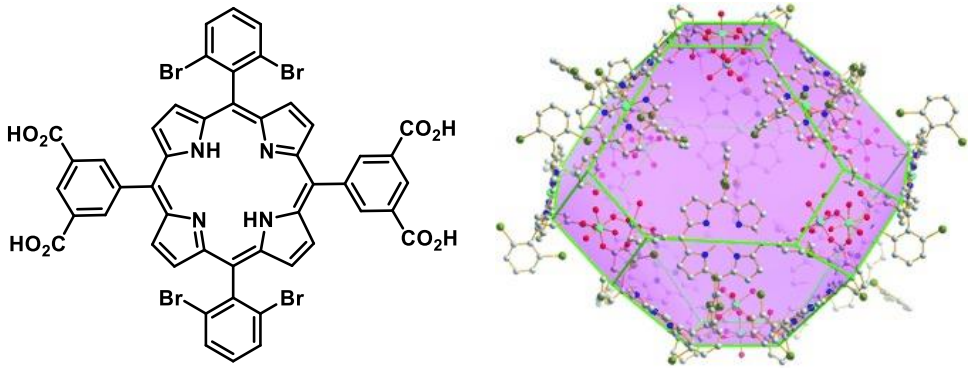

Figure 1.18: The novel porphyrin ligand used in synthesis of MMPF-3 (left) and the structure of one of the catalytically active polyhedral 'cages' within the material (right). Adapted from ref. 69.

Taking a biomimetic approach, porphyrin MOFs have also been developed which contain iron as the metal centre akin to *heme*, including PCN-222(Fe)[70], a member of the wider Porous Coordination Network MOF series. Synthesised from the commonly used tetrakis (4-carboxyphenyl) porphyrin ligand (TCPP), PCN-222(Fe) has been shown to catalyse a variety of oxidation reactions using hydrogen peroxide. In an extension of the biomimetic theme, it has also been demonstrated that the substrate shows better affinity for the MOF than a natural peroxidase enzyme. This is likely explained by the significantly higher concentration of available binding sites in the 3-D framework compared to an enzyme, which may typically have only one.

Whilst the majority of research has focused on the catalysis of oxidation reactions, natural given the similarities of porphyrin ligands to the *heme* functionality which efficiently catalyses such reactions, other types of reaction have also been investigated. For example, porphyrin MOFs are among the materials that have been investigated as catalysts for the synthesis of organic molecules from carbon dioxide. The zirconium-tetracarboxyphenylporphyrin MOF PCN-224 has proved effective in catalysing the reaction between CO_2 and propylene oxide, affording a cyclic carbamate with potentially useful applications.[71] It has also demonstrated the highest apparent surface area of any porphyrin MOF, at 2600 m^2/g.

1.5.2 Phthalocyanine MOFs

Whilst, as outlined, the chemistry of porphyrin MOFs is well-established, only in very recent years have the first true phthalocyanine-based MOFs been reported. Due to the particular symmetry of phthalocyanines, these have been based on ligands in which all of the peripheral positions contain functional groups involved in coordination to the metal ions in the SBU, with the majority employing

catecholate bonds.[72] Several examples of 2D layered MOFs have been synthesised in which the octahydroxyphthalocyanine ligand is coordinated to metals such as copper, cobalt, nickel, iron and zinc[73,74,75] (**Figure 1.19**). These materials have generally been exploited in electrocatalysis, taking advantage of the ability of the catechol functionalities to be oxidised to *ortho*-quinones. The porosity of the materials has also been studied, with apparent BET surface areas of up to 412 m^2/g being reported.[74] Beyond these catecholate MOFs, a 2D layered structure composed of octaamino phthalocyanine ligands has also been reported.[76]

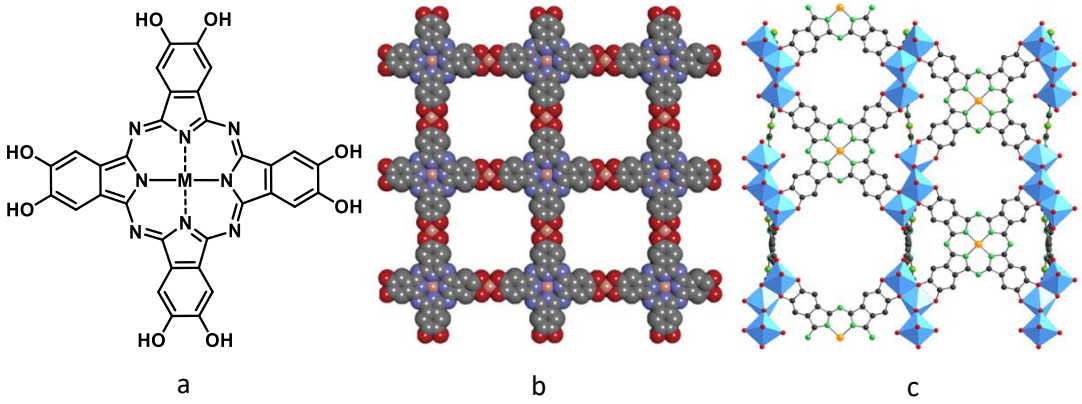

Figure 1.19: The structures of a) the octahydroxyphthalocyanine ligand most commonly employed in reported PcMOFs b) the 2D MOF Cu-CuPc (grey = C, blue = N, red = O, orange = Cu) and c) the 3D MOF MOF-1992 (black = C, green = N, red = O, orange = Co, blue polyhedral = Fe). Adapted from refs. 73 and 77.

As well as the numerous 2D MOF structures, Yaghi and co-workers have reported a 3D MOF also incorporating the octahydroxyphthalocyanine ligand. In this case, the structure featured an iron-based trinuclear SBU coordinated to six ligands, as compared to the previous 2D layered structured which contained mononuclear SBUs each coordinated to two ligands.[77] This is also the only PcMOF in which the structure has been determined by single crystal diffraction, as shown in **Figure 1.19**. It has shown promise in the electrochemical reduction of CO_2 and has also been shown to have a very high surface area of 1471 m^2/g.

1.6 Porous molecular crystals

Beyond the covalently and ionically bonded structures discussed in previous sections, much work has been undertaken in recent years on the study of porous materials held together by only weak inter-molecular forces. Some example structures are shown **Figure 1.20**, with one of the earliest being tris-*o*-phenylenedioxycyclotriphosphazene, which was shown to have a nanoporous crystal structure and to efficiently adsorb gases such as carbon dioxide and methane.[78] A significant advance in the area was the development of highly porous crystals of triptycenetrisbenzimidazolone, which have been found to have a BET surface area of 2796 m^2/g.[79]

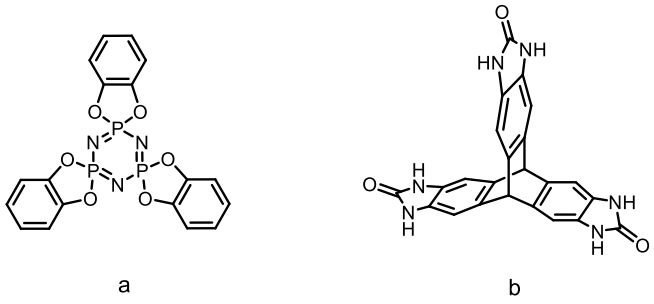

Figure 1.20: The structures of a) tris-*o*-phenylenedioxycyclotriphosphazene and b) triptycenetrisbenzimidazolone, used to form porous molecular crystals.

There have also been reports of macrocycles forming such crystal structures. Porphyrins, particularly tetraphenylporhyrins, had long been known to crystallise as structures containing large pores, but these were always occupied by guest molecules.[80] As with other molecular crystals however, progress has recently been made. One example is a diaminotriazinyl functionalised tetraphenylporphyrin[81] in which hydrogen bonding between the functional groups leads to the porphyrin macrocycles adopting a distorted 2-D layered structure, somewhat analogous to 2-D layered porphyrin MOFs, as shown in **Figure 1.21**. This extra stability allows it to be permanently microporous, though with a relatively low BET surface area of 124 m^2/g.

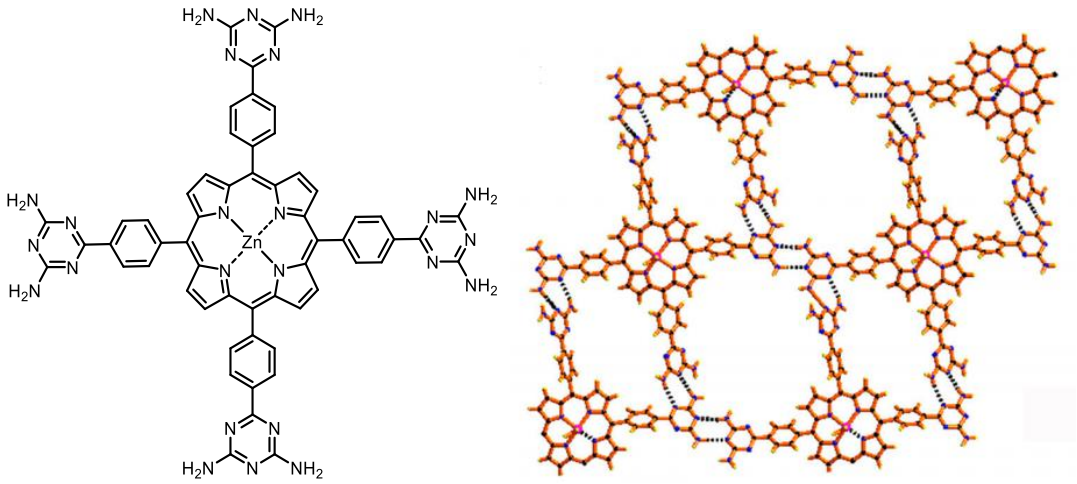

Figure 1.21: The structures of the diaminotriazinyl functionalised tetraphenylporphyrin, and the distorted 2-D layered structure it adopts because of intermolecular hydrogen bonding. Adapted from ref. 81.

1.6.1 Phthalocyanine molecular crystals

An important area of study in recent years within our research group has been phthalocyanine-based molecular crystals. In order to avoid the inherent insolubility associated with phthalocyanines, bulky diisopropylphenoxy groups have been introduced in the peripheral sites of the phthalocyanine. The resulting molecule, shown in **Figure 1.22**, has been found to form large crystals in the unusual $Pn\bar{3}n$ space group, with a unit cell containing 12 molecules of the phthalocyanine.[82] Although the structure contains significant pore space, this is entirely occupied by solvent molecules, and upon evacuation using vacuum the porous structure generally collapses.

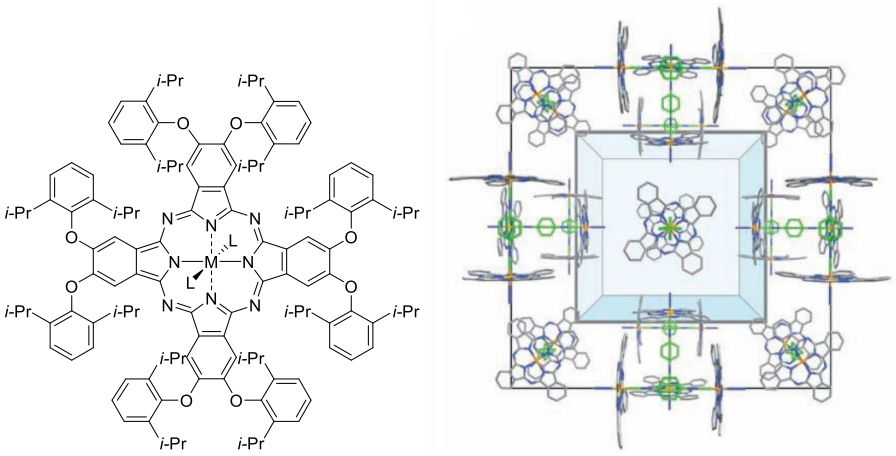

Figure 1.22: The substituted phthalocyanine from which the molecular crystal was formed, and the permanently nanoporous structure obtained using the bidentate ligands.

This limitation was subsequently overcome with the discovery that using bidentate ligands to axially link two metal centres on adjacent phthalocyanines can result in the retention of crystallinity even upon complete removal of solvent.[13] As well as the structural support, it has been noted that the bidentate ligand can also provide for electronic conjugation between metal centres, which in turn can stabilise particular oxidation states. Beyond Fe^{2+}, it has also proved possible to incorporate a wide variety of potentially catalytically useful metal centres, such as Co^{2+}, Mn^{2+} and Ru^{2+} with no significant change in structure. The material displays BET surface areas of over 1000 m^2/g, and with the accessible metal sites described as engineered versions of those observed in *heme* units, is particularly promising for catalysis.

More recently, the unique structure of this particular phthalocyanine has allowed the formation of different materials by co-crystallisation with other molecules. It was determined that fullerenes C_{60} or C_{70} could be incorporated into the phthalocyanine (**Figure 1.23**), and indeed they seem to favour the formation of the crystalline nanoporous structure.[83] Although the fullerene blocks the cavities between the phthalocyanines, the large void is still accessible to guest molecules, and a high BET surface area of 970 m^2/g was measured. The porous crystal is also remarkably stable to hydrolytic conditions and to high pressures.

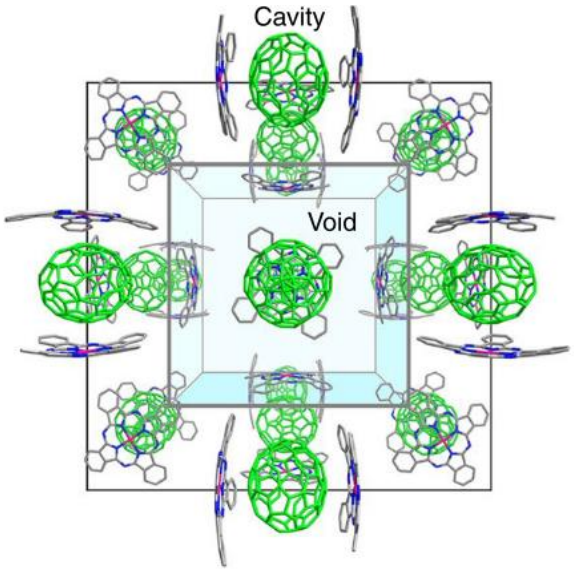

Figure 1.23: The nanoporous structure formed from co-crystallisation of fullerenes with the phthalocyanine, with the occupied cavities and unoccupied voids highlighted. Adapted from ref. 79.

More recently, work within the group has also examined the co-crystallisation of tetraphenylporphyrins (TPPs) with the phthalocyanine. In, as yet unpublished work, it was initially shown to co-crystallise with TPP connected to the phthalocyanine via a nitride bridge between the

metal centres of the two macrocycles. It has subsequently been determined that the unlinked, and indeed metal-free molecules are able to co-crystallise in the $Pn\bar{3}n$ space group due to favourable interactions between their peripheral phenyl groups, as shown in **Figure 1.24.** Further work has shown that a variety of metals can be incorporated into the phthalocyanine with retention of the $Pn\bar{3}n$ cubic structure.

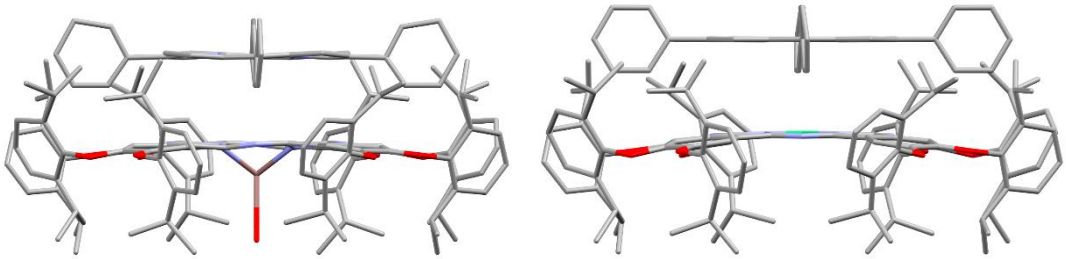

Figure 1.24: Crystal structures obtained from the co-crystallisation of metal-free TPP with a) Indium phthalocyanine and b) Nickel phthalocyanine.

1.7 Aims and Objectives

The principal aim of the PhD project was therefore to expand the scope for the use of phthalocyanines in porous structures, with an ultimate aim of producing materials with useful catalytic properties. Several potential strategies to achieve this were identified. In the first, outlined in **Chapters 2** and **3,** alternative phthalocyanine ligands were to be developed which could coordinate to known metal-organic framework secondary building unit morphologies. Specifically, the use of carboxylate groups to form SBUs, analogous to previously reported tetracarboxyphenylporphyrin MOFs, could significantly expand the range of phthalocyanine MOFs beyond the previously reported catecholate structures.

The second potential route was to build on the work previously carried out within the group on porous phthalocyanine network polymers, which is described in **Chapter 4**. Previous examples of both the specific phthalocyanine employed and the groups used to link them were limited and so it was thought that there would be scope to expand the range of functionalities and polymerisation methodologies.

Finally, the recent results from within the group concerning phthalocyanine-based nanoporous molecular crystals were to be further explored. As discussed in **Chapter 5**, there was considerable scope to vary the nature of the tetraphenylporphyrin molecules used in the co-crystallisations, both by changing the metal ion and by adding various substituents at different positions on the phenyl rings. It was thought that this would allow the nature of the phthalocyanine-porphyrin interactions to be tailored.

2 Attempted synthesis of MOFs from tetracarboxyimidophthalocyanine

2.1 Background and Aims

With the absence in literature of any previous phthalocyanine carboxylate MOF syntheses, initial focus was on conditions used to synthesise the most comparable MOFs. These included those containing analogous tetracarboxyphenylporphyrins, generally 5,10,15,20-tetrakis(4-carboxyphenyl)porphyrin (TCPP) as well as the small number of phthalocyanine catecholate MOFs. Such conditions were found to vary widely in terms of the metal source used, the solvent system, and parameters such as temperature and reaction time. Additives were also frequently added in order to tune the synthetic environment.

TCPP-based MOFs were however found to generally contain one of a small number of different Secondary Building Units (SBUs). As TCPP MOFs consisting of zirconium clusters were the most common, it was decided to initially focus on attempting to synthesise phthalocyanine analogues of these. Numerous reports of such structures were identified, as summarised in **Table 2.1**.

MOF Name	Tetraacid	Metal Source	Additive	Solvent	Temp. (°C)	Time (hrs)
MOF 525[84]	Cu(II) TCPP	$ZrOCl_2$	Acetic Acid	DMF	65	72
MOF 545[84]	Cu(II) TCPP	$ZrOCl_2$	Formic Acid	DMF	130	72
PCN-221[85]	Cu(II) TCPP	$ZrCl_4$	Benzoic Acid	DMF	120	12
PCN-222[70]	Cu(II) TCPP	$ZrCl_4$	Benzoic Acid	DEF	120	48
PCN-224[71]	Co(II) TCPP	$ZrCl_4$	Benzoic Acid	DMF	120	24
PCN-225[86]	Zn(II) TCPP	$ZrCl_4$	Benzoic Acid	DEF	120	12

Table 2.1: Literature conditions for TCPP Zr cluster MOF synthesis.

An additional type of TCPP MOF identified in the literature was those containing a linear trinuclear metal cluster as the SBU, as in PIZA-1.[65] The synthesis in this case involved heating the metal-free TCPP with cobalt(II) chloride in a 1:1 mixture of pyridine and H_2O.

There were also a number of reports of MOFs consisting of 2D sheets of tetraacid ligands connected by a bidentate bipyridyl (bpy) linker, generally 4,4'-bipyridine or a derivative, summarised in **Table 2.2** and **Figure 2.1**. Although ZnPO-MOF did not incorporate a tetracarboxyphenylporphyrin ligand, the

tetracarboxyphenylbenzene used was considered to be suitably analogous for the conditions to be worth replicating.

MOF Name	Tetraacid	Bpy linker	Metal Source	Additive	Solvent	Temp. (°C)	Time (hrs)
ZnPO-RPM[87]	(M)TCPP	**bpy 1**	$Zn(NO_3)_2.6H_2O$	HNO_3	DMF/EtOH (1:1)	80	20
PPF-11[88]	(M)TCPP	**bpy 2**	$Co(NO_3)_2.6H_2O$	N/A	DMF/EtOH (3:1)	80	24
ZnPO-MOF[66]	1,2,4,5-tetrakis(4-carboxyphenyl)benzene	**bpy 1**	$Zn(NO_3)_2.6H_2O$	N/A	DMF	100	48

Table 2.2: Literature conditions for TCPP bpy linked MOF synthesis.

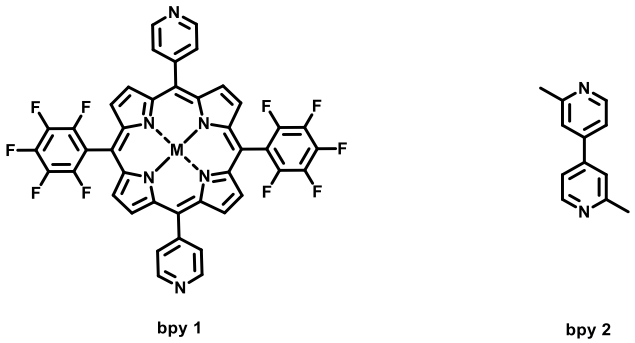

Figure 2.1: The structures of the bipyridine ligands used as linkers in selected TCPP bpy linked MOFs.

Finally, the conditions employed for the syntheses of the small number of previously reported phthalocyanine MOFs were examined (**Table 2.3**).

MOF Name	Pc Ligand	Metal Source	Additive	Solvent	Temp. (°C)	Time (hrs)
NiPc–MOF[76]	NiPc-$(NH_2)_8$	$NiCl_2.6H_2O$	NH_3	DMSO	60	12
PcCu-O_8-Co MOF[74]	CuPc-$(OH)_8$	$Co(acac)_2$	NH_3	DMF/H_2O	120	40
MOF Cu-CuPc[73]	CuPc-$(OH)_8$	$Cu(CF_3acac)_2$	NH_3	DMF/H_2O	120	36
MOF-1992[77]	CoPc-$(OH)_8$	$FeCl_2$	N/A	DMF/H_2O/MeOH	150	16

Table 2.3: Literature conditions for Pc MOF synthesis.

The catecholate and amino phthalocyanine MOFs described in the previous chapter had incorporated substitution at all eight of the peripheral positions but it was clear that the four-fold symmetry of TCPP was key to the formation of all the successfully synthesised porphyrinic carboxylate MOFs structures. In order to introduce metal carboxylate SBUs into phthalocyanine MOFs, a phthalocyanine ligand replicating this four-fold symmetry was therefore required, which would not be possible by substitution of any of the individual peripheral or non-peripheral sites on a standard phthalocyanine ring. To this end, a ligand design was developed with a five-membered imide ring bonded to the phthalocyanine benzene ring. This ring was to be formed using an aromatic amine, the *para*-functionalisation of which would allow the correct symmetry of carboxyl groups, as outlined in **Figure 2.2**.

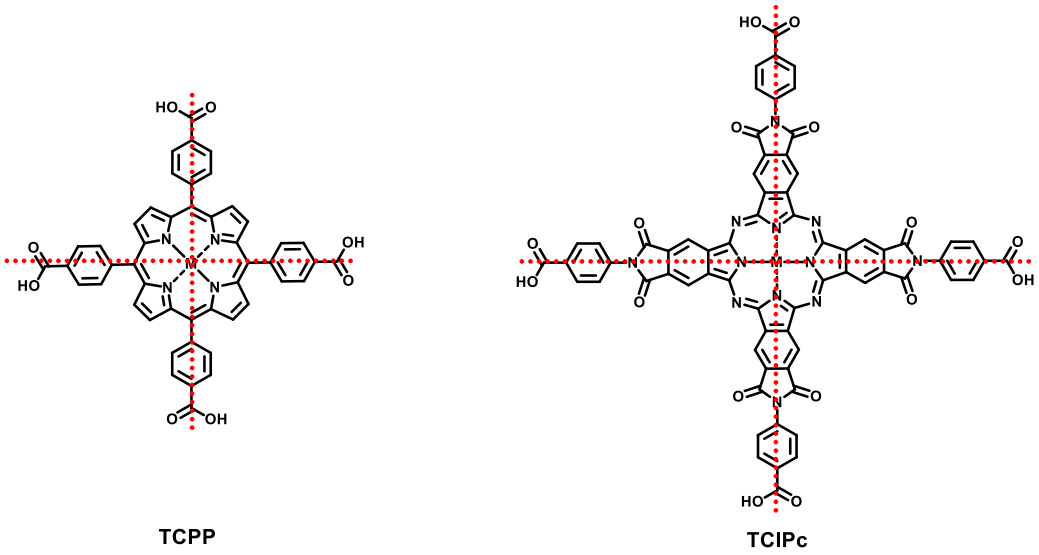

Figure 2.2: The structures of TCPP and the proposed novel tetracarboxyimidophthalocyanine (TCIPc) ligand, highlighting the conserved four-fold symmetry.

2.2 Tetracarboxyimidophthalocyanine ligand synthesis

It was initially assumed that the synthesis of the desired TCIPc ligand would be relatively straightforward, as the necessary synthetic steps had previously been reported in the synthesis of similar compounds. One example was a synthesis described by Sakamoto and Ohno,[89] which was the basis for initial investigation. This started from pyromellitic dianhydride, from which unsubstituted tetraimidophthalocyanine could be formed via a urea melt, and which was in turn hydrolysed to give octacarboxyphthalocyanine. This would then be ring-closed to form the tetraanhydride, the reaction of which with *p*-aminobenzoic acid would produce the desired phthalocyanine. As shown in **Scheme**

2.1, zinc was employed so that it would be possible to characterise the synthesised phthalocyanine by NMR spectroscopy. However, this synthetic route ultimately proved unviable due to poor solubility of various intermediates. Whilst analysis was difficult, it appeared that a degree of polymerisation was occurring, rather than the formation of discrete molecular phthalocyanine as expected.

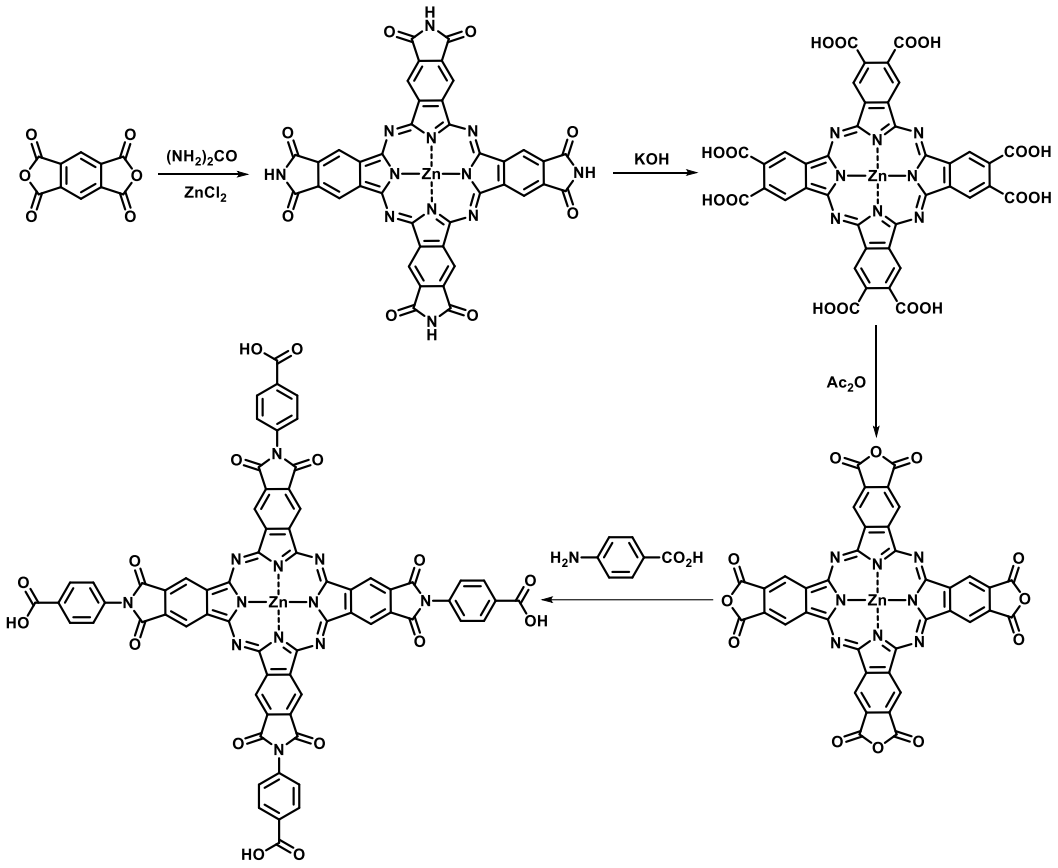

Scheme 2.1: The proposed synthetic route to Zn(II) TCIPc via a urea melt with pyromellitic dianhydride.

Although forming TCIPc from pyromellitic anhydride had not proved possible, it was thought that initially forming the imido-anhydride and then forming the phthalocyanine may be more successful, since it would avoid the inherent polymerisation potential of the dianhydride. By using equimolar quantities of pyromellitic dianhydride and *p*-aminobenzoic acid, the imido-anhydride was obtained (**Scheme 2.2**)

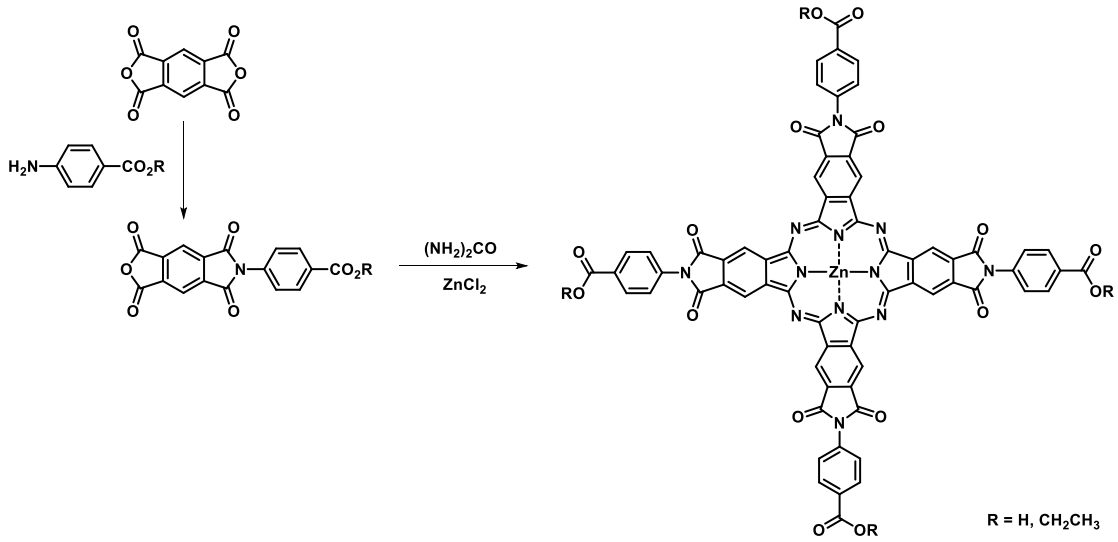

Scheme 2.2: The proposed synthetic route to Zn(II) TCIPc via a urea melt with the imido-anhydride intermediate.

Once again however, attempting the phthalocyanine synthesis using Sakamoto and Ohno's urea melt method[89] resulted in an entirely insoluble black solid. It was presumed that either the carboxyl or imide group was not stable to the reaction conditions and was becoming involved in a polymerisation reaction. Use of an ethyl-ester protected version resulted in the same outcome. When the reaction was further investigated by the use of a diisopropyl analogue of the imido anhydride, polymerisation did not appear to occur, but it proved impossible to isolate a pure product form the complex phthalocyanine mixture obtained.

Further examination of the literature for potential synthetic routes identified a 1972 paper from Boston and Bailar which described a strategy involving the synthesis of discrete phthalocyanines via tetracyanobenzene,[90] as shown in **Scheme 2.3**. Since this reagent is expensive at the scale required, it was first synthesised using a procedure reported by Wohrle[91] in which pyromellitic anhydride was heated in formamide in order to obtain the diimide, which was then converted to the tetraamide using ammonium solution. Tetracyanobenzene was then obtained by reaction of the tetraamide with thionyl chloride.

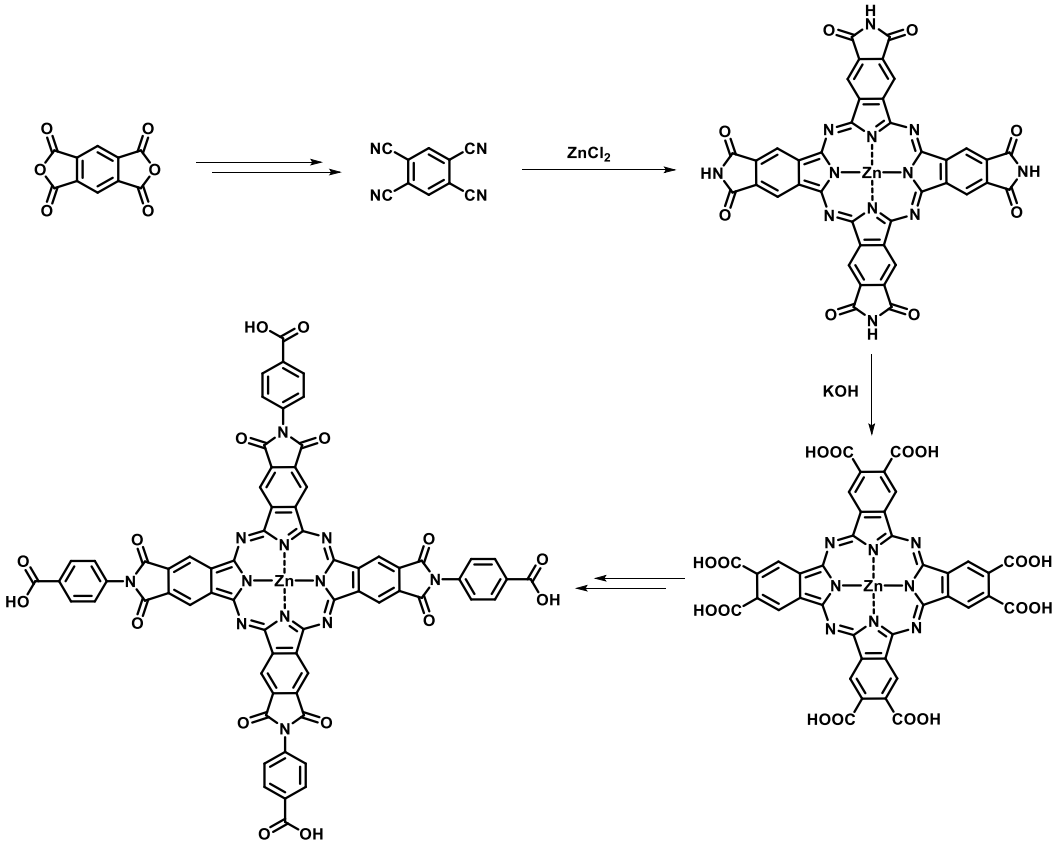

Scheme 2.3: The proposed synthetic route to Zn(II) TCIPc via tetracyanobenzene.

However, subsequent reaction of tetracyanobenzene with a metal salt as per the literature conditions did not afford the desired tetraimidophthalocyanine. Instead, a black, completely insoluble solid was obtained, suggesting that polymerisation had again taken place. The conversion of the imido-anhydride in **Scheme 2.2** to an imido-phthalonitrile was also attempted using Wohrle's methodology. However, after reaction with formamide, only the symmetrical unsubstituted diimide was obtained, as the *N*-substituted imide was apparently not stable to the reaction conditions. Ziegler had reported in that conversion of an anhydride to phthalimide could also be carried out by means of a urea melt,[92] and so this was attempted. Once again however, only the symmetrical phthalimide was obtained.

Given the difficulties experienced in obtaining a pure phthalocyanine product by the synthetic routes previously employed, an alternative strategy was developed. Adapted from a procedure described by Opris,[93] this was planned as a six or seven stage synthesis starting from *o*-xylene, shown in **Scheme 2.4**. The first step involved bromination in order to obtain 4,5-dimethyl-1,2-dibromobenzene. This was subsequently oxidised to the dicarboxylic acid using potassium permanganate. Initially this was done as an aqueous suspension, as described by Opris *et al*, however this generally resulted in large quantities of unreacted starting material settling in the bottom of the flask, even with vigorous stirring. It was found that using a 1:1 solution of water: pyridine afforded conversion to the diacid in high yield.

It was however necessary to use a very large excess of potassium permanganate, up to 20 equivalents, in order to ensure that both aromatic methyl groups were fully oxidised. Formation of the anhydride from the diacid proved unexpectedly challenging. Initially a standard procedure of refluxing in acetic anhydride was employed, but this led to significant quantities of an insoluble by-product being formed, and the solution rapidly darkening from colourless to dark brown. Although the product could eventually be isolated from the solution upon solvent removal, multiple reprecipitation and recrystallisation steps were required, and the yield was correspondingly low, not more than 20%. Sublimation was also investigated as a means of obtaining the pure anhydride, as this has previously been described as means of both forming and purifying similar molecules.[94] However, although a pure product could be obtained, conversion was low, with significant quantities of unreacted diacid remaining even after subliming for up to 12 hrs under vacuum at high temperature.

After further examination of the literature an alternative procedure for the ring closing of dicarboxylic acids to cyclic anhydrides was identified. First described by Mombaini *et al*, this involved using a combination of thionyl chloride and sodium carbonate in a mixture of dichloromethane and 1,4-dioxane.[95] It was found that removal of the inorganic components by washing with water afforded the product in high purity upon removal of the solvent, without the need for any additional purification, although the reaction proceeded slowly, going to completion in around 48 hours. Reaction of the anhydride with *p*-aminobenzoic acid to give the phthalimide was found to take place readily upon refluxing in glacial acetic acid. Conversion of the dibromophthalimide to the phthalonitrile however proved challenging. Attempting the classic Rosenmund–Von Braun synthesis, only the copper(II) phthalocyanine could be obtained. Even by using the mildest possible conditions, carrying out the reaction at 120 ^{o}C and highly diluting the starting material, the desired phthalonitrile product could not be isolated in significant yield.

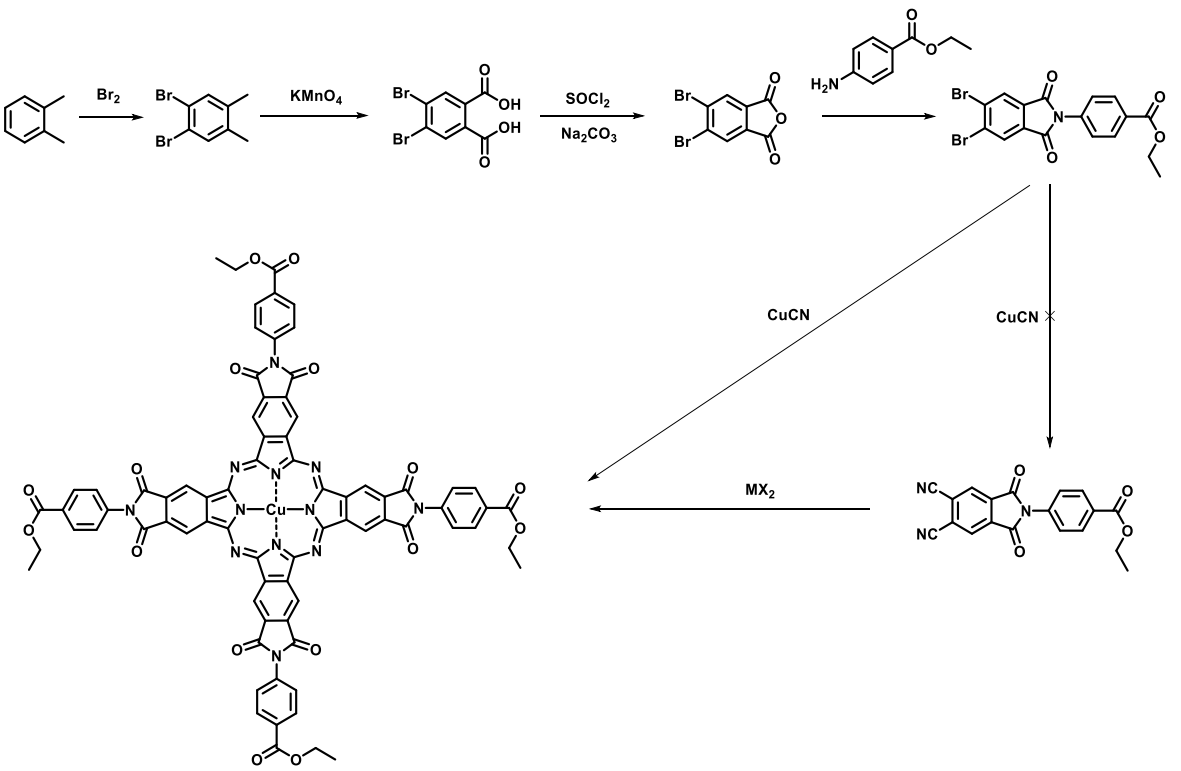

Scheme 2.4: The synthetic route to ester-protected Cu(II) TClPc via phthalonitrile.

In addition, the phthalocyanine obtained by reaction of the unprotected carboxyl dibromophthalimide appeared highly impure, being pale in colour rather that the intense blue/green expected from highly light-absorbing phthalocyanine macrocycles. It is likely that this was a result of the reactive carboxyl group interfering with the cyanation and/or tetracyclomerisation reactions. As a result, the procedure was adapted by the substitution of *p*-aminobenzoic acid for ethyl *p*-aminobenzoate, with the expectation that the ethyl ester protection would allow the phthalocyanine formation to proceed more cleanly. This proved successful, with a deep blue solid isolated from the phthalocyanine formation reaction. Following synthesis of the ester-protected phthalocyanine, the ester could be hydrolysed relatively simply using alkaline conditions (**Scheme 2.5**). TClPc was seen to dissolve in the alkaline solution as the reaction progressed, and following cooling could be precipitated by acidification of the solution. The yields for the ester hydrolysis step were however relatively low.

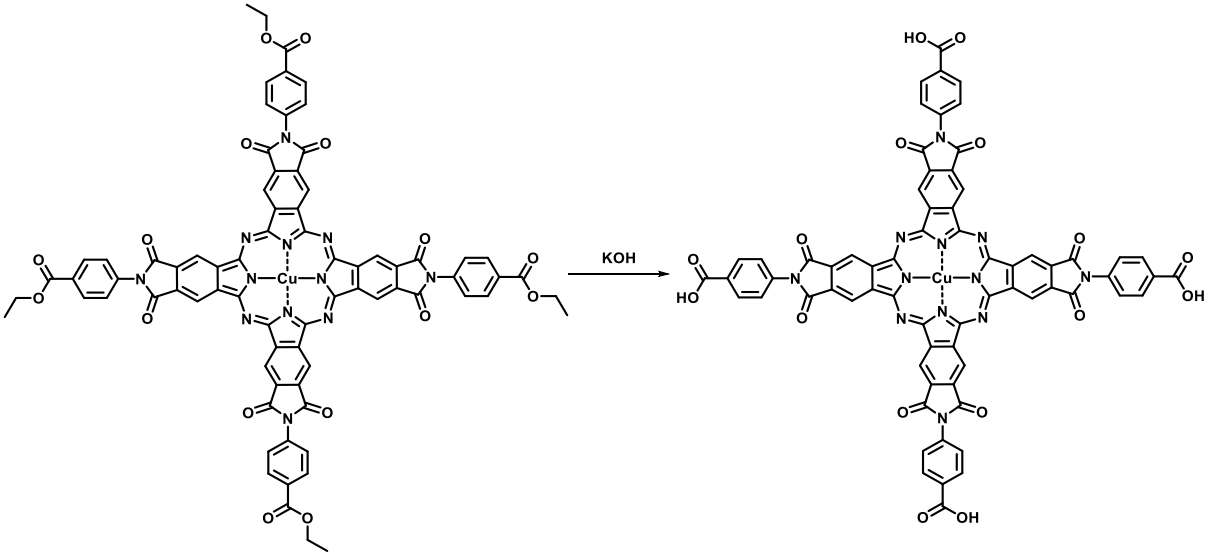

Scheme 2.5: The hydrolysis of the ester-protected phthalocyanine to the final tetraacid product.

Analysis of the synthesised phthalocyanine ligand was hampered by its poor solubility, which along with the paramagnetic nature of the incorporated Cu^{2+} metal centre made NMR analysis impossible. By finely dispersing a sample in acetone, MALDI-TOF analysis was however successfully carried out in order to verify that the molecule had the expected mass, as shown in **Appendix 8.1**. Given the highly absorbing nature of the extended conjugation system in the phthalocyanine, UV-visible spectroscopy was also a useful technique, and due to the very low concentrations needed for such highly absorbing samples, the poor solubility of the ligand was not a significant problem.

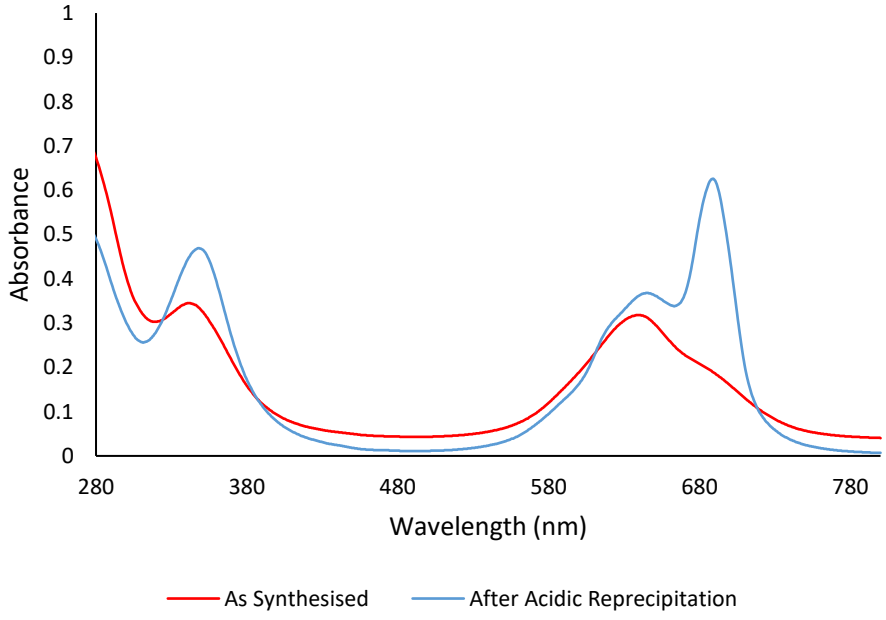

Figure 2.3: The change in absorbance of Cu(II) TCIPc with acidic reprecipitation.

Analysis of the spectrum in **Figure 2.3** shows two distinct peaks in the Q-band region of the spectrum characteristic of phthalocyanine absorption spectroscopy. As it is known that the orbital symmetry of metallated phthalocyanines generally leads to a single peak in this region, it can be assumed that they corresponded to the discrete molecular phthalocyanine, and a separate absorption from aggregation of π-stacked phthalocyanine molecules.[7] Experimental validation for this is provided by the fact that upon dissolving the originally synthesised phthalocyanine in 1M sodium hydroxide solution, and then reprecipitating with 1M hydrochloric acid, a significant increase in observed solubility corresponded to an increase in the area of the Q band peak at 690 nm compared to that at 650 nm.

This was further explored by examining the effect of the binding of a ligand to the free axial sites of the copper metal ion in the phthalocyanine. Whilst the square planar configuration of the d^9 copper(II) ion means that coordination to axial ligands is generally weak,[96] it was known it was possible for a nitrogen coordinating ligand such as pyridine to bind axially to the phthalocyanine overcoming the attractive π-stacking force, and so increase the ratio of free phthalocyanine to stacked dimer.[97] Pyridine was therefore added dropwise to the solution of acid-reprecipitated phthalocyanine in the spectrometer, with the spectrum recorded after addition of every 3 drops (**Figure 2.4**). It was seen that addition of pyridine did indeed increase intensity of the peak at 690 nm corresponding to molecular phthalocyanine, though the effect appeared to decrease after addition of approximately 9 drops, suggesting saturation of the axial sites. This result suggests that while the π-stacking of the synthesised phthalocyanine was significant, it could possibly be overcome by judicious choice of reaction conditions.

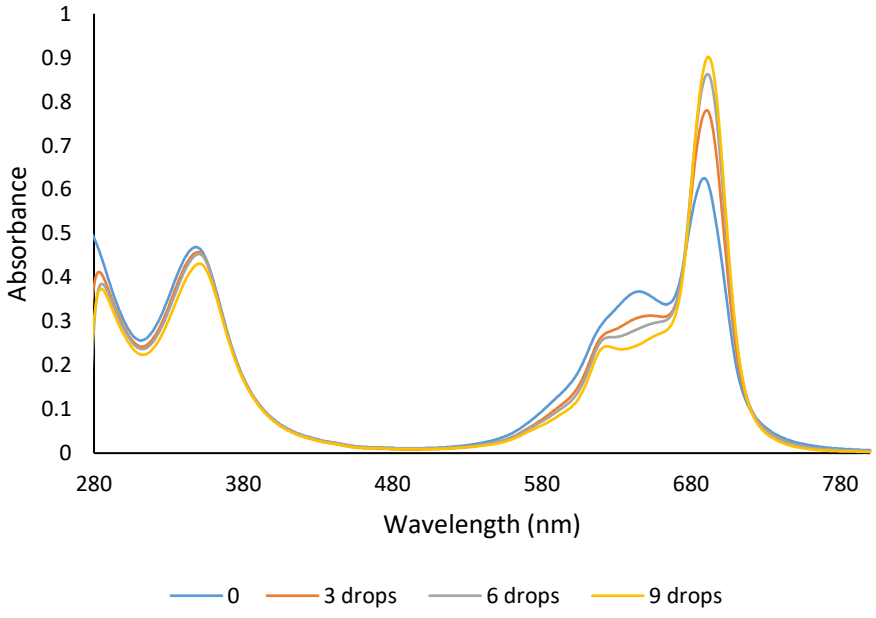

Figure 2.4: The change in absorbance of Cu(II) TClPc with addition of pyridine.

2.3 Attempted Tetracarboxyimidophthalocyanine Metal Organic Framework Synthesis

2.3.1 Zirconium cluster MOFs

With the desired tetrafunctionalised ligand successfully synthesised, initial MOF synthesis reactions focussed on replicating structures analogous to those previously outlined containing Zr_6O clusters linked with porphyrin ligands. As such, analogous reaction conditions were also employed, using the copper(II) substituted TCIPc ligand with zirconium tetrachloride as a readily available source for the zirconium metal, as outlined in **Table 2.4**. In all cases, Cu(II) TCIPc was added along with zirconium tetrachloride and the specified additive to a vial, and dissolved with sonication for at least 20 minutes. The vials were sealed and heated in a metal block for the stated reaction time. Cooling was ramped slowly, at a rate of 20 °C per hour, and upon reaching room temperature, the solid contents of the vial were filtered and washed with the cold relevant solvent, followed by acetone.

Cu(II) TCIPc	$ZrCl_4$	Additive	Solvent	Temp. (°C)	Time (hrs)	Quantity Obtained
10 mg (0.0075 mmol)	10 mg (0.043 mmol)	250 mg Benzoic acid	2.0 ml DMSO	120	12	16 mg
10 mg (0.0075 mmol)	10 mg (0.043 mmol)	250 mg Benzoic Acid	2.0 ml DMF	120	12	29 mg
13.3 mg (0.01 mmol)	1.8 mg (0.0077 mmol)	0.7 ml Acetic Acid	2.7 ml DMF	65	72	9 mg
10 mg (0.0075 mmol)	30 mg (0.129 mmol)	400 mg Benzoic acid	2.0 ml DMF	120	24	13 mg

Table 2.4: Initial synthesis conditions for Cu(II) TCIPc MOF.

The success of the MOF synthesis reactions was determined by examining the crystallinity of the product, and the degree to which it possessed internal surface area. No single crystals were obtained, and powder X-ray diffraction confirmed that the products were entirely amorphous. Measurement of surface area using BET analysis also revealed the structures to have no accessible porosity. From the failure of these reactions to successfully produce a crystalline porous structure, it was determined that literature conditions would require significant adaption in order to tailor them to the properties of the new ligand. Since the TCIPc ligand was considerably less soluble than the porphyrin-based ligands previously examined in literature, examination of the solvent system used in the reaction was considered one of the most important variables. Various polar, high boiling point solvents were therefore employed, with all other variables still based on a literature precedent, as outlined in **Table 2.5**. The scale was also increased, in order to more easily analyse the products produced.

Cu(II) TCIPc	$ZrCl_4$	Solvent	Temp. (°C)	Time (hrs)	Quantity Obtained
40 mg (0.03 mmol)	40 mg (0.17 mmol)	DMF	120	24	21 mg
40 mg (0.03 mmol)	40 mg (0.17 mmol)	DEF	120	24	36 mg
40 mg (0.03 mmol)	40 mg (0.17 mmol)	NMP	120	24	12 mg
40 mg (0.03 mmol)	40 mg (0.17 mmol)	DMSO	120	24	0 mg
40 mg (0.03 mmol)	40 mg (0.17 mmol)	1M $NaOH_{(aq)}$	120	24	8 mg

Table 2.5: Variation of solvent in MOF synthesis with Cu(II) TCIPc.

With *N*-methyl-2-pyrrolidone (NMP), DMSO and aqueous alkaline solution, very little or no solid material was recovered upon cooling, suggesting that the phthalocyanine ligand may have been too soluble in these solvents. Material was recovered from reactions using both DMF and DEF, but the yield was significantly improved with the latter. In both cases, the samples were found to be amorphous and non-porous. An additional variable to investigate was the concentration of phthalocyanine and metal salt. This had initially been based on literature, using approximately the same number of moles as equivalent reactions with TCPP, and was subsequently varied as shown in **Table 2.6**. It was determined however that the highest yields of isolable solid could be obtained with the original conditions.

Cu(II) TCIPc	$ZrCl_4$	DEF	Temp. (°C)	Time (hrs)	Quantity Obtained
40 mg (0.03 mmol)	40 mg (0.17 mmol)	4 ml	120	24	58 mg
10 mg (0.0075 mmol)	40 mg (0.17 mmol)	4 ml	120	24	17 mg
40 mg (0.03 mmol)	10 mg (0.043 mmol)	4 ml	120	24	35 mg
40 mg (0.03 mmol)	40 mg (0.17 mmol)	8 ml	120	24	43 mg
10 mg (0.0075 mmol)	40 mg (0.17 mmol)	8 ml	120	24	11 mg
40 mg (0.03 mmol)	10 mg (0.043 mmol)	8 ml	120	24	28 mg

Table 2.6: Variation of phthalocyanine and metal salt concentration in MOF synthesis with Cu(II) TCIPc.

In all of the reactions, the heating and cooling rates had simply been carried out at the highest rates possible, with no ramping of temperature. As it was known that this could have a significant impact on the success of MOF synthesis reactions,[98] the effect of various rates of heating and cooling was examined (**Table 2.7**). The former was deceased to 120 °C per hour and the latter varied from the most

rapid possible, approximately 240 °C per hour, down to 20 °C per hour. As an additional factor, the use of mechanical stirring was also investigated. Previous studies on MOF synthesis conditions had suggested that this may have a significant impact upon the formation of intermediates and therefore the crystallinity of the final product.[99]

Time (hrs)	Temperature (°C)	Heating rate (°C/hr)	Cooling rate (°C/hr)	Mechanical stirring	Quantity Obtained
12	150	240	240	No	64 mg
12	150	240	120	No	53 mg
12	150	120	20	No	61 mg
12	150	120	20	Yes	48 mg
16	150	240	240	No	42 mg
16	150	120	20	No	49 mg

Note: In all cases 40 mg of Cu(II) TClPc (0.03 mmol) and $ZrCl_4$ (0.17 mmol), with 4 ml DEF were used

Table 2.7: Variation of heating and cooling rate, along with stirring, in MOF synthesis with Cu(II) TClPc.

As with previous experiments, single crystals could not be obtained. However, using a reaction time of 150 °C for 12 hours, and with a gradual cooling rate of 20 °C/hr a sample was obtained which did show distinct sharp peaks in the powder X-ray diffraction pattern, as shown in **Figure 2.5**. The same result was also obtained with a rection time of 16 hours while the use of mechanical stirring was found to result in an entirely amorphous product. However, the low number of peaks, especially at low values if 2θ, is not what would be expected given the large unit cell that would exist in a truly crystalline structure incorporating a ligand such as TClPc,[100] which suggests that it was not formed.

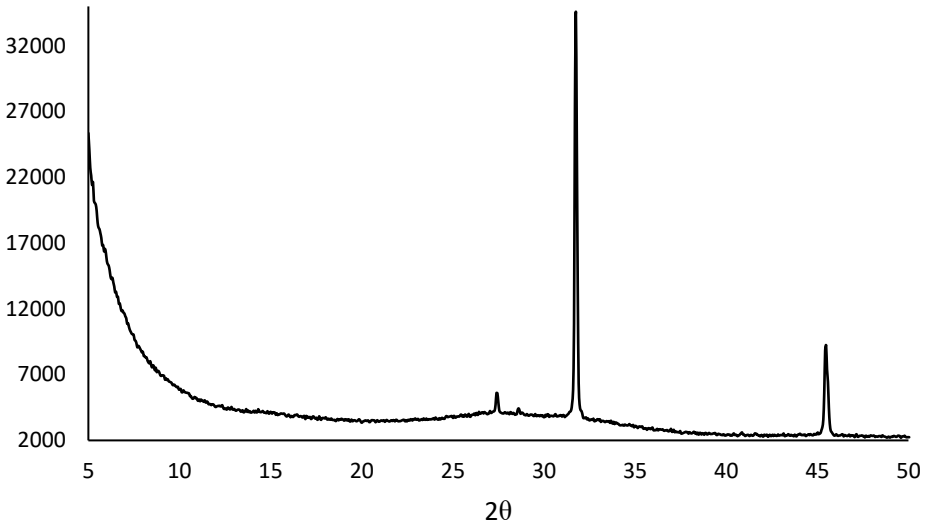

Figure 2.5 Powder XRD pattern for the semi-crystalline Cu(II) TCIPc-Zr product.

The IR spectrum of the synthesised product was recorded, and compared to that of the molecular phthalocyanine ligand, as shown in **Figure 2.6.** Numerous differences could be observed, which may suggest that phthalocyanine functionalities were coordinating to the zirconium. The peak at 1699 cm^{-1} in the spectrum of the ligand, likely attributable to carboxyl C=O stretch,[101] was largely absent in the spectrum of the TCIPc-Zr product, though it must be noted that this could not be conclusively distinguished from a potential imide C=O peak. Additionally, the appearance of a large peak centred at 1370 cm^{-1} could be consistent with literature reports of absorbances in metal-carboxylate MOFs such as MOF-5.[102] The broad peak at 3300 cm^{-1} corresponding to the carboxyl O-H stretch also appeared less intense, though broadened, in the product spectrum, suggesting that at least a portion of the acid groups had indeed become coordinated to zirconium atoms. The fact that it was still evident however implies this coordination was not universal, as would be expected in the predicted crystalline structure.[99] It is also possible however that this absorbance could have been a result of the fact that certain functionalities, for example the imide bonds, were not entirely stable to the identified MOF synthesis conditions and had undergone degradation.

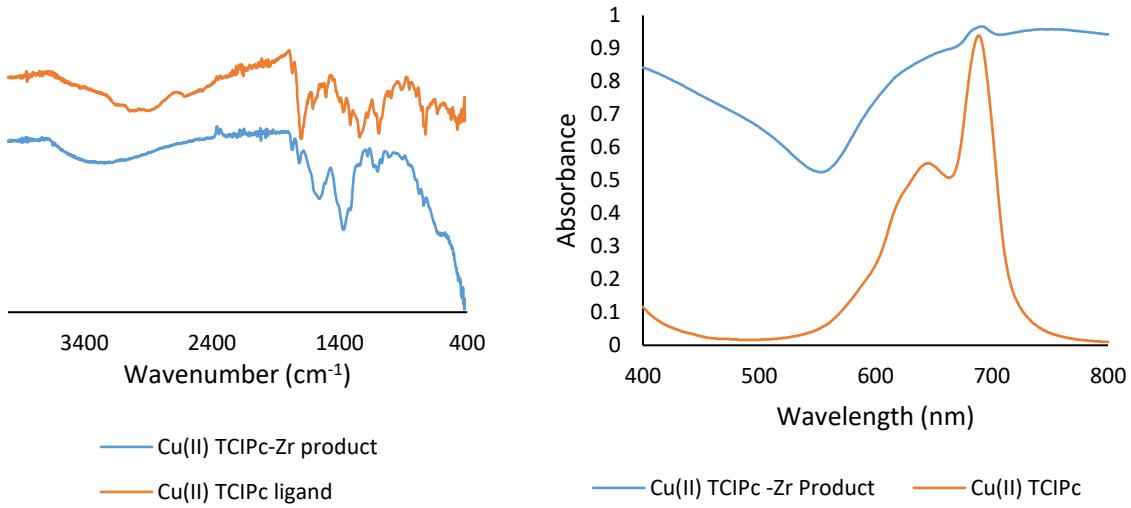

Figure 2.6 Comparison of the IR and UV-vis spectra of the TCIPc ligand and the synthesised TCIPc-Zr semi-crystalline product.

As with the investigation of the molecular phthalocyanine, the highly absorbing nature of the ligand made UV-vis spectroscopy an attractive technique to probe the nature of the synthesised product. This was measured by finely suspending the solid in an appropriate solvent, in this case 1-chloronaphthalene. Since it has been determined previously that the zirconium SBU itself does not have significant absorbances in the UV-vis visible wavelengths examined,[103] the observed spectrum was solely due to the phthalocyanine functionality. Comparison to that of the discrete phthalocyanine ligand, showed that the spectrum was much less clearly defined, with a consistently high baseline. This is due to significant scattering, probably due to a mismatch between the refractive index of the solvent and that of the solid.[104] However the broad spectrum suggests a large amount of Pc aggregation which would be avoided in the desired crystalline structure, again suggesting that the desired MOF had not formed.

Evidence for the failure of formation of true crystalline structure was further enhanced by the BET surface area measurements. With such a large ligand a crystalline MOF would be expected to have a network of large internal pores[105] and therefore likely a large internal surface area. BET measurements however showed a maximum surface area of 27 m^2/g, no higher than had been obtained with the truly amorphous samples. In addition, as shown by the isotherm in **Figure 2.8**, there was no significant N_2 absorption at low partial pressure, which suggests that there was not a significant quantity of pores in the microporous size range.

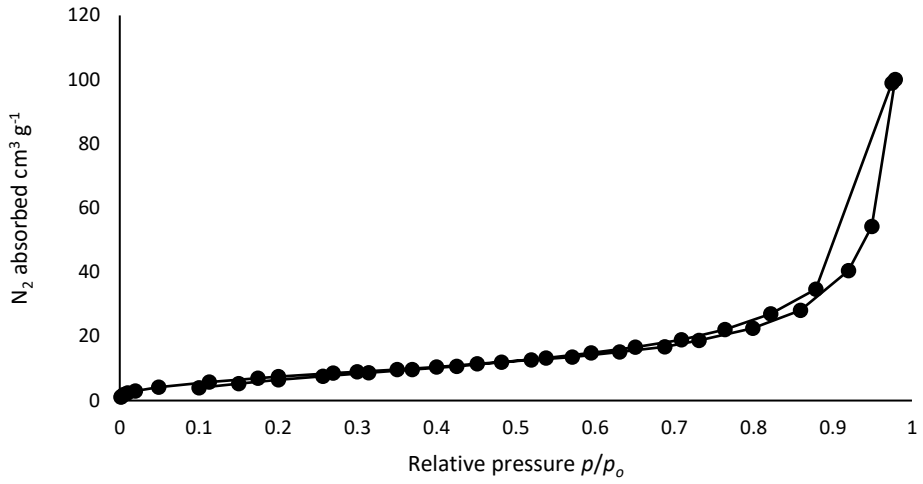

Figure 2.8: The BET isotherm for the semi-crystalline Cu(II) TCIPc-Zr product.

The material was also examined using Inductively Coupled Plasma Mass Spectrometry (ICP-MS) in order to determine the relative quantities of copper and zirconium present. It was found that the quantity of zirconium was greatly in excess of what would be expected in potential MOFs incorporating the TCIPc ligand with Zr_6 SBUs, suggesting that a significant excess of uncoordinated zirconium, likely the oxide, remained within the material. This adds weight to the hypothesis that the excessive aggregation of the TCIPc ligand prevented the formation of the desired structures, and taken together with the other analysis undertake, suggests that the attempted MOF synthesis reactions resulted in only a disordered sample of the starting materials being obtained

2.3.2 Alternative MOF morphologies

As well as the zirconium clusters, an attempt was also made to adapt the carboxy-copper paddlewheel MOF structures previously reported in the literature to the new ligand. Using the conditions that had appeared most successful, the ligand was heated in a sealed vial with copper nitrate in diethylformamide for 12 hours at 150 °C. As before, no single crystals were obtained, so the product was washed with additional diethylformamide and acetone and dried before being ground to a fine powder. XRD analysis of this, shown in **Figure 2.9**, initially yielded only amorphous material, however repetition did result in a product that displayed several sharp peaks on the diffraction spectrum, albeit with a significant background consistent with the amorphous material.

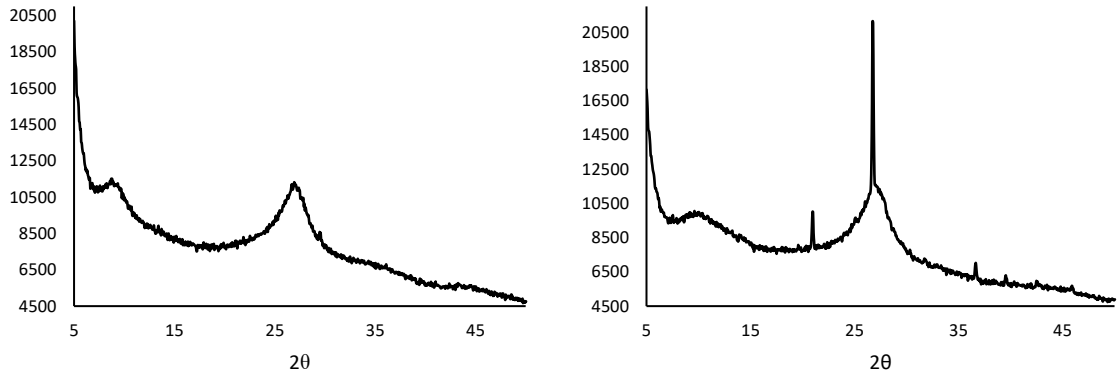

Figure 2.9: The powder XRD patterns for the amorphous (left) and semi-crystalline (right) Cu(II) TCIPc-Cu products.

The pattern of sharp peaks appeared largely consistent with that obtained from zirconium MOF synthesis attempts, but with shifted value of 2θ. As with the previous zirconium cluster samples, measurement of the BET surface area determined that the sample had no internal porosity.

In a final attempt to obtain crystalline MOF materials, the literature reports of bipyridyl-linked structures discussed previously were adapted to use the synthesised TCIPc ligand. Several bipyridyl molecules were considered, as shown in **Figure 2.10**. 4,4'-Bipyridine was initially used as the most simple and commercially available pillar ligand. As per the claims in the reporting of PPF-11, it was thought that the modified dimethyl bipyridyl ligand could be more effective[88] due to the increased steric strain of the methyl group resulting in reduced competition from the phthalocyanine metal centre for binding with the pyridyl functionality. Since the required 2,2'-dimethyl-4,4'-bipyridine was found to be expensive, it was synthesised from 2-methylpyridine following literature procedure.[106] An attempt was made to synthesise the (5, 15-(4,4'-Bipyridyl)-10, 20-bis(pentafluorophenyl))porphyrin ligand as used in the ZnPO-MOF and ZnPO-RPM, however this was not successful.

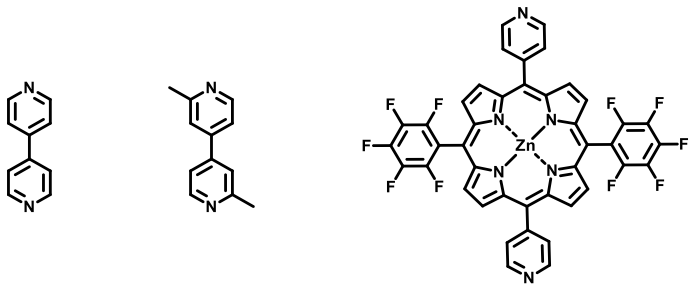

Figure 2.10: The bipyridyl ligands intended to be used in MOF synthesis reactions with Cu(II) TCIPc.

Adapting the synthesis conditions from literature, several reactions were carried out using the bipyridyl ligands, as outlined in **Table 2.8**.

Bpy linker	Metal Source	Additive	Solvent	Temp. (°C)	Time (hrs)
4,4'-Bipyridine	$Zn(NO_3)_2.6H_2O$	N/A	DMF	80	20
4,4'-Bipyridine	$Zn(NO_3)_2.6H_2O$	HNO_3	DMF/EtOH (1:1)	80	20
2,2'-dimethyl,4,4'-bipyridine	$Zn(NO_3)_2.6H_2O$	HNO_3	DMF/EtOH (1:1)	80	20
2,2'-dimethyl,4,4'-bipyridine	$Co(NO_3)_2.6H_2O$	N/A	DMF/EtOH (3:1)	80	24

Table 2.8:F The conditions used in bipyridyl-linked MOF synthesis reactions with Cu(II) TCIPc.

In all cases however, the materials obtained were determined to be entirely amorphous, and also found to have no significant internal surface area by BET analysis. In addition, examination of the filtrate obtained following isolation of the solid product showed the presence of significant quantities of the bipyridyl linkers, suggesting that little if any had coordinated strongly to the TCIPc ligands.

2.4 Conclusions

A novel copper(II) tetracarboxyimidophthalocyanine ligand was developed and characterised, although attempts to synthesise alternatively metallated versions were unsuccessful. Numerous strategies were explored for the incorporation of the ligand into metal organic frameworks, largely based on literature precedent. The majority aimed to replicate the significant number of reports of structures based on zirconium cluster secondary building units, but while semi-crystalline materials were obtained, the overall lack of crystallinity, along with very low porosity of the materials produced were evidence of the failure to form true MOFs. The same outcome resulted from attempts to incorporate the ligand into copper cluster and bipyridine-linked layered MOFs.

This failure to form porous structures can likely be assigned to the extremely high attractive forces between molecules of the phthalocyanine ligand. This was evidenced during its synthesis by its low solubility in all solvents, and by UV-vis studies showing significant aggregation. As a result, it is likely that the potential interactions with the metal clusters could not overcome the phthalocyanine-phthalocyanine interactions, and so the materials obtained remained uncoordinated molecular ligands.

3 Attempted synthesis of MOFs from octacarboxyphthalocyanine and related ligands

3.1 Background and Aims

With the synthesis of MOFs from the initially devised imide-based phthalocyanine proving ultimately unsuccessful, other means of incorporating coordinating functionalities onto phthalocyanines were investigated. While the initial development of the tetra-substituted phthalocyanine had been driven by a desire to mirror the symmetry of tetracarboxyphenylporphyrin MOFs, examination of the literature suggested that this was not necessarily a requirement for the successful synthesis of crystalline structures. In particular, it was considered that it may be possible to form structures where, in addition to functional groups forming part of the secondary building unit, extra groups could be present, which would not coordinate but rather hang pendant within the pore space. This was based on reports such as that of the MOF UiO-66-$(COOH)_2$, shown in **Figure 3.1**, in which additional non-coordinating carboxyl groups had been added to the benzenedicarboxylic acid linkers in UiO-66, with crystallinity retained.[107]

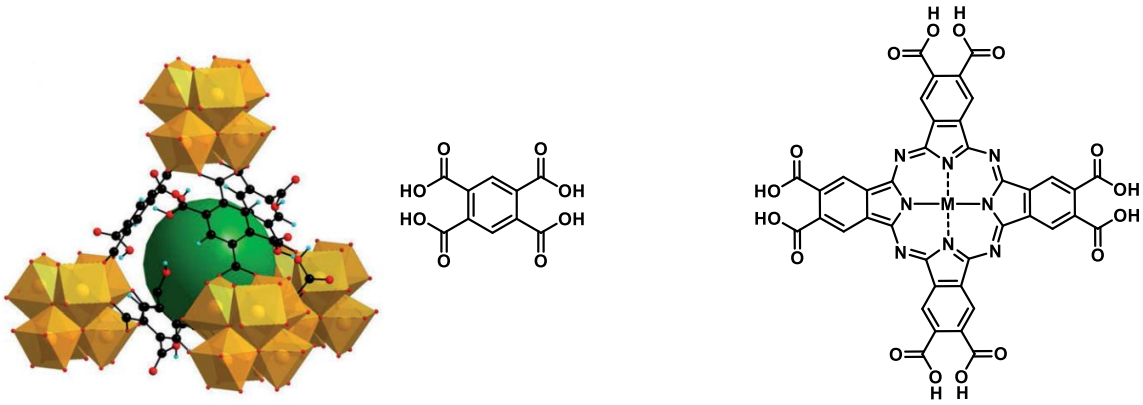

Figure 3.1: The structure of the carboxylate MOF UiO-66-$(COOH)_2$ with its constituent benzenedicarboxylic acid linker (left) compared to octacarboxyphthalocyanine (right).

Accordingly, it was thought that a simple phthalocyanine with additional non-coordinating carboxyl groups may also be appropriate for forming MOFs. Octacarboxyphthalocyanine (OCPc) was identified as a relatively simple synthetic target meeting the criteria, with carboxyl groups that would coordinate to metal ions in the secondary building unit, as well as additional pendant groups.

3.2 Octacarboxyphthalocyanine ligand synthesis

Using parts of the methodology developed for the synthesis of the tetraimidophthalocyanine, a synthetic route to the metallated OCPc was identified, shown in **Scheme 3.1**.

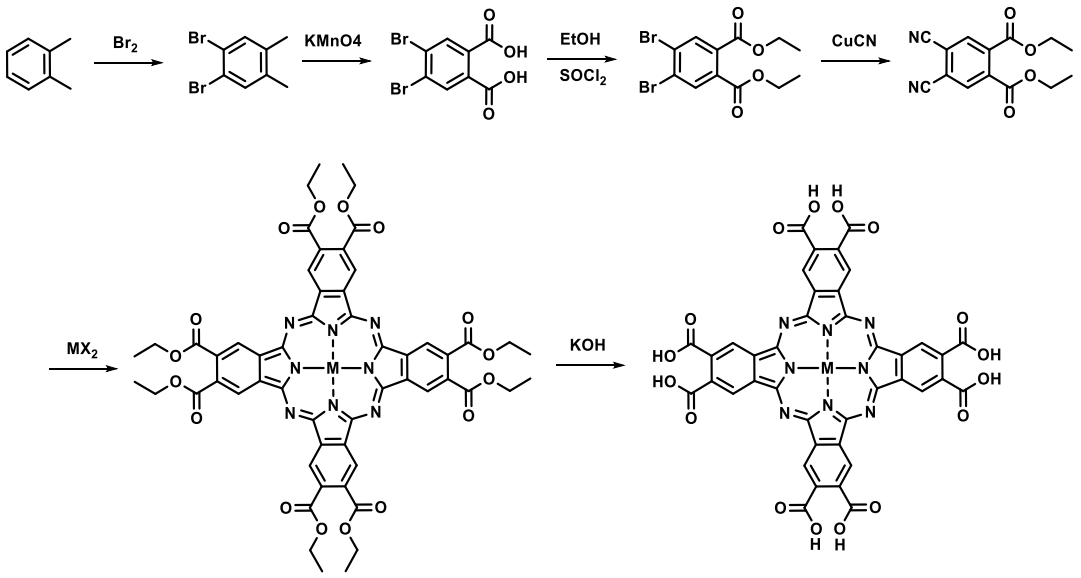

Scheme 3.1: The synthetic route to metallated octacarboxyphthalocyanine.

Initially this followed the same route as the tetraimidophthalocyanine, with the bromination of *o*-xylene followed by oxidation of the dibrominated product to the dicarboxylic acid using potassium permanganate. Subsequently, the acid group was transformed to the ethyl ester using thionyl chloride in ethanol. Initially, this step was not implemented, but it was determined that the diacid was not compatible with the conditions employed in subsequent reaction steps, in particular the Rosenmund-von Braun cyanation step. No further purification of the diethyl ester was necessary, and the Rosenmund-Von Braun reaction of the protected product was found to proceed readily. Indeed, as with the TCIPc synthesis, the reaction was prone to proceeding directly to the phthalocyanine making isolation of the desired phthalonitrile challenging. Again, conditions such as the concentration, temperature, reaction time, and relative quantity of copper cyanide were varied, though no significant improvement in the yield was observed. However, following a report by Chen *et al*, potassium iodide was added to the standard reaction conditions.[108] By careful monitoring of the reaction progress, this allowed the phthalonitrile to be isolated from the reaction mixture with yields of up to 21%.

The successful isolation of the phthalonitrile meant that unlike with TCIPc, metals other than copper, with greater potential catalytic utility, could be incorporated into the octaethyl ester phthalocyanine, as summarised in **Table 3.1.**

Metal Ion Incorporated in Phthalocyanine	Metal salt	Conditions	Yield (%)[a]
Copper(II)	CuCN	DMF, 160 °C, 16 hrs	85[b]
Cobalt(II)	$Co(OAc)_2$	NMP, 180 °C, 2 hrs	14
Manganese(II)	$Mn(OAc)_2$	NMP, 180 °C, 6 hrs	12
Iron(III)	$FeCl_3$	Quinoline, 180 °C, 6 hrs	0

[a] Yields calculated from quantity of diethyl 4,5-dibromo-1,2-dibenzoate.

[b] Obtained directly from dibromo via Rosenmund-Von Braun reaction.

Table 3.1: The conditions and yields of different metallated OCPc ligands.

With the cobalt(II) and manganese(II) salts, the formation of the phthalocyanine from the phthalonitrile was found to proceed readily and with good yields although the low yield in which the phthalonitrile could be obtained mean that the overall quantities were still limited. With the iron(III) salt, no formation of the phthalocyanine was observed. This may have been due to the alternative synthesis conditions employed, which were based on those for an alternative phthalocyanine ligand as the opportunity to tailor the conditions in order to obtain the iron(III) OCPc was limited by the low quantity of the phthalonitrile which was available.

In order to convert the ethyl-ester protected phthalocyanine to the carboxyl functionality desired for MOF synthesis, simple acid and base-catalysed ester hydrolysis reactions were initially attempted. However, even after several days, and despite wide variation of reaction conditions such as temperature, solvent and concentration, conversion of the ethyl ester could not be achieved. Literature-inspired strategies such as the use of biphasic systems[109] and crown ethers[110] in order to improve the solubility of inorganic bases also proved unsuccessful. Unpublished conditions that had previously been identified within the group to effectively hydrolyse multiple ester groups in aromatic systems, employing hydrobromic acid with acetic acid as a solvent were also examined. Whilst these did result in hydrolysis, reaction times were extremely long, and a mixture of fully and partially hydrolysed esters was generally obtained. The isopropyl and butyl ester variant of the phthalocyanines were also synthesised in order to see if they could be more easily hydrolysed than the ethyl ester, but this did not prove to be the case. Eventually it was determined that a base catalysed ester hydrolysis, using a concentrated methanolic potassium hydroxide solution, was the most effective route to obtain

the tetraacid. Long reaction times of up to seven days were still necessary, but the pure product could be obtained with complete conversion.

Although OCPc could be synthesised more reliably and was not as extremely insoluble as the tetraimidophthalocyanine, similar problems in characterisation were encountered. Small quantities could be dissolved in NMR solvents, but due to the lack of protons present, little information could be gained from ^{1}H NMR, and the sample could not be made concentrated enough for good quality ^{13}C spectra. As a substitute, NMR analysis was carried out of the ester protected product, and an isopropyl analogue which it was hoped would be more soluble, as shown in **Experimental 7.3**. Whilst the peaks corresponding to the aliphatic ester protons could be clearly distinguished, information about the phthalocyanine core was more difficult to infer.

As OCPc was relatively soluble in alkaline aqueous solution, it could however be analysed by UV-vis spectroscopy (**Figure 3.2**). As expected, a Q-band peak was observed with maximum absorbance at 688 nm, consistent with the peak form generally observed in metallated phthalocyanines.[7] The relatively broadened nature of the peak, with a shoulder also being observed around 620 nm, may suggest that the monomeric phthalocyanine ligand was coexisting with dimeric or oligomeric clusters of π-stacked macrocycles.[111] UV-vis spectra were also recorded for manganese(II) and cobalt(II) OCPc under identical conditions. In the case of manganese, the maximum absorbance was blue-shifted slightly to 680 nm, reflecting the altered energy of the frontier molecular orbitals due to the substitution of the metal centre. The maximum absorbance for the cobalt(II) ligand was found at an intermediate value of 682 nm. The baseline was also higher with Co(II) OCPc, particularly below 500 nm, which suggests that the solubility in the alkaline aqueous solvent was lower than with the other metallated phthalocyanines, and as a result the scattering previously described for suspended particles was more prevalent.

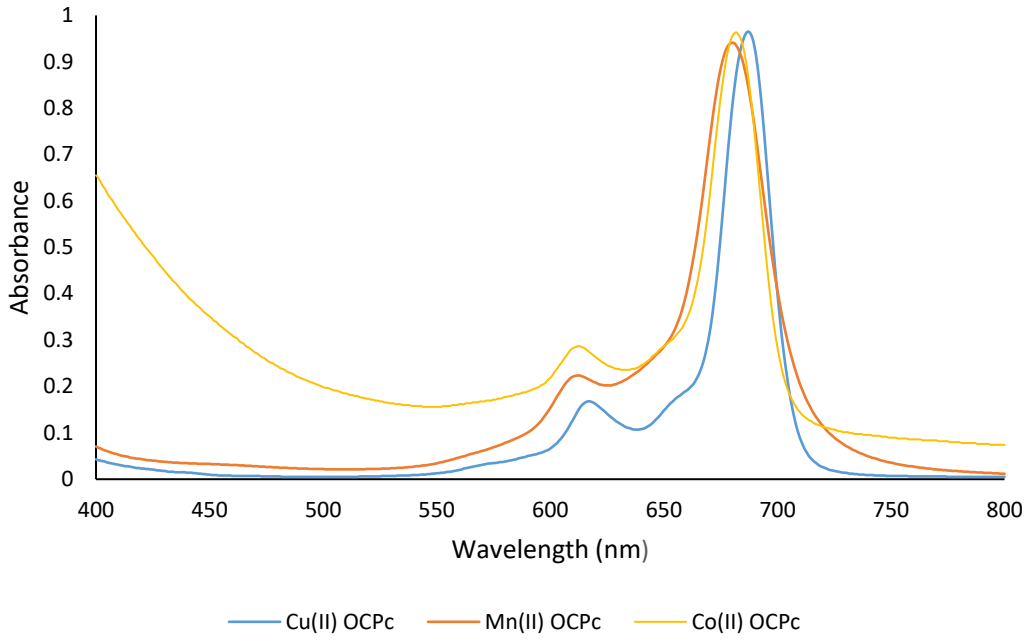

Figure 3.2: UV-vis spectra of metallated OCPc ligands.

The copper(II) OCPc ligand was also examined by powder X-ray diffraction in order to determine whether it self -arranged to form a crystalline structure (see **Appendix 8.1**). It was found that the product obtained using hydrobromic acid in the final ester hydrolysis step did tend to show sharp peaks in the XRD pattern consistent with at least a degree of crystallinity in packing structure. This may be explained by the fact that the relatively poor solubility of the product obtained by this methodology meant that the π-stacking was undisturbed, and so was extended enough to cause long range order with the sample. The ordered stacking of similar powdered phthalocyanines has previously been noted, and indeed exploited.[112] Interestingly, a separate sample, prepared under apparently identical conditions, gave a powder XDR pattern that was quite different. This suggests that the exact crystalline phase adopted by the phthalocyanine solid may be highly dependent on subtle differences during its formation. Contrastingly, powder XRD analysis of the sample obtained following ester hydrolysis using concentrated potassium hydroxide solution over long periods of time showed it to be almost entirely amorphous. This may be a result of the more extensive dissolution of the sample interrupting the initial π-stacking.

3.3 Octacarboxyphthalocyanine Metal Organic Framework Synthesis

Since the copper(II) substituted OCPc could be reliably obtained on multi-gram scale, investigation and optimisation of MOF synthesis was based on this ligand. As with TCIPc, MOF synthesis using the OCPc ligand was initially adapted from literature precedent, as shown in **Table 3.2.** Specifically, reports of UiO-66-$(COOH)_2$,[27] which used benzenetetracarboxylic acid as a linker, as well as the numerous reports of MOFs containing tetracarboxyphenylporphyrin (TCPP).[1-3] Due to the significantly different chemistry of their formation, the synthetic conditions for the octahydroxyphthalocyanine MOFs were not considered applicable in the case of the OCPc ligand.

Cu(II) OCPc	$ZrCl_4$	Additive	Solvent	Temp. (°C)	Time (hrs)	Quantity Obtained
50 mg (0.053 mmol)	15 mg (0.064 mmol)	N/A	H_2O	100	24	22 mg
50 mg (0.053 mmol)	50 mg (0.215 mmol)	Benzoic acid	DMF	120	12	43 mg
50 mg (0.053 mmol)	150 mg (0.644 mmol)	Benzoic acid	DMF	120	24	74 mg
62.5 mg (0.067 mmol)	30 mg (0.129 mmol)	Acetic Acid	DMF	65	72	39 mg

Table 3.2: Initial OCPc MOF synthesis conditions.

In all cases however, the single crystals reported in literature were not obtained, but instead fine powders following washing and drying. As with TCIPc, other forms of analysis and interpretation of the results of the MOF synthesis reactions using the OCPc ligand were also hampered by difficulty in characterising the products. As insoluble network structures, liquid state techniques such as NMR and solution UV-vis spectroscopy were not applicable and the information that could be gained from others such as IR spectroscopy was reduced by the relative lack of distinctive functional groups in the ligand. Powder X-ray diffraction was therefore left as the main means of determining the success or otherwise of MOF synthesis. Specifically, the success or failure of each synthesis attempt could be determined by whether the diffraction pattern corresponded to a crystalline or amorphous product.

The initial MOF synthesis reactions following conditions adapted from literature, shown in **Table 3.2**, resulted in products that were found by powder XRD to be entirely amorphous, with a clear lack of sharp peaks that would have been indicative of a crystalline product. It could therefore be concluded that in these cases the solid obtained following the reaction was simply a mixture of the randomly oriented starting materials with the phthalocyanine molecules being arranged amorphously rather than as the α or β polymorphs, which appears consistent with solution-deposition at the relatively low temperatures involved.[113]

The failure of these initial attempt to form the desired crystalline solids can presumably be explained by the significant difference in geometry between OCPc and the other ligands preventing the formation of the desired network structures, highlighted in **Figure 3.3**, as well as its comparatively poor solubility impacting the available stoichiometry.

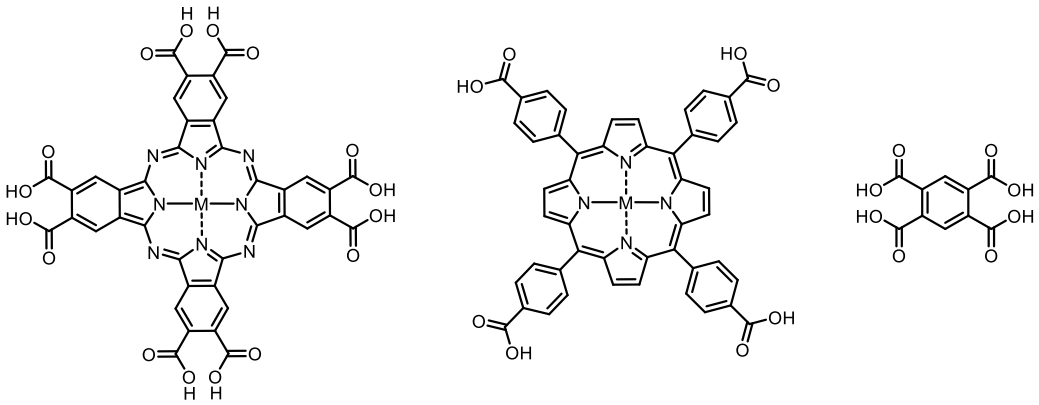

Figure 3.3: The structures of the carboxylate ligands OCPc (left), tetracarboxyphenylporphyrin (centre) and benzenedicarboxylic acid (right).

It was therefore concluded that OCPc MOF synthesis would require the development and optimisation of bespoke conditions. The first factor investigated was the choice of solvent, summarised in **Table 3.4**. This was limited by the fact that even with extensive sonication the phthalocyanine ligand was soluble only in a limited range of solvents, namely polar high boiling solvents such as DMF, DEF, and DMSO. Additionally, given the acid functionality, it was also soluble in alkaline aqueous solutions.

Cu(II) OCPc	$ZrCl_4$	Solvent	Temp. (°C)	Time (hrs)	Quantity Obtained
100 mg (0.108 mmol)	105 mg (0.450 mmol)	DMF	120	24	101 mg
100 mg (0.108 mmol)	105 mg (0.450 mmol)	DEF	120	24	126 mg
100 mg (0.108 mmol)	105 mg (0.450 mmol)	DMSO	120	24	49 mg
100 mg (0.108 mmol)	105 mg (0.450 mmol)	1M $NaOH_{(aq)}$	120	24	38 mg

Table 3.4: OCPc MOF synthesis solvent screen.

While the yields of solid products recovered by filtration varied significantly, in all cases no single crystals were obtained. Powder diffraction analysis also suggested that only amorphous products had been formed. Further optimisation was therefore undertaken, involving the varying of the temperature profile of the reaction (**Table 3.5**) which considered both the maximum reaction temperature but also the rate of initial heating and especially final cooling, since this had been found to be an important factor in the synthesis of TCIPc-based materials.

Maximum Temp. (°C)	Heating rate (°C/hr)	Time (hrs)	Cooling rate (°C/hr)	Crystalline by XRD?	Quantity Obtained
120	240	24	240	No	84 mg
120	240	24	20	No	102 mg
120	20	24	240	No	71 mg
120	20	24	20	No	124 mg
150	240	24	240	No	63 mg
150	240	24	20	Yes	116 mg
150	20	24	240	No	75 mg
150	20	24	20	Yes	98 mg

Note: In all cases 100 mg (0.108 mmol) of Cu(II) OAPc and 105 mg (0.450 mmol) of $ZrCl_4$, with 4 ml DEF were used

Table 3.5: Examination of heating and cooling parameters in OCPc MOF synthesis.

Whilst single crystals were not obtained in any of the resulting products, powder XRD did reveal apparent crystallinity in the case of the sample heated to 150 °C and gradually cooled, as ultimately shown in **Figure 3.4**. In contrast, the rate of heating did not appear to affect the outcome of the synthesis reactions. Whilst literature precedent for this particular result is scant, there are reports which mention very specific ramping rates for heating and cooling being employed.[114] This is likely due to the specific requirements for growth of recoverable crystalline particles.[115] These identified conditions were therefore retained and optimisation was continued via the investigation of the effect of reactant concentration, as detailed in **Table 3.6**. The concentration of Pc ligand in diethylformamide was varied from 5.4 mM to 21.7 mM, with the quantity of $ZrCl_4$ varied proportionally. Additional experiments maintaining the same concentration and varying the absolute quantity were also carried out.

Cu(II) OCPc	$ZrCl_4$	DEF	Temp. (°C)	Time (hrs)	Crystalline by XRD?	Quantity Obtained
100 mg (0.108 mmol)	105 mg (0.450 mmol)	16 ml	150	24	No	49 mg
50 mg (0.054 mmol)	52.5 mg (0.225 mmol)	8 ml	150	24	No	28 mg
100 mg (0.108 mmol)	105 mg (0.450 mmol)	8 ml	150	24	Yes	143 mg
100 mg (0.108 mmol)	105 mg (0.450 mmol)	4 ml	150	24	No	178 mg
50 mg (0.054 mmol)	52.5 mg (0.225 mmol)	4 ml	150	24	Yes	74 mg
50 mg (0.054 mmol)	52.5 mg (0.225 mmol)	2 ml	150	24	No	91 mg

Table 3.6: Examination of ligand concentration in OCPc MOF synthesis.

It was determined that there was a range of phthalocyanine ligand concentrations of approximately 6.5 – 13.5 mM within which the reactions could result in crystalline products, while at either higher or lower concentrations, only amorphous products were obtained. This appears to be in agreement with reported studies of MOF formation, both experimental and computational, which generally suggest that at low concentration the reactions proceed slowly with poor yields, but excessively high concentrations afford either a mixture of products or the crystalline ligand.[99, 116] In the specific case of the OCPc ligand, at low concentration a large quantity of the ligand remained soluble upon cooling and therefore did not form strong interactions with the zirconium metal ions, whereas with high concentrations only a very small quantity could dissolve upon initial heating and therefore, despite the large amounts of product recovered, the bulk of the material was simply unreacted discrete phthalocyanine.

Following this, the reactions were repeated using the successful ligand and metal source concentrations, but with the addition of benzoic acid and phthalic acid as modulators in an attempt to improve the outcome, shown in **Table 3.7**. Addition of the former has been shown to be a highly effective strategy with UiO-66-type MOFs[117] and it was thought that phthalic acid may more closely correspond to the octacarboxy ligand with pendant acid groups. These modulators were used in concentrations of between 5.5 M and 1.4 M.

Additive	DEF	Temp. (°C)	Time (hrs)	Quantity Obtained
Benzoic acid – 5.4 g (0.044 mol)	8 ml	150	24	236 mg
Benzoic acid – 2.7 g (0.022 mol)	8 ml	150	24	163 mg
Benzoic acid – 1.35 g (0.011 mol)	8 ml	150	24	119 mg
Phthalic acid – 2.7 g (0.016 mol)	8 ml	150	24	142 mg
Phthalic acid – 1.35 g (0.008 mol)	8 ml	150	24	97 mg

Note: In all cases 100 mg (0.108 mmol) of Cu(II) OAPc and 105 mg (0.450 mmol) of $ZrCl_4$ were used

Table 3.7: Examination of the effect of benzoic acid in OCPc MOF synthesis.

With all quantities of both benzoic and phthalic acid, significant amounts of excess modulator were found to remain upon completion of the reaction, which were extremely difficult to remove. Even after refluxing several times in a variety of solvents, NMR analysis showed the presence of considerable quantities of the acids in the filtrate upon separation of the solid product. Powder XRD analysis also determined that all the samples were amorphous. It appeared that, rather than being incorporated into a crystalline structure, the modulators were instead simply coordinating to the other reaction components due to strong hydrogen bonding interactions with the large number of carboxyl groups on the OCPc ligand, which was likely compounded by the π-π interactions between the highly planar phthalocyanine and the aromatic acids employed. The failure of the modulators to function as suggested by the literature could potentially be explained by the large size disparity between the small carboxylic acid molecules used and the phthalocyanine ligand.[118] Employing a ligand featuring carboxyl groups on only one benzene ring may have been more effective, but such asymmetrically substituted phthalocyanine molecules are synthetically challenging.[119]

A further reaction parameter that was investigated was the physical environment of the reaction (**Table 3.8**). In general, sealed borosilicate glass vials were used, following the main literature consensus. These were available in different sizes, which was also considered a potential factor given the resultant difference in solvent surface area and headspace. Alternative conditions were also investigated based on reports of analogous carboxylate MOFs synthesised in unsealed round bottomed flasks.[120] As with the attempted synthesis using TCIPc, the presence or absence of mechanical stirring was also thought likely to affect the formation of the desired products.

Reaction vessel	Mechanical stirring	Solvent	Temp. (°C)	Time (hrs)	Product Obtained
Sealed vial – 8 ml	Yes	DEF	150	24	97 mg
Sealed vial – 8 ml	No	DEF	150	24	88 mg
Sealed vial – 14 ml	Yes	DEF	150	24	102 mg
Sealed vial – 14 ml	No	DEF	150	24	79 mg
RBF – 25 ml	Yes	DEF	150	24	132 mg
RBF – 25 ml	No	DEF	150	24	128 mg

Note: In all cases 100 mg (0.108 mmol) of Cu(II) OAPc and 105 mg (0.450 mmol) of $ZrCl_4$, with 4 ml DEF were used

Table 3.8: Examination of mechanical factors in OCPc MOF synthesis.

Whilst the change from 8 ml to 14 ml sealed vial did not affect the crystallinity of the products obtained, attempting the reactions in a round bottomed flask resulted in an entirely amorphous product. It was observed that a significant quantity of the solvent was lost during the syntheses in these cases, and the resulting greater concentration of phthalocyanine ligand was likely outwith the parameters previously established for successful formation of crystalline material. An amorphous product was also the result when the reactions carried out in sealed vials were subject to mechanical stirring. An undisturbed environment was therefore determined to be crucial in the formation of the extended networks in the MOF material of interest. It has been previously postulated with other MOFs that this effect may be a result of stirring stabilising intermediates rather than the final desired structure, due to the most favourable concentrations of reactants being located in certain pockets of the solvothermal mixture rather than the bulk.[99]

The intolerance to slight differences in the reaction conditions as a result of the properties of the OCPc ligand mean that a narrow band of conditions were found during the extensive optimisation process to favour the formation of more crystalline products, namely using diethylformamide as a solvent, heating for 24 hrs at 150 °C with slow cooling, summarised in **Scheme 3.2**. Determination of the precise yield of reactions was not possible however, due to the fact that the specific structure of the MOF material could not be elucidated.

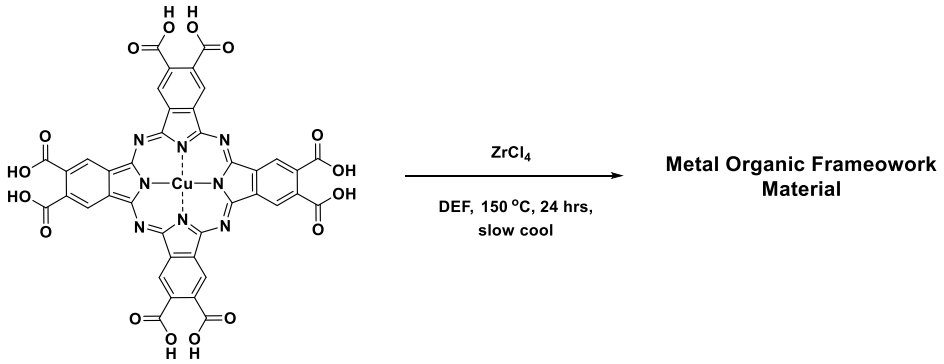

Scheme 3.2: The optimised reaction conditions for the synthesis of Cu(II) OCPc MOF materials.

Powder XRD analysis of the solid product thus obtained gave the pattern shown in **Figure 3.4**, which features the sharp peaks indicative of a more successful reaction. Due to the large size of OCPc, the unit cell of the resulting crystal structure would be expected to be large,[121] and this is supported by the low 2θ of the majority of the peaks observed in the spectrum. This is also consistent with the published pXRD patterns of the small number of reported catecholate phthalocyanine MOFs, which generally show a small number of sharp peaks in the 0-10-degree range.[74] Significantly, the pattern was also different from that obtained from non-amorphous samples of the OCPc ligand alone.

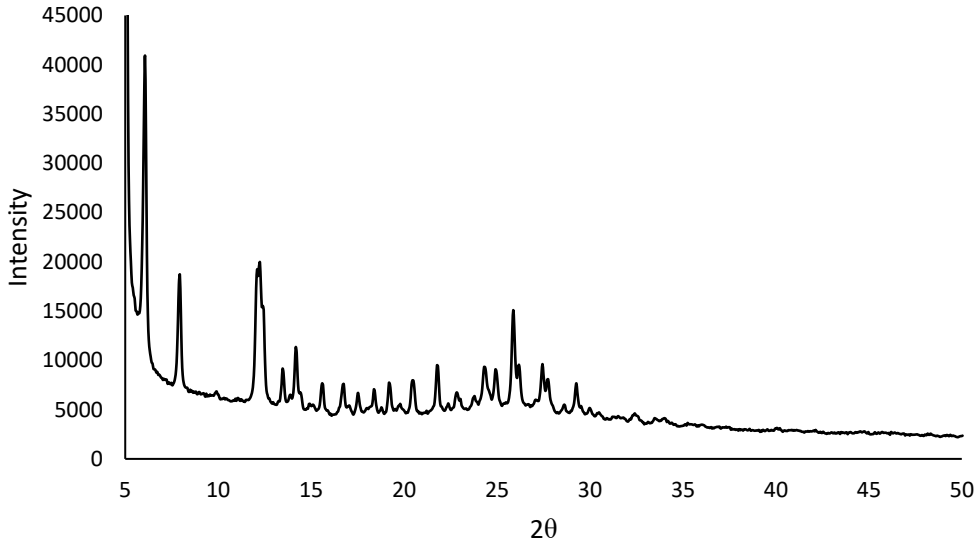

Figure 3.4 Powder XRD pattern for crystalline Cu(II) OCPc MOF material.

The synthesised MOF-type product was also analysed by IR spectroscopy, shown in **Figure 3.5**. Compared to the spectrum of the OCPc ligand, many of the same peaks were observed, as expected given the retention of the functional groups. In particular, the carboxyl O-H stretch at 3300 cm^{-1} was still observed in the synthesised material, which supports the idea of uncoordinated pendant carboxyl groups being present. A number of changes observed in the spectrum of the OCPc MOF do suggest that coordination to the Zr-based SBU may have altered the stretching or bending vibrations of

functionalities in the phthalocyanine. As discussed in the previous chapter, changes in the peaks at 1710 and 1560 cm^{-1}, likely assignable to carboxyl C=O stretching,[101] suggest differences between the ligand and the product that could be attributed to coordination to the zirconium clusters . Additionally, the significant increase in the relative size of the peak centred at 1365 cm^{-1} is consistent with literature reports of absorbances in metal-carboxylate MOFs such as MOF-5.[102] The overall form of the spectrum, with many individual absorbances retained from the ligand spectrum, is also similar to the reported spectra from analogous MOFs, including porphyrinic carboxylate[70] and phthalocyanine catecholate[73] structures.

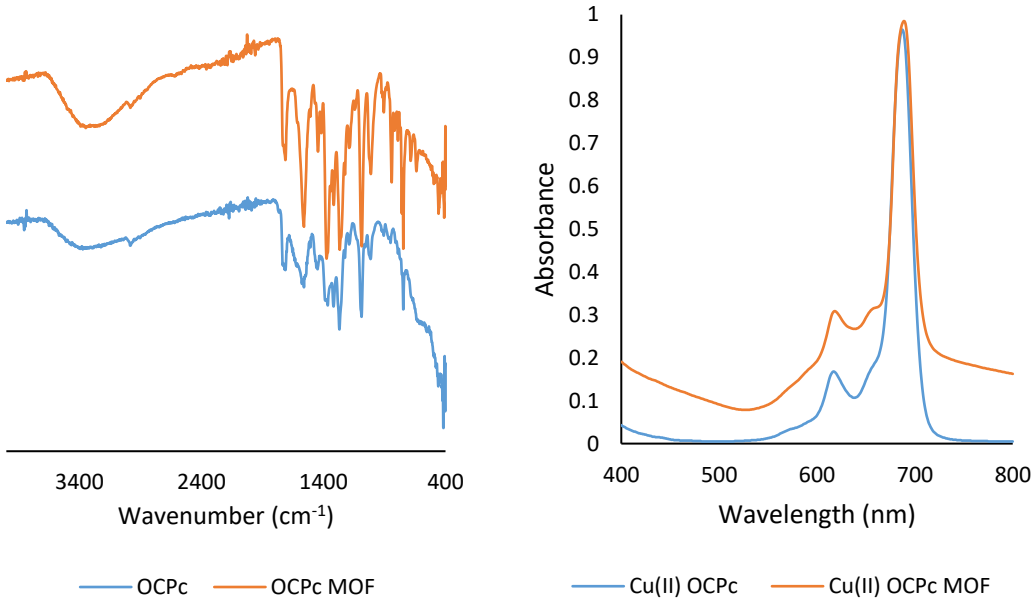

Figure 3.5 Comparison of the IR and UV-vis spectra of the discrete Cu(II) OCPc ligand and the Cu(II) OCPc MOF material.

In attempt to gain more insight into the electronic environment of the phthalocyanine rings within the MOF-type material, it was investigated by UV-vis spectroscopy. As before, this could be carried out by finely suspending small particles of the material in an aromatic solvent, namely 1-chloronaphthalene. While the baseline was higher due to the scattering of the solid particles, the spectrum obtained showed a similar pattern to that of the discrete OCPc ligand. The single large Q-band peak had a maximum absorbance at a slightly longer wavelength of 690 nm compared to 687 nm. It is notable that there was no peak corresponding to additional aggregation of the phthalocyanine ligand in the product, which is strong evidence that the solid product did not consist of π-stacked molecular phthalocyanines. This appears to be consistent with reported well-defined spectra for porphyrinic MOFs,[122] which describe the maintenance of the characteristic Q-band peaks and so suggests that the ligands were coordinated in a more open structure as a result of MOF-type bonding. As mentioned in

the previous chapter, none of the small number of descriptions of reported phthalocyanine MOFs contain any information about the solid-state UV-vis spectra of the products, making comparison impossible.

ICP-MS was employed in order to verify whether the quantities of copper and zirconium present in the OCPc material were consistent with a potential MOF-type structure. It was found that there was an approximate zirconium: copper ratio of 9:1 in the samples examined. This may be consistent with potential Zr-based SBUs coordinating to the phthalocyanine ligand, however, assuming Zr_6 clusters were present, this would equate to the coordination of only three carboxyl groups per cluster. Whilst the relatively large size of the OCPc ligand and steric hindrance from the pendant carboxyl groups would mean that it would likely not be able to coordinate densely to the SBU, this is a considerably lower degree of coordination than in analogous non-phthalocyanine MOFs. Hence it is possible that, as in the case of the TCIPc material, some uncoordinated zirconium oxide remained within the structure.

Having identified the optimal conditions for the synthesis of the copper(II) OCPc MOF material, synthesis was also undertaken of the cobalt(II) and manganese(II) versions. The small quantity of these metallated OCPc ligands that could be obtained meant that it was not possible to further optimise the conditions for the change in metal centre, but as the success or failure of the MOF synthesis reactions appeared to be most strongly influenced by the symmetry and solubility of the phthalocyanine ligands, it was thought that the altered electronic environment upon substituting copper for cobalt would have relatively little impact, particularly as spectroscopic studies of variously metallated phthalocyanines had shown that changing the metal centre had only minor effects on the energy of the molecular orbitals.[7]

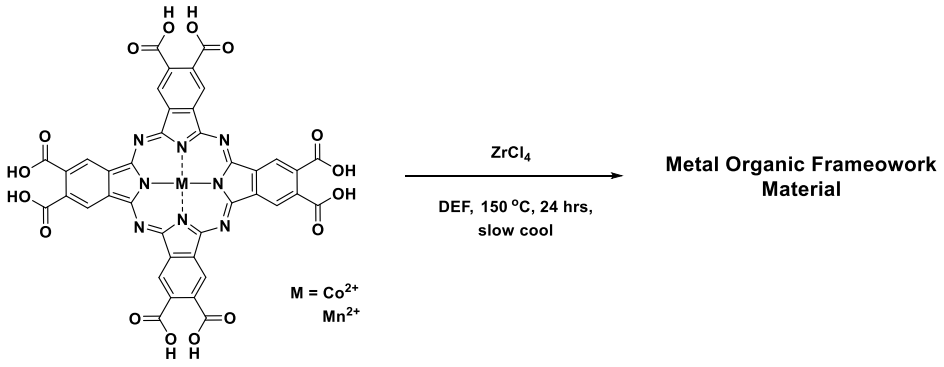

Scheme 3.3: The synthesis of Co(II) and Mn(II) OCPc MOF materials.

Following this reasoning, the reactions were carried out as per **Scheme 3.3** to obtain appreciable quantities of powder products for both the Co(II) OCPc MOF and Mn(II) OCPc MOF products. XRD

analysis however showed that both products were entirely amorphous, suggesting that the impact of the metal centre on the formation of crystalline structures may be significantly greater than thought. The two materials were also analysed by UV-vis spectroscopy, using the same methodology as with the Cu(II) MOF-type material. In both cases, the peaks observed were much less distinct, showing a high degree of scattering as opposed to distinct absorbances, and pointing to a potential lack of structural homogeneity and a high degree of aggregation in these structures. This is also likely to explain the fact that the broad peaks that could be observed had maximum absorbances at considerably higher wavelengths than the copper(II) MOF-type structure, with the cobalt(II) and manganese(II) materials showing maximum absorbance at 707 nm and 723 nm respectively. As the substitution of metal centres has been shown not to significantly affect the wavelength of maximum absorbance, this shift could instead be explained by peaks corresponding to aggregated phthalocyanines swamping those of the discrete molecular ligands.[123] ICP analysis of the Co(II) OCPc product however did show that the ratio of zirconium to cobalt was approximately 6 to 1. Again assuming the presence of Zr_6 clusters, this would correspond to the coordination of 4 carboxyl groups per cluster, which may be consistent with expected coordination structures formed from the ligand.

3.3.1 Porosity measurements

Once samples had been identified in which X-ray powder diffraction analysis suggested that a desired porous structure may be present, this was probed by measuring the specific surface area, calculated using the Brunauer–Emmett–Teller (BET) theory. This involved treating the samples as outlined, generally by refluxing in solvent systems for an extended period of time, and then thoroughly drying them for at least 16 hours in a vacuum oven, before degassing using dedicated instruments. Generally, best practice calls for larger quantities of sample for such measurements in order to ensure reproducibility of results,[124] but in some cases less than 100 mg was available and so smaller amounts had to be used.

Conditions	XRD Pattern	BET Surface area (m^2/g)
DEF, 150 ^oC, 24 hrs	Crystalline	81
DEF, 150 ^oC, 24 hrs, dilute concentration	Crystalline	38
DEF, 150 ^oC, 24 hrs, H_2O refluxed	Crystalline	15

Table 3.9: BET surface area measurements of initial samples.

As outlined in **Table 3.9** above, initial measurements with some of the samples that had appeared potentially promising by powder XRD resulted in surface areas that were disappointingly low, with the vast majority being less than 20 m^2/g, indicating that there was effectively no internal porosity. The highest value obtained of 81 m^2/g is just outwith the range normally observed from simple external gas adsorption on the finely powdered particles,[125] so may be consistent with that sample having a low amount of internal surface area. This observed lack of internal free volume may be explained by the fact that the desired coordination structure simply failed to form as expected in these samples, with the significant attractive force between individual OCPc ligands due to their strong π-π interactions likely to be a contributing factor. The role of pendant carboxyl groups, and their potential to coordinate other than in the expected way, could also be a factor in restricting free pore volume. It is also possible that the crystalline porous MOF structure did form as hoped in the samples, but that the large pores were blocked and therefore unavailable for gas adsorption. This could be explained by the trapping of uncoordinated OCPc ligand within them during the formation of the structure, which would be difficult to subsequently remove due both to the low solubility of the ligand, and also the high potential for its carboxyl groups to coordinate to different parts of the structure.

However results for later samples from further optimised conditions did show higher BET surface areas. As with XRD measurements of crystallinity, it was found that using a slower cooling rate in the MOF material synthesis was favourable in the formation of structures with higher BET surface areas (**Table 3.10**).

Conditions	XRD Pattern	BET Surface area (m^2/g)
DEF, 150 °C, 24 hrs, slow cool	Crystalline	209
DEF, 150 °C, 16 hrs, slow cool	Crystalline	170
DEF, 150 °C, 36 hrs, slow cool	Crystalline	145
DEF, 180 °C, 24 hrs, slow cool	Crystalline	177
DEF, 130 °C, 24 hrs, slow cool	Crystalline	116

Table 3.10: BET surface area measurements of samples from optimised conditions.

From the form of the isotherm of the higher surface area sample (**Figure 3.6**), it was clear that the adsorption is reversible, given the lack of significant hysteresis observed between the adsorption and desorption curves. This suggests that the small N_2 molecules could diffuse relatively easily within the structure. It can also be seen that there is a relatively large amount of gas absorbed at very low relative pressures. As previously discussed, this type of adsorption is consistent with a structure with a higher

internal surface area, and so may be indicative of at least partial success in the formation of such structures, despite the relatively low area measured. This could be seen clearly by comparison of the isotherms of the higher surface area samples to those of the previously examined non-porous materials, with the latter showing effectively no gas uptake at these low partial pressures.

As the substitution of copper(II) for cobalt(II) and manganese(II) in the phthalocyanine metal centre had resulted in materials that were entirely amorphous, the extent to which this was also reflected in the surface areas of such structures was investigated, also shown in **Figure 3.6**. It was found that the materials containing cobalt(II) and manganese(II) were indeed non-porous as well as non-crystalline, with BET surface areas of less than 20 m^2/g.

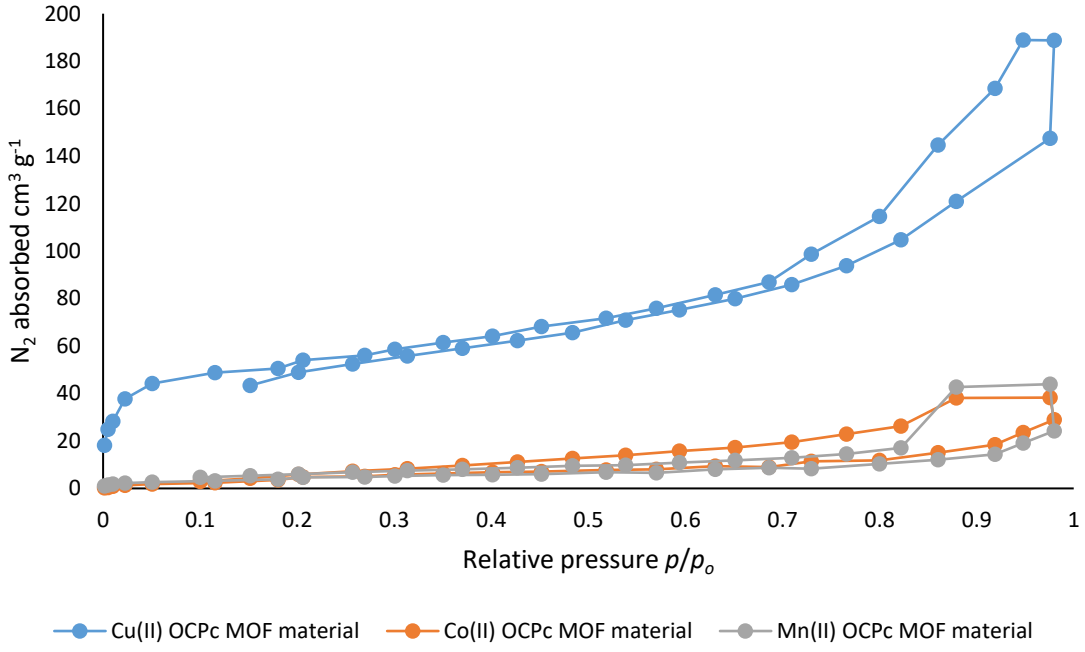

Figure 3.6: Comparison of N_2 adsorption of MOF samples synthesised using OCPc ligands containing different metals.

The uptake of carbon dioxide by the synthesised MOFs was also measured. All of the samples were found to poorly adsorb CO_2, with a maximum uptake of 14 cm^3/g. While this low CO_2 adsorption could have been a result of there being no significant porosity in the sample, this would somewhat contradict the result from the N_2 adsorption experiments. It is therefore likely that the result was due to the large size of the OCPc ligand resulting in pores which were too large to efficiently adsorb CO_2 at the temperature of 273 K which was employed, as adsorption of CO_2 at this temperature is generally only seen in pores with a diameter of less than 0.6 nm.[126] This is also consistent with the observed lack of correlation between the apparent BET surface areas as measured by nitrogen adsorption and the quantity of carbon dioxide adsorbed, as illustrated in **Figure 3.7**.

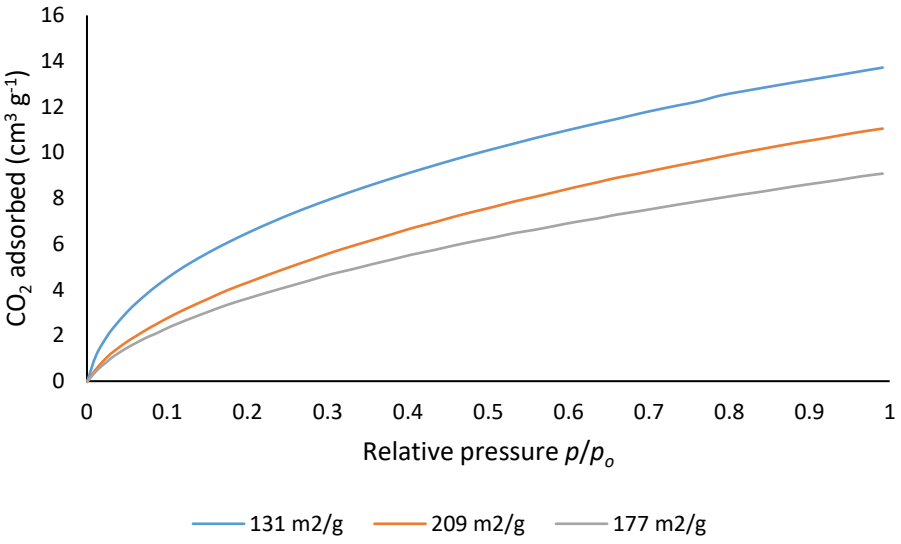

Figure 3.7: Comparison of CO_2 adsorption of samples of different BET surface areas.

3.3.2 Post-synthetic treatment

As stated, the general procedure for the collection of the products of MOF synthesis reactions involved the filtering of solid products using a sintered glass funnel. The recovered solids were then first washed with the solvent used in the reaction, which was the standard practice to remove as much of the remaining uncoordinated phthalocyanine ligand as possible.[127] The success of this was evidenced by the fact that the filtrate from such washings was frequently the intense blue colour of the ligand, suggesting that significant quantities of uncoordinated ligand had initially remained. In addition to the ligand, it was likely that metal salt and the additives, where used, would remain in the sample, as would the solvent, given the high boiling points of those used.[127] The presence of these substances within the pores of the desired materials would likely act to reduce their apparent porosity, which could account for the low BET surface areas measured.[128]

It was therefore desirable to determine the extent to which the materials produced could be treated post-synthetically in order to improve their porosity and hence potential utility. It was also important to examine the extent to which they could withstand exposure to various environments in order to understand their potential usability in future applications. The simplest treatment was to wash the samples with additional solvent following the reaction solvent. Acetone and methanol were generally used due to their low boiling points and miscibility with the polar, high boiling point solvents in question. Water could also be used, though its higher boiling point and polarity made it more difficult to remove. In general however, the additional solvent could be removed in turn either by simply drying

in air, or more thoroughly by heating, particularly with the use of a vacuum oven. In all cases, the samples appeared more visibly dry, and those that were initially found to be crystalline by powder XRD maintained their crystallinity following treatment. No significant improvement in surface area was observed following such treatment however, so harsher methodologies were employed. Instead of simply washing the samples with solvent, they were stirred at reflux for up to 48 hours. As with the cold washing, when refluxed in acetone the structure of the materials did not appear to be significantly degraded, as judged by the powder XRD, but no significant increase in surface areas was obtained.

Additional solvents were therefore employed, with a sample initially refluxed in methanol for a period of 24 hours, then with water. As with acetone, powder XRD analysis after refluxing in methanol suggested that the structure was still largely intact, though as shown in **Figure 3.8**, the pattern did appear to have altered slightly, and broad background peaks corresponding to an amorphous material could begin to be seen. After refluxing in water, complete degradation of the structure was observed as evidenced by the total absence of sharp peaks in the powder XRD spectrum. These results likely suggest that the metal ion-carboxyl linkages in the secondary building unit were vulnerable to attack by the more polar solvent molecules under higher temperature conditions. The large size of the Cu(II) OCPc ligand is likely to at least partly explain the decomposition observed, as previous studies have found that replacing the small 1,4-benzene dicarboxylate linker in UiO-66 with longer aromatic molecules increases its susceptibility to degradation by water and other highly polar solvents.[129]

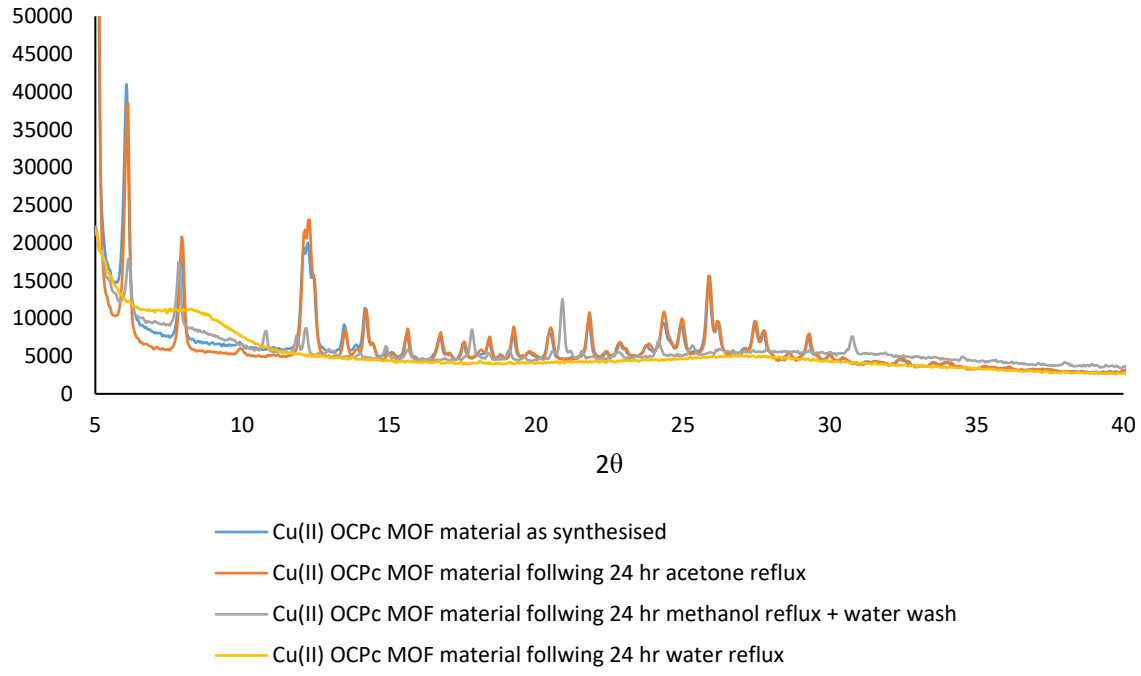

Figure 3.8: Comparison of powder XRD patterns of treated and untreated products showing degradation.

An alternative to the use of solvents to remove potential contaminants, heating at high temperatures, potentially under vacuum, was investigated. Although samples were generally heated in a vacuum oven at 100 °C prior to BET measurements, it was thought that this temperature may not be sufficient to remove less volatile compounds, such as the high boiling point solvents used in the synthesis. This would also be somewhat analogous to the calcination-type processes traditionally used to activate materials such as zeolites, and similar treatments had previously been shown to be effective in improving the porosity of certain MOFs.[130] To this end, thermogravimetric analysis (TGA) was used to examine the change in weight of the samples as they were heated up to approximately 800 °C. Particular losses of mass could then be identified as corresponding to the loss of particular compounds. In order to specifically investigate the relevance of this to the porosity of individual MOF-type products, samples with the highest and lowest apparent BET surface areas obtained, 209 and 12 m^2/g respectively, were compared by TGA, as summarised in **Figure 3.9**.

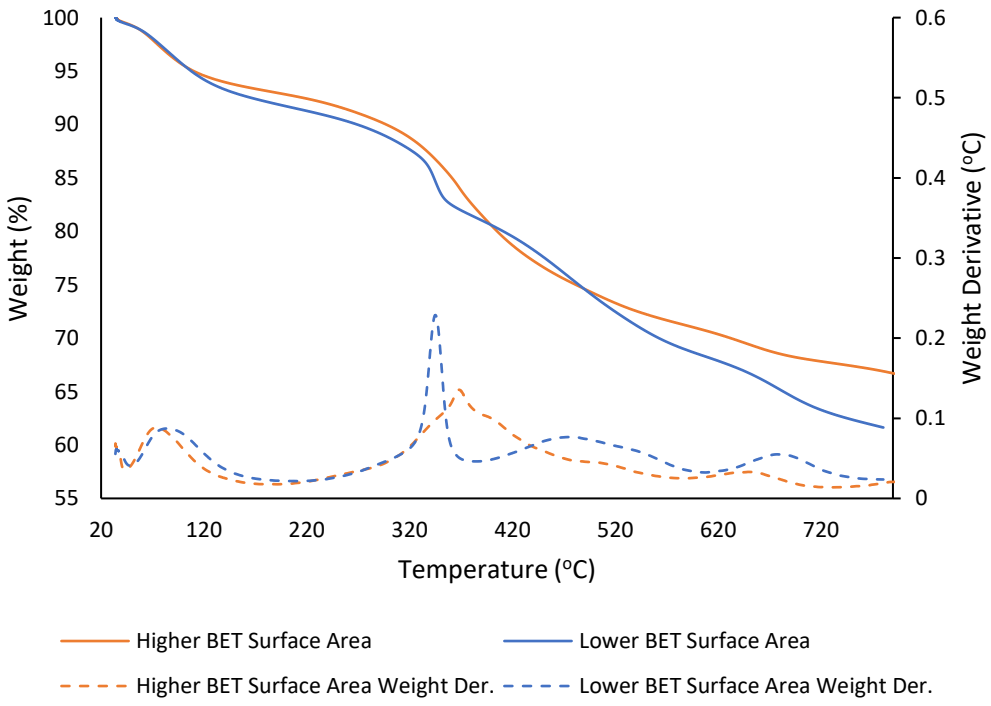

Figure 3.9: Comparison of TGA results for Cu(II) OCPc MOF samples with BET surface areas of 209 m^2/g and 12 m^2/g respectively.

Loss of mass of approximately 7% below 120 °C was observed with both samples, consistent with residual water being driven off. However no significant mass loss was seen that would indicate the presence of DEF in the sample, suggesting that washing with acetone and water had been sufficient to remove it. The large loss of mass around 350 °C, particularly abrupt in the low surface area sample,

is likely evidence of a contaminant remaining, as the phthalocyanine ligand is known to be stable beyond this temperature.[131] Additional loss of mass likely also occurred due to the decarboxylation of the octacarboxy ligand, although as these processes are reported to occur in a series of small steps at temperatures over 300 °C,[132] they are difficult to identify. Overall, the higher surface area sample showed a mass loss of 33% below 800 °C, compared to 39% for the lower surface area sample. This is therefore consistent with residual molecular contaminants within the pores of the material being at least partly responsible for the relatively low surface areas measured. It is also evidence of a reasonable degree of thermal stability of the materials produced.

3.4 Tetracarboxyphthalocyanine

As pendant uncoordinated carboxyl groups thought to be oriented within the pores were believed to play a significant role in determining the properties of the OCPc MOF-type material, it was thought that this could be further explored by contrast with a structure that lacked such groups. To this end, a tetracarboxypthalocyanine ligand was synthesised by adaptation of the previously developed synthetic route (**Scheme 3.4**), starting from commercially available 3,4-dibromotoluene. It was not possible to control the regioselectivity of the tetramerisation reaction, and as separation of phthalocyanine isomers is notoriously difficult and generally depends on the presence of solubilising functionalities absent from the molecule in question,[133] the product obtained was a mixture of isomers with the carboxyl groups in the two possible peripheral positions.

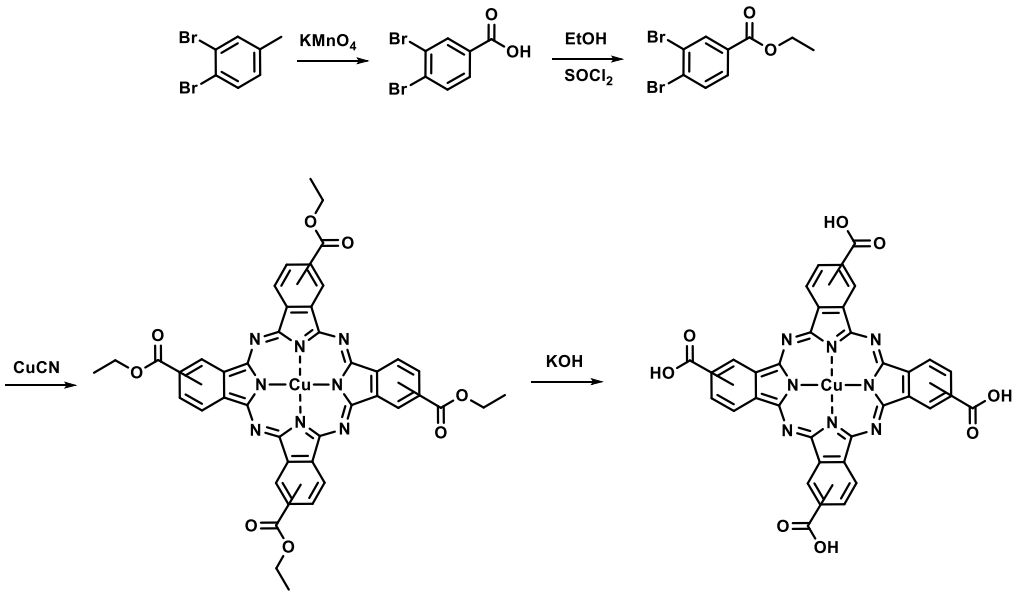

Scheme 3.4: The synthetic route to copper(II) tetracarboxyphthalocyanine.

The MOF synthesis conditions developed for OCPc were then used in an attempt to synthesise a MOF using the tetracarboxyphthalocyanine ligand. Powder XRD analysis however determined that the product formed was not consistent with the expected crystalline structure, instead appearing largely amorphous. It was also found to be non-porous, with an apparent BET surface area of only 19 m^2/g. The failure to form crystalline porous structures may be due to the inability to isolate isomers of the phthalocyanine, which would have led to a statistical majority of the ligand molecules in the reaction having reduced symmetry. Whilst a few reports exist describing the successful synthesis of porous MOFs with low symmetry ligands,[134] the vast majority of carboxylate MOFs with permanent porosity have been synthesised from highly symmetrical ligands, since this most easily allows the formation of repetitive units in the crystalline structure.[135]

3.5 Octacarboxypyrazinoporphyrazine

Whilst the synthesis of the OCPc ligands had been successfully accomplished, the numerous challenges encountered often resulted in yields that were low or inconsistent. The most frequently encountered problems were with the aromatic substitution reactions required to form the phthalonitrile, so methods were examined that could avoid this step entirely. Attention focussed on the potential to use pyrazinoporphyrazine (azaPc) as a backbone for the synthesis of porous materials, in place of phthalocyanine. As previously discussed, and highlighted in **Figure 3.10**, the two macrocycles are closely related, with four benzene rings in the phthalocyanine substituted for pyrazine rings. Whilst this has a significant impact on the electronic properties of the ring, the crucial planar rigidity is conserved, as is the highly accessible nature of the metal centre.

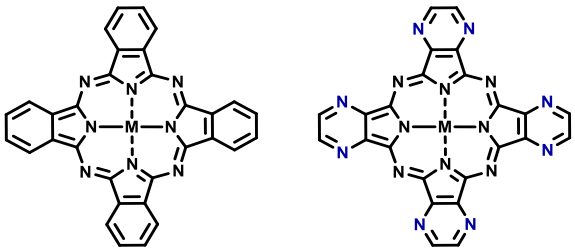

Figure 3.10: The structure of phthalocyanine ligand compared with that of pyrazinoporphyrazine.

The major advantage of using pyrazinoporphyrazine was that rather than requiring the substitution of aryl halide groups with nitriles via the relatively harsh and difficult to control conditions of the Rosenmund-Von Braun reaction, they could be synthesised with the nitrile groups already in place, via

a number of routes, for example the condensation reaction of an appropriate primary diamine and diketone.

A synthetic route to the pyrazinoporphyrazine analogue of OCPc was therefore identified starting from diethyl tartrate (**Scheme 3.5**). This was oxidised by adapting a procedure from literature using *N*-bromosuccinimide in to give diethyldioxosuccinate.[136] Likely as a result of the decision to use 1,2-dichloroethane as the solvent in place of carbon tetrachloride due to the environmental concerns associated with the latter, it proved extremely difficult to isolate the pure product at this stage, but it was eventually discovered that refluxing the impure product in ethanol with an excess of diaminomaleonitrile resulted in a mixture, from which the desired dicyanopyrazine could be isolated easily by column chromatography. Evaluation of various reaction conditions using easily obtained 1,2,5,6 tetracyanopyrazine as an analogue revealed that the best yield for the tetracyclomerisation reaction were obtained by following a literature procedure in which sulfolane was used as a solvent.[137] The octaethylester-substituted copper(II) pyrazinoporphyrazine was prepared in reasonable yield by application of the identified conditions. This was then hydrolysed to the octacarboxypyrazinoporphyrazine using potassium hydroxide, as had been done in the synthesis of OCPc.

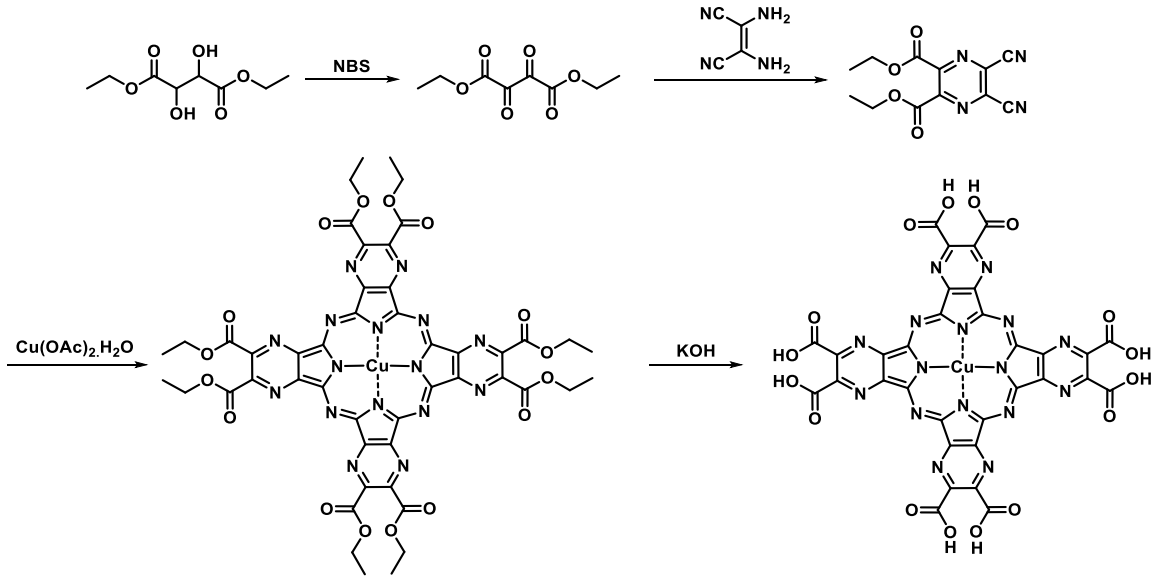

Scheme 3.5: The synthetic route to copper(II) octacarboxypyrazinoporphyrazine.

As with the OCPc, analysis and characterisation of the azaphthalocyanine was complicated by its poor solubility in common organic solvents. The particular lack of protons also prevented characterisation by ^{1}H NMR. UV-vis spectroscopy was possible due to the ability to dissolve small amounts of the azaPc in alkaline aqueous solution. As shown in **Figure 3.15**, the spectrum showed the same characteristic Q-band as the phthalocyanine, but with the peak shifted slightly to 640 nm. The peak was also seen

to have a higher baseline overall, suggesting both greater aggregation of the individual macrocycles and a higher degree of scattering from solid particles. These differences from the OCPc ligand can be explained due to the electronic differences resulting from the pyrazine rings and are consistent with previous studies of similar metallated azaphthalocyanines, which have shown maximum absorbance at lower wavelengths than corresponding phthalocyanines due to the difference in energy of the relevant molecular orbitals.[138]

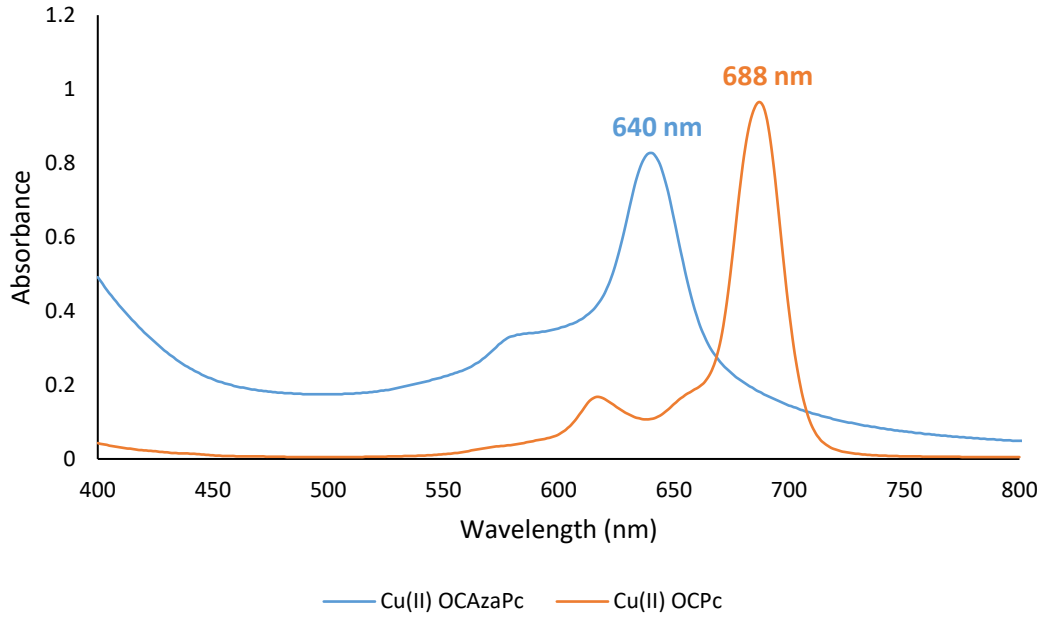

Figure 3.11: Comparison of the UV-vis spectra ofCu(II) OCazaPc and Cu(II) OCPc.

Despite the differences in the electronic structure as evidenced by the UV-vis spectra, due to the identical geometry and peripheral functionality of the synthesised copper(II) octacarboxypyrazinoporphyrazine and the corresponding phthalocyanine, it was thought that the MOF synthesis conditions optimised for the latter may still be applicable. On this basis, a MOF synthesis attempt was undertaken using the same concentration, reaction time and heating profile as previously, with a powder product being obtained (**Scheme 3.6**).

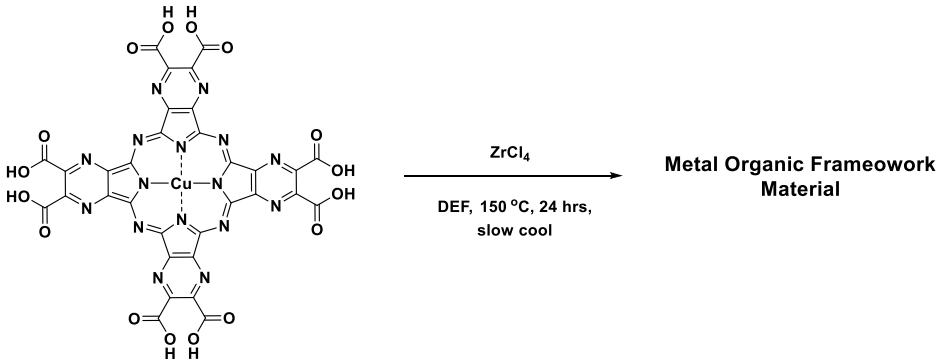

Scheme 3.6: The attempted synthesis of a Cu(II) OCazaPc MOF material.

However, upon analysis the MOF synthesis reaction was again found to be unsuccessful. The UV-vis spectrum (**Figure 3.16**), recorded as previously by finely suspending the solid in 1-chloronaphthalene, did show the typical Q-band peak, with a maximum absorbance at a lower wavelength of 671 nm reflecting the different electronic environment in the pyrazinoporphyrazine ring when compared to the phthalocyanine. However the baseline absorbance was significantly higher, which as with spectra from failed MOF synthesis attempts previously described, indicates a high degree of scattering likely attributable to aggregation of the ligands rather than formation of crystalline porous structures.[104] Although there is little discussion of pyrazinoporphyrazine materials in literature, aggregation has been highlighted as an issue in their application.[139]

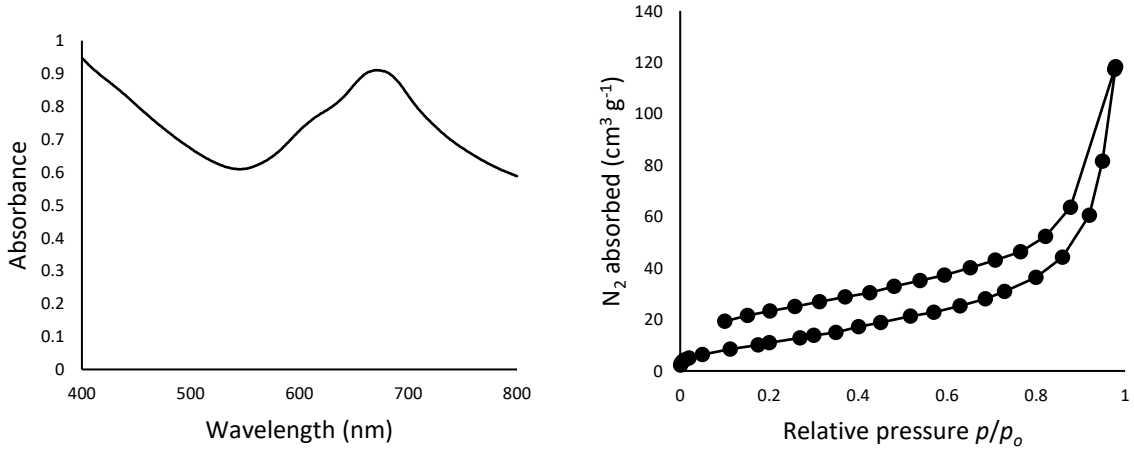

Figure 3.12: The UV-vis spectrum (left) and nitrogen adsorption isotherm (right) for the Cu(II) octacarboxypyrazinoporphyrazine MOF material.

This was also consistent with the measured BET surface area of only 38 m^2/g. The lack of any significant gas uptake as seen in the nitrogen adsorption isotherm in **Figure 3.12** further showed the lack of porosity within the material. As TGA analysis did not suggest a significant quantity of solvent or other volatile contaminants remained within the material, this finding is instead attributable to

failure to form any type of potentially porous network structure upon substitution of phthalocyanine for pyrazinoporphyrazine.

3.6 Conclusions

The octacarboxyphthalocyanine ligand was synthesised with the incorporation of a variety of metals. Procedures for its incorporation into metal organic frameworks were developed and crystalline materials with a modest degree of internal porosity were obtained based on the copper(II) phthalocyanine ligand. Repetition of the synthesis using phthalocyanines containing alternative metals were however unsuccessful. The synthesised crystalline materials were found to be reasonably robust, withstanding refluxing in a variety of solvents. Full elucidation of the structure of the material was hampered by the failure to obtain single crystals for diffraction.

Further attempts to synthesis analogous crystalline materials using the similar tetracarboxyphthalocyanine and octacarboxypyrazinoporphyrazine ligands were unsuccessful, likely ascribable to the considerable differences in geometry and solubility respectively.

4 Phthalocyanine Network Polymers

4.1 Background and Aims

As a result of the difficulties encountered in obtaining highly porous metal-organic frameworks containing the phthalocyanine moieties of interest, attention turned to other types of materials into which they could be incorporated using the precursors prepared as part of this study. As has been discussed, work previously published by the group had shown the effectiveness of amorphous phthalocyanine network polymers as porous materials.[44] Given the huge numbers of porous polyimides also reported in the literature,[140] one promising area of investigation was the incorporation of the newly developed tetraimidophthalocyanine functionality into such a structure.

Since it had not proven possible to obtain the tetraanhydridophthalocyanine, which would be necessary for a true polyimide reaction, the polymers were to be constructed using the tetracyclomerisation reaction as the polymerisation step (**Scheme 4.1**), as had been shown to be effective for the synthesis of Pc network polymers. This therefore required the synthesis of a series of bifunctionalised tetrabromo monomers, formed from the reaction of two equivalents of the previously synthesised 4,5-dibromophthalic anhydride with a suitable diamine.

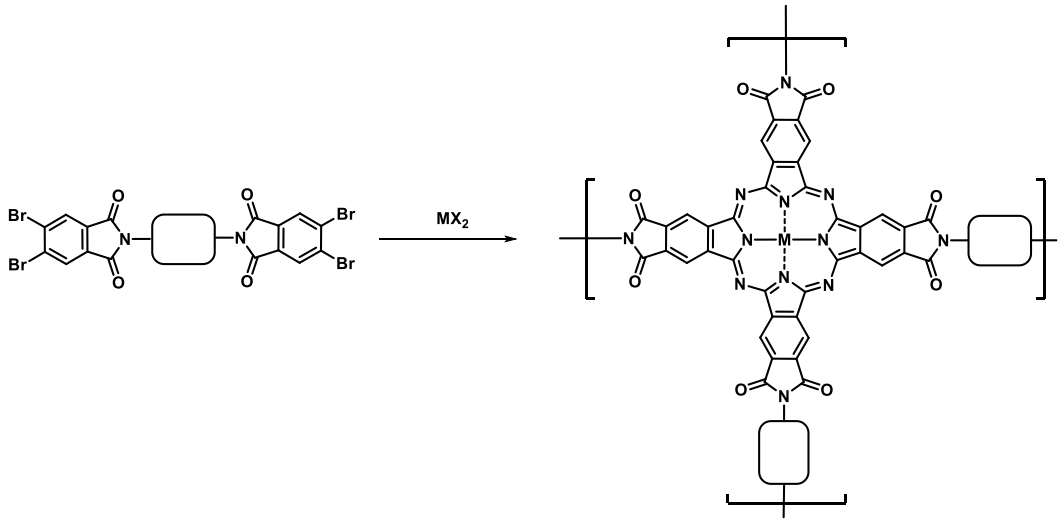

Scheme 4.1: The synthetic plan for a series of imidophthalocyanine network polymers.

4.2 Imidophthalocyanine polymers using commercial diamines

Initially *p*-phenylenediamine was chosen as the simplest possible diamine, but the product formed in the subsequent reaction was found to be insoluble in all organic solvents and therefore difficult to analyse, such that an NMR spectrum could not be obtained. Using instead 2,3,5,6 -tetramethyl-1,4-phenylenediamine, a more soluble product could be obtained. NMR and IR analysis however showed that refluxing in acetic acid, as had proved successful in all the monoimide syntheses, resulted in the formation of the amic-acid intermediate, even with extended reaction times, as shown in **Scheme 4.2**. Once isolated, it also proved impossible to effect the ring closure of this to the desired diphthalimide by heating in high boiling point solvents such as DMF. It was subsequently determined however, that simply carrying out the initial reaction in DMF gave the desired product in reasonable yield.

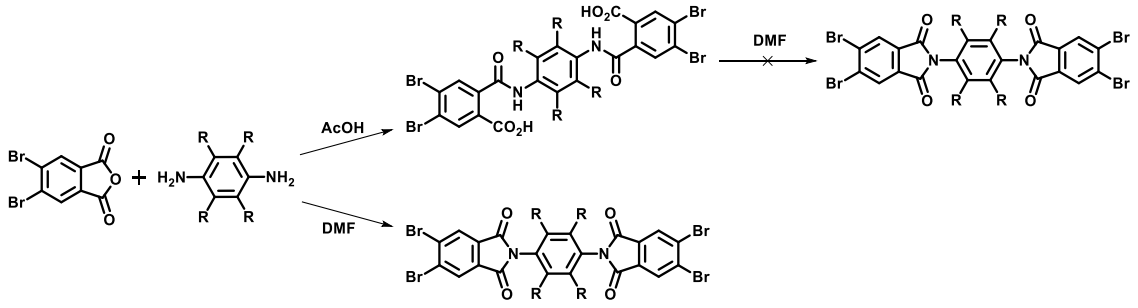

Scheme 4.2: The synthetic conditions explored for diphthalimides monomers using commercial diamines.

Using this methodology, a series of diphthalimides was prepared using a variety of available diamines, highlighted in **Figure 4.1**. Whilst some, such as 2,3,5,6 -tetramethyl-1,4-phenylenediamine would be expected to form planar phthalocyanine sheets, others were chosen in the hope that their structure would force the formation of more contorted structures that would likely be more microporous. In all cases, the network polymers were synthesised from the corresponding diphthalimide by reacting with a slightly superstoichiometric quantity of copper(I) cyanide in DMF. Although the unsubstituted *p*-phenylenediamine-based bis-imide was poorly soluble in the solvent, it was found to undergo polymerisation nonetheless, presumably due to the reaction of the small quantity that was able to dissolve in the solution. As with the discrete phthalocyanines, the network polymers were isolated upon completion by washing with aqueous ammonia solution to remove unreacted copper cyanide, and then with hot DMF in an attempt to remove unreacted diphthalimide.

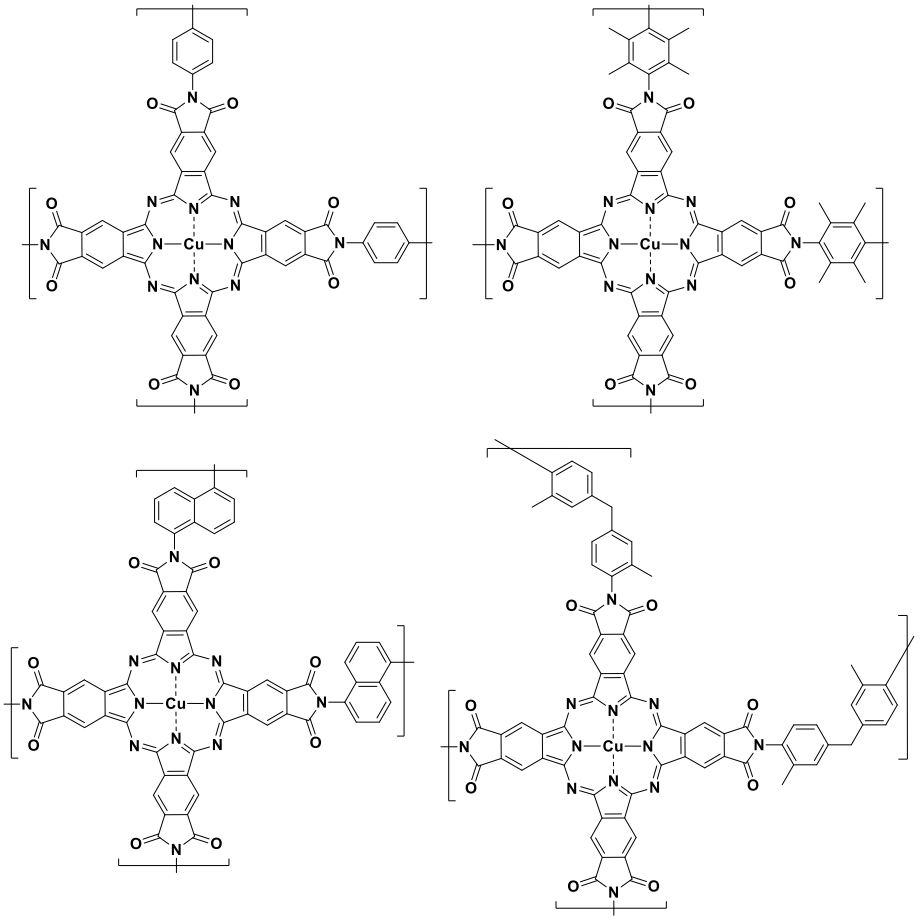

Figure 4.1: The structures of the initial non-porous tetraimidophthalocyanine network polymers.

A series of four tetraimidophthalocyanine network polymers were thus obtained. Analysis was limited by their intrinsic insolubility, but IR analysis was carried out, and by suspending the polymers in a suitable solvent UV-Vis spectroscopy was also employed. Both gave spectra consistent with the presence of the phthalocyanine and imide functionalities. Powder XRD analysis showed that, as expected, the samples were amorphous. BET surface area analysis gave apparent surface areas of all the polymers of less than 20 m^2/g. This is likely to be due to the fact that the structure of the diamine linkages used did not prevent rotation, nor introduce enough contortion to prevent the aggregation of phthalocyanine polymer sheets stopping the formation of accessible pores. This is consistent with previous reports of phthalocyanine polymers, as with the exception of materials containing ladder-like linkages specifically designed for porosity, very low surface areas have been recorded.[44] It was also thought possible that unreacted monomer, or partially reacted dimeric or trimeric by-products could have remained trapped within the structure following its synthesis, rather than being removed upon washing with solvent. These would then block any pores that did exist, reducing the apparent porosity of the material. Whilst literature reports do generally assume the removal of unreacted or partially reacted monomer by vigorous Soxhlet extraction with polar solvents,[141] it is likely that the

less soluble nature of the monomers employed could explain the failure of that methodology in this case.

4.3 Imidophthalocyanine polymers using bespoke diamines

It was clear from initial results that the commercial diamines, whilst easily available, were not suitable for the production of porous polymers using this methodology. They did not introduce enough steric hindrance or contortion to prevent the stacking of adjacent phthalocyanine macrocycles, and this also meant that unreacted diphthalimide monomer was insufficiently soluble to be removed from the synthesised polymer. It was therefore clearly necessary to design specific diamines that could avoid these problems and hopefully form polymers with the desired porosity and accessible phthalocyanine metal centres.

To this end, two specific diamines were proposed that would meet the criteria, shown in **Figure 4.2**. In both, two substituted aniline rings were bonded via a single atom to a bulky substituent. In one case, this was the rigid, tricyclic adamantane group, and in the other the planar, polycyclic fluorene. The aniline rings themselves were also substituted at the 2 and 6 positions in order to hinder rotation around the single bond with the phthalimide ring upon formation by steric clash with its oxygen atoms.

Figure 4.2: The structures of the two specifically designed diamines designed to prevent phthalocyanine stacking.

The fluorene-based diamine was synthesised via an adapted literature procedure reacting 2,6-dimethylaniline with 9-fluorenone in the presence of hydrochloric and triflic acid.[142] While the literature procedure called for the reaction to be carried out under pressure, the highly acidic conditions were incompatible with the pressure vessels available, and so it was performed at atmospheric pressure. This may account for the reduced yield compared to that reported in literature. Synthesis of the adamantane diamine was also based initially on literature precedent, though in this case a reaction to form the similar diamine with only a single *ortho*-methyl substitution, which described simply heating the aniline, its hydrochloride salt and 2-adamantanone.[143] Following this procedure with 2,6-dimethylaniline however resulted in complex mixture, from which the desired

product could not be isolated. Using the conditions successfully employed in the synthesis of the fluorene-based diamine similarly failed to give the desired product. However, following an adapted procedure from unpublished work within the group did eventually allow the adamantane diamine to be obtained, albeit with relatively low yield.

By reacting the synthesised diamines with 4,5-dibromophthalic anhydride, the corresponding diphthalimides were obtained. Interestingly and in direct contrast to the commercial diamines, using DMF as a solvent was not successful, with only the starting diamine and an unidentified impurity being recovered. However, refluxing in acetic acid, as previously employed for monoimide synthesis, did allow the products to be obtained cleanly in good yields, with no purification required. This is likely due to the considerable differences in solubility between diphthalimides derived from the commercial and bespoke amines. The former could only be dissolved, with heating, in solvents such as DMF and DMSO, whereas the latter readily dissolved in a variety of common organic solvents. As previously, the polymerisation step was then carried out using copper(I) cyanide in DMF to afford the polymers in **Figure 4.3**. Following precipitation of the solution into aqueous ammonia, green solids were obtained. Due to the high solubility of the monomers, refluxing in acetone was sufficient to purify the polymers.

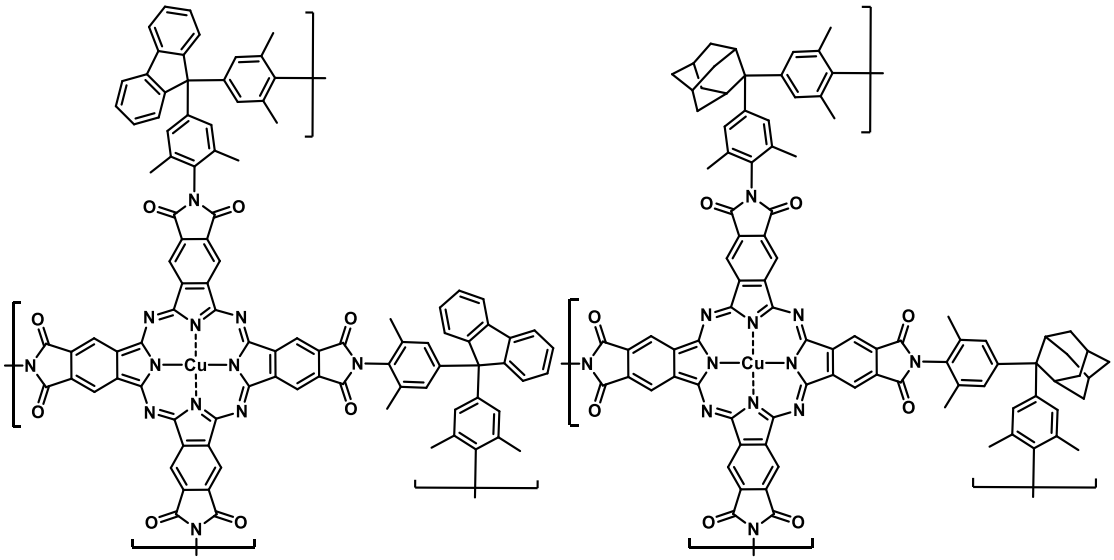

Figure 4.3: The structures of the fluorene (left) and adamantane (right) based tetraimidophthalocyanine network polymers.

The BET surface areas of the resultant network polymers were then measured (**Figure 4.4**). Both were found to be somewhat microporous, with the adamantane-based polymer having an apparent BET surface area of 236 m^2/g and the fluorene-based polymer a surface area of 183 m^2/g. The difference may be explained by the less planar adamantane group more effectively disrupting the π-π stacking

of the extended ring systems. The fact that the values were still relatively low however suggests that neither polymer was able to fully overcome this issue. Although methyl groups are generally reported to prevent rotation around the C-N single bonds in polyimides,[144] it is possible that incomplete inhibition of this rotation could have further contributed to lowering the internal free volume of the structure. A significant degree of hysteresis can also be observed in the isotherms of both polymers. As the effect extends to low relative pressures, it is consistent with swelling of the polymer structures following gas uptake.[145] Whilst the phthalocyanine molecule might be expected to impart enough rigidity to the polymer structure to prevent this swelling, it has previously been suggested in the literature that flexibility of the linking group allows swelling.[146]

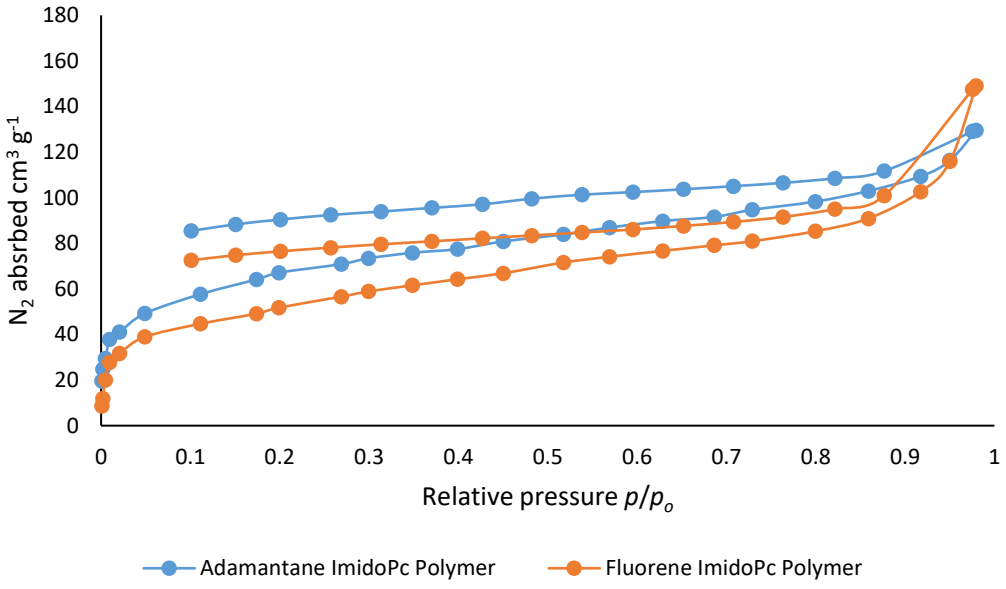

Figure 4.4: Comparison of the N_2 adsorption isotherms for the two polymers using bespoke diamines.

The CO_2 adsorption capability of both polymers was also measured, with the maximum adsorption at 1 atmosphere found to be 26 cm^3/g and 32 cm^3/g for the fluorene and adamantane-based polymers, respectively. These values were still relatively low, which as previously discussed was likely to be at least partly explained by the large size of the phthalocyanine functionality resulting in pores that were too large to effectively adsorb CO_2. This was however more than twice the CO_2 uptake previously recorded for the Pc MOF-type materials with similar apparent BET surface areas. This may be due to the fact that more polar, nitrogen-containing functionalities have been found to have a high affinity for CO_2.[147] Both the imide group, and the nitrogen atoms in the phthalocyanine ring could potentially form favourable interaction with carbon dioxide molecules. Indeed, a report in the literature describes a porous phthalocyanine as having a particularly high CO_2 adsorption capacity, although in that case

primary amine groups were included in the structure to maximise the favourable R-N(δ^-) - C(δ^+)=O_2 interactions.[148]

In order to determine whether the porosity was being inhibited by potential contaminants trapped within the pores, and also to gauge their potential utility in different applications, the thermal stability of the polymers was examined by thermogravimetric analysis, shown in **Figure 4.5**. As with previous materials, a mass loss of approximately 5% was observed below 120 °C, corresponding to the loss of volatile solvent contaminants such as water. No loss was seen at slightly higher temperatures however, which suggests that DMF solvent from the polymerisation reactions was effectively removed by the washing regime. The total mass loss up to 800 °C was 43% for the fluorene-based polymer and 49% for the adamantane-based polymer. The latter showed a particularly rapid loss of mass at around 530 °C, which is consistent with the thermal decomposition of the adamantane functionality as reported in the literature.[149] Despite the reported decomposition of fluorene-based polymers at approximately the same temperature,[150] no such rapid degradation was observed in this case, suggesting that interactions with the similarly planar phthalocyanine may have had an effect on the stability of the polymer.

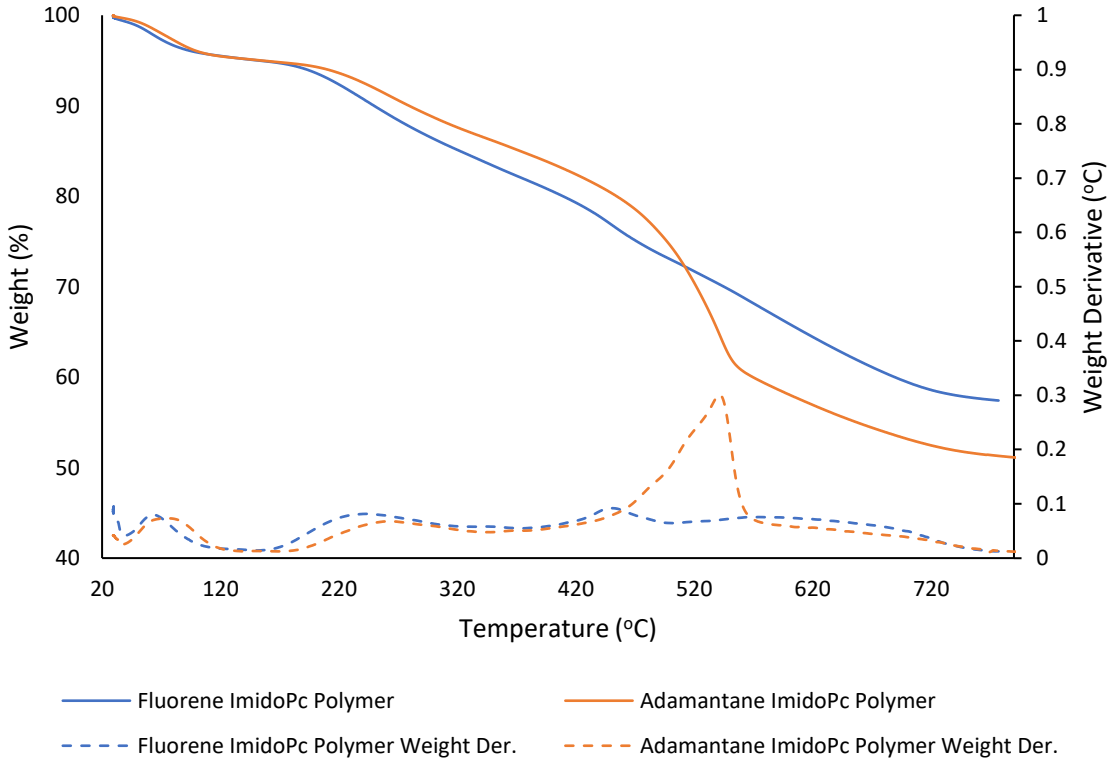

Figure 4.5: Comparison of the TGA for the two polymers using bespoke diamines.

4.4 Pyrazinoporphyrazine polymers

As the pyrazinoporphyrazine functionality had been successfully synthesised and its incorporation into metal-organic frameworks in the place of phthalocyanine examined, it also appeared a promising structural unit for making network polymers analogous to the phthalocyanine-based examples described. Specifically, *bis*-functionalised phthalonitrile pyrazines could be used as monomers in polymerisation reactions in which the formation of the pyrazinoporphyrazine macrocycle would itself be the polymerisation step (**Figure 4.6**).

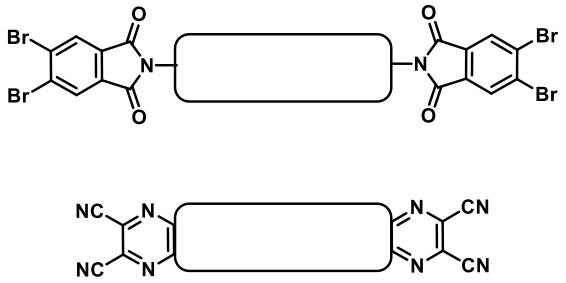

Figure 4.6: Comparison of the *bis*-functionalised monomers used in the synthesis of the tetraimidophthalocyanine (top) and pyrazinoporphyrazine (bottom) network polymers.

As with the discrete octacarboxy-functionalised pyrazinoporphyrazine, the significant advantage of this method was the very different synthetic route. This had the potential to allow the incorporation of a wide variety of different substituents into the polymer, as well as avoiding the unreliable and potentially hazardous aryl halide substitution step.

4.4.1 Bifunctional phthalonitrile pyrazine monomer synthesis

Obtaining polymers with a reasonable degree of internal surface area had been shown to require a means of avoiding extensive π-π stacking reactions, so it was again necessary to build in functionalities that prevented this. The pyrazine formation required *bis*-diketones, which opened the possibility of adapting previous work within the group in order to include sites of contortion such as spiro centres and triptycene-like structures. As with the adamantane and fluorene functionalities incorporated into the phthalocyanine network polymers, these were thought likely to force the formation of non-planar molecules in which the macrocycles could not stack efficiently.

4.4.1.1 1,4-Bisbenzil as precursor for network polymers

The first such possibility examined was the use of a system containing five aromatic rings, in which it was hoped that the avoidance of sterically unfavourable interactions between such bulky substituents would prevent the undesirable stacking of macrocycles. This approach mirrored that of what appeared to be the only published example of a true pyrazinoporphyrazine polymer, in which *tert*-butyl groups had been appended to the structure.[48] This monomer was also chosen due to its extremely simple synthetic route, since, as shown in **Scheme 4.3**, it could be produced in a single step by the reaction of commercially available 1,4-Bisbenzil with diaminomaleonitrile.

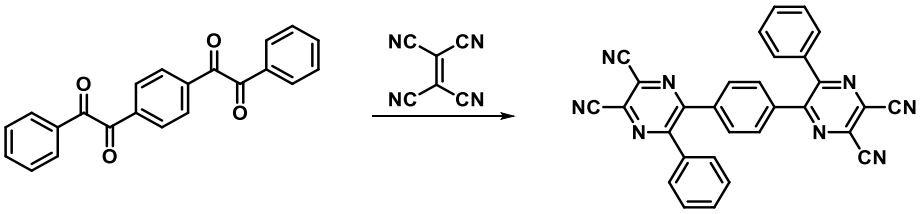

Scheme 4.3: The synthesis of the 1,4-bizbenzil-based monomer.

The reaction was found to proceed cleanly upon reflux in acetic acid, and the bifunctional monomer was obtained easily in near quantitative yield without the need for purification.

4.4.1.2 Monomers from synthesised *bis*-diketones

While the phenyl groups in the 1,4-bisbenzil monomer were thought likely to restrict rotation to only a limited extent, other functionalities which exploited this more, or had other means of achieving a large internal free volume, were desirable. Based upon experience within the group, spirobisindane, anthracene and ethanoanthracene were identified as likely to be effective. Unlike bisbenzil however, the *bis*-diketones containing these functionalities were not available commercially, so syntheses were devised, as shown in **Scheme 4.4**.

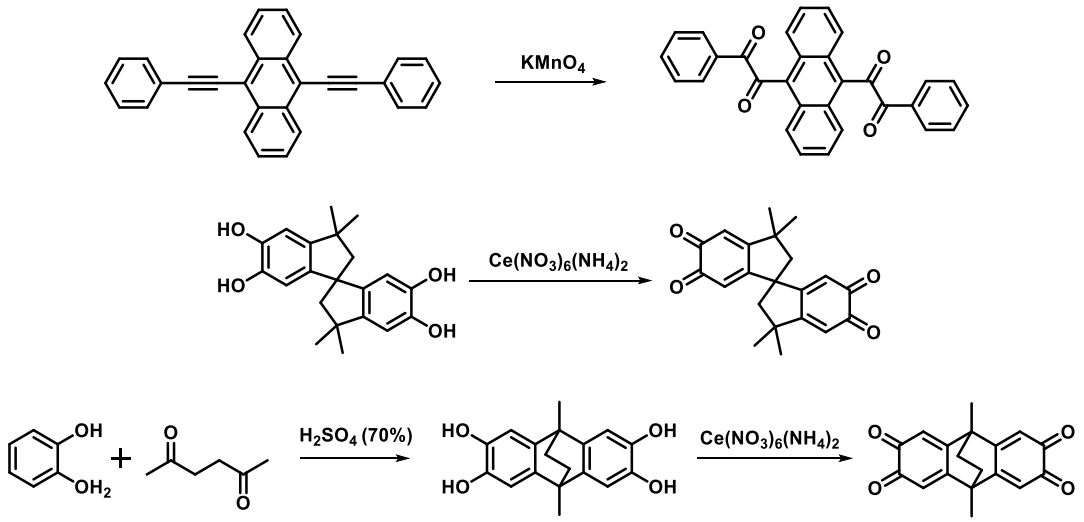

Scheme 4.4: The synthetic routes to additional *bis*-diketones.

It was thought that an anthracene derivative, 9,10-(1-phenylethane-1,2-dione) anthracene, could be synthesised relatively simply from the *bis*-phenylethynyl equivalent, by oxidation with a slight excess of potassium permanganate. This proved to be the case, with the reaction taking place with reasonable yield. A highly contorted *bis*-diketone containing the spiro centre functionality was also synthesised. This was made simpler due to the commercially availability of 5,5',6,6'-tetrahydroxy-3,3,3',3'-tetramethyl-1,1'-spirobisindane (TTSBI) as a starting material. In order to oxidise this to the *bis*-quinone, a mixture of nitric acid and acetic acid was initially used as the oxidant, however this was found to form a complex mixture from which the product could not be isolated. It was found however that using cerium ammonium nitrate as the oxidant, the product could be obtained in good yield and purity without the need for any purification steps. The final synthesised *bis*-diketone was based on the ethanoanthracene functionality. As well as preventing stacking, the triptycene-like structure also had the advantage of an intrinsic intramolecular free volume, which could increase the porosity of a resulting network polymer, as had also been demonstrated with a previous phthalocyanine polymer reported by the group.[145] Tetrahydroxyethanoanthracene was first formed in good yield via the acid mediated reaction between 1,2-catechol and 2,5-hexanedione.[151] This was then oxidised to form the *bis*-quinone using the same cerium ammonium nitrate-based oxidation procedure previously employed with TTSBI, with the quinone again obtained in good yield.

The synthesised *bis*-diketones were then reacted with diaminomaleonitrile to form the *bis*-phthalonitrile pyrazine monomers. In all cases however, this reaction did not proceed as expected. Refluxing in acetic acid, as had been done with the 1,4-bisbenzil monomer, resulted in only the recovery of starting material in the case of 9,10-(1-phenylethane-1,2-dione) anthracene, and a crude

mixture that did not appear to contain the desired product in the case of the ethanoanthracene and spirobisindane molecules, suggesting that these *bis*-quinones were susceptible to degradation. Repeating the reactions with a large range of solvents, temperatures, reaction times, concentrations and with the addition of various potential catalysts resulted in the same outcome, and so it did not prove possible to obtain the necessary *bis*-phthalonitrile pyrazine monomers.

4.4.2 Pyrazinoporphyrazine polymer synthesis

With copper having been the metal most commonly incorporated into previously synthesised phthalocyanine polymers, it was identified as the metal to initially be incorporated into the pyrazinoporphyrazine network polymer. Following the procedure that had been used for the molecular pyrazinoporphyrazine, the successfully synthesised 1,4-bisbenzil phthalonitrile pyrazine monomer was refluxed in sulfolane for 2 hours, resulting in the formation of a dark-green/black solid precipitate (**Scheme 4.5**). This was washed with water and acetone, before being refluxed in acetone for 24 hours in order to remove unreacted monomer. A yield of 74% was obtained. Alternative conditions employing *N*-methyl-2-pyrrolidone and DMF as solvents were also investigated, but were found to result in reduced yields.

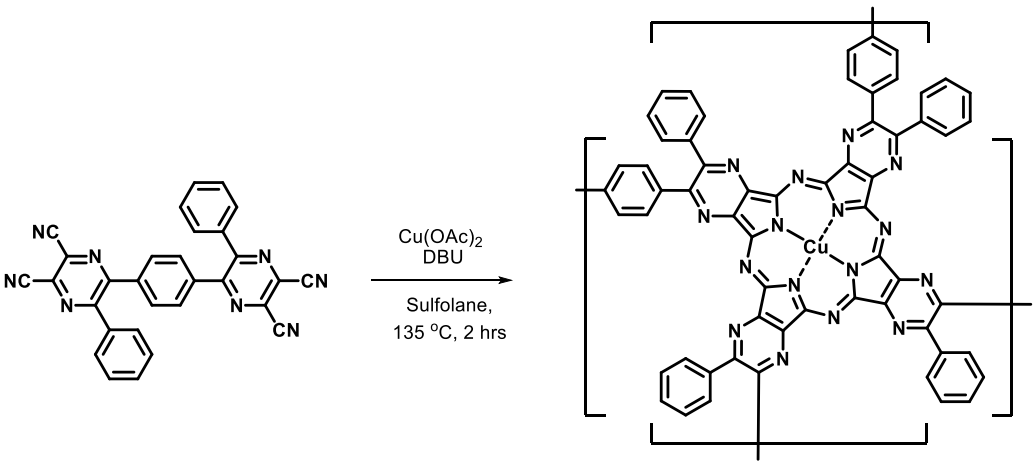

Scheme 4.5: The polymerisation reaction of the 1,4-bisbenzil based pyrazine monomer using copper(II) acetate.

Following successful synthesis of the copper(II) pyrazinoporphyrazine polymer, alternative metal salts were used. Cobalt (II) and zinc(II) versions were synthesised via the same procedure using the corresponding acetate salts, with slightly reduced yields of 69% and 65% respectively obtained. Once again, analysis was hampered by the insoluble network nature of the polymers, but as previously, they were dispersed in 1-chloronaphthalene in order to record UV-vis spectra, shown in **Figure 4.7**. The

copper(II) polymer was found to have a very similar absorbance to the previously synthesised copper(II) phthalocyanine materials, which tallies with the energy of the electronic transitions within the macrocycle resulting in absorbance at similar wavelengths in pyrazinoporphyrazines and phthalocyanines.[152] The form of the spectra was also consistent across the different metal centres, with the Q-band peak and associated shoulder visible in all cases, despite considerable scattering. The maximum absorbance of the copper(II) polymer was at 689 nm, with that of the cobalt(II) polymer occurring at a slightly lower 687nm and the zinc(II) polymer at 684 nm. Although the large degree of scattering present in the spectrum of the latter two made it difficult to draw definitive conclusions, the slightly blue-shifted value of the maximum absorbance wavelength when moving from copper to cobalt to zinc is consistent with a previously reported study of metallated molecular pyrazinoporphyrazines.[153]

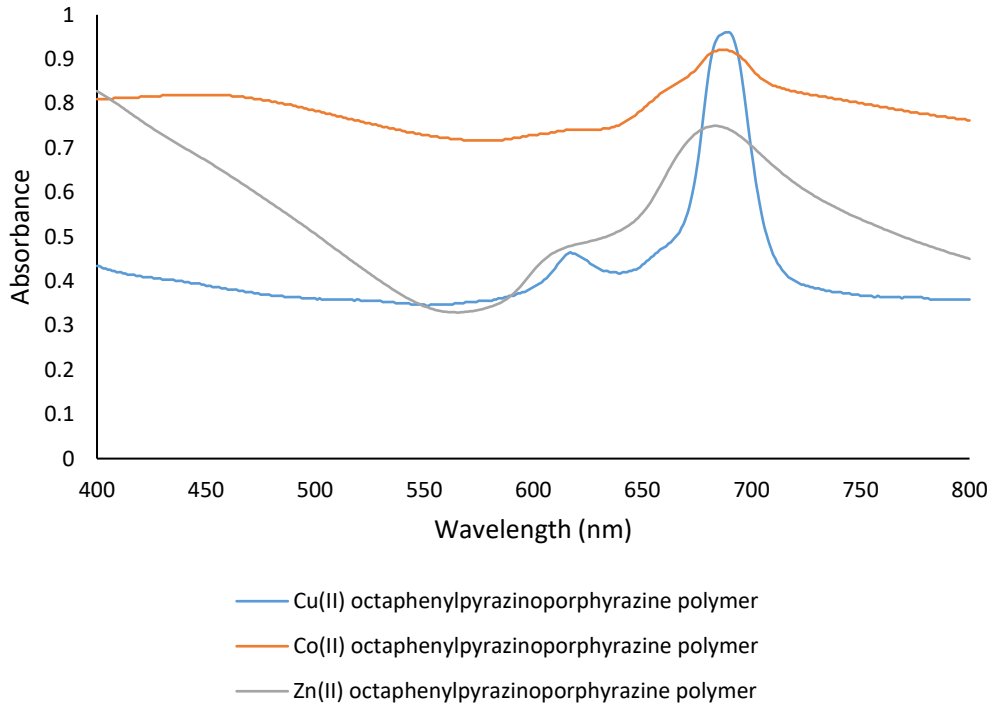

Figure 4.7: The UV-vis spectra of the synthesised metallated pyrazinoporphyrazine polymers.

Measurement of the apparent BET surface areas showed that all of the polymers had a low degree of internal porosity, with values of 69 m^2, 4 m^2 and 55 m^2 for the Co(II), Cu(II) and Zn(II) polymers respectively. Even within the low range of values recorded, the slightly larger degree of porosity measured with the Co(II), and to a lesser extent Zn(II) polymers does suggest that the metal ion used in the formation of the pyrazinoporphyrazine ring has an influence on the nature of the resultant polymer. Interestingly, and in contrast to what had been observed with other synthesised materials,

there was no correlation between the degree of scattering in the solid-state UV-vis spectrum and a higher apparent surface area within this series of network polymers.

4.5 Conclusions

A variety of novel network polymers featuring the tetraimidophthalocyanine functionality were developed and characterised. An initial series involving commercial diamines was produced, but the materials were found to be entirely non-porous, likely as a result of their relatively planar structure failing to inhibit aggregation. An additional pair of polymers designed to overcome this limitation by incorporating bulky functionalities were found to possess a degree of porosity.

The synthesis of pyrazinoporphyrazine-based network polymers was also examined. An initial structure containing multiple aryl rings was successfully produced, but the surface area of the material was limited. Attempts to expand this area of investigation with the incorporation of contorted functionalities did not prove possible synthetically.

5 Phthalocyanine Molecular Crystals

5.1 Background and Aims

As previously outlined, in recent years, work on phthalocyanines within our research group has largely concentrated on molecular crystals formed from a highly substituted 2,3,9,10,16,17,23,24-octa(2',6'-diisopropylphenoxy)phthalocyanine ((dipPhO)$_8$PcM). Due to the steric clash resulting from the isopropyl groups, aggregation is avoided, and highly porous molecular crystals of cubic symmetry can be formed.[82] The crystal structure has been shown to accept guests such as 4,4-bipyridine and fullerenes,[83] which are both able to act as "wall-ties" to stabilise the crystal towards solvent removal(**Figure 5.1**).

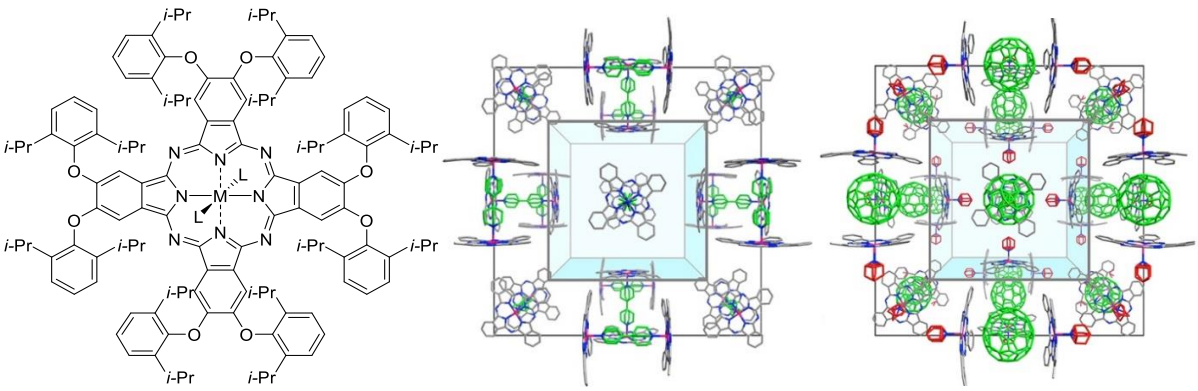

Figure 5.1: The structure of the sterically hindered phthalocyanine ((dipPhO)$_8$PcM)., and the molecular crystal formed using 4,4-bipyridyl and C_{60} "wall-ties", which stabilise the crystal towards solvent removal. Adapted from refs. 82-83.

More recently, metal-free tetraphenylporphyrin (TPP) has also been shown to be successfully incorporated into the nanoporous cubic crystal structure by co-crystallisation. Furthermore, it has been shown that a variety of metal ions can be incorporated into the Pc, including Al^{3+}, Ti^{4+}, Mn^{3+}, Fe^{3+}, Co^{2+}, Ni^{2+}, Cu^{2+}, Zn^{2+}, Ga^{3+}, Ag^{2+}, In^{3+} and Au^3, without disrupting the formation of nanoporous cubic crystals. As shown in **Figure 5.2**, this co-crystallisation involves close interaction between the (dipPhO)$_8$PcM and TPP ligands.

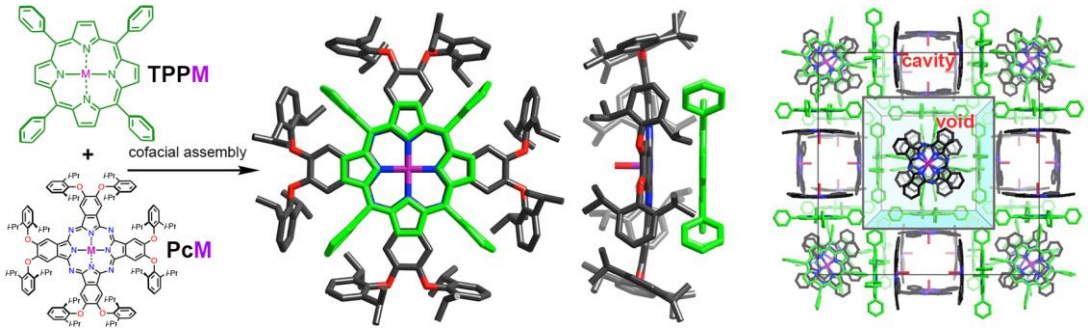

Figure 5.2: The structure of the molecular crystal formed from $(dipPhO)_8PcM$ and TPP.

Therefore, it was of interest to investigate the effect of the introduction of different substituents and metals on the ability of the porphyrin macrocycle to form Pc-TPP dimers and nanoporous crystals. The variation in in structure of the TPP was predicted to result in different interactions between the $(dipPhO)_8PcM$ and TPP upon co-crystallisation and also in solution. Investigation of this area was also made attractive by the simple synthetic route to the substituted derivatives of TPP and its metal complexes. Pc-TPP dimer interactions could then be studied by a combination of the formation of single crystals analogous to those previously obtained, and by UV-vis spectroscopy , which was known to be effective in related systems.[154]

5.2 Synthesis of 2,3,9,10,16,17,23,24-octa(2',6'-diisopropylphenoxy)phthalocyanine

Using a route previously employed within the group,[82] shown in **Scheme 5.1**, the substituted phthalocyanine could be prepared using a four-step reaction starting from commercially available 4,5-dichlorophthalic anhydride. By first refluxing with formamide, the cyclic imide could be obtained. The cyclic imide was then transformed to the diamide using aqueous ammonia, and then in turn to the phthalonitrile by dehydrating with thionyl chloride. This was reacted with 2,6-diisopropylphenol via an aromatic nucleophilic substitution reaction. For the latter reaction, good yields were generally obtained, albeit with reaction times of several days, and the formation of small quantities of the phthalocyanine was also generally observed, though the pure phthalonitrile could be easily obtained by recrystallisation.

From the phthalonitrile, metal free $(dipPhO)_8Pc$ was synthesised by refluxing in *n*-pentanol with a small quantity of lithium metal. Upon completion, acetic acid was added. This displaced the weakly coordinated lithium ion that had templated the formation of the phthalocyanine, resulting in the

metal free variant. Generally, purification required reprecipitation by methanol of the phthalocyanine dissolved in chloroform.

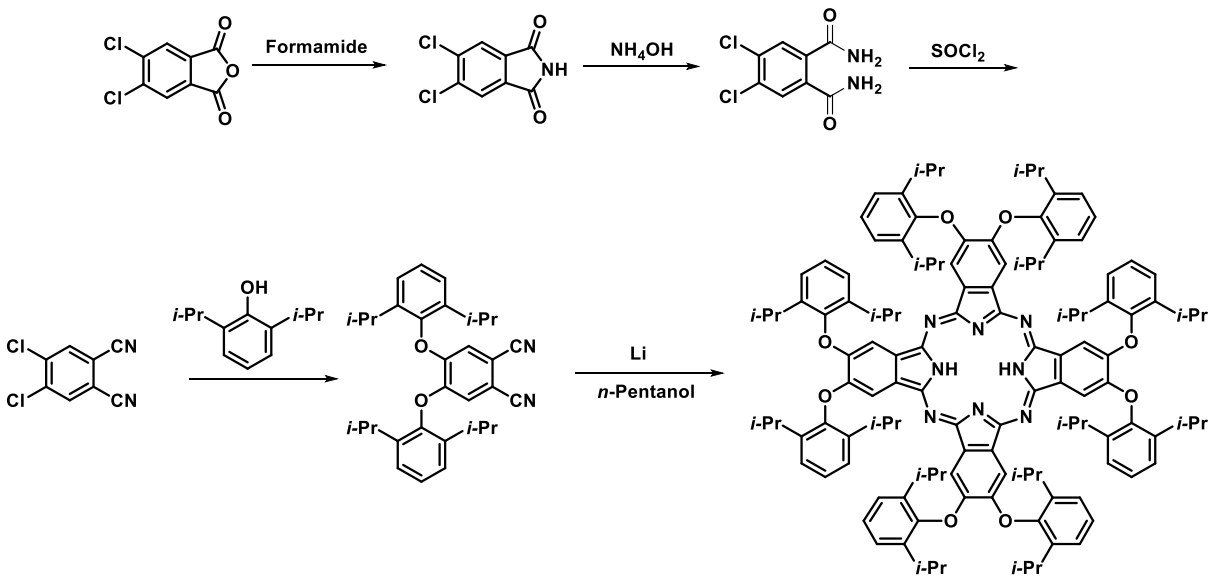

Scheme 5.1: The synthetic route to metal-free $(dipPhO)_8Pc$.

Metallated versions of the $(dipPhO)_8Pc$ were also produced. Previous work within the group had developed syntheses for the incorporation of the vast majority of d and f-block metals into the phthalocyanine. It was decided to focus on a few common transition metals initially, as the synthetic procedures for these were generally simpler and had proved most reliable. Zinc(II) and cobalt(II) phthalocyanines ($(dipPhO)_8PcZn$ and $(dipPhO)_8PcCo$) were both synthesised from the phthalonitrile, by heating with an equimolar quantity of the corresponding metal(II) acetate salt. Upon completion, the solutions were precipitated into water to afford the solid. As with the metal-free phthalocyanine, purification was carried out by reprecipitating a solution of the phthalocyanine dissolved in chloroform into methanol. This generally had to be repeated several times to afford the pure product. The copper(II) phthalocyanine ($(dipPhO)_8PcCu$) was synthesised using a different methodology in which the metal-free phthalocyanine was heated in solution with copper(II) acetate. Again, purification by reprecipitation was required. In all three cases, acceptable yields of 30 - 50% were obtained.

5.3 Metallated phthalocyanine/tetraphenylporphyrin interactions

5.3.1 Spectroscopic studies of solution-state metallated phthalocyanine/porphyrin interactions

The $(dipPhO)_8PcCu$ complex was chosen as a model system for examination of the reactions due to its sharper peaks in UV-vis spectroscopy which had proved to be an effective method for evaluating the interactions between $(dipPhO)_8PcM$ and TPP in previous studies. After recording the spectra of the pure Pc and TPP, it was known from literature precedent that the appearance of an additional peak at a higher wavelength of around 730 nm in the spectra of the mixed solution of the two could be used to evaluate the Pc-TPP interactions and to gauge the degree of aggregation.[155] The single Q-band peak present in metal Pc would simplify visualisation of this adjacent aggregation peak. Copper in particular was believed likely to have an additional benefit, as the lack of axial ligands coordinating to the Cu^{2+} ion as a result of its square planar geometry may enhance aggregation.

An appropriate concentration of the ligands had to first be determined in order to maximise the intensity of the appropriate peaks without exceeding the limits of absorbance that could be recorded by the spectrometer. To this end, the cuvette path length was reduced from the standard 10 mm to 1 mm, so that for a given absorbance, the concentration could be increased by a factor of 10. This way, the optimal concentration of the two ligands was determined to be 25 µM. The concentration of the $(dipPhO)_8PcCu$ therefore maintained at this level, while the quantity of the TPP was changed in order to measure the effect of its concentration on the aggregation with the phthalocyanine, as shown in **Figure 5.3**. The additional peak corresponding to Pc/TPP aggregation could be seen adjacent to the main phthalocyanine Q-band peak, with a maximum absorbance at 732 nm. Whilst earlier initial results had suggested that a 1:3 dichloromethane: methanol solvent mixture maximised aggregation, it was found that the $(dipPhO)_8PcCu$ was not fully soluble in this solvent mixture. As a result, a 1:1 dichloromethane: methanol solution was used instead. From this study, with the assumption that the dimer was the only aggregate formed, it could be estimated that the association constant (K_a) for the CuPc-TPP dimer is in the range 1.4-1.8 x 10^5 M^{-1} for this solvent mixture. A good correlation was found between the molar ratio of CuPc/TPP versus the ration of the $(dipPhO)_8PcCu$ Q-band at 680 nm and the dimer peak at 732 nm. Hence, this peak ratio was subsequently used to evaluate the *relative* ability of TPP metal complexes and substituted TPPs to aggregate with $(dipPhO)_8PcM$.

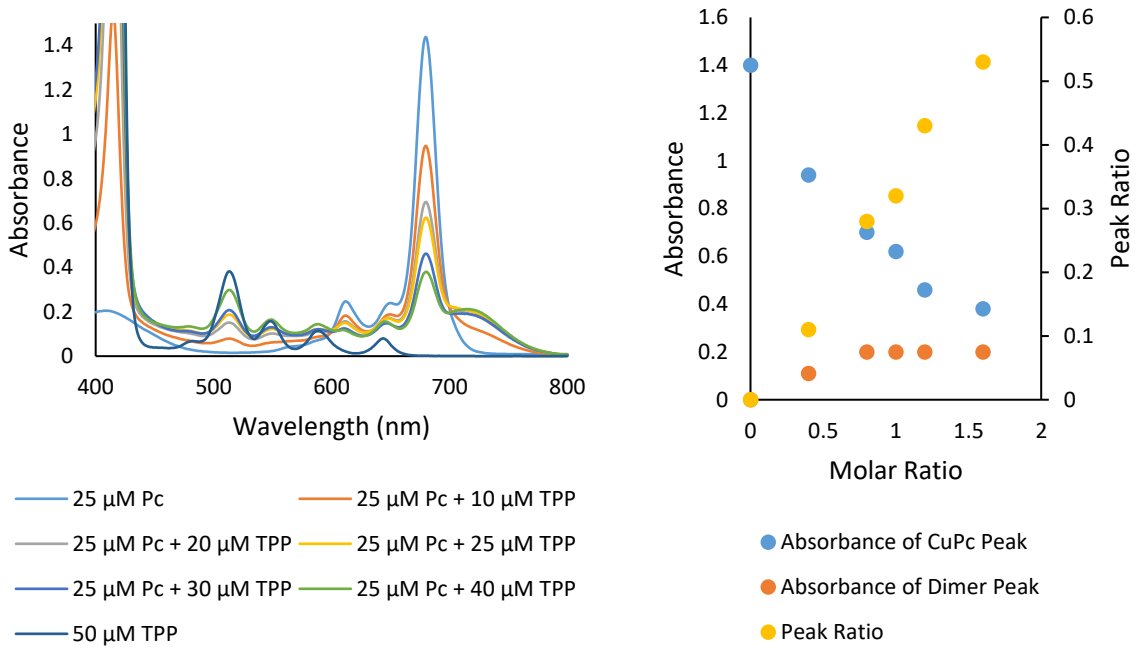

Figure 5.3: The UV-vis spectra of $(dipPhO)_8PcCu/H_2TPP$ aggregation with increasing TPP concentration and change in absorbance peaks with increasing TPP/Pc molar ratio. Note that peak ratio refers to the ratio of the intensity of the $(dipPhO)_8PcCu$ Q-band at 680 nm with that of the peak due to aggregation at 732 nm.

Having examined the interactions between the $(dipPhO)_8PcCu$ and H_2TPP, a logical next step was to examine the change in the aggregation the TPP containing metal centres (TPPM). To this end, a series of metal-containing TPPs were combined in solution with the metal-free phthalocyanine ($(dipPhO)_8PcH_2$), using a 1:3 dichloromethane: methanol solvent mixture. The metal-free phthalocyanine was used to avoid of any competing effects from metal-metal interactions. As shown in **Figure 5.3**, the metal centre was found to have a significant impact on the degree of aggregation. Comparison of the $(dipPhO)_8PcH_2$ Q-band peak to that of the aggregation could be quantified in order to obtain a numerical measure of the strength of the interactions. Copper-substituted TPP in particular appeared to exhibit considerably stronger aggregation than any other metal substitution, with zinc and chromium showing the weakest, and the other metals falling in the range between. The particular affinity of the copper may be explained by the square planar geometry resulting in particularly tight, rigid binding of the copper ion to the macrocycles such as the phthalocyanine ligand, and the previously-mentioned lack of axial ligand binding on either face of the ligand.[96]

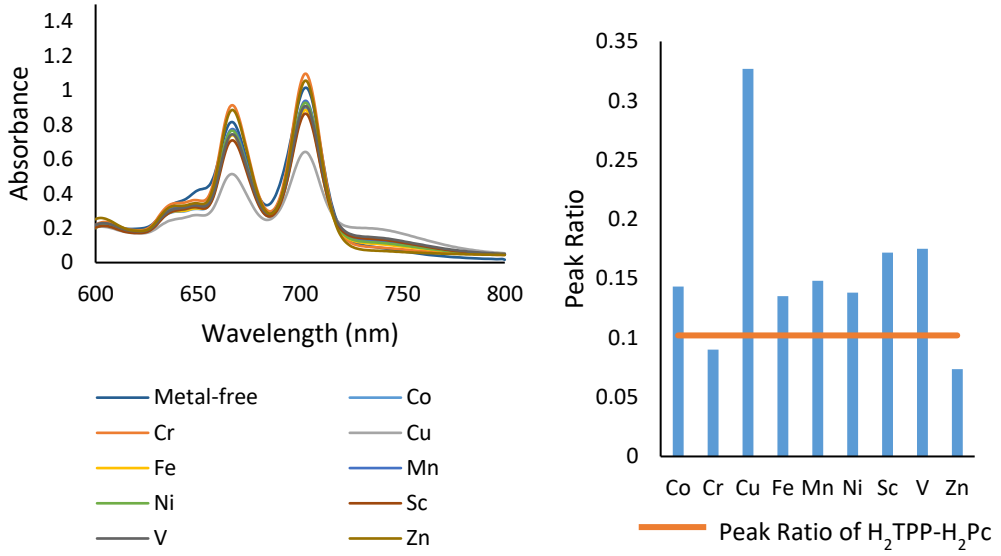

Figure 5.4: The UV-vis spectra of the $(dipPhO)_8PcH_2$/TPPM mixtures and the ratio of the Pc/TPP peak for each TPPM.

Having examined the impact of varying the tetraphenylporphyrin metal centre on the aggregation, the next step was to look at the combination of this with metalation of the phthalocyanine. ZnPc, CoPc and CuPc previously produced were used alongside the commercially available Zn, Co and CuTPP. Due to the previously mentioned varying solubility of the MPcs in the solvent system employed, the solvent ratio again had to be adjusted to 1:1 dichloromethane: methanol, and so the results are not directly comparable to the previous H_2Pc-MTPP study. With the rest of the previously identified conditions maintained, all combinations of MPc and MTPP were investigated. A summary of the results is shown in **Figure 5.5**, with the ratio of Q-band to aggregate peak calculated and the spectra being shown in **Appendix 8.3**. Trends can be identified, with the CuPc showing a significant degree of aggregation with all of the TPPs, and ZnPc contrastingly showing very little aggregation exhibited with any of the TPPs. Aggregation of the TPPs with the CoPc generally fell between the two extremes. It could therefore be concluded that the aggregation was highly dependent on the nature of the metal centre in the Pc but that the TPP metal centre had a more limited impact. This may suggest that metal-metal interactions between the centres of the two ligands were less important than the ligand-ligand interactions.

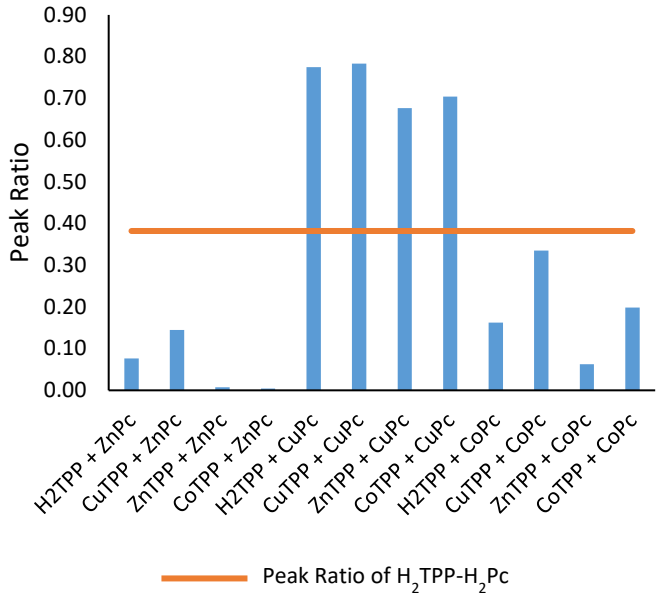

	H_2 TPP	Cu TPP	Zn TPP	Co TPP
CuPc	0.78	0.78	0.68	0.70
ZnPc	0.08	0.14	0.01	0.00
CoPc	0.16	0.34	0.06	0.20

Figure 5.5: The peak ratios of the Q-band and dimer peaks for each of the MTPP-MPc combinations, compared to that of H_2TPP-H_2Pc in the same conditions.

5.3.2 Crystallographic studies of metallated phthalocyanine/porphyrin interactions

Whilst useful information could be gleaned from spectroscopic studies about the nature of the interactions between the phthalocyanine and tetraphenylporphyrin in solution, in order to obtain a greater understanding of the solid-state nature of the structure formed from the two macrocycles it was important to perform single-crystal X-ray diffraction studies. Again building on work that had been carried out previously within the group, co-crystallisation was performed by slow vapour diffusion of methanol into a solution of the $(dipPhO)_8$PcM and TPP dissolved in chloroform.

Accordingly, crystal structures were obtained of the CoTPP/$(dipPhO)_8$PcCo and CuTPP/$(dipPhO)_8$PcCu products, as shown in **Figure 5.6**. As had previously been found with the system, both crystallised in the cubic $Pn\bar{3}n$ space group. Examining the interactions between the two macrocycles, it was found that the metal-metal distance in the [*v*CuTPP/CuPc] structure was 3.447 Å, whilst that in the [*v*CoTPP/CoPc] structure was 3.567 Å. This correlates with the significantly greater degree of aggregation observed in the UV-vis spectra, suggesting that the important interactions are conserved between the solution and solid-state systems.

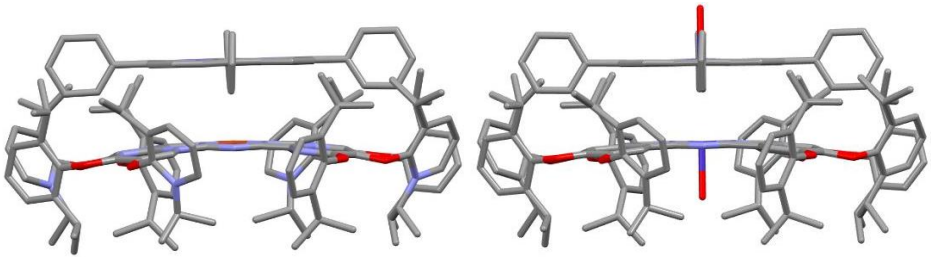

Figure 5.6: The molecular crystal structures of [*v*CuTPP/CuPc] (left) and [*v*CoTPP/CoPc] (right).

Additionally, attempts were made to obtain single crystals of the H_2Pc/MTPP dimers. Disappointingly, isolable crystals could not be acquired in the majority of cases. As shown in **Figure 5.7** however, crystals were successfully obtained for the ZnTPP/(dipPhO)$_8$PcH_2 and CuTPP/(dipPhO)$_8$PcH_2 products. The [*v*ZnTPP/H_2Pc] product was found to crystallise in the same $\mathrm{Pn\bar{3}n}$ space group as obtained in most cases of Pc-TPP co-crystallisation. The [*v*CuTPP/H_2Pc] structure however was unexpectedly found to crystallise in the monoclinic $\mathrm{P2_1/c}$ space group.

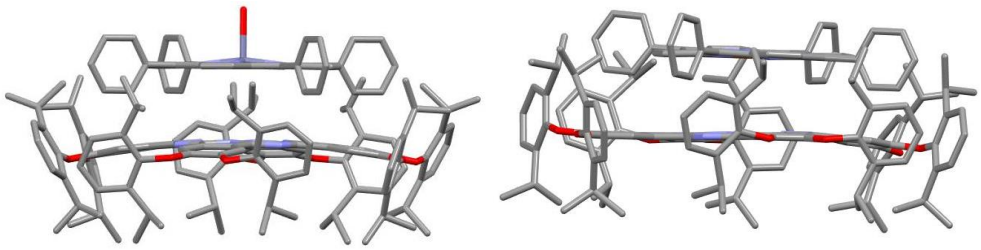

Figure 5.7: The molecular crystal structures of [*v*ZnTPP/H_2Pc] (left) and [*v*CuTPP/H_2Pc] (right).

5.4 Phthalocyanine aggregation with substituted tetraphenylporphyrin derivatives

5.4.1 Synthesis of a library of substituted tetraphenylporphyrins

As previously discussed, an advantage of the TPP system was the ability to introduce substituents to the phenyl rings in in order to fine-tune the properties of the resulting Pc/TPP molecular crystals. To this end, it was desirable to examine the effect of a variety of substituents in various positions on the TPP on its ability to interact with Pc. While both metal-free and a range of metallated unsubstituted TPPs were available commercially, the substituted TPPs had to be synthesised. This was done using the methodology initially outlined by Adler and Longo, which involves refluxing pyrrole with a corresponding aldehyde in propionic acid.[156] Yields for this reaction are generally poor, being highly dependent on a number of factors such as temperature, initial concentration, acidity and atmospheric

oxygen availability, and numerous polymeric side products are almost invariably produced. However, the relative simplicity, and the commercial availability of a large library of substituted benzaldehydes, made it a suitable synthetic method despite these disadvantages.

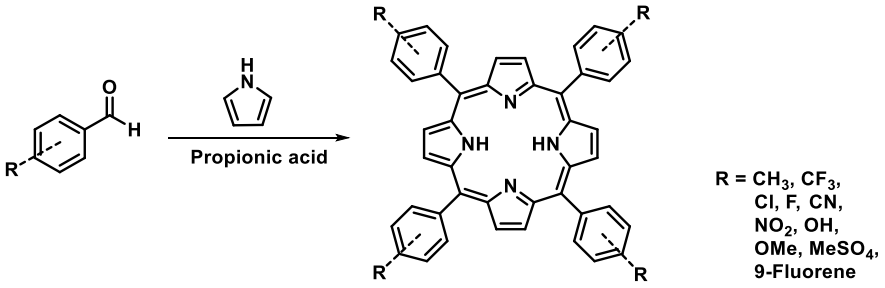

Scheme 5.2: The synthesis of the substituted TPPs.

Initial work, carried out in conjunction with supervised undergraduate project students, led to the synthesis of a series of TPPs with a variety of substituents, from electron-withdrawing to electron-donating groups, as well as others with considerable steric bulk. In some cases, several isomers of the benzaldehyde were available, and so the position of the substitution was also varied in order to explore the effect this had on the interactions with the $(dipPhO)_8Pc$. In others, only the *para*-substituted version could be synthesised.

TPP	Yield (%)	TPP	Yield (%)	TPP	Yield (%)
2-CH_3	5.2	2-Cl	3.2	4-CN	0
3-CH_3	0.1	3-Cl	1.5	4-NO_2	0.4
4-CH_3	1.8	4-Cl	7.7	4-OH	0
2-CF_3	3.1	2-F	4.6	4-OMe	1.2
3-CF_3	4.0	3-F	6.5	4-$MeSO_2$	0.2
4-CF_3	5.1	4-F	10.4	Fluorene	0

Table 5.1: The synthesised substituted TPPs.

With some of the reactions, upon cooling the reaction mixture, the tetraphenylporphyrin product could be isolated simply by filtration as a lustrous purple solid and was found to be highly pure without further purification. In others, no significant quantity of solid material was obtained at this stage, but following dilution with methanol and freezing, small quantities were successfully isolated. In some cases, the product could only be recovered by removal of solvent and purification of the residue. Where required, purification was carried out by column chromatography, although it was sometimes

necessary to repeat this to obtain the pure product. In all cases, the yields were low, as expected. *Para*-substitution appeared to result in higher yields, which may have been a result of the greater inherent symmetry resulting in the more favourable formation of crystals. The attempted syntheses of the cyano and hydroxyl-substituted TPPs were not successful, and the nitro and methylsulfonyl-substituted products were obtained with extremely low yields. This could likely be explained by the greater tendency of these functionalities to undergo undesirable side reactions upon exposure to the relatively harsh reaction conditions. In contrast, the methyl, trifluoromethyl, chloro and fluoro-substituted TPPs appeared more stable to the reaction conditions, and were obtained in quantities usable for screening.

The synthesised TPPs were characterised via NMR, IR and LDI mass spectrometry, but as with the phthalocyanine ligands discussed in previous chapters, the most insightful technique was UV-vis spectroscopy. As shown in **Appendix 8.3**, almost all of the TPP exhibited the expected form of the spectrum, with a large Soret-band peak and a series of smaller Q-band peaks. In the cases of the 4-NO_2 and 4-$MeSO_4$-substituted examples, the peaks were much less clearly defined, which may have been a result of their reduced solubility due to the presence of the highly polar functionalities.

5.4.2 Screening of solution-state phthalocyanine/porphyrin interactions

The aggregation of the synthesised TPP derivatives with $(dipPhO)_8PcH_2$ was then examined using UV-vis spectroscopy. Although the spectra were slightly more difficult to interpret as a result of the split Q-band of $(dipPhO)_8PcH_2$, this was outweighed by both the greater availability of the metal-free ligand and the desire to maintain consistency with previous studies. In the large majority of cases, the additional peak assigned to the aggregated complex was observed at higher wavelength, as seen in **Figure 5.8**. As with the spectra of the TPPs alone, 4-NO_2 and 4-$MeSO_4$ substitution resulted in higher baselines and broader peaks in the spectra, likely due to the lower solubility and hence higher porphyrin-porphyrin aggregation in these molecules. For most of the other tetraphenylporphyrins, the expected aggregation peak could be seen clearly, with the most aggregation observed for the fluoro- and methyl-substituted TPPs, the methoxy-substituted showing an intermediate amount, and relatively little aggregation in the case of the chloro- and trifluoromethyl TPPs. Due to the considerable differences in solubility and potential for this to affect the obtained spectra, it was not thought appropriate to attempt to precisely quantify the peak ratios.

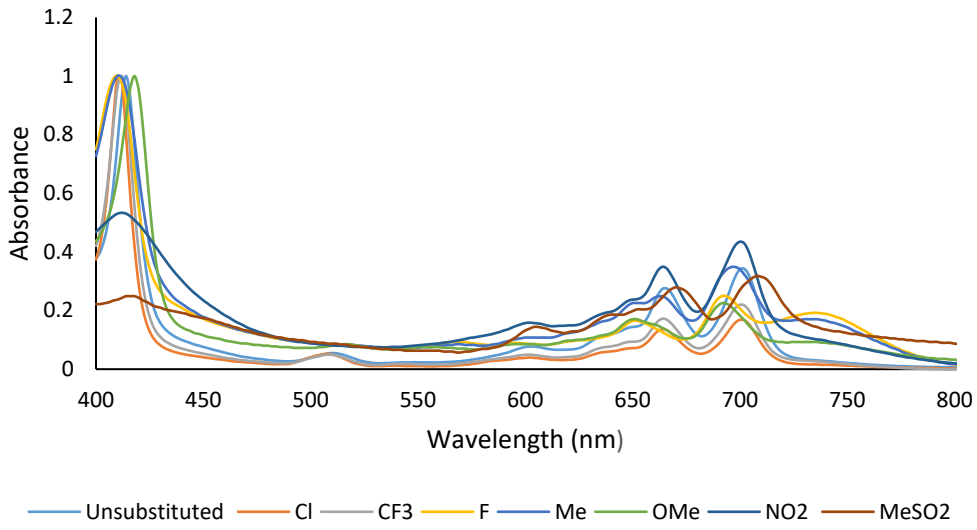

Figure 5.8: The UV-vis spectra of the H_2Pc:*para*-substituted-TPP dimers.

5.4.3 Crystallographic studies of phthalocyanine/porphyrin interactions

As with the variation of the metal centre, it was also desirable to compare the solution-state data of $(dipPhO)_8PcH_2$/TPP interaction with crystallographic information. However, relatively few samples resulted in isolable crystals, and often only self-crystallised phthalocyanine or porphyrin were obtained. Nevertheless, two of the desired structures were obtained, as shown in **Figure 5.9**. Co-crystallisation with 4-fluoro-substituted TPP gave a crystal structure with the cubic $Pn\bar{3}n$ space group generally associated with the nanoporous crystal system, whereas with methyl substitution crystals with orthorhombic $Pnma$ were found. It could therefore be concluded that such substitution could have a significant impact on the formation of crystal structures of the aggregate.

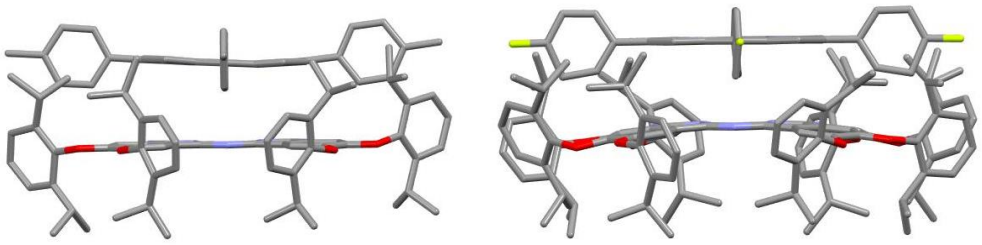

Figure 5.9: The molecular crystal structures of [$\nu H_2TPP(4CH_3)_4/H_2Pc$] (left) and [$\nu H_2TPP(4F)_4/H_2Pc$] (right).

5.5 Phthalocyanine/fluorinated-tetraphenylporphyrin interactions

5.5.1 Synthesis of fluorinated tetraphenylporphyrins

As fluorine-functionalised TPPs had appeared to show some particularly interesting results, and given the wide commercial availability of fluorinated benzaldehyde precursors, it was decided to expand investigation in this area via the synthesis of a large library of fluorine-containing TPPs. Again following Adler and Longo's methodology, and in collaboration with supervised undergraduate students, 15 such porphyrins were synthesised in sufficiently large quantities to be studied (**Figure 5.10**).

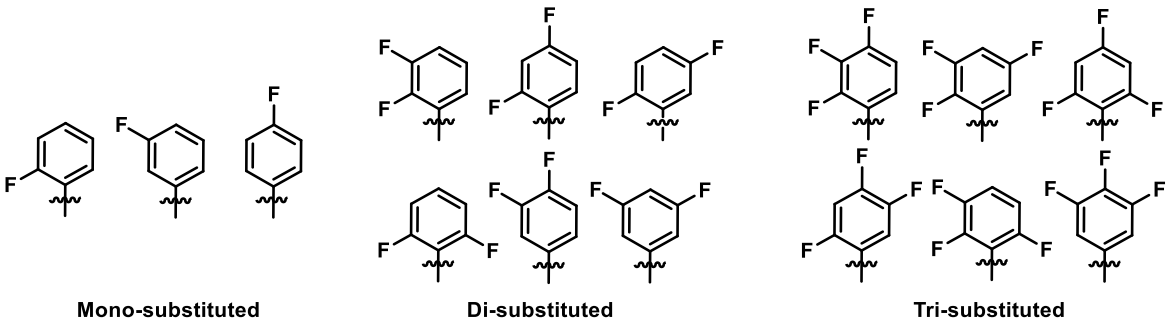

Figure 5.10: The different fluorinated substituents on the tetraphenylporphyrins produced.

As summarised in **Table 5.2**, yields were generally low, varying from a minimum of 3% to a maximum of 26%. A trend seemed evident in which the mono-substituted tetraphenylporphyrins were formed in greater yields, as well as those multi-fluorinated products featuring substitution in the *para* position. This may have been a result of electronic effects activating the tetracyclomerisation reaction, or it may have been that the greater symmetry of such products caused the formation of larger, more isolable crystals.

TPP – 1F	Yield (%)	TPP – 2F	Yield (%)	TPP – 3F	Yield (%)
2-F	15	2,3-F	7	2,3,4-F	8
3-F	22	2,4-F	14	2,3,5-F	3
4-F	26	2,5-F	3	2,4,6-F	6
		2,6-F	9	2,4,5-F	6
		3,4-F	10	2,3,6-F	3
		3,5-F	7	3,4,5-F	14

Table 5.2: The yields obtained for the synthesis of the fluorinated TPPs.

The synthesised fluorinated TPPs were characterised using NMR and UV-vis spectroscopy again, with the spectra also included in **Appendix 8.3**. As with the variably-substituted TPPs previously described, all products showed the expected form of the spectrum, confirming successful synthesis of the porphyrin macrocycle.

5.5.2 Spectroscopic studies of solution-state phthalocyanine/fluorinated-tetraphenylporphyrin interactions

The fluorinated TPPs were combined with $(dipPhO)_8PcH_2$ using the previously identified conditions, and the UV-vis spectra recorded in **Figure 5.11**. Due to the reduced variability in solubility of the TTPs the spectra were of a more consistent form. As a result, the aggregation peaks are more clearly visible, with a maximum generally at or around 732 nm.

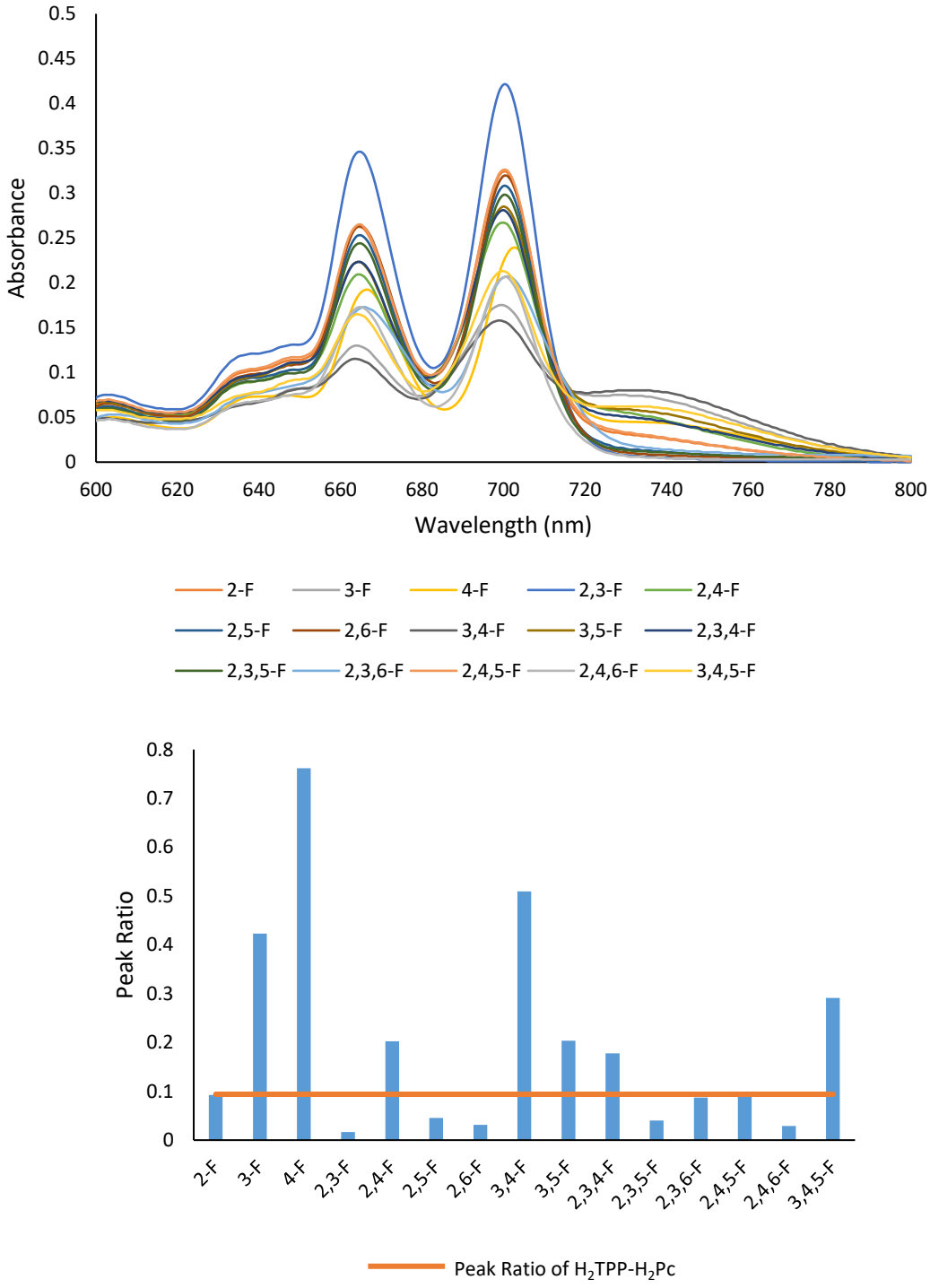

Figure 5.11: The UV-vis spectra of the H_2Pc/fluoro-substituted-TPP dimers, together with the peak ratios of the Q-band and aggregation peaks, compared to H_2TPP/H_2Pc.

As previously, the ratio of the maximum absorbance of the Q-band peak and the dimer peak was calculated for each case, resulting in the chart shown in **Figure 5.11**. By comparison to the equivalent value for $(dipPhO)_8PcH_2/H_2TPP$, the degree to which the fluorine atoms are encouraging or hindering

aggregation relative to the unsubstituted TPP can be determined. The 4-fluoro-TPP appeared to exhibit by far the strongest aggregation. This added to the evidence from the variably-substituted TPPs that functionalisation at this position most strongly favours the Pc/TPP interactions. Since the atomic radius of fluorine is slightly larger than hydrogen, it is likely that the observed favouring of aggregation at the *para*-position is dominated by electronic rather than steric effects. The high electronegativity of fluorine would be expected to reduce the electron density of the π-system in the porphyrin ring, favouring aggregation with the electron-rich $(dipPhO)_8PcH_2$. A general trend of TPPs containing fluorine in the *para*-position having a greater degree of aggregation is confirmed by the enhanced aggregation of the 3,4-, 2,3,4 and 3,4,5-subsituted TPPs. Substitution at the *meta*-position was also found to favour aggregation to a lesser extent, though when present at both the 3 and 5 positions the effect was lessened. This is likely due to the fact that rotation around the porphyrin-phenyl bond can allow the *meta*-substituted fluorine to be positioned where it cannot interfere sterically with the aggregation. In the case of the 3,5-substituted TPP however, one fluorine atom will always be in a position to hinder aggregation.

In contrast, substitution at the *ortho*-position was found to result in less aggregation in almost all cases. This may be as a result of steric hindrance inhibiting aggregation and the lack of a favourable interaction between the *ortho*-hydrogen and the meso-nitrogen of $(dipPhO)_8PcH_2$. The previously discussed rotation around the phenyl-porphyrin single bond is believed to be relatively slow, which can result in multiple isomers of the *ortho*-substituted TPP that can interact with $(dipPhO)_8PcH_2$. The aggregation of each of these will be different, with the isomer in which all of the fluorine atoms are positioned to avoid interfering with aggregation being most favoured (as in seen in the X-ray structure below). Notably, with the 2,6-difluoro and 2,4,6-trifluoro-substituted TPPs, in which four fluorine atoms will unavoidably be placed between the Pc and TPP, no aggregation is seen. To conclude, these results suggest that the electronegative fluorine atoms reduce the electron density of the extended π-system of the TPP and hence favour aggregation, which is consistent with similar effects in other systems in literature.[157] However, *ortho*-substitution of the TPP phenyl groups results in unfavourable steric interactions for aggregation.

Finally, the aggregation of several of the fluorinated TPPs with the previously synthesised metallated phthalocyanines was examined. The 3,4-difluoro, 2,3,4-trifluoro and 2,5-difluoro TPPs were selected, representing porphyrins that had exhibited a high, intermediate and low level of aggregation with the $(dipPhO)_8PcH_2$ respectively. As previously found when comparing phthalocyanines, examination of the results was made slightly more difficult by the considerable differences in the position of the Q-band peaks between the $(dipPhO)_8PcH_2$ and metallated Pc complexes. Nonetheless, as shown in **Figure 5.12**, it could be determined that aggregation was most strongly favoured with $(dipPhO)_8PcCu$, as had been

the case with the unsubstituted TPP. Indeed, the ratio of the aggregation peak to the Q-band peak was considerably greater in every case than with $(dipPhO)_8PcH_2$. Little aggregation was seen with $(dipPhO)_8PcZn$ and $(dipPhO)_8PcCo$, with levels considerably less than the corresponding FTPP-H_2Pc dimer. Overall, it is evident that the metal ion in the phthalocyanine has a considerably bigger effect on the degree of aggregation than substitution of the TPP. The spectra for all of the PcM/FTPP combinations are shown in **Appendix 8.3**.

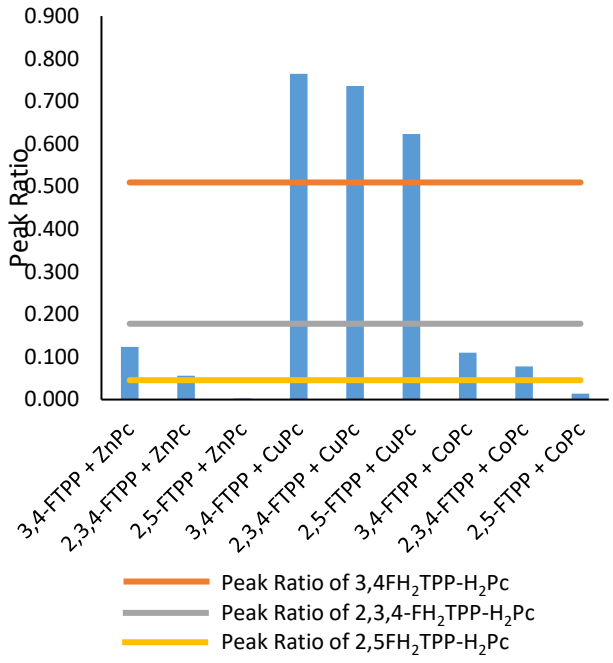

	3,4F TPP	2,3,4F TPP	2,5F TPP
CuPc	0.765	0.736	0.623
ZnPc	0.124	0.056	0.002
CoPc	0.110	0.078	0.014

Figure 5.12: The peak ratios of the Q-band and dimer peaks for each of the PcM/FTPP combinations, compared to that of the fluorine-substituted H_2TPP-H_2Pc dimers in the same conditions.

5.5.3 Crystallographic studies of phthalocyanine/fluorinated-tetraphenylporphyrin interactions

As the structures were assumed to be similar to those previously reported, the same methodologies were employed for the co-crystallisations with fluorinated TPPs. For most of the synthesised FTPPs, co-crystallisation resulted in the successful formation of cubic green crystals, which were submitted for diffraction. In several cases however, these were found to consist solely of the phthalocyanine, without included TPP.

In total, data was gathered for 7 structures with the Pc successfully coordinated to the fluorinated TPP. In 5 cases, the co-crystallisation resulted in the retention of the standard $Pn\bar{3}n$ cubic space group.

This was the case, for example, with all of the singly substituted fluorinated TPPs, but also with other TPPs such as 2,4-difluoro, as shown in **Figure 5.13.**

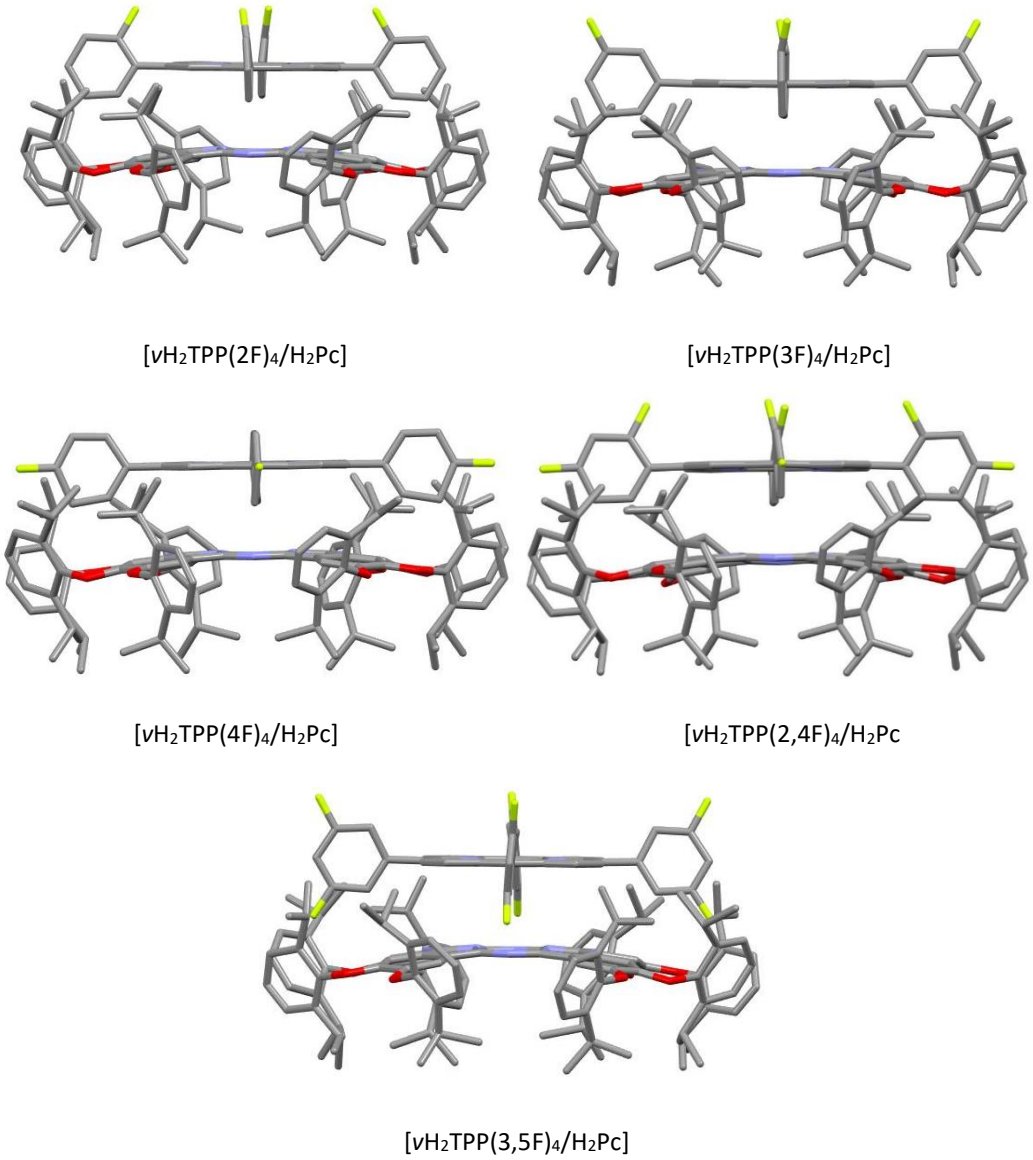

[*v*H_2TPP(2F)$_4$/H_2Pc] [*v*H_2TPP(3F)$_4$/H_2Pc]

[*v*H_2TPP(4F)$_4$/H_2Pc] [*v*H_2TPP(2,4F)$_4$/H_2Pc

[*v*H_2TPP(3,5F)$_4$/H_2Pc]

Figure 5.13: The molecular crystal structures of the FTPP: H_2Pc dimers

In contrast, with the 3,4-difluoro and 3,4,5-trifluoro-substituted TPP co-crystallisations resulted in the formation of crystals with the $\mathrm{l4mm}$ space group, as shown in **Figure 5.14**.

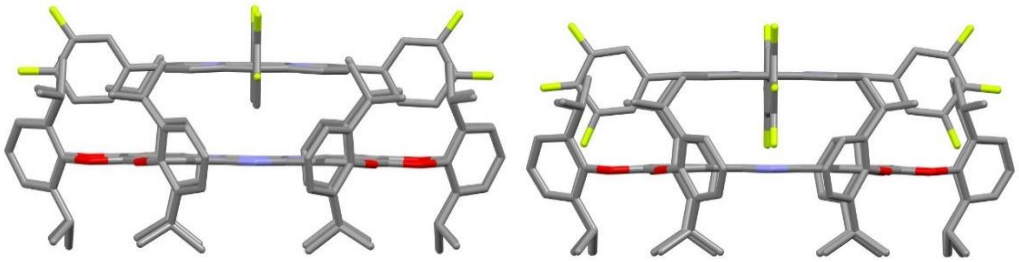

Figure 5.14: The molecular crystal structures of [*v*H_2TPP(3,4F)$_4$/H_2Pc] (left) and [*v*H_2TPP(3,4,5F)$_4$/H_2Pc] (right).

As summarised in **Table 5.3**, these differences seemed to also be reflected in both the intermolecular distances between the macrocycles in the crystal structures, and the curvature imparted to the otherwise planar (dipPhO)$_8$PcH_2 by the TPP-induced cubic crystal formation. A trend appeared to be present within the singly fluorinated co-crystals, in which moving from *ortho* to *meta* to *para* substitution increased the distance between the macrocycles and the distortion of the phthalocyanine ring.

Structure	Space group	Macrocycle to macrocycle distance (Å)	Phthalocyanine curvature (degrees)
[*v*H_2TPP/H_2Pc]	Cubic ($Pn\bar{3}n$)	3.461(7)	18.60
[*v*H_2TPP(2F)$_4$/H_2Pc]	Cubic ($Pn\bar{3}n$)	3.423(6)	19.57
[*v*H_2TPP(3F)$_4$/H_2Pc]	Cubic ($Pn\bar{3}n$)	3.417(6)	18.79
[*v*H_2TPP(4F)$_4$/H_2Pc]	Cubic ($Pn\bar{3}n$)	3.380(7)	17.12
[*v*H_2TPP(2,4F)$_4$/H_2Pc]	Cubic ($Pn\bar{3}n$)	3.482(7)	17.25
[*v*H_2TPP(3,4F)$_4$/H_2Pc]	Tetragonal ($I4mm$)	3.645(7)	1.31
[*v*H_2TPP(3,5F)$_4$/H_2Pc]	Cubic ($Pn\bar{3}n$)	3.399(7)	23.04
[*v*H_2TPP(3,4,5F)$_4$/H_2Pc]	Tetragonal ($I\bar{4}mm$)	3.716(8)	2.73

Table 5.3: Summary of the crystallographic data of the phthalocyanine/fluorinated-tetraphenylporphyrin structures

The apparent correlation between the decrease in the macrocycle to macrocycle distance and increase in the contortion of the (dipPhO)$_8$PcH_2 caused by aggregation with the TPP is shown graphically in **Figure 5.15**.

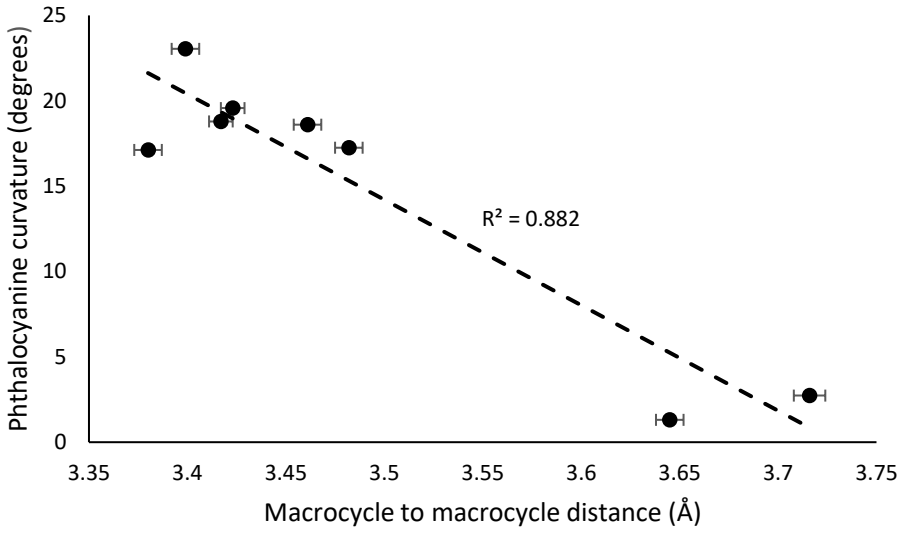

Figure 5.15: The relationship between the macrocycle to macrocycle distance and the curvature of the phthalocyanine ring for each of phthalocyanine/fluorinated-tetraphenylporphyrin structures. Note that while the estimated standard deviation for the macrocycle distances could be calculated, this was not possible when examining the curvature, due to the way in which planes were constructed in the software.

Comparing the crystallographic data to the results previously obtained from spectroscopy does appear to suggest that the steric and inductive effects of the different fluorine substitutions on the aggregation are at least somewhat consistent between solid and solution-state, though interpretation of this must be caveated by the fact that there was a degree of uncertainty in both the crystallographic and spectroscopic results. Even given these caveats, the 2-fluoro substituted TPP does seem to be an exception to the correlation, as it has a short macrocycle distance despite showing a relatively small aggregation ratio. This is likely explained by the previously discussed ability of rotation of the phenyl ring in TPP to position the *ortho*-substituted fluorine atoms towards or away from the phthalocyanine ring. Whilst crystallisation exclusively results in the more energetically favourable conformation, the solution-state system consists of a mixture of four conformers at equilibrium, and is therefore less favoured, as shown in **Figure 5.16**.

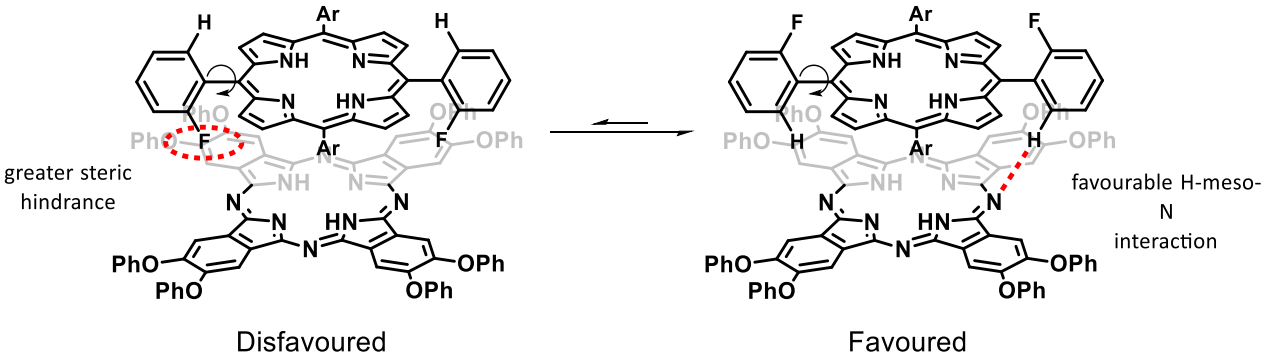

Figure 5.16: The equilibrium between the two conformations of the 2-F substituted TPP, showing variation of the interactions with the phthalocyanine.

While the by the $I4mm$ space group in which the 3,4-difluro and 3,4,5-trifluorosubstituted TPPs were found to co-crystallise with the $(dipPhO)_8PcH_2$ evidently corresponded to reduced strength of the Pc/TPP interactions, interest was piqued by the presence of linear channels within the crystals, as visualised in **Figure 5.17**.

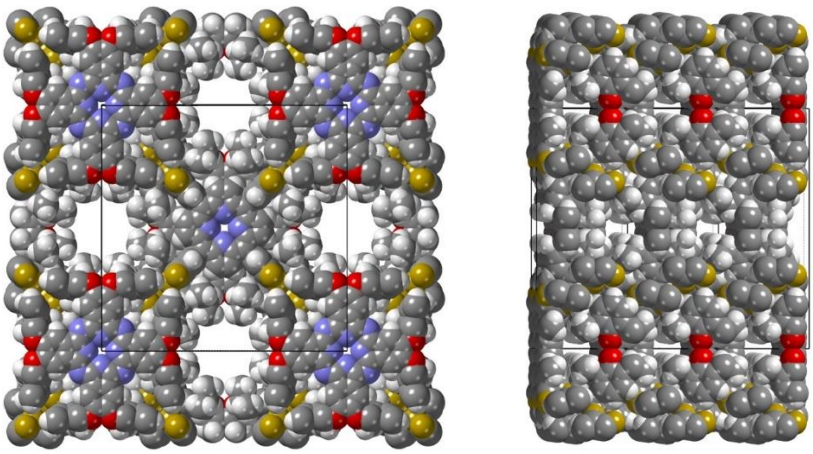

Figure 5.17: The tetragonal structure of the co-crystals of $(dipPhO)_8PcH_2$/3,4,5-FH_2TPP showing the 1-D channels (approx. 0.8 nm in diameter) which run along the Z-axis of the crystal

It was therefore decided to investigate whether this alternative structure could also result in the formation of a permanently porous crystal. Following the previously established procedure, the 3,4,5-trifluorosubstituted TPP and metal-free phthalocyanine were co-crystallised at a larger scale, with 150 mg of the co-crystal product being obtained. The maintenance of the crystal structure was confirmed by powder X-ray diffraction**.** The resulting product was found to have a small amount of internal porosity, with an apparent BET surface area of 180 m^2/g (**Figure 5.18**), suggesting that the evacuated 3,4,5-FH_2TPP/$(dipPhO)_8PcH_2$ structure does maintain its porous structure on evacuation of solvent.

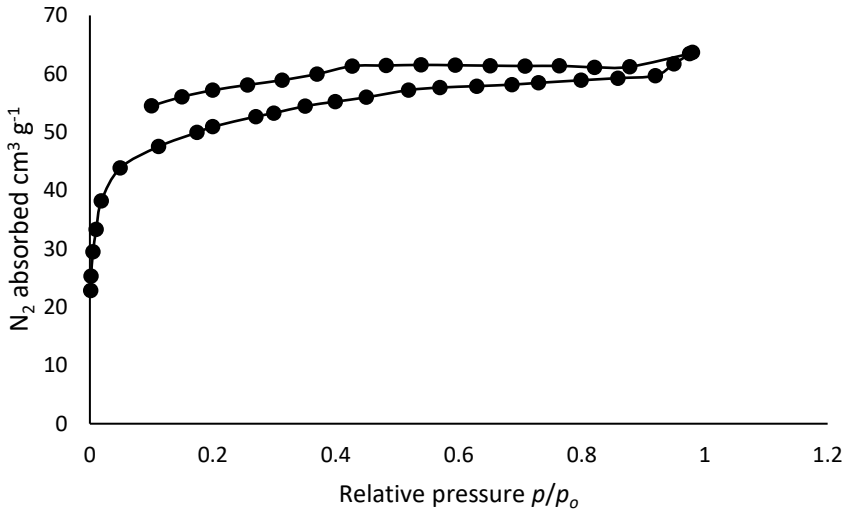

Figure 5.18: The BET isotherm of the 3,4,5-FH_2TPP/H_2Pc crystal

5.6 Conclusions

The range and scope of potential interactions between both metallated and metal-free $(dipPhO)_8$Pc and a wide variety of TPPs was examined. Various metals were substituted into both macrocycles, which was found to have a significant effect on the aggregation of the two, as determined via UV-vis spectroscopy. Specifically, in both cases, copper(II) substitution was found to favour aggregation, and zinc(II) disfavour it. Crystal structures were also obtained for two samples showing the solid-state nature of the system.

The substitution of various functionalities onto the TPP was also investigated. Once again, a significant impact on the strength of the aggregation was observed, with methyl- and fluoro-substitution at the *para* position most favourable, for which crystal structure data was also obtained. Based on this, a variety of mono, di and trifluorinated tetraphenylporphyrins were synthesised, and their aggregation with the phthalocyanine examined. Again, *para*-substitution was found to be most suitable. A number of crystal structures were obtained, most in the cubic space group which had previously been found to have potential as a nanoporous material. However, a new tetragonal packing arrangement of the co-crystal of $(dipPhO)_8PcH_2$/3,4,5-FH_2TPP also proved to possess permanent porosity.

6 Overall Conclusions and Future Work

Some of the intriguing potential utility of both novel and previously reported phthalocyanine ligands in the construction of porous materials has been demonstrated. A novel tetracarboxyimidophthalocyanine ligand has been developed, but despite sharing similarities with ligands previously used in Metal Organic Frameworks, its very high intermolecular attractive forces appear to preclude its use. Octacarboxyphthalocyanine has also been investigated as a ligand in MOF syntheses, and was found to result in the formation of crystalline structures with a small degree of internal porosity. Full structural information could not be determined due to the inability to obtain single crystals, and available data was not conclusively supportive of the formation of the expected MOFs.

Use of the tetraimidophthalocyanine functionality has also been expanded by its incorporation into a series of network polymers, using the tetracyclomerisation step for polymerisation. Initial examples displayed negligible surface areas, which can be ascribed to lack of inhibition of dense packing of the phthalocyanine rings. However, two examples of network polymers designed to overcome this problem did show greater internal surface areas.

Finally, new molecular crystals have been produced showing the interactions between a wide ranges of tetratraphenylporphyrin ligands with a phthalocyanine widely studied in the group. The results have confirmed that the nature of the interactions can be significantly altered, both by variation of the metal centre and by substitution of different functionalities onto the phenyl rings. A new type of co-crystal with tetragonal packing was also shown to possess permanent porosity.

6.1 Computational Evaluation of Phthalocyanine MOF formation

To explain the failure to obtain truly crystalline MOF products with the TCIPc and OCPc ligands, it would be desirable to computationally investigate the energetic favourability of the structures likely to be formed. Initial attempts to construct models of the potential carboxylate zirconium-cluster MOFs containing both TCIPc and OCPc in order to facilitate this were undertaken, but time constraints and software issues prevented this being completed during the course of the project. From these models, the energy of formation of such structures could be calculated and this could be compared to the energies of formation of the MOFs which had inspired the Pc MOF syntheses, based on their published CIF files. The expected energetic unfavorability of Pc MOF formation compared to that of porphyrin

or benzenetetracarboxylic acid-based MOFs would then rationalise the observed failure of the attempts to synthesise the former.

It would also be useful to use these modelled structures in order to obtain a predicted powder X-ray diffraction pattern. Comparison of this to the obtained patterns could allow the definitive determination of whether the synthesised OCPc MOF material was consistent with the hypothesised structure.

6.2 Further Phthalocyanine Metal Organic Frameworks

Formation of crystalline phthalocyanine MOFs is believed to have been most significantly impacted by the poor solubility of the ligands employed. Given this, increasing their solubility in common solvents would be desirable. To this end, initial attempts to modify the structures of both the tetracarboxyimidophthalocyanine and octacarboxyphthalocyanine ligands by the addition of substituents in the non-peripheral positions were undertaken, as outlined in **Schemes 6.1** and **6.2**. Unfortunately, the necessary phthalonitrile or *ortho*-dibromo intermediates could not be isolated during the period of the work. It is likely however that this could be overcome with further synthetic investigation, which may lead to improvements in the outcome of MOF synthesis reactions, and also the ability to remove uncoordinated ligands upon completion. Additionally, variation of the substituents may allow tailoring of the environment within porous crystalline MOFs.

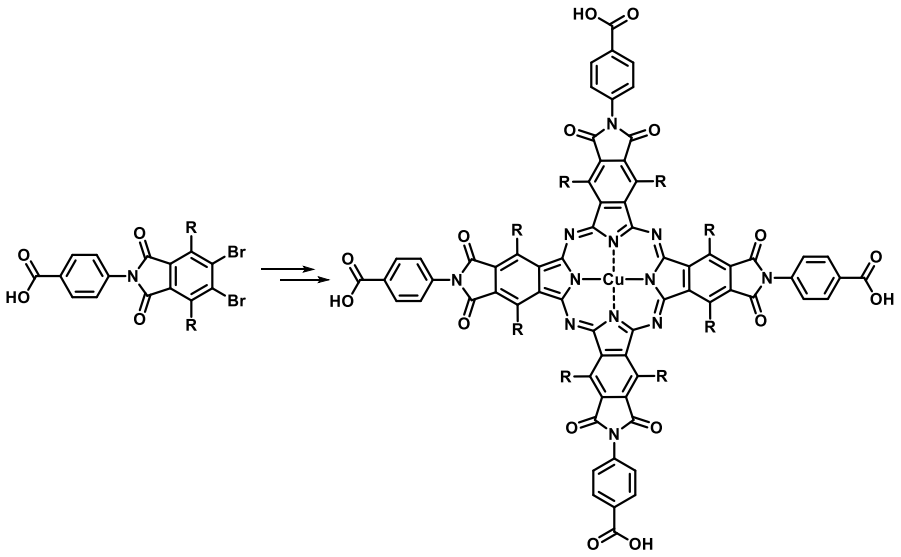

Scheme 6.1: The propose substituted tetracarboxyimidophthalocyanine

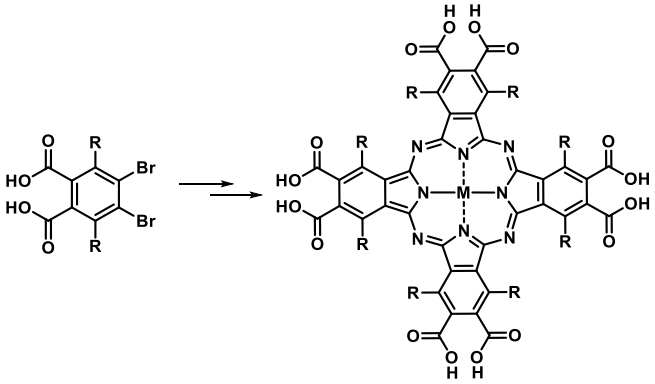

Scheme 6.2: The propose substituted octacarboxyphthalocyanine

6.3 Further Phthalocyanine Network Polymers

Another area which could be explored in greater detail is the further potential for the synthesis of network polymers featuring the developed phthalocyanine functionalities. In order to minimise the aggregation of the phthalocyanine, which had been found to prevent porosity in the materials, additional bulky functionalities, for example triptycenes, could be incorporated.

It would also be desirable to successfully produce a wider range of pyrazinoporphyrazine polymers. Whilst this had been prevented during the period of the project by the unexpected repeated failure of the pyrazine-forming reaction, it is likely that this obstacle could be overcome given sufficient time to probe the variable synthetic conditions. This should allow the production of porous polymers incorporating the functionality.

6.4 Phthalocyanine Covalent Organic Frameworks

Whilst crystalline organic/inorganic MOFs and amorphous organic polymers were thoroughly investigated during the course of the project, a potential future area of investigation would be the synthesis of purely organic, crystalline Covalent Organic Frameworks. As with the network polymers, these could potentially be based on the tetraimidophthalocyanine functionality. Changing the linking unit between the phthalocyanines from strong, largely irreversible bonds such as imides to reversible bonds such as boronate ester linkages or imines should allow the eventual formation of the thermodynamically more stable products. To this end synthesis of alternative versions of the phthalocyanine ligand containing aldehyde and amine functionality could be investigated, via the route shown in **Figure 6.1**.

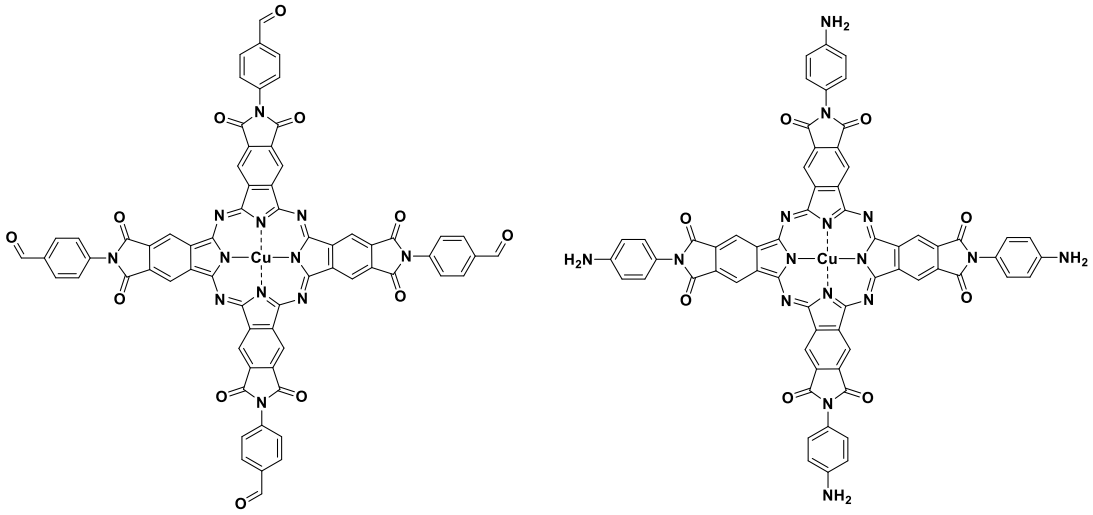

Figure 6.1: The structures of the aldehyde and amine functionalised phthalocyanines

Reaction with an appropriate amine or aldehyde to form novel imine Pc COFs could then be possible. Materials could be synthesised as layered 2D COFs by using terephthaldehyde and *p*-phenylenediamine, as shown in **Figure 6.2** This could then be built on by using tetrafunctionalised linkers to produce 3D COFs that may improve the accessibility of the phthalocyanine metal centres.

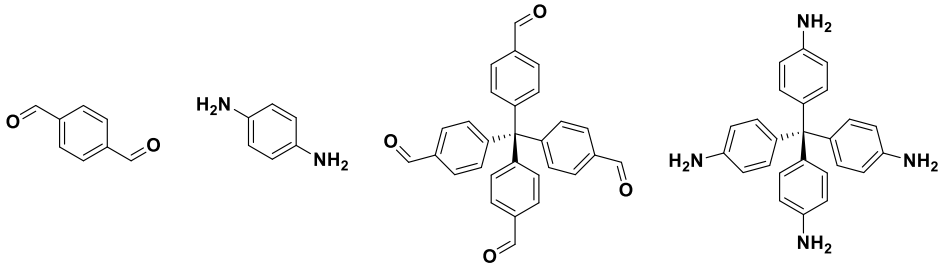

Figure 6.2: Examples of COF linkers

7 Experimental

7.1 Equipment

Reagents and purification

Unless a synthetic procedure is provided, reagents were purchased from commercial sources and used without further purification. Thin layer chromatography (TLC) was used to monitor the progress of most reactions reported using aluminium-backed plates coated with Merck TLC silica gel 60 F254. Column chromatography used for the purification of some compounds was performed over silica gel (pore size 60 Å, particle size 40-63 µm) as the stationary phase.

Melting Points (Mp)

Melting points were recorded using a Stuart SMP10 melting point apparatus and are uncorrected.

Infra-red Spectroscopy (IR)

Infrared adsorption spectra were recorded using powdered samples in the range of 4000-400 cm^{-1} using a Shimadzu IR Affinity-1S FTIR spectrophotometer.

Ultraviolet-visible light spectroscopy (UV-vis)

UV-vis spectra were recorded using a Shimadzu UV-1800 spectrophotometer, with soluble analytes in various solvents as described, with either a 1 or 10 mm path length quartz cuvette. Insoluble samples were first finely suspended in 1-chloronaphthalene using sonication.

Nuclear Magnetic Resonance Spectrometry (NMR)

^{1}H and ^{13}C NMR spectra were acquired using a suitable deuterated solvent (chloroform, acetone, dimethyl sulphoxide) using the following instruments: Avance Bruker AVA 400, AVA 500, PRO 500 or AVA 600 instrument.

Mass Spectrometry (MS)

Small molecule low-resolution mass spectrometry (LRMS) and high resolution mass spectrometry (HRMS) was performed by using a Fison VG Platform II quadrupole instrument plus Thermo Finnigan MAT 900 XP, Electron Ionisation Sector MS utilising electron impact (EI), Matrix Assisted Laser Desorption/Ionization (MALDI) or simply Laser Desorption/Ionization (LDI).

BET Surface Areas (BET)

Low-temperature (77 K) nitrogen and carbon dioxide (273 K) adsorption/desorption isotherms were obtained using a Quantachrome Quadrasorb*evo* automated surface area analyser. Accurately

weighed powdered samples of roughly 100 mg were degassed for 16 h at 100 °C under high vacuum prior to analysis.

Thermal-gravimetric Analysis (TGA)

Thermo-gravimetric analysis (TGA) was conducted using a Thermal Analysis SDT Q600 system with a sample heating rate of 10°C min^{-1} up to 800°C.

Powder X-ray Diffraction

Powder X-ray diffraction was carried out using Bruker D2 Phaser and D8 Advance instruments.

X-ray Crystallography

X-ray crystal structure analysis was accomplished using a Bruker Smart Apex CCD diffractometer with MoKα radiation λ = 0.71073 Å at 150 K; Oxford Diffraction SuperNova diffractometer with CuKα radiation λ = 1.5405 Å at 120 K.

7.2 Synthetic procedures for phthalocyanine precursors

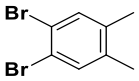

4,5-Dimethyl-1,2-dibromobenzene[158]

A solution of iodine (0.10 g, 0.79 mmol) in *o*-xylene (25.0 ml, 22.0 g, 0.21 mol) was cooled to 0 °C, and bromine (22 ml, 62.3 g, 0.43 mol) was added dropwise over 2 h under a nitrogen atmosphere. The solution was warmed to room temperature and left stirring for a further 20 h. The resulting solid was dissolved in diethyl ether (100 ml) and washed with 2 M sodium hydroxide (2 x 50 ml) and water (2 x 50 ml). The organic phase was dried with magnesium sulphate, and the solvent removed under reduced pressure to afford an off-white solid. The crude product was purified by recrystallisation from methanol to give 4,5-dimethyl-1,2-dibromobenzene as a white solid (38.7 g, 0.15 mol, 70.4%). Mp 84-86 °C [Lit: 85-87 °C]; IR (ATR): ν_{max} = 2976, 2947, 2918, 1439, 1340, 1157, 642 cm^{-1}; ^{1}H NMR (500 MHz,

$CDCl_3$): δ_H = 7.38 (s, 2H, Ar *H*), 2. 20 (s, 6H C*H*$_3$) ppm; LRMS (EI, m/z): calculated $C_8H_8Br_2$ 261.9, found: 261.9 [M+].

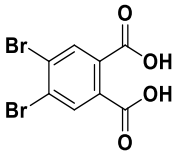

4,5-Dibromophthalic acid[93]

To a 1:1 (v/v) solution of pyridine:water (600 ml) was added 4,5-dimethyl-1,2-dibromobenzene (15 g, 0.05 mol). The mixture was heated to 100 °C under a nitrogen atmosphere and potassium permanganate (109 g, 0.90 mol) was added in portions over 1 h. The mixture was heated for a further 48 h, and filtered hot, with the manganese dioxide solid further washed with hot water. The filtrate was collected, and the solvent removed under reduced pressure to give a yellow-white solid. The solid was dissolved in warm water, and the solution acidified with 6M hydrochloric acid until the pH < 2, at which point a white solid precipitated. This was collected by filtration, washed with 0.01 M hydrochloric acid, and dried in air to give 4,5-dibromophthalic acid as a white solid (17.2 g, 0.053 mol, 89 %). Mp: Sublimes at 220 °C; IR (ATR): ν_{max} = 3093, 2917(br) 1710cm, 1520, 1413, 1232, 1086, 594 cm^{-1}; ^{1}H NMR (500 MHz, $CDCl_3$): δ_H = 8.25 (s, 2H, Ar *H*) ppm.

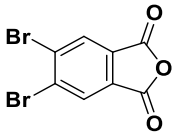

4,5-Dibromophthalic anhydride[95]

To a 1:1 (v/v) mixture of dichloromethane and 1,4-dioxane (96 ml) were added 4,5-dibromophthallic acid (2.50 g, 7.8 mmol) and anhydrous sodium carbonate (0.83 g, 7.8 mmol) and heated to 70 °C under a nitrogen atmosphere. Thionyl chloride (5.70 ml, 9.35 g, 79 mmol) was added dropwise over 30 min. The mixture was heated for a further 48 h, then cooled to room temperature. The mixture was washed with water (2 x 50 ml), dried with magnesium sulphate, and the solvent removed under reduced pressure. The solid obtained was washed with *n*-hexane and dried in air to afford 4,5-dibromophthalic anhydride as a white solid (1.87 g, 6.2 mmol, 79%). Mp: Sublimes at > 220 °C. IR (ATR): ν_{max} = 3091, 1822, 1767, 1300, 1236, 1084, 914, 702 cm^{-1}; ^{1}H NMR (500 MHz, $CDCl_3$): δ_H = 8.28 (s, 2H, Ar *H*) ppm; ^{13}C NMR (126 MHz, $CDCl_3$): δ_C = 160.8, 134.5, 131.0, 130.6 ppm; LRMS (EI, m/z): calculated $C_8H_2Br_2O_3$ 303.8, found: 303.9 [M+].

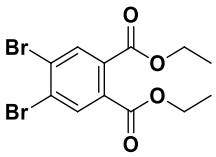

Diethyl 4,5-dibromo-1,2-dibenzoate

A suspension of 4,5-dibromophthalic acid (3.00 g, 9.3 mmol) in ethanol (30 ml) was heated to 80 °C under a nitrogen atmosphere. Thionyl chloride (6.70 ml, 11.00 g, 93 mmol) was added dropwise over 30 min. The mixture was heated for a further 48 h, then cooled to room temperature. Water (100 ml) was added, and the mixture was then extracted with chloroform (2 x 100 ml) The combined organic layers were washed with 1M sodium hydrogen carbonate (2 x 100 ml) then water (100 ml), dried with magnesium sulphate, and the solvent removed under reduced pressure to obtain diethyl 4,5-dibromo-1,2-dibenzoate as a white solid (1.87 g, 6.2 mmol, 79%). Mp: 55-57 °C. IR (ATR): ν_{max} = 3091, 2985, 1714, 1577, 1242, 1230, 1080, 779 cm^{-1}; ^{1}H NMR (500 MHz, $CDCl_3$): δ_H = 7.98 (s, 2H, Ar *H*), 4.39 (q, *J* = 7.1 Hz, 4H, C*H*$_2$) 1.39 (t, *J* = 7.1 Hz, 6H, C*H*$_3$) ppm; ^{13}C NMR (126 MHz, $CDCl_3$): δ_C = 160.8, 134.5, 131.0, 130.6 ppm; LRMS (EI, m/z): calculated $C_{12}H_{12}Br_2O_4$ 380.0, found: 379.9 [M+].

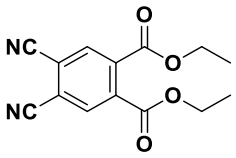

Diethyl 4,5-dicyano-1,2-dibenzoate[159]

To a solution of diethyl 4,5-dibromo-1,2-dibenzoate (5.00 g, 13.2 mmol) in anhydrous dimethylformamide (100 ml) was added copper cyanide (2.60 g, 28.5 mmol) and potassium iodide (4.40 g, 26.5 mmol) and the solution was heated to 120 °C for 4 hours under a nitrogen atmosphere. Upon cooling, the solution was poured slowly into aqueous ammonium hydroxide solution (200 ml. 10%). The precipitate obtained was filtered off and washed with further ammonia solution and water alternately until the washings were colourless and dried in air to afford a pale blue solid. This was then washed with hot chloroform (3 x 100 ml) and the filtrate concentrated under reduced pressure to obtain a pale yellow oil. This was purified by column chromatography with hexane: ethyl acetate (3:1) as an eluent to obtain the product as a white solid (0.75g, 2.75 mmol, 21%). Mp: 127-129 °C [Lit: 124-125 °C]. IR (ATR): ν_{max} = 2997, 2252, 1731, 1375, 1301, 1253, 1106, 904 cm^{-1}; ^{1}H NMR (500 MHz, $CDCl_3$): δ_H = 8.14 (s, 2H, Ar *H*), 4.43 (q, *J* = 7.2 Hz, 4H, C*H*$_2$) 1.40 (t, *J* = 7.2 Hz, 6H, C*H*$_3$) ppm; ^{13}C NMR (126 MHz,

$CDCl_3$): δ_C = 164.1, 136.5, 133.9, 118.1, 114.0, 63.2, 14.0. ppm; LRMS (EI, m/z): calculated $C_{14}H_{12}N_2O_4$ 272.3, found: 272.1 [M+].

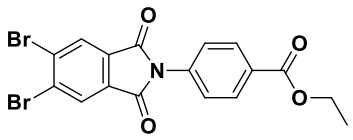

***N*-(4-ethylbenzoate)-4,5-dibromophthalimide**

To glacial acetic acid (170 ml) were added 4,5-dibromophthalic anhydride (2.88 g, 9.5 mmol) and ethyl *p*-aminobenzoate (1.92 g, 11.6 mmol) and the solution was heated to reflux for 16 hrs under a nitrogen atmosphere. Upon cooling, the solution was poured into water in order to precipitate a white solid. This was filtered off, washed with water and dried in air to afford the product without further purification (2.79 g, 6.2 mmol, 65%). Mp >300°C; IR (ATR): ν_{max} = 3088, 2986, 1778, 1709, 1366, 1275, 742 cm^{-1}; ^{1}H NMR (500 MHz, DMSO-d_6): δ_H = 8.37 (s, 2H, Ar *H*) 8.14-8.09 (m, 2H, Ar *H*), 7.65-7.60 (m, 2H, Ar *H*), 4.35 (q, *J* = 7.1 Hz, 2H, CH_2), 1.35 (t, *J* = 7.1 Hz, 3H, CH_3) ppm; ^{13}C NMR (126 MHz, $CDCl_3$): δ_C = 170.3, 170.2, 141.0, 137.2, 136.1, 135.0, 133.8, 133.6, 132.2, 66.2, 19.4 ppm; LRMS (MALDI-TOF, m/z): calculated $C_{17}H_{11}Br_2NO_4$: 450.91, found: 450.93 [M+].

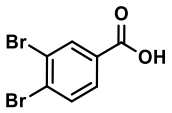

3,4-Dibromobenzoic acid[160]

To a 1:1 (v/v) solution of pyridine:water (240 ml) was added 3,4-dibromotoluene (5.0 g, 20.0 mmol). The mixture was heated to 100 °C under a nitrogen atmosphere and potassium permanganate (38.0 g, 0.24 mol) was added in portions over 1 h. The mixture was heated for a further 48 h, and filtered hot, with the manganese dioxide solid further washed with hot water. The filtrate was collected, and the solvent removed under reduced pressure to give a yellow-white solid. The solid was dissolved in warm water, and the solution acidified with 2M hydrochloric acid until the pH < 2, at which point a white solid precipitated. This was collected by filtration, washed with 0.01 M hydrochloric acid, and dried in air to give the product as a white solid (3.75 g, 13.4 mmol, 67 %). Mp: 228-230°C [Lit: 230-232 °C]; IR (ATR): ν_{max} = 3093, 2900(br) 1701, 1411, 1284, 1232, 1086, 889 cm^{-1}; ^{1}H NMR (500 MHz, DMSO-d_6): δ_H = 13.48 (s, 1H, COO*H*), 8.17 (d, *J* = 1.9 Hz, 1H, Ar *H*), 7.91, (d, *J* = 8.3 Hz, 1H, Ar *H*), 7.82 (dd, *J* =

8.3, 1.9 Hz, 1H, Ar *H*) ppm; ^{13}C NMR (126 MHz, DMSO-d_6): δ_C = 165.9, 134.7, 134.5, 132.4, 130.3, 129.6, 124.7 ppm.

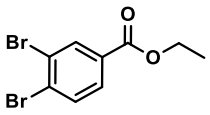

Ethyl 3,4-dibromobenzoate[161]

A suspension of 3,4-Dibromobenzoic acid (3.75 g, 13.4 mmol) in ethanol (75 ml) was heated to 80 °C under a nitrogen atmosphere. Thionyl chloride (4.0 ml, 6.57 g, 55.5 mmol) was added dropwise over 30 min. The mixture was heated for a further 48 h, then cooled to room temperature. Upon cooling, water (150 ml) was added, and the mixture was then extracted with chloroform (2 x 100 ml) The combined organic layers were washed with 1M sodium hydrogen carbonate (2 x 100 ml) then water (100 ml), dried with magnesium sulphate, and the solvent removed under reduced pressure to obtain the product as an off-white solid (3.43 g, 11.2 mmol, 84%). Mp: 62-64 °C. IR (ATR): ν_{max} = 2985, 2878, 1716, 1446, 1282, 1229, 1084, 902, 777 cm^{-1}; ^{1}H NMR (500 MHz, $CDCl_3$): δ_H = 8.26 (d, *J* = 2.0 Hz, 1H, Ar *H*), 7.81 (dd, *J* = 8.3, 2.0 Hz, 1H, Ar *H*), 7.69 (d, J = 8.3 Hz, 1H, Ar *H*), 4.39 (q, J = 7.1 Hz, 2H, CH_2), 1.40 (t, J = 7.1 Hz, 3H, CH_3) ppm; ^{13}C NMR (126 MHz, $CDCl_3$): δ_C = 164.7, 134.6, 133.7, 131.0, 130.2, 129.2, 125.0, 61.6, 14.3 ppm; LRMS (EI, m/z): calculated $C_9H_8Br_2O_2$ 305.9, found: 305.9 [M+].

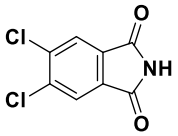

4,5-Dichlorophthalimide[91]

To formamide (40 ml) was added 4,5-dichlorophthalic anhydride (21.0 g, 96.8 mmol), and the solution was heated to reflux for 2 hours under a nitrogen atmosphere. Upon cooling a thick paste formed, which was filtered, and the resulting solid washed with water and dried in air to afford an off white product (9.78 g, 45.3 mmol, 47%). Mp: 196 - 198 °C [Lit: 193 - 195 °C]; IR (ATR): ν_{max} = 3680, 3473, 2980, 2713, 1724, 1651, 1350, 1057, 737 cm^{-1}; ^{1}H NMR (500 MHz, $CDCl_3$): δ_H = 8.08 (s, 1H, N*H*), 7.94 (s, 2H, Ar *H*) ppm; ^{13}C NMR (126 MHz, $CDCl_3$): δ_C = 165.8, 139.4, 131.7, 125.7.ppm; LRMS (EI, m/z): calculated $C_8H_3Cl_2NO_2$: 214.95, found: 214.92 [M+].

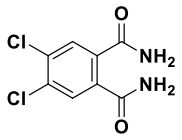

4,5-Dichlorobenzene-1,2-diamide[91]

To aqueous ammonium hydroxide solution (25%, 125 ml) was added 4,5-dichlorophthalimide (9.00 g, 41.7 mmol), and the suspension stirred for 24 hours at room temperature under a nitrogen atmosphere. Additional aqueous ammonium hydroxide solution (33%, 50 ml) was then added, and the suspension stirred for a further 24 hours. It was then filtered, and the solid obtained was washed with water and dried in air to afford an off-white product (8.19 g, 35.1 mmol, 84%). Mp: 250 – 252 °C [Lit: 245 - 247 °C]; IR (ATR): ν_{max} = 3680, 3426, 3138, 2980, 1651, 1603, 1402, 1055, 1031, 897cm^{-1}; ^{1}H NMR (500 MHz, $CDCl_3$): δ_H = 7.83 (s, 2H, Ar *H*), 7.68 (s, 4H, N*H*$_2$) ppm; ^{13}C NMR (126 MHz, $CDCl_3$): δ_C = 167.7, 136.5, 131.8, 129.5 ppm; LRMS (EI, m/z): calculated $C_8H_6Cl_2N_2O_2$: 231.98, found: 232.01 [M+].

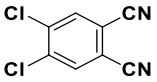

4,5-Dichlorobenzene-1,2-dicyanobenzene[91]

To anhydrous dimethylformamide (50 ml) at 0 °C was added thionyl chloride (33.0 ml, 54.1 g, 0.45 mol) and the solution was stirred under a nitrogen atmosphere for 1 hour. To this was added 4,5-dichlorobenzene-1,2-diamide (8.00 g, 34.3 mmol), and the mixture was stirred for a further 4 hours at 0 °C followed by 20 hours at room temperature. The mixture was then poured into ice water to precipitate a solid, which was filtered, washed with water and dried. The solid was then recrystallized from methanol to afford the product as a white solid (5.20 g, 26.4 mmol, 77%). Mp: 184 - 186 °C [Lit: 182 - 184 °C]; IR (ATR): ν_{max} =3084, 2237, 1466, 1350, 1221, 1340, 1026, 914 cm^{-1}; ^{1}H NMR (500 MHz, $CDCl_3$): δ_H = 7.93 (s, 2H, Ar *H*) ppm; ^{13}C NMR (126 MHz, $CDCl_3$): δ_C = 139.1, 135.0, 115.1, 113.6.ppm; LRMS (EI, m/z): calculated $C_8H_2Cl_2N_2$: 196.0, found: 196.0 [M+].

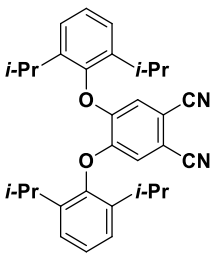

4,5-Di-(2,6-diisopropyl)-phenoxyphthalonitrile[82]

To a solution of 4,5-dichlorobenzene-1,2-dicyanobenzene (4.80 g, 24.4 mmol) in anhydrous dimethylformamide (72 ml) were added dry potassium carbonate (13.1 g, 94.8 mmol) and 2,6-diisopropylphenol (13.3 ml, 12.8 g, 71.8 mmol). The solution was then heated to 65 °C under a nitrogen atmosphere for 72 hours. Upon cooling, the solution was poured into water (200 ml) to precipitate a dark solid, which was filtered and washed with water and then methanol until the washings were clear. The crude product was then recrystallised from methanol to give the product as an off-white solid (6.89 g, 14.3 mmol, 59%). Mp: 162 – 164 °C; IR (ATR): ν_{max} =2965, 2225, 1620, 1501, 1339, 1283, 1203, 1093, 791 cm^{-1}; ^{1}H NMR (500 MHz, $CDCl_3$): δ_H = 7.26-7.37 (m, 6H, Ar *H*), 6.75 (s, 2H, Ar *H*), 2.95 (hept, *J* = 6.8 Hz, 4H, C*H*), 1.21 (d, *J* = 6.8 Hz, 24H, CH_3) ppm; ^{13}C NMR (126 MHz, $CDCl_3$): δ_C = 151.5, 147.2, 140.7, 127.4, 125.2, 117.9, 115.3, 109.2, 50.9, 27.5 ppm; LRMS (EI, m/z): calculated $C_{32}H_{36}N_2O_2$: 480.2, found: 480.2 [M+].

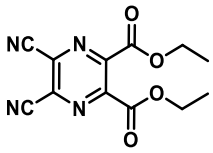

5,6-Diethylesterpyrazine-2,3-dicarbonitrile

To a solution of diethyltartrate (8.80g, 42.7 mmol) in 1,2-dichloroethane (80 ml) was added *N*-bromosuccinimide (32.3 g, 181 mmol) and the solution heated to 75 °C for 48 hours under a nitrogen atmosphere. Upon cooling, diethyl ether (100 ml) was added, and the solution filtered. The solution was washed with water (2 x 100 ml) and dried with magnesium sulphate and the solvent was then removed under reduced pressure to give a yellow oil. This crude product was added to a solution of diaminomaleonitrile (9.23 g, 85.4 mol) in ethanol (500 ml) and heated at reflux for 1 hour under a nitrogen atmosphere. A brown solid was obtained, which was purified by column chromatography using an ethyl acetate: hexane (1:1) eluent to obtain the product as a pale yellow solid (2.57 g, 9.38 mmol, 22%). Mp: 89-91 °C; IR (ATR): ν_{max} = 2986, 1724, 1418, 1288, 1146, 1039, 1011, 864 cm^{-1}; ^{1}H NMR (500 MHz, $CDCl_3$): δ_H = 4.56 (q, *J* = 7.1 Hz, 4H, CH_2), 1.47 (t, J = 7.1 Hz, 6H, CH_3). ppm; ^{13}C NMR

(126 MHz, $CDCl_3$): δ_C = 161.4, 146.6, 133.4, 111.7, 64.2, 13.9. ppm; LRMS (EI, m/z): calculated $C_{12}H_{10}N_4O_4$: 274.2, found: 274.1 [M+].

7.3 Synthetic procedures for molecular phthalocyanines

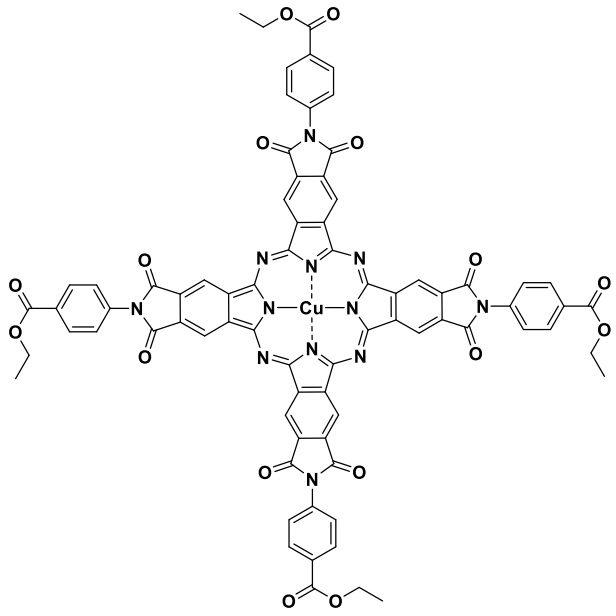

Copper(II) tetrakis(*N*-(4-ethylbenzoate)imido)phthalocyanine (Cu(II) TEtEstIPc)

To a solution of *N*-(4-ethylbenzoate)-4,5-dibromophthalimide (12.50 g, 28.2 mmol), in anhydrous dimethylformamide (250 ml) was added copper cyanide (7.5 g, 83.7 mmol) and heated to 160 °C under a nitrogen atmosphere for 16 hrs. Upon cooling, the solution was poured slowly into a 10 % ammonium hydroxide solution. The precipitate obtained was filtered off and washed with further 10 % ammonia solution and water alternately until the washings were colourless, and dried in air to afford a dark blue solid (3.42 g, 20.1 mmol, 34%). Mp > 300 °C; IR (ATR): ν_{max} = 3348, 3177, 2108, 1651, 1599, 1342, 1311, 1167, 785 cm^{-1}; UV-vis (DMSO) λ_{max}: 681, 655, <400 nm; HRMS (MALDI-TOF, m/z): calculated $C_{76}H_{44}CuN_{12}O_{16}$ 1443.229, found: cluster of peaks centred at 1444.267 [MH+].

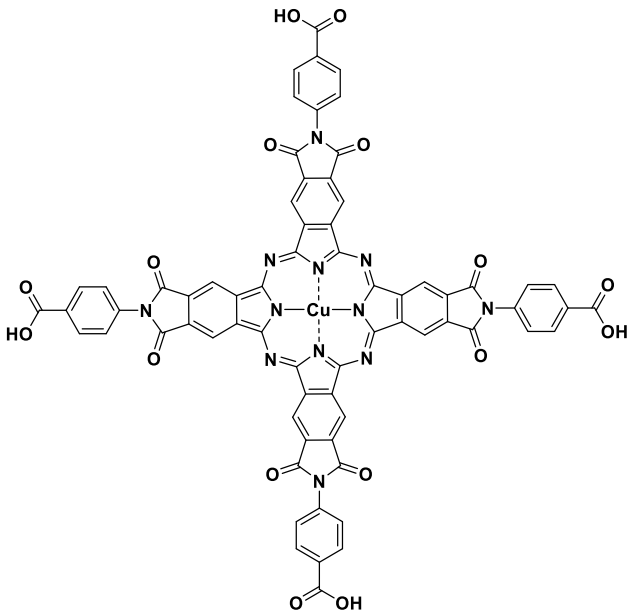

Copper(II) tetrakis(*N*-(4-carboxyphenyl)imido)phthalocyanine (Cu(II) TCIPc)

To an aqueous solution of potassium hydroxide (100 mml, 1M) was added copper(II) tetrakis(N-(4-ethylbenzoate)imido)phthalocyanine (3.25 g, 2.25 mmol) and the suspension was heated at 50 °C for 2 hours. Upon cooling, the solution was filtered to remove any undissolved material, and the filtrate was then precipitated by the addition of 2M hydrochloric acid. The precipitate was filtered, washed with water and acetone, and dried in air to afford the solid as a dark blue solid. (2.19 g, 1.64 mmol, 73%). Mp > 300 °C; IR (ATR): ν_{max} = 3240(br), 2359, 1594, 1508, 1364, 1010, 908, 783 cm^{-1}; UV-vis (H_2O) λ_{max}: 674, 641, 343 nm; LRMS (MALDI-TOF, m/z): calculated $C_{68}H_{28}CuN_{12}O_{16}$ 1331.1037, found: cluster of peaks centred at 1331.1113 [MH+].

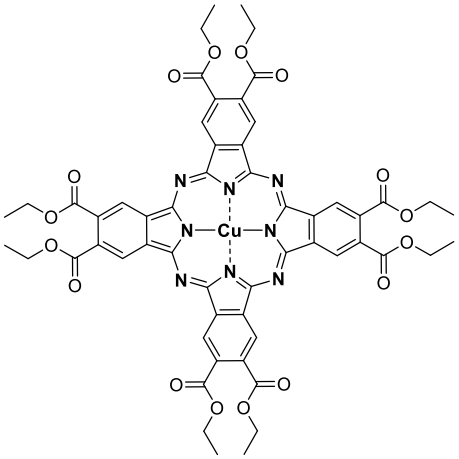

Copper(II) tetrakis(diethyl-1,2-dibenzoate)phthalocyanine

To a solution of diethyl 4,5-dibromo-1,2-dibenzoate (4.50 g, 11.9 mmol), in anhydrous dimethylformamide (75 ml) was added copper cyanide (3.19 g, 35.7 mmol) and heated to 160 ^{o}C under a nitrogen atmosphere for 16 hrs. Upon cooling, the solution was poured slowly into a 10 % ammonium hydroxide solution. The precipitate obtained was filtered off and washed with further 10 % ammonia solution and water alternately until the washings were colourless and dried in air to afford a blue solid. (2.91 g, 2.53 mmol, 85%). Mp > 300 ^{o}C; IR (ATR): ν_{max} = 2984, 1731, 1506, 1326, 1262, 1181, 1072, 1004, 751 cm^{-1}; UV-vis (DMSO) λ_{max}: 679, 641, 613 nm; LRMS (MALDI-TOF, m/z): calculated $C_{56}H_{48}CuN_8O_{16}$ 1151.25, found: 1151.21 [M+].

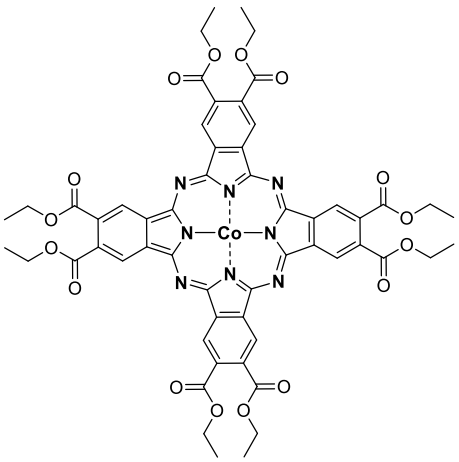

Cobalt(II) tetrakis(diethyl-1,2-dibenzoate)phthalocyanine

To a solution of diethyl 4,5-cyano-1,2-dibenzoate (0.50 g, 1.54 mmol), in anhydrous *N*-methyl-2-pyrrolidone (10 ml) was added cobalt(II) acetate (0.82 g, 4.62 mmol) and the solution heated at 180

°C under a nitrogen atmosphere for 2 hours. Upon cooling, the solution was poured into water, and the resulting precipitate was filtered off, washed with water, methanol and acetone and dried in air to afford the product as a green-black solid (0.30 g, 0.26 mmol, 67%). Mp > 300 °C; IR (ATR): ν_{max} = 2997, 1735, 1522, 1334, 1252, 1080, 1021, 738 cm^{-1}; ^1H NMR (500 MHz, DMSO-d_6): δ_H = 8.40 (s, 8H, Ar *H*), 3.77 (br, 16H, CH_2), 2.03 (br, 24 H, CH_3)) ppm; UV-vis (DMSO) λ_{max}: 674, 638, ,400 nm; LRMS (MALDI-TOF, m/z): calculated $C_{56}H_{48}CoN_8O_{16}$ 1147.25, found: 1147.28 [M+].

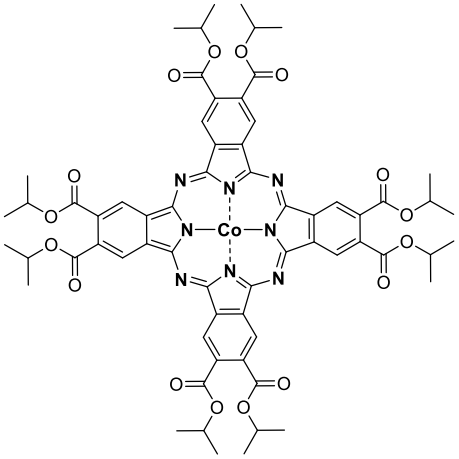

Cobalt(II) tetrakis(diispropyl-1,2-dibenzoate)phthalocyanine

To a solution of diispropyl 4,5-cyano-1,2-dibenzoate (0.20 g, 0.49 mmol), in anhydrous *N*-methyl-2-pyrrolidone (4 ml) was added cobalt(II) acetate (0.24 g, 1.38 mmol) and the solution heated at 180 °C under a nitrogen atmosphere for 2 hours. Upon cooling, the solution was poured into water, and the resulting precipitate was filtered off, washed with water, methanol and acetone and dried in air to afford the product as a green-black solid (0.32 g, 0.25 mmol, 73%). Mp > 300 °C; IR (ATR): ν_{max} = 3012, 2994, 1738, 1532, 1328, 1082, 1056, 749 cm^{-1}; ^1H NMR (500 MHz, DMSO-d_6): δ_H = 8.32 (s, 8H, Ar *H*), 3.78 (br, 8H, C*H*), 1.27 (br, 48 H, CH_3)) ppm; UV-vis (DMSO) λ_{max}: 672, 6333, ,400 nm; LRMS (MALDI-TOF, m/z): calculated $C_{64}H_{64}CoN_8O_{16}$ 1260.19, found: 1260.27 [M+].

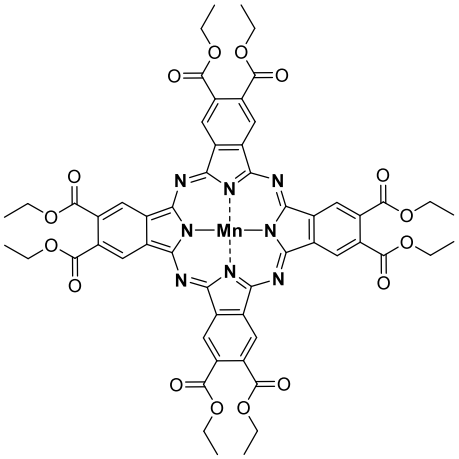

Manganese(II) tetrakis(diethyl-1,2-dibenzoate)phthalocyanine

To a solution of diethyl 4,5-cyano-1,2-dibenzoate (0.50 g, 1.54 mmol), in anhydrous *N*-methyl-2-pyrrolidone (10 ml) was added manganese(II) acetate (0.80 g, 4.62 mmol) and the solution heated at 180 °C under a nitrogen atmosphere for 6 hours. Upon cooling, the solution was poured into water, and the resulting precipitate was filtered off, washed with water, methanol and acetone and dried in air to afford the product as a green-black solid (0.25 g, 0.22 mmol, 57%). Mp > 300 °C; IR (ATR): ν_{max} = 2959, 1554, 1512, 1367, 1256, 1051, 758 cm^{-1}; ^1H NMR (500 MHz, DMSO-d_6): δ_H = 8.38 (s, 8H, Ar *H*), 3.77 (br, 16H, CH_2), 2.04 (br, 24 H, CH_3) ppm; UV-vis (DMSO) λ_{max}: 672, 636, 611 nm; LRMS (MALDI-TOF, m/z): calculated $C_{56}H_{48}MnN_8O_{16}$ 1143.26, found: 1143.23 [M+].

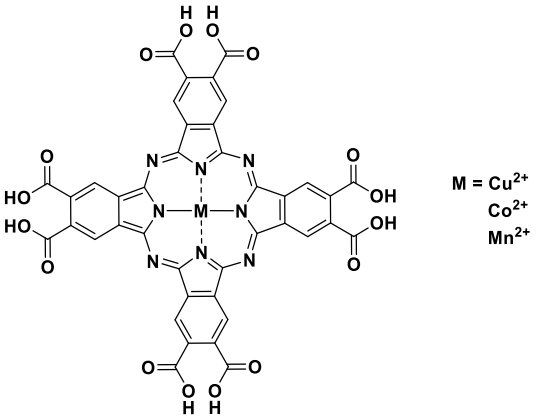

General procedure for the ester hydrolysis of metallated tetrakis(diethyl-1,2-dibenzoate) phthalocyanines

To a stirring solution of potassium hydroxide in methanol was added the metallated tetrakis(diethyl-1,2-dibenzoate)phthalocyanine. The suspension was heated at reflux for 7 days under a nitrogen atmosphere, over which time the solid was seen to dissolve. Upon cooling, any remaining solid was

removed by filtration, and the filtrate was then precipitated with 2M hydrochloric acid to afford a dark solid, which was isolated by filtration and dried in air. This was then dissolved in sodium hydroxide solution (1M, 50 ml) with sonication, before being reprecipitated by the addition of 2M hydrochloric acid. The precipitate was filtered, washed with water and acetone, and dried in air to afford the product.

Copper(II) tetrakis(1,2-dicarboxy)phthalocyanine (Cu(II) OCPc)[93]

Following the general procedure, potassium hydroxide (1.56 g, 27.8 mmol) in methanol (25 ml) was reacted with copper(II) tetrakis(diethyl-1,2-dibenzoate)phthalocyanine (2.00 g, 1.70 mmol) to afford the product as a dark blue solid (1.23 g, 1.31 mmol, 78%). Mp > 300 ^{o}C; IR (ATR): ν_{max} = 3291(br), 2984, 1713, 1560, 1375, 1267, 1087, 1013, 746 cm^{-1}; UV-vis (H_2O) λ_{max}: 687, 654, 618 nm; LRMS (MALDI-TOF, m/z): calculated 927.00, found: 927.05 [M+].

Cobalt(II) tetrakis(1,2-dicarboxy)phthalocyanine (Co(II) OCPc)[93]

Following the general procedure, potassium hydroxide (0.20g, 3.48 mmol) in methanol (5 ml) was reacted with cobalt(II) tetrakis(diethyl-1,2-dibenzoate)phthalocyanine (0.25 g, 0.21 mmol) to afford the product as a dark green solid (0.16 g, 0.17 mmol, 82%). Mp > 300 ^{o}C; IR (ATR): ν_{max} = 3246(br), 2458, 1704, 1658, 1564, 1244, 1070, 747cm^{-1}; UV-vis (H_2O) λ_{max}: 682, 615, <400 nm; LRMS (MALDI-TOF, m/z): calculated 923.00, found: 923.05 [M+].

Manganese(II) tetrakis(1,2-dicarboxy)phthalocyanine (Mn(II) OCPc)[162]

Following the general procedure, potassium hydroxide (0.20 g, 3.48 mmol) in methanol (5 ml) was reacted with manganese(II) tetrakis(diethyl-1,2-dibenzoate)phthalocyanine (0.25 g, 0.21 mmol) to afford the product as a dark solid (0.14 g, 0.16 mmol, 74%). Mp > 300 ^{o}C; IR (ATR): ν_{max} = 3184(br), 2879, 1686, 1616, 1311, 1230, 1083, 721 cm^{-1}; UV-vis (H_2O) λ_{max}: 680, 644, 613 nm; LRMS (MALDI-TOF, m/z): calculated 919.01, found: 919.05 [M+].

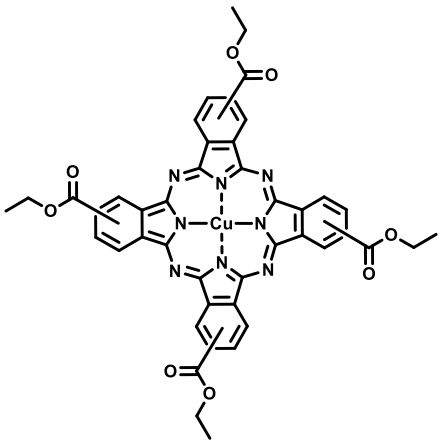

Copper(II) tetrakis(ethyl-1/2-benzoate) phthalocyanine

To a solution of ethyl 3,4-dibromobenzoate (3.43 g, 11.2 mmol), in anhydrous dimethylformamide (50 ml) was added copper cyanide (3.01 g, 33.6 mmol) and heated to 160 ^{o}C under a nitrogen atmosphere for 16 hrs. Upon cooling, the solution was poured slowly into a 10 % ammonium hydroxide solution. The precipitate obtained was filtered off and washed with further 10 % ammonia solution and water alternately until the washings were colourless and dried in air to afford a blue solid (2.03 g, 2.35 mmol, 83%). Mp > 300 ^{o}C; IR (ATR): ν_{max} = 2987, 2868, 1713, 1585, 1366, 1240, 1083, 1049, 733 cm^{-1}; UV-vis (DMSO) λ_{max}: 683, 672, 608 nm; LRMS (MALDI-TOF, m/z): calculated $C_{44}H_{22}CuN_8O_8$ 863.16, found: 863.12 [M+].

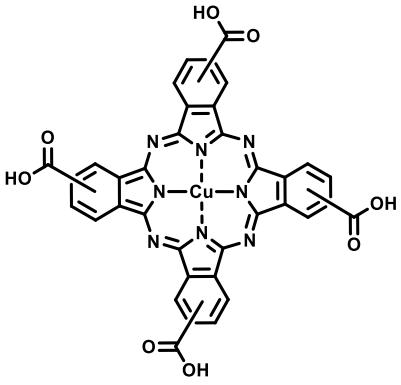

Copper (II) tetracarboxyphthalocyanine[163]

To a stirring solution of potassium hydroxide (1.56 g, 27.8 mmol) in methanol (25 ml) was added copper(II) tetrakis(ethyl-1/2-benzoate phthalocyanine (2.00 g, 2.31 mmol). The suspension was heated at reflux for 7 days under a nitrogen atmosphere, over which time the solid was seen to dissolve. Upon cooling, remaining solid was removed by filtration, and the filtrate was then precipitated with 2M hydrochloric acid to afford a deep blue solid, which was isolated by filtration and

dried in air. This was then dissolved in sodium hydroxide solution (1M, 50 ml) with sonication, before being reprecipitated by the addition of 2M hydrochloric acid. The precipitate was filtered, washed with water and acetone, and dried in air to afford the product as a dark blue solid (1.44 g, 1.92 mmol, 83%). Mp > 300 °C; IR (ATR): ν_{max} = 3049(br), 2359, 1681, 1614, 1373, 1250, 1150, 1088, 735 cm^{-1}; UV-vis (H_2O) λ_{max}: 694, 597, <400 nm.

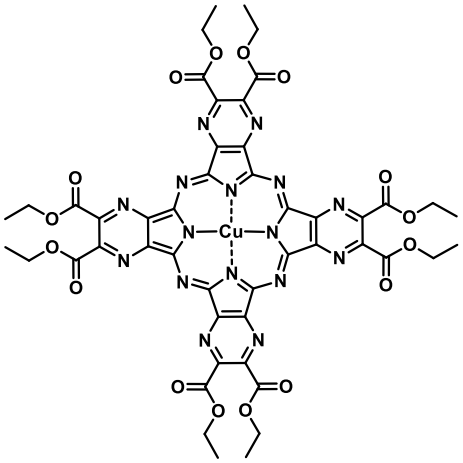

Copper(II) tetrakis(diethyl-1,2-dipyrazinoate)pyrazinoporphyrazine[164]

To a solution of 5,6-diethylesterpyrazine-2,3-dicarbonitrile (1.00 g, 3.65 mmol), in anhydrous *N*-methyl-2-pyrrolidone (20 ml) was added copper acetate monohydrate (0.24 g, 1.21 mmol) and the solution heated to 135 °C under a nitrogen atmosphere for 2 hours. Upon cooling, the solution was poured into water (30 ml). The precipitate obtained was filtered off, washed with water, and dried in air to afford a dark green solid. (0.62 g, 0.53 mmol, 58%). Mp > 300 °C; IR (ATR): ν_{max} = 2981, 2860, 1663, 1502, 189, 1252, 1048, 757 cm^{-1}; UV-vis (DMSO) λ_{max}: 751, 641, <400 nm; LRMS (MALDI-TOF, m/z): calculated $C_{48}H_{40}CuN_{16}O_{16}$ 1159.21, found: 1160.20 [MH+].

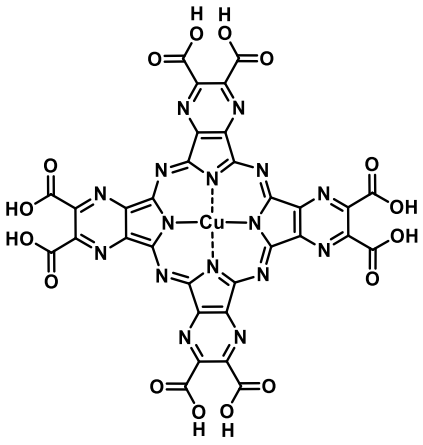

Copper(II) tetrakis(1,2-dicarboxy) pyrazinoporphyrazine[164]

To a stirring solution of potassium hydroxide (0.48 g, 8.32 mmol) in methanol (10 ml) was added copper(II) tetrakis(diethyl-1,2-dipyrazinoate)pyrazinoporphyrazine (0.60 g, 0.52 mmol). The suspension was heated at reflux for 7 days under a nitrogen atmosphere, over which time the solid was seen to dissolve. Upon cooling, remaining solid was removed by filtration, and the filtrate was then precipitated with 2M hydrochloric acid to afford a deep blue solid, which was isolated by filtration and dried in air. This was then dissolved in sodium hydroxide solution (1M, 10 ml) with sonication, before being reprecipitated by the addition of 2M hydrochloric acid. The precipitate was filtered, washed with water and acetone, and dried in air to afford the product as a dark green solid (0.40 g, 0.43 mmol, 83%) ν_{max} = 3312(br), 2160, 1587, 1406, 1357, 1263, 759 cm^{-1}; UV-vis (H_2O) λ_{max}: 746, 646, 581 nm; LRMS (MALDI-TOF, m/z): calculated $C_{32}H_8CuN_{16}O_{16}$: 934.96, found: 934.94 [M+].

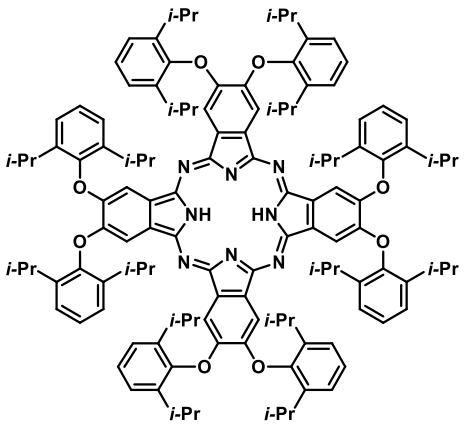

2,3,9,10,16,17,23,24-Octa-(2,6-diisopropyl)-phenoxy)phthalocyanine[13]

A solution of 4,5-di-(2,6-diisopropyl)-phenoxyphthalonitrile (3.00 g, 6.31 mmol) in *n*-pentanol (15 ml) was heated to reflux under a nitrogen atmosphere. Lithium metal (0.1 g) was added, and the solution heated at reflux for 5 hours. Upon cooling acetic acid solution (3 ml, 0.1 M) was added, and the solvent was then removed under reduced pressure to give a crude green solid. This was dissolved in chloroform and then precipitated from methanol to give the product as a green solid (1.45 g, 0.75 mmol, 48%). Mp >300°C; IR (ATR): ν_{max} = 2961, 1597, 1437, 1327, 1265, 1182, 1091, 875, 789cm^{-1}; UV-vis (DCM) λ_{max}: 703, 668, 606 nm; ^{1}H NMR (500 MHz, $CDCl_3$): δ_H = 8.15 (s, 8H, Ar *H*), 7.47-7.61 (m, 24H, Ar *H*), 3.40 (hept, 16H, *J* = 6.5 Hz, C*H*), 1.16-1.38 (m, 96H, CH_3), -0.72 (s, 2H, NH) ppm; ^{13}C NMR (126 MHz, $CDCl_3$): δ_C = 152.3, 151.2, 149.4, 142.0, 140.0, 132.5, 126.7, 124.9, 107.7, 27.8, 24.1, 23.9 ppm; LRMS (LDI-TOF, m/z): calculated $C_{128}H_{146}N_8O_8$: 1923.13, found: 1924.13 [MH+].

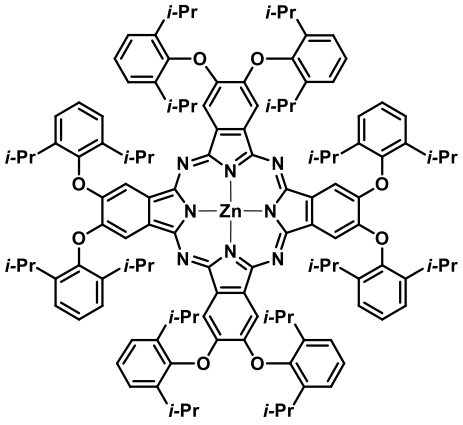

Zinc (II) 2,3,9,10,16,17,23,24-Octa-(2,6-diisopropyl)-phenoxy)phthalocyanine[82]

A solution of 4,5-di-(2,6-diisopropyl)-phenoxyphthalonitrile (3.00 g, 6.31 mmol) and zinc(II) acetate (1.10 g, 6.02 mmol) in *N*-methyl-2-pyrrolidone (10 ml) was heated at 165 ^{o}C under a nitrogen atmosphere for 16 hours. Upon cooling, the solution was poured into water, and the precipitate formed was filtered to give a crude green solid. This was dissolved in chloroform and then precipitated from methanol to give the pure product as a green solid (1.81 g, 0.91 mmol, 58%). Mp >300^{o}C; IR (ATR): ν_{max} = 2958, 1609, 1460, 1333, 1272, 1186, 1094, 895, 788^{-1}; UV-vis (DCM) λ_{max}: 680, 648, 613 nm; ^{1}H NMR (500 MHz, $CDCl_3$): δ_H = 8.16 (s, 8H, Ar *H*), 7.45-7.58 (m, 24H, Ar *H*), 3.36 (sept, 16H, *J* = 6.5 Hz, C*H*), 1.19-1.35 (m, 96H, C*H*3) ppm; ^{13}C NMR (126 MHz, $CDCl_3$): δ_C = 152.8, 151.1, 149.4, 141.8, 140.2, 132.6, 126.9, 124.8, 107.4, 27.8, 24.0, 23.8 ppm; LRMS (LDI-TOF, m/z): calculated $C_{128}H_{144}ZnN_8O_8$: 1985.04, found: 1986.04 [MH+].

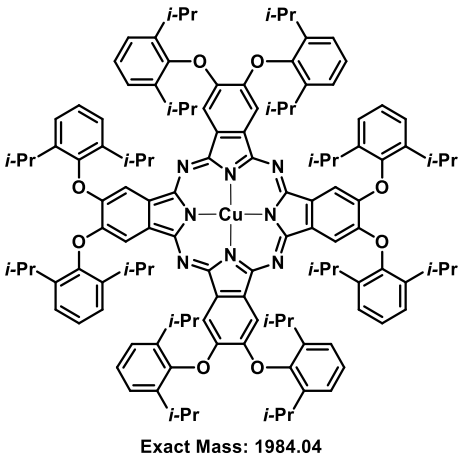

Copper (II) 2,3,9,10,16,17,23,24-Octa-(2,6-diisopropyl)-phenoxy)phthalocyanine

A solution of 4,5-di-(2,6-diisopropyl)-phenoxyphthalonitrile (1.00 g, 0.50 mmol) and a large excess of copper(II) acetate (4.70 g, 24.9 mmol) in dry *n*-pentanol (50ml) was heated at reflux for four hours.

After cooling, the mixture was dissolved in toluene and filtered to remove the excess of copper(II) acetate and the solvent was removed under reduced pressure to give a crude green solid. This was dissolved in chloroform and then precipitated from methanol to give the pure product as a green solid. (0.71 g, 0.36 mmol, 72%). Mp >300°C; IR (ATR): ν_{max} = 2960, 1613, 1462, 1351, 1270, 1184, 1097, 1032, 902, 797 cm^{-1}; UV-vis (DCM) λ_{max}: 681, 613, 409 nm; LRMS (LDI-TOF, m/z): calculated $C_{128}H_{144}CuN_8O_8$: 1984.04, found: 1985.04 [MH+].

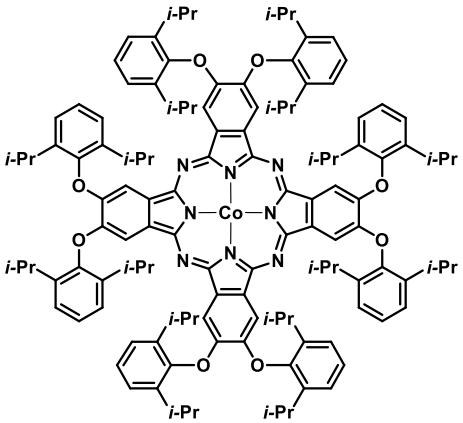

Cobalt (II) 2,3,9,10,16,17,23,24-Octa-(2,6-diisopropyl)-phenoxy)phthalocyanine[13]

A solution of 4,5-di-(2,6-diisopropyl)-phenoxyphthalonitrile (3.00 g, 6.31 mmol) and cobalt(II) acetate (1.08 g, 6.1 mmol) in *N*-methyl-2-pyrrolidone (10 ml) was heated at 165 °C under a nitrogen atmosphere for 16 hours. Upon cooling, the solution was poured into water, and the precipitate formed was filtered to give a crude green solid. This was dissolved in chloroform and then precipitated from methanol to give the pure product as a green solid (2.03 g, 1.02 mmol, 65%). Mp >300°C; IR (ATR): ν_{max} = 2972, 1619, 1458, 1416, 1348, 1190, 1091, 1044, 864, 797, 755 cm^{-1}; UV-vis (DCM) λ_{max}: 668, 642, 602 nm; LRMS (LDI-TOF, m/z): calculated $C_{128}H_{144}CoN_8O_8$: 1980.04, found: 1981.04 [M+].

7.4 Synthetic procedures for phthalocyanine metal-organic framework (MOF) materials

Copper(II) tetrakis(*N*-(4-carboxyphenyl)imido)phthalocyanine MOF materials (Cu(II) TAIPc MOF)

In a typical procedure, copper(II) tetrakis(N-(4-ethylbenzoate)imido)phthalocyanine (0.04 g, 0.03 mmol), and zirconium tetrachloride (0.04 g, 0.17 mmol), were added to a sealed vial with diethylformamide (4 ml), and heated in an enclosed heating block at 150 ^{o}C for 16 hours. Upon cooling, the mixture obtained was filtered, and the solid washed with a small quantity of fresh diethylformamide and dried in air. It was then suspended in acetone and heated to reflux for 24 hours before being filtered once more and dried under vacuum to afford a blue-green solid (0.3 g). Mp > 300 ^{o}C; IR (ATR): ν_{max} = 3219(br), 3034, 1713, 1630, 1317, 1215, 1065, 732 cm^{-1}; UV-vis (1-chloronaphthalene) λ_{max}: 751, 693, 493 nm; BET surface area: 27 m^2/g; TGA analysis: Initial weight loss due to thermal degradation commencing at ~350 °C with a 42% loss of mass below 800 °C.

Copper(II) tetrakis(1,2-dicarboxy)phthalocyanine MOF material (Cu(II) OCPc MOF)

In a typical procedure, copper(II) tetrakis(1,2-dicarboxy)phthalocyanine (0.11 g, 0.12 mmol), and zirconium tetrachloride (0.12 g, 0.52 mmol), were added to a sealed vial with diethylformamide (4 ml), and heated in an enclosed heating block at 150 ^{o}C for 16 hours. Upon cooling, the mixture obtained was filtered, and the solid washed with a small quantity of fresh diethylformamide and dried in air. It was then suspended in acetone and heated to reflux for 24 hours before being filtered once more and dried under vacuum to afford a blue-green solid (0.07g). Mp > 300 ^{o}C; IR (ATR): ν_{max} = 3289(br), 2986, 1732, 1565, 1365, 1317, 1269, 1087, 746 cm^{-1}; UV-vis (1-chloronaphthalene) λ_{max}: 689, 559, 619 nm; BET surface area: 209 m^2/g; TGA analysis: Initial weight loss due to thermal degradation commencing at ~ 300 °C with a 33% loss of mass below 800 °C.

Cobalt(II) tetrakis(1,2-dicarboxy)phthalocyanine MOF material (Co(II) OCPc MOF)

To a vial containing cobalt(II) tetrakis(1,2-dicarboxy)phthalocyanine (0.11 g, 0.12 mmol), and zirconium tetrachloride (0.12 g, 0.52 mmol) was added diethylformamide (4 ml) .The vial was sealed and heated in an enclosed heating block at 150 ^{o}C for 16 hours. Upon cooling, the mixture obtained was filtered, and the solid washed with a small quantity of fresh diethylformamide and dried in air. It was then suspended in acetone and heated to reflux for 24 hours before being filtered once more and dried under vacuum to afford a dark green solid (0.06 g). Mp > 300 ^{o}C; IR (ATR): ν_{max} = 3313(br), 1553, 1452, 1313, 1144, 1092, 752 cm^{-1}; UV-vis (1-chloronaphthalene) λ_{max}: 704, 653, <400 nm; BET surface area: 19 m^2/g.

Manganese(II) tetrakis(1,2-dicarboxy)phthalocyanine MOF material (Mn(II) OCPc MOF)

To a vial containing manganese(II) tetrakis(1,2-dicarboxy)phthalocyanine (0.11 g, 0.12 mmol), and zirconium tetrachloride (0.12 g, 0.52 mmol) was added diethylformamide (4 ml) .The vial was sealed

and heated in an enclosed heating block at 150 °C for 16 hours. Upon cooling, the mixture obtained was filtered, and the solid washed with a small quantity of fresh diethylformamide and dried in air. It was then suspended in acetone and heated to reflux for 24 hours before being filtered once more and dried under vacuum to afford a dark green solid (0.06) Mp > 300 °C; IR (ATR): ν_{max} = 3264(br), 1701, 1618, 1523, 1446, 1377, 1315, 1097, 750 cm^{-1}; UV-vis (1-chloronaphthalene) λ_{max}: 723, 656 <400 nm; BET surface area: 17 m^2/g.

Copper(II) tetracarboxyphthalocyanine MOF material (Cu(II) TCPc MOF)

To a vial containing copper(II) tetracarboxyphthalocyanine (0.11 g, 0.15 mmol), and zirconium tetrachloride (0.15 g, 0.63 mmol) was added diethylformamide (4 ml). The vial was sealed and heated in an enclosed heating block at 150 °C for 16 hours. Upon cooling, the mixture obtained was filtered, and the solid washed with a small quantity of fresh diethylformamide and dried in air. It was then suspended in acetone and heated to reflux for 24 hours before being filtered once more and dried under vacuum to afford a dark green solid (0.08 g). Mp > 300 °C; IR (ATR): ν_{max} = 3223(br), 3080, 2789, 1693, 1585, 1386, 1329, 1088, 737 cm^{-1}; UV-vis (1-chloronaphthalene) λ_{max}: 712, 656, 373 nm; BET surface area: 19 m^2/g.

Copper(II) tetrakis(1,2-dicarboxy) pyrazinoporphyrazine MOF material (Cu(II) OCazaPc MOF)

To a vial containing copper(II) tetrakis(1,2-dicarboxy) pyrazinoporphyrazine (0.11 g, 0.12 mmol), and zirconium tetrachloride (0.12 g, 0.52 mmol) was added diethylformamide (4 ml). The vial was sealed and heated in an enclosed heating block at 150 °C for 16 hours. Upon cooling, the mixture obtained was filtered, and the solid washed with a small quantity of fresh diethylformamide and dried in air. It was then suspended in acetone and heated to reflux for 24 hours before being filtered once more and dried under vacuum to afford a dark green solid (0.7 g). Mp > 300 °C; IR (ATR): ν_{max} = 3280(br), 3003, 2164, 1589, 1364, 1265, 1109, 752 cm^{-1}; UV-vis (1-chloronaphthalene) λ_{max}: 671, 613, <400 nm; BET surface area: 38m^2/g; Initial weight loss due to thermal degradation commencing at ~ 250 °C with a 38% loss of mass below 800 °C.

7.5 Synthetic procedures for tetrabromo monomers

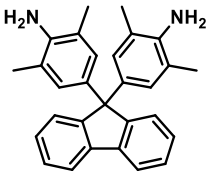

9,9-Bis(4-amino-3,5-dimethylphenyl)fluorene[142]

To 2,6-dimethylaniline (6.05 g, 50 mmol) were added concentrated hydrochloric acid (6.0 ml) and water (3.0 ml). 9-Fluorenone (3.00 g, 16.7 mmol) was added, followed by trifluoromethanesulfonic acid (1.5 ml, 2.55 g, 17.0 mmol). The mixture was heated at reflux under a nitrogen atmosphere for 48 hours, then stirred at room temperature for a further 120 hours. Aqueous sodium hydroxide solution (30 ml, 2M) was added to obtain a thick paste, which was filtered and washed with 2M hydrochloric acid, then acetone. The solid was stirred in aqueous ammonia solution (50 ml, 35%) for 30 minutes, then filtered and dried in air. The crude product was then washed with cold toluene to obtain the product as a white solid (2.56 g, 6.35 mmol, 38 %). Mp >300°C; IR (ATR): ν_{max} = 3399, 3047, 2920, 1618, 1487, 1440, 1300, 1159, 858 cm^{-1}; ^{1}H NMR (500 MHz, DMSO-d_6): δ_H = 7.81-7.85 (m, 2H, Ar *H*), 7.30-7.37 (m, 4H, Ar *H*), 7.24-7.28 (m, 2H, Ar *H*), 4.39 (s, 4H, NH_2), 1.94 (s, 12H, CH_3) ppm; ^{13}C NMR (126 MHz, DMSO-d_6): δ_C = 152.9, 143.1, 139.7, 133.6, 127.8, 127.6, 127.3, 126.5, 120.6, 120.5, 64.1, 18.6.; HRMS (ESI, m/z): calculated $C_{29}H_{28}N_2$: 404.2325, found: 404.2323 [MH+].

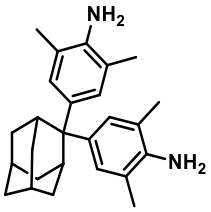

2,2-Bis(4-amino-3,5-dimethylphenyl)adamantane

A mixture of 2-adamantanone (2.00 g, 13.3 mmol), 2,6-dimethylaniline (4.8 ml, 4.72 g, 39.0 mmol) and 2,6-dimethylaniline hydrochloride (4.62 g, 29.3 mmol) was thoroughly combined and heated to 180 °C under a nitrogen atmosphere for 72 hours. After cooling to 140 °C, water (20 ml) was added and the mixture heated for a further 1 hour. It was then poured into aqueous ammonia solution (50 ml, 35%) and extracted with chloroform (3 x 50 ml). The combined organic phases were washed with water (3 x 50 ml), dried with magnesium sulphate and the solvent removed under reduced pressure to give a brown oil. This was purified by column chromatography using a Hexane: Ethyl acetate (3:2) eluent to obtain a pale brown solid, which was washed with cold methanol to give the product as an off-white solid. (0.47 g, 1.25 mmol, 9%). Mp >300°C; IR (ATR): ν_{max} = 3379, 2904, 2851, 2362, 1734, 1616, 1489, 1292, 1150, 864, 742cm^{-1}; ^{1}H NMR (500 MHz, $CDCl_3$): δ_H = 6.96 (s, 4H, Ar *H*), 3.45 (s, 4H, NH_2), 2.14 (s, 12H, CH_3), 2.07-2.11 (m, 5H, C*H*), 1.66-2.81 (s, 9H, CH_2) ppm; ^{13}C NMR (126 MHz, $CDCl_3$):

δ_C = 139.1, 139.0, 125.5, 121.7, 48.8, 38.3, 33.5, 31.9, 27.7, 18.2.ppm; LRMS (LDI-TOF, m/z): calculated $C_{26}H_{34}N_2$: 375.2795, found: 375.2787 [MH+].

General procedure for synthesis of bis-imides from commercial diamines

A stirring solution of two equivalents of 4,5-dibromophthalic anhydride and one equivalent of the appropriate diamine in anhydrous *N,N*-dimethylformamide was heated to reflux until the reaction was complete. Upon cooling, the solution was poured into water in order to precipitate a solid. This was filtered off, washed with water and other solvents if appropriate and dried in air. The solid product was generally obtained without further purification.

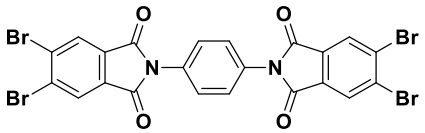

1,4-bis(4,5-dibromophthalimide)-benzene

Following the general procedure, 4,5-dibromophthalic anhydride (1.00 g, 3.2 mmol) and *p*-phenylenediamine (0.17 g, 1.6 mmol) in dimethylformamide (10 ml) was heated to reflux for 16 hrs under a nitrogen atmosphere. Upon cooling, the solution was poured into water in order to precipitate a beige solid. This was filtered off, washed with water and dried in air to afford the product without further purification. Mp >300^{o}C; IR (ATR): ν_{max} = 3286, 2996, 2342, 1769, 1705, 1349, 1317, 756cm^{-1}.

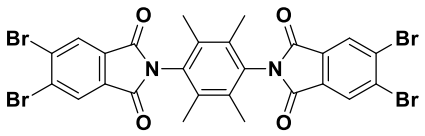

2,3,5,6-tetramethyl-1,4-bis(4,5-dibromophthalimide)-benzene

Following the general procedure, 4,5-dibromophthalic anhydride (0.44 g, 1.4 mmol) and 2,3,5,6-tetramethylphenylenediamine (0.12 g, 0.7 mmol) in dimethylformamide (10 ml) was heated to reflux for 16 hrs under a nitrogen atmosphere. Upon cooling, the solution was poured into water in order to precipitate a beige solid. This was filtered off, washed with water and dried in air to afford the product without further purification. Mp >300^{o}C; IR (ATR): ν_{max} = 3381, 3008, 2382, 1776, 1711, 1369, 1321,

746cm^{-1}; ^{1}H NMR (500 MHz, DMSO-d_6): δ_H = 8.43 (s, 4H, Ar *H*), 2.03 (s, 12 H, C*H*$_3$) ppm; ^{13}C NMR (126 MHz, DMSO-d_6): δ_C = 162.3, 133.9, 131.6, 131.2, 130.6, 128.9, 15.1 ppm.

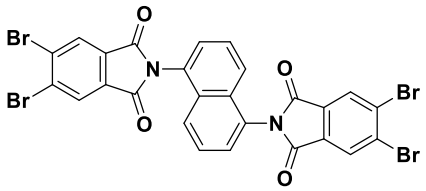

1,5-bis(4,5-dibromophthalimide)-naphthalene

Following the general procedure, 4,5-dibromophthalic anhydride (1.50 g, 4.9 mmol) and 1,5-diaminonaphthalene (0.39 g, 2.4 mmol) in anhydrous dimethylformamide (20 ml) was heated to reflux for 16 hrs under a nitrogen atmosphere. Upon cooling, the solution was poured into water in order to precipitate an off-white solid. This was filtered off, washed with water and dried in air to afford the product without further purification. Mp >300^{o}C; IR (ATR): ν_{max} = 3137, 3008, 2926, 1771, 1721, 1465, 1257, 1197, 734cm^{-1}; ^{1}H NMR (500 MHz, DMSO-d_6): δ_H = 8.44 (s, 4H, Ar *H*), 8.08-8.12 (m, 2 H, Ar *H*), 7.73-7.77 (m, 2 H, Ar *H*), 7.67-7.71 (m, 2 H, Ar *H*) ppm; ^{13}C NMR (126 MHz, DMSO-d_6): 166.1, 138.4, 133.6, 131.1, 129.3, 128.7, 127.0, 126.3, 121.4 ppm.

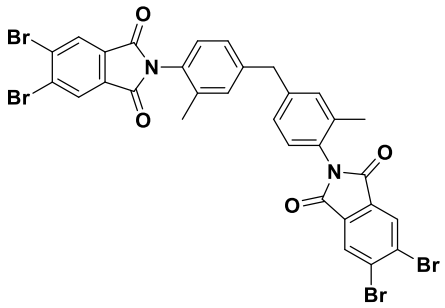

4,4'-bis-(3,4-dibromophthalimide)-3,3'-dimethyldiphenylmethane

Following the general procedure, 4,5-dibromophthalic anhydride (1.50 g, 4.9 mmol) and 4,4'-diamino-3,3'-dimethyldiphenylmethane (0.56 g, 2.4 mmol) in anhydrous dimethylformamide 20 ml) was heated to reflux for 16 hrs under a nitrogen atmosphere. Upon cooling, the solution was poured into water in order to precipitate a beige solid. This was filtered off, washed with water and dried in air to afford the product without further purification. Mp >300^{o}C; IR (ATR): ν_{max} = 2980, 2864, 1778, 1710, 1502, 1368, 1301, 1107, 1032, 739 cm^{-1}; ^{1}H NMR (500 MHz, DMSO-d_6): δ_H = 8.36 (s, 4H, Ar *H*), 7.31-7.34 (m, 2H, Ar *H*), 7.23-7.29 (m, 4H, Ar *H*), 4.02 (s, 2H, C*H*$_2$) 2.11 (s, 6H, C*H*$_3$) ppm; ^{13}C NMR (126 MHz, DMSO-d_6): δ_C = 165.8, 142.6, 136.8, 132.6, 131.5, 131.2, 129.6, 129.1, 129.0, 127.5, 40.3, 17.9 ppm.

General procedure for synthesis of bis-imides from synthesised diamines

In a typical reaction, the synthesised diamine was added with 4,5-dibromophthalic anhydride to glacial acetic acid and heated to reflux under a nitrogen atmosphere for 16 hours. Upon cooling, the solution was poured into water to precipitate a solid, which was filtered off, washed with water, and dried in air.

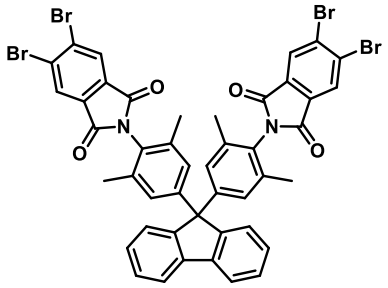

9,9-Bis(4-(4,5-dibromophthalimide)-3,5-dimethylphenyl)fluorene

Following the general procedure, 9,9-bis(4-amino-3,5-dimethylphenyl)fluorene (0.60 g, 1.48 mmol) and 4,5-dibromophthalimide (0.90 g, 2.96 mmol) were refluxed in glacial acetic acid (40 ml). Following work-up, the product was obtained as an off-white solid without further purification (1.34 g, 1.37 mmol, 92%). Mp >300°C; IR (ATR): ν_{max} = 3084, 1720, 1485, 1367, 1308, 1215, 1112, 850 cm^{-1}; ^{1}H NMR (500 MHz, DMSO-d_6): δ_H = 8.38 (s, 4H, Ar *H*), 7.97 (d, *J* = 7.6 Hz, 2H, Ar *H*), 7.64 (d, *J* = 7.6 Hz, 2H, Ar *H*), 7.46 (td, *J* = 7.6, 1.1 Hz, 2H, Ar *H*) 7.38 (td, *J* = 7.6, 1.1 Hz, 2H, Ar *H*), 7.02 (s, 4H, Ar *H*) 1.99 (s, 12H, CH_3) ppm; ^{13}C NMR (126 MHz, DMSO-d_6): δ_C = 165.5, 150.2, 147.0, 140.0, 137.2, 132.1, 131.6, 129.3, 128.9, 128.7, 128.5, 127.7, 126.8, 121.2, 65.0, 18.3. ppm; LRMS (LDI-TOF, m/z): calculated $C_{45}H_{28}Br_4N_2O_4$: 975.88, found: 976.88 [MH+].

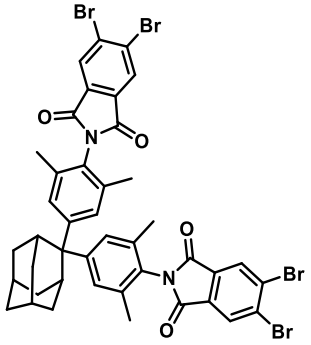

2,2-Bis(4-(4,5-dibromophthalimide)-3,5-dimethylphenyl)adamantane

Following the general procedure, 2,2-bis(4-amino-3,5-dimethylphenyl)adamantane (0.50 g, 1.34 mmol) and 4,5-dibromophthalimide (0.81 g, 2.68 mmol) were refluxed in glacial acetic acid (30 ml). Following work-up, the product was obtained as an off-white solid without further purification (1.10

g, 1.15 mmol, 86%). Mp >300°C; IR (ATR): ν_{max} = 3680, 2972, 2864, 1710, 1369, 1055, 1031, 1011, 844, 746cm^{-1}; ^{1}H NMR (500 MHz, $CDCl_3$): δ_H = 8.21 (s, 4H, Ar *H*), 7.22 (s, 4H, Ar *H*), 4.02 (s, 2H, C*H*$_2$) 2.06-2.13 (m, 5H, C*H*), 2.11 (s, 12H, C*H*$_3$), 1.71-1.87 (m, 9H, C*H*$_2$) ppm; ^{13}C NMR (126 MHz, $CDCl_3$): δ_C = 175.2, 165.32, 148.9, 136.3, 131.7, 128.9, 126.4, 126.3, 50.1, 38.0, 33.3, 32.3, 27.4, 18.6 ppm; LRMS (LDI-TOF, m/z): calculated $C_{42}H_{34}Br_4N_2O_4$: 945.93, found: 946.93 [MH+].

7.6 Synthetic procedures for phthalocyanine network polymers

General procedure

In a typical reaction, copper cyanide was added in portions to a solution of the tetrabromo bis-imide in anhydrous *N,N*-dimethylformamide and the solution was heated at 160 °C under nitrogen for 16 hours. Upon cooling, the mixture was precipitated into a 10% aqueous ammonia solution, and the solid filtered off, washed with further a 10% aqueous ammonia solution until the washings were clear, then dried in air. The solid was then suspended in a variety of different solvents and heated at reflux for 24 hours, before being filtered and dried to obtain the desired network polymer.

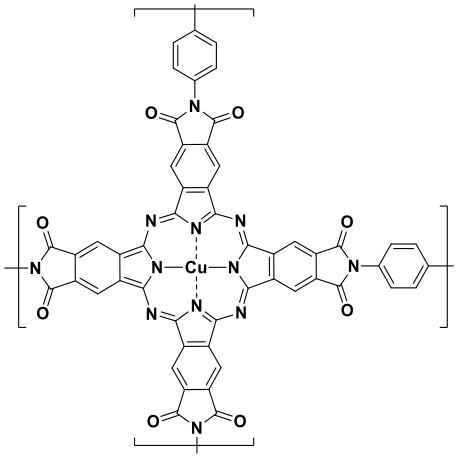

1,4-bisimidobenzene phthalocyanine copper(II) polymer

Following the general procedure, to a suspension of 1,4-bis(4,5-dibromopthalimide)-benzene (1.00 g, 1.3 mmol), in anhydrous dimethylformamide (40 ml) was added copper cyanide (0.70 g, 7.8 mmol) and the solution heated to 160 °C under a nitrogen atmosphere for 16 hrs. Upon work-up, a dark solid was obtained. This was suspended in acetone and heated to reflux for 24 hours, before being filtered and dried, and then refluxed again in methanol and dried in air to afford the product as a dark solid. (0.62 g, 83%). Mp > 300 °C; IR (ATR): ν_{max} = 3258, 1717, 1597, 1514, 1369, 1122, 1101, 741 cm^{-1}; UV-vis (1-chloronaphthalene) λ_{max}: 739, 651, <400 nm; BET surface area: 7 m^2/g.

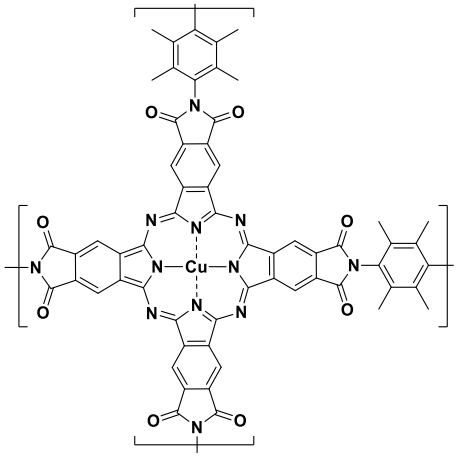

1,4-bisimido-2,3,5,6-tetramethylbenzene phthalocyanine copper(II) polymer

Following the general procedure, to a solution of 2,3,5,6-tetramethyl-1,4-bis(4,5-dibromopthalimide)-benzene (1.00 g, 1.5 mmol), in anhydrous dimethylformamide (40 ml) was added copper cyanide (0.75 g, 8.4 mmol) and the solution heated to 160 ^{o}C under a nitrogen atmosphere for 16 hrs. Upon work-up, a dark solid was obtained. This was suspended in acetone and heated to reflux for 24 hours, before being filtered and dried, and then refluxed again in methanol and dried in air to afford the product as a dark solid. (0.56 g, 77%). Mp > 300 ^{o}C; IR (ATR): ν_{max} = 3164, 1726, 1610, 1534, 1372, 1123, 1081, 835, 741 cm^{-1}; UV-vis (1-chloronaphthalene) λ_{max}: 734, 648, <400 nm; BET surface area: 17 m^2/g.

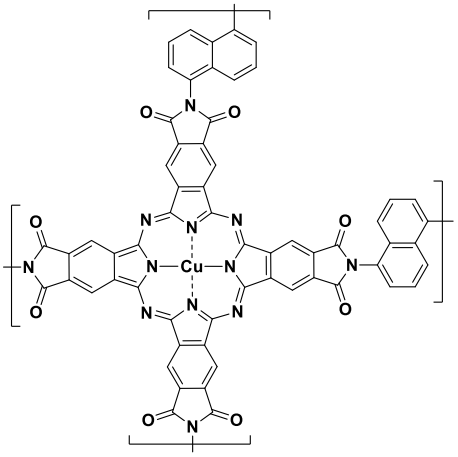

1,5-bisimidonaphthalene phthalocyanine copper(II) polymer

Following the general procedure, to a solution of 1,5-bis(4,5-dibromophthalimide)-naphthalene (1.00 g, 1.4 mmol), in anhydrous dimethylformamide (40 ml) was added copper cyanide (0.73 g, 8.1 mmol) and the solution heated to 160 °C under a nitrogen atmosphere for 16 hrs. Upon work-up, a dark solid was obtained. This was suspended in acetone and heated to reflux for 24 hours, before being filtered and dried, and then refluxed again in methanol and dried in air to afford the product as a dark solid. (0.51 g, 71%). Mp > 300 °C; IR (ATR): ν_{max} = 3184, 2959, 2885, 1734, 1609, 1324, 1114, 1008, 763 cm^{-1}; UV-vis (1-chloronaphthalene) λ_{max}: 721, 638, 343 nm; BET surface area: 20 m^2/g.

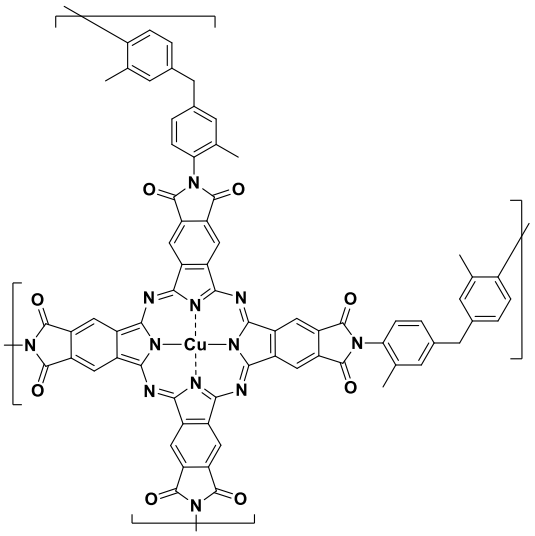

4,4'-bisimido-3,3'-dimethyldiphenylmethane phthalocyanine copper(II) polymer

Following the general procedure, to a solution of 4,4'-bis(4,5-dibromophthalimide)-3,3'-dimethyldiphenylmethane (1.00 g, 1.2 mmol), in anhydrous dimethylformamide (40 ml) was added copper cyanide (0.65 g, 7.2 mmol) and the solution heated to 160 °C under a nitrogen atmosphere for 16 hrs. Upon work-up, a dark solid was obtained. This was suspended in acetone and heated to reflux for 24 hours, before being filtered and dried, and then refluxed again in methanol and dried in air to afford the product as a dark solid. (0.32 g, 43%). Mp > 300 °C; IR (ATR): ν_{max} = 3230, 2899, 1764, 1708, 1414, 1154, 1073, 762 cm^{-1}; UV-vis (1-chloronaphthalene) λ_{max}: 729, 641, <400 nm; BET surface area: 19 m^2/g.

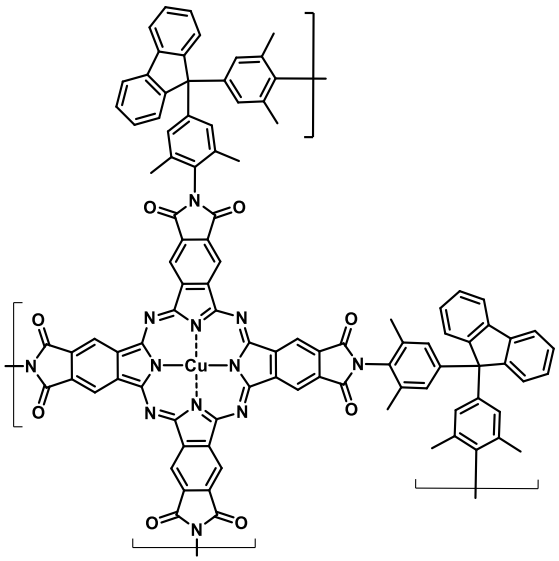

9,9-Bis(4-imido-3,5-dimethylphenyl)fluorene phthalocyanine copper(II) polymer

Following the general procedure, to a solution of 9,9-bis(4-(4,5-dibromophthalimide)-3,5-dimethylphenyl)fluorene (0.30 g, 0.31 mmol), in anhydrous dimethylformamide (15 ml) was added copper cyanide (0.17 g, 1.86 mmol) and the solution heated to 160 °C under a nitrogen atmosphere for 16 hrs. Upon work-up, a green solid was obtained. This was suspended in acetone and heated to reflux for 24 hours, before being filtered and dried, and then refluxed again in chloroform and dried in air to afford the product as a green solid (0.14 g, 58%). Mp > 300 °C; IR (ATR): ν_{max} = 3260, 3061, 2364, 1776, 1719, 1593, 1362, 1113, 728 cm^{-1}; UV-vis (1-chloronaphthalene) λ_{max}: 721, 659, <400 nm; BET surface area: 183 m^2/g. Initial weight loss due to thermal degradation commencing at ~ 200 °C with a 49% loss of mass below 800 °C.

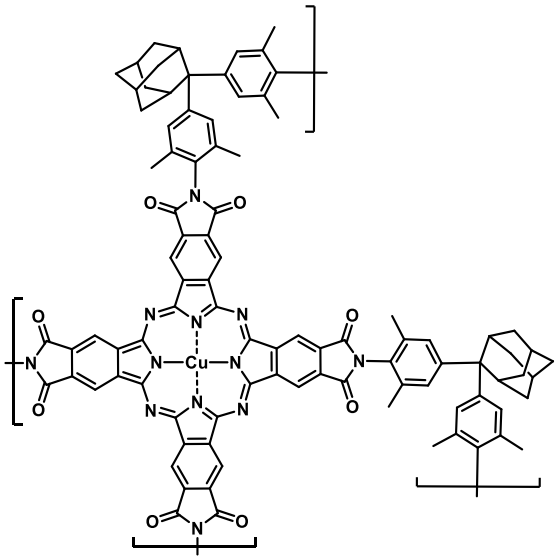

2,2-Bis(4-imido-3,5-dimethylphenyl)adamantane phthalocyanine copper(II) polymer

Following the general procedure, to a solution of 2,2-bis(4-(4,5-dibromophthalimide)-3,5-dimethylphenyl)adamantane (0.40 g, 0.42 mmol), in anhydrous dimethylformamide (15 ml) was added copper cyanide (0.23 g, 2.54 mmol) and the solution heated to 160 °C under a nitrogen atmosphere for 16 hrs. Upon work-up, a green solid was obtained. This was suspended in acetone and heated to reflux for 24 hours, before being filtered and dried, and then refluxed again in chloroform and dried in air to afford the product as a green solid (0.17 g, 53%). Mp > 300 °C; IR (ATR): ν_{max} = 3275, 2912, 2653, 1776, 1717, 1593, 1360, 1228, 1113, 739 cm^{-1}; UV-vis (1-chloronaphthalene) λ_{max}: 725, 640, <400 nm; BET surface area: 236 m^2/g. Initial weight loss due to thermal degradation commencing at ~ 200 °C with a 43% loss of mass below 800 °C.

7.7 Synthetic procedures for phthalonitrile pyrazine monomers

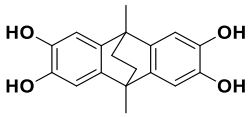

2,3,6,7-Tetrahydroxy-9,10-dimethyl-9,10-ethanoanthracene[165]

To ice cooled sulphuric acid was added powdered 1,2-benzenediol, freshly recrystallised from toluene, to give a colourless suspension. To this, 2,5-hexanedione was added drop-wise to form a green mixture. After 1 hour of stirring, the ice bath was removed, and the mixture was stirred for an additional 5 days at room temperature. The precipitate formed was then removed from the acid by filtration, washed with water and dried in air to afford the product as an off-white solid. Mp >300°C; IR (ATR): ν_{max} = 3468, 3302, 2947, 1599, 1447, 1294, 1134, 812, 797 cm^{-1}; ^{1}H NMR (500 MHz, DMSO-d_6): δ_H = 8.40 (s, 4H, O*H*), 6.22 (s, 4H, Ar *H*), 1.69 (s, 4H, CH_2), 1.41 (s, 6H, CH_3) ppm; ^{13}C NMR (126 MHz, $CDCl_3$): δ_C = 142.2, 138.1, 109.2, 21.2, 19.0 ppm; HRMS (EI, m/z): calculated $C_{18}H_{18}O_4$: 298.11996, found: 298.11923 [M+].

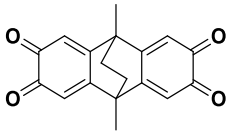

2,3,6,7-Tetraketone-9,10-dimethyl-9,10-ethanoanthrabisquinone[166]

To a 3:1 (v/v) solution of acetonitrile:water (550 ml) was added 2,3,6,7-tetrahydroxy-9,10-dimethyl-9,10-ethanoanthracene (5.50 18.5 mmol) and ammonium cerium nitrate (40.50 g, 73.8 mmol) in portions, and the mixture stirred at room temperature for 3 hours. The acetonitrile was then removed

under reduced pressure, brine (200 ml) was added, and the mixture was extracted with chloroform (3 x 150 ml). The organic phase was washed with water (3 x 150 ml), dried with magnesium sulphate, and the solvent removed under reduced pressure. The solid obtained was washed with water to give the product as a green solid (3.27 g, 11.1 mmol, 60%) Mp >300°C; IR (ATR): ν_{max} = 3064, 2978, 1657, 1566, 1458, 1333, 1273, 891, 802 cm^{-1}; ^{1}H NMR (500 MHz, DMSO-d_6): δ_H = 6.29 (s, 4H, Ar *H*), 2.06 (s, 4H, CH_2), 1.54 (s, 6H, CH_3) ppm; ^{13}C NMR (126 MHz, $CDCl_3$): δ_C = 179.5, 155.0, 121.9, 41.1, 32.3, 18.1 ppm; HRMS (EI, m/z): calculated $C_{18}H_{14}O_4$: 294.0887, found: 295.0979 [M+].

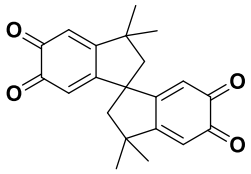

5,5',6,6'-Tetraketone-3,3,3',3'-tetramethyl-1,1'-spirobisindane[166]

To a 3:1 (v/v) solution of acetonitrile:water (800 ml) was added 5,5',6,6'-tetrahydroxy-3,3,3',3'-tetramethyl-1,1'-spirobisindane (5.00 14.7 mmol) and ammonium cerium nitrate (33.1 g, 60.3 mmol) in portions, and the mixture stirred at room temperature for 3 hours. The acetonitrile was then removed under reduced pressure, brine (200 ml) was added, and the mixture was extracted with chloroform (3 x 150 ml). The organic phase was washed with water (3 x 150 ml), dried with magnesium sulphate, and the solvent removed under reduced pressure. The solid obtained was washed with water to give the product as a red-orange solid (4.14 g, 12.3 mmol, 84%) Mp >300°C; IR (ATR): ν_{max} = 2968, 1651, 1587, 1350, 1260, 1159, 846, 758 cm^{-1}; ^{1}H NMR (500 MHz, $CDCl_3$): δ_H = 6.29 (s, 2H, Ar *H*), 6.19 (s, 2H, Ar *H*), 2.40 (d, *J* = 13.4 Hz, 2H, CH_2), 2.26 (d, *J* = 13.4 Hz, 2H, CH_2), 1.43 (s, 6H, CH_3), 1.41 (s, 6H, CH_3) ppm; ^{13}C NMR (126 MHz, $CDCl_3$): δ_C = 178.4, 178.3, 167.8, 167.0, 125.0, 122.0, 56.6, 54.8, 43.1, 30.3, 28.6 ppm; HRMS (EI, m/z): calculated $C_{21}H_{20}O_4$: 336.1356, found: 336.1360 [M+].

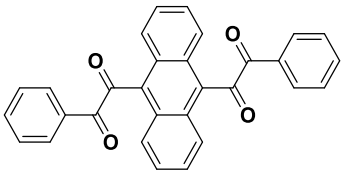

9,10-(1-Phenylethane-1,2-dione) anthracene

To a solution of 9,10-bis(phenylethynyl)anthracene (2.00 g, 5.3 mmol) in acetone (315 ml) was added a solution of sodium hydrogen carbonate (0.08 g 0.95 mmol) in water (190 ml). Potassium

permanganate (8.00 g, 50.6 mmol) was then added slowly with vigorous stirring, and the mixture stirred at room temperature for 72 hours. Sodium nitrite (18.0 g, 0.26 mol) was added, followed by sulphuric acid (10%, 95 ml) and finally concentrated sulphuric acid (1.1 ml). To this mixture was added sodium chloride (300 g, 5.1 mol). Following vigorous stirring, the solids were filtered off, and the filtrate extracted with dichloromethane (3 x 200 ml). The organic phase was washed with water (3 x 150 ml), dried with magnesium sulphate, and the solvent removed under reduced pressure. The resulting solid was washed with cold methanol to afford the product as a yellow solid (0.96 g, 2.2 mmol, 41%). Mp: 234-236°C; IR (ATR): ν_{max} = 3063, 2924, 1676, 1442, 1261, 1179, 1101, 975, 844, 732 cm^{-1}; ^{1}H NMR (500 MHz, $CDCl_3$): δ_H = 8.40 (d, *J* = 6.9, Hz, 4H, Ar *H*), 8.01 (dd, J = 6.8, 3.2 Hz, 4H, Ar *H*), 7.80 (m, 2H, Ar *H*), 7.67 (m, 4H, Ar *H*), 7.52 (dd, J = 6.8, 3.2 Hz, 4H, Ar *H*) ppm; ^{13}C NMR (126 MHz, $CDCl_3$): δ_C 198.03, 190.08, 135.10, 135.00, 131.86, 130.80, 129.27, 128.90, 127.58, 125.12 ppm; HRMS (ESI, m/z): calculated $C_{30}H_{18}O_4$: 442.1278, found: 443.1276 [MH+].

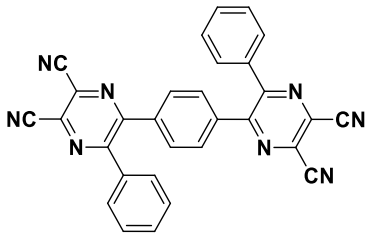

2,2'-(1,4-Phenylene)bis(3-phenyl-5,6-dicyanopyrazine)[167]

To glacial acetic acid (150 ml) was added 2,2-(1,4-phenylene)bis(1-phenylethane-1,2-dione) (1.71 g, 5.0 mmol) and diaminomaleonitrile (1.08 g, 10.0 mmol) and the solution was heated to reflux for 6 hrs under a nitrogen atmosphere. Upon cooling, a precipitate formed, which was filtered off, washed with water and dried in air to afford the product without further purification as a pale yellow solid (2.32 g, 4.8 mmol, 96%). Mp:>300°C; IR (ATR): ν_{max} = 2358, 1508, 1373, 1229, 1194, 1078, 854, 771, 696 cm^{-1}; ^{1}H NMR (500 MHz, DMSO-d_6): δ_H = 7.52 (s, 4H, Ar *H*), 7.42-7.50 (m, 10H, Ar *H*) ppm; ^{13}C NMR (101 MHz, DMSO-d_6): δ_C 155.4, 154.3, 137.9, 135.7, 131.3, 130.9, 130.5, 130.4, 130.2, 129.2, 114.6, 114.5 ppm; LRMS (EI, m/z): calculated $C_{32}H_{16}N_6$: 486.1, found: 486.1 [M+].

7.8 Synthetic procedures for pyrazinoporphyrazine network polymers

General procedure

In a typical reaction, the bis(dicyanopyrazine) monomer and metal salt were added to sulfolane and heated. 1,8-Diazabicyclo-[5,4,0]-undecene-7 was then added, and the solution refluxed. Upon cooling, the mixture was poured into water, and the solid formed filtered off, washed with water and acetone, and dried. The product was then refluxed in additional solvents for 24 hour periods.

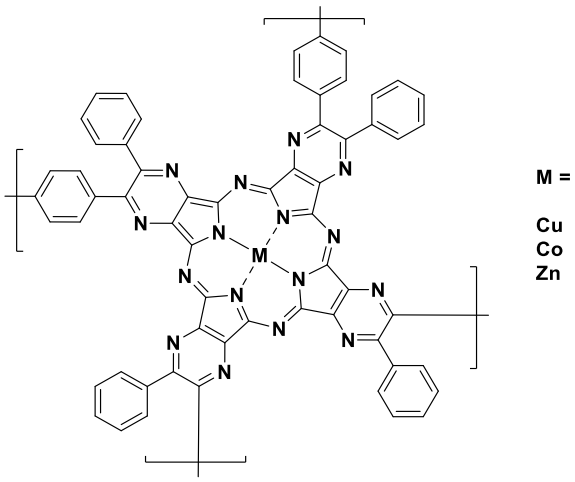

Octaphenylpyrazinoporphyrazine copper(II) polymer

To sulfolane (15 ml) was added 2,2'-(1,4-phenylene)bis(3-phenyl-5,6-dicyanopyrazine) (1.00 g, 2.1 mmol) and copper(II) acetate monohydrate (0.30 g, 1.50 mmol), and the solution heated to 135 °C. 1,8-Diazabicyclo-[5,4,0]-undecene-7 (0.05 ml, 0.33 mmol) was then added, and the solution heated for a further 2 hours. Upon cooling, the mixture was poured into water, and the precipitate formed was filtered off, washed with further water and acetone, and dried. The solid was then refluxed in acetone and then chloroform, for 24 hours each time, to obtain a dark green solid (0.80 g, 74%). Mp > 300 °C; IR (ATR): ν_{max} = 3183, 3022, 1567, 1447, 1342, 1234, 1113, 950, 694 cm^{-1}; UV-vis (DMSO) $\lambda_{max:}$ 689, 658, 617 nm; BET surface area: 4 m^2/g; Initial weight loss due to thermal degradation commencing at ~ 200 °C with a 34% loss of mass below 800 °C.

Octaphenylpyrazinoporphyrazine cobalt(II) polymer

To sulfolane (15 ml) was added 2,2'-(1,4-phenylene)bis(3-phenyl-5,6-dicyanopyrazine) (1.00 g, 2.1 mmol) and cobalt(II) acetate tetrahydrate (0.37 g, 1.50 mmol), and the solution heated to 135 °C. 1,8-Diazabicyclo-[5,4,0]-undecene-7 (0.05 ml, 0.33 mmol) was then added, and the solution heated for a

further 2 hours. Upon cooling, the mixture was poured into water, and the precipitate formed was filtered off, washed with further water and acetone, and dried. The solid was then refluxed in acetone and then chloroform, for 24 hours each time, to obtain a dark green solid (0.73 g, 69%). Mp > 300 °C; IR (ATR): ν_{max} = 3216, 3049, 1602, 1556, 1344, 1238, 1155, 1074, 694 cm^{-1}; UV-vis (DMSO) λ_{max}: 688, 621, 460 nm; BET surface area: 69 m^2/g; Initial weight loss due to thermal degradation commencing at ~ 220 °C with a 37% loss of mass below 800 °C.

Octaphenylpyrazinoporphyrazine zinc (II) polymer

To sulfolane (15 ml) was added 2,2'-(1,4-phenylene)bis(3-phenyl-5,6-dicyanopyrazine) (1.00 g, 2.1 mmol) and zinc(II) acetate dihydrate (0.33 g, 1.50 mmol), and the solution heated to 135 °C. 1,8-Diazabicyclo-[5,4,0]-undecene-7 (0.05 ml, 0.33 mmol) was then added, and the solution heated for a further 2 hours. Upon cooling, the mixture was poured into water, and the precipitate formed was filtered off, washed with further water and acetone, and dried. The solid was then refluxed in acetone and then chloroform, for 24 hours each time, to obtain a dark green solid (0.70 g, 65%). Mp > 300 °C; IR (ATR): ν_{max} = 3296, 1670, 1612, 1346, 1246, 1165, 1107, 945, 696 cm^{-1}; UV-vis (DMSO) λ_{max}: 684, 612, <400 nm; BET surface area: 55 m^2/g; Initial weight loss due to thermal degradation commencing at ~ 200 °C with a 41% loss of mass below 800 °C.

7.9 Synthesis procedures for fluorinated tetraphenylporphyrins

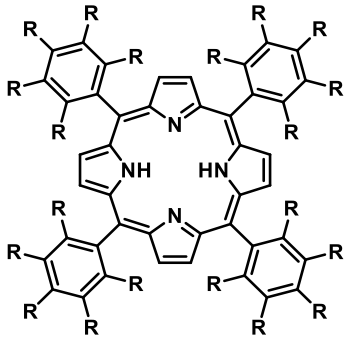

R = F, H

General procedures

Procedure A – To propionic acid were added pyrrole and the corresponding fluorinated benzaldehyde, and the solution was heated at a temperature of 140 °C for 30 mins. Upon cooling, the solution was

filtered, and the solid was washed with methanol and dried in air to afford the product as a lustrous purple solid.

Procedure B - To propionic acid were added pyrrole and the corresponding fluorinated benzaldehyde, and the solution was heated at a temperature of 140 °C for 30 mins. Upon cooling methanol was added, and the solution was cooled at freezer temperature for 24 hours. The solution was then filtered to obtain a brown-purple solid, which was washed with methanol and dried in air to afford the product as a purple solid.

Procedure C - To propionic acid were added pyrrole and the corresponding fluorinated benzaldehyde, and the solution was heated at a temperature of 140 °C for 30 mins**.** Upon cooling, the solvent was removed under reduced pressure to leave a dark brown residue. This was purified by column chromatography using with CH_2Cl_2:Hexane (1:1 v/v) as eluent, to obtain, upon removal of solvent, a purple solid.

5,10,15,20-tetrakis(2-fluorophenyl)porphyrin[168]

Following procedure A, to propionic acid (50 ml) was added pyrrole (0.81 ml, 0.78 g, 11.6 mmol) and 2-fluorobenzaldehyde (0.79ml, 0.93 g, 7.5 mmol). Upon work-up, a purple solid was obtained (0.19 g, 0.28 mmol, 15 %). Mp >300°C; IR (ATR): ν_{max} = 3322, 1603, 1578, 1543, 1478, 1312, 1274, 1173, 991, 782 cm^{-1}; UV-vis (DCM/MeOH) λ_{max}: 587, 509, 411 nm; ^{1}H NMR (500 MHz, CD_2Cl_2): δ_H = 8.97 (s, 4H, Ar *H*), 8.17-8.22 (m, 4H, Ar *H*), 7.85-7.92 (m, 4H, Ar *H*), 7.59-7.66 (m, 8H, Ar *H*), -2.79 (s, 2H, N*H*) ppm; HRMS (LDI-TOF, m/z): calculated $C_{44}H_{26}F_4N_4$: 686.20881, found: cluster of peaks at 686.20916 [M+].

5,10,15,20-tetrakis(3-fluorophenyl)porphyrin[168]

Following procedure B, to propionic acid (50 ml) was added pyrrole (0.84 ml, 0.81 g, 12.1 mmol) and 3-fluorobenzaldehyde (0.93 ml, 1.09 g, 8.8 mmol). Upon work-up, a purple solid was obtained (0.33 g, 0.48 mmol, 22%). Mp >300°C; IR (ATR): ν_{max} = 3308, 1611, 1569, 1512, 1474, 1341, 1273, 1123, 979, 790 cm^{-1}; UV-vis (DCM/MeOH) λ_{max}: 587, 512, 489 nm; ^{1}H NMR (500 MHz, CD_2Cl_2): δ_H = 8.95 (s, 8H, Ar *H*), 8.04-8.10 (m, 4H, Ar *H*), 7.96-8.03 (m, 4H, Ar *H*), 7.76-7.82 (m, 4H, Ar *H*), 7.55-7.61 (m, 4H, Ar *H*), -2.84 (s, 2H, N*H*) ppm; HRMS (LDI-TOF, m/z): calculated $C_{44}H_{26}F_4N_4$: 686.20881, found: cluster of peaks at 686.20999 [M+].

5,10,15,20-tetrakis(4-fluorophenyl)porphyrin[168]

Following procedure A, to propionic acid (50 ml) was added pyrrole (0.84 ml, 0.81 g, 12.1 mmol) and 4-fluorobenzaldehyde (0.86 ml, 1.00 g, 8.1 mmol). Upon work-up, a purple solid was obtained (0.35 g,

0.51 mmol, 26 %). Mp >300°C; IR (ATR): ν_{max} = 3310, 3042, 1599, 1504, 1468, 1348, 1219, 1153, 966, 787 cm^{-1}; UV-vis (DCM/MeOH) λ_{max}: 589, 513, 413, nm; ^{1}H NMR (500 MHz, CD_2Cl_2): δ_H = 8.90 (s, 8H, Ar *H*), 8.23 (s, 8H, Ar *H*), 7.53 (s, 8H, Ar *H*), -2.94 (s, 2H, N*H*) ppm; HRMS (LDI-TOF, m/z): calculated $C_{44}H_{26}F_4N_4$: 686.20881, found: cluster of peaks at 686.20889 [M+].

5,10,15,20-tetrakis(2,3-difluorophenyl)porphyrin

Following procedure B, to propionic acid (75 ml) was added pyrrole (1.58 ml, 1.53 g, 22.8 mmol) and 2,3-difluorobenzaldehyde (1.52 ml, 1.98 g, 13.9 mmol). Upon work-up, a purple solid was obtained (0.17 g, 0.22 mmol, 6%). Mp >300°C; IR (ATR): ν_{max} = 3309, 1622, 1598, 1472, 1335, 1271, 1161, 1053, 924, 791 cm^{-1}; UV-vis (DCM/MeOH) λ_{max}: 587, 508, 413 nm; ^{1}H NMR (500 MHz, CD_2Cl_2): δ_H = 8.94 (s, 8H, Ar *H*), 7.92-8.03 (m, 4H, Ar *H*), 7.70-7.77 (m, 4H, Ar *H*), 7.55-7.62 (m, 4H, Ar *H*), -2.85 (s, 2H, N*H*) ppm; LRMS (LDI-TOF, m/z): calculated $C_{44}H_{22}F_8N_4$: 758.17112, found: cluster of peaks at 758.17195 [M+].

5,10,15,20-tetrakis(2,4-difluorophenyl)porphyrin[169]

Following procedure A, to propionic acid (150 ml) was added pyrrole (2.94 ml, 2.84 g, 42.3 mmol) and 2,4-difluorobenzaldehyde (3.16 ml, 4.11 g, 28.9 mmol). Upon work-up, a purple solid was obtained (0.77 g, 1.01 mmol, 14 %). Mp >300°C; IR (ATR): ν_{max} 3314, 3022, 1600, 1558, 1465, 1328, 1260, 1153, 1087, 982, 774 cm^{-1}; UV-vis (DCM/MeOH) λ_{max}: 587, 508, 413 nm; ^{1}H NMR (500 MHz, CD_2Cl_2): δ_H = 8.92 (s, 8H, Ar *H*), 8.08-8.25 (m, 4H, Ar *H*), 7.33-7.45 (m, 8H, Ar *H*), -2.85 (s, 2H, N*H*) ppm; HRMS (LDI-TOF, m/z): calculated $C_{44}H_{22}F_8N_4$: 758.17112, found: cluster of peaks at 758.17019 [M+].

5,10,15,20-tetrakis(2,5-difluorophenyl)porphyrin[170]

Following procedure B, to propionic acid (75 ml) was added pyrrole (1.60 ml, 1.55 g, 23.1 mmol) and 2,5-difluorobenzaldehyde (1.61 ml, 2.10 g, 14.8 mmol). Upon work-up, a purple solid was obtained (0.09 g, 0.12 mmol, 3%). Mp >300°C; IR (ATR): ν_{max} = 3322, 1606, 1597, 1537, 1422, 1384, 1255, 1129, 10988, 965, 782 cm^{-1}; UV-vis (DCM/MeOH) λ_{max}: 586, 508, 411 nm; ^{1}H NMR (500 MHz, CD_2Cl_2): δ_H = 8.96 (s, 8H, Ar *H*), 7.90-7.81 (m, 4H, Ar *H*), 7.54-7.62 (m, 8H, Ar *H*), -2.85 (s, 2H, N*H*) ppm; HRMS (LDI-TOF, m/z): calculated $C_{44}H_{22}F_8N_4$: 758.17112, found: cluster of peaks at 758.17159 [M+].

5,10,15,20-tetrakis(2,6-difluorophenyl)porphyrin[169]

Following procedure A, to propionic acid (75 ml) was added pyrrole (1.60 ml, 1.55 g, 23.1 mmol) and 2,6-difluorobenzaldehyde (1.60 ml, 2.11 g, 14.8 mmol). Upon work-up, a purple solid was obtained (0.24 g, 0.32 mmol, 9%). Mp >300°C; IR (ATR): ν_{max} 3305, 1608, 1583, 1457, 1355, 1264, 1158, 1057, 978, 777 cm^{-1}; UV-vis (DCM/MeOH) λ_{max}: 586, 505, 411 nm; ^{1}H NMR (500 MHz, CD_2Cl_2): δ_H = 8.97 (s,

8H, Ar *H*), 7.94-7.86 (m, 4H, Ar *H*), 7.45-7.55 (m, 8H, Ar *H*), -2.80 (s, 2H, N*H*) ppm; HRMS (LDI-TOF, m/z): calculated $C_{44}H_{22}F_8N_4$: 758.17112, found: cluster of peaks at 758.17070 [M+].

5,10,15,20-tetrakis(3,4-difluorophenyl)porphyrin[170]

Following procedure A, to propionic acid (75 ml) was added pyrrole (1.55 ml, 1.50 g, 22.4 mmol) and 3,4-difluorobenzaldehyde (1.61 ml, 2.08 g, 14.6 mmol). Upon work-up, a purple solid was obtained (0.29 g, 0.38 mmol, 10%). Mp >300°C; IR (ATR): ν_{max} = 3315, 1601, 1528, 1475, 1367, 1253, 1141, 1068, 969, 788 cm^{-1}; UV-vis (DCM/MeOH) λ_{max}: 589, 511, 414 nm; ^{1}H NMR (500 MHz, CD_2Cl_2): δ_H = 8.93 (s, 8H, Ar *H*), 8.06-8.13 (m, 4H, Ar *H*), 8.00 (s, 4H, Ar *H*), 7.60-7.68 (m, 4H, Ar *H*), -2.92 (s, 2H, N*H*) ppm; HRMS (LDI-TOF, m/z): calculated $C_{44}H_{22}F_8N_4$: 758.17112, found: cluster of peaks at 758.17196 [M+].

5,10,15,20-tetrakis(3,5-difluorophenyl)porphyrin[171]

Following procedure C, to propionic acid (150 ml) was added pyrrole (3.67 ml, 3.55 g, 52.9 mmol) and 3,5-difluorobenzaldehyde (3.33 ml, 4.31g, 30.3 mmol). Upon work-up, a purple solid was obtained (0.39 g, 0.51 mmol, 7%). Mp >300°C; IR (ATR): ν_{max} 3311, 1602, 1581, 1444, 1368, 1293, 1221, 1049, 993, 781cm^{-1}; UV-vis (DCM/MeOH) λ_{max}: 586, 509, 413 nm; ^{1}H NMR (500 MHz, CD_2Cl_2): δ_H = 8.98 (s, 8H, Ar *H*), 7.81-7.91 (m, 8H, Ar *H*), 7.35-7.41 (m, 4H, Ar *H*), -2.93 (s, 2H, N*H*) ppm; HRMS (LDI-TOF, m/z): calculated $C_{44}H_{22}F_8N_4$: 758.17112, found: cluster of peaks at 758.17159 [M+].

5,10,15,20-tetrakis(2,3,4-trifluorophenyl)porphyrin[172]

Following procedure B, to propionic acid (75 ml) was added pyrrole (0.97 ml, 1.91 g, 28.5 mmol) and 2,3,4-trifluorobenzaldehyde (1.78 ml, 2.50 g, 15.6 mmol). Upon work-up, a purple solid was obtained (0.27 g, 0.33 mmol, 8%). Mp >300°C; IR (ATR): ν_{max} = 3312, 1607, 1505, 1470, 1300, 1273, 1234, 1055, 1010, 924, 789 cm^{-1}; UV-vis (DCM/MeOH) λ_{max}: 586, 509, 410 nm; ^{1}H NMR (500 MHz, CD_2Cl_2): δ_H = 8.94 (s, 8H, Ar *H*), 7.89-7.99 (m, 4H, Ar *H*), 7.47-7.55 (m, 4H, Ar *H*), -2.90 (s, 2H, N*H*) ppm; HRMS (LDI-TOF, m/z): calculated $C_{44}H_{18}F_{12}N_4$: 830.13344, found: cluster of peaks at 830.13170 [M+].

5,10,15,20-tetrakis(2,3,5-trifluorophenyl)porphyrin

Following procedure C, to propionic acid (75 ml) was added pyrrole (1.62 ml, 1.57 g, 23.4 mmol) and 2,3,5-trifluorobenzaldehyde (1.49 ml, 2.09 g, 13.1 mmol). Upon work-up, a purple solid was obtained (0.07 g, 0.08 mmol, 3%). Mp >300°C; IR (ATR): ν_{max} = 3309, 1621, 1556, 1424, 1350, 1293, 1202, 1070, 978, 782 cm^{-1}; UV-vis (DCM/MeOH) λ_{max}: 585, 508, 408 nm; ^{1}H NMR (500 MHz, CD_2Cl_2): δ_H = 9.01 (s, 8H, Ar *H*), 7.74-7.83 (m, 4H, Ar *H*), 7.52-7.59 (m, 4H, Ar *H*), -2.90 (s, 2H, N*H*) ppm; HRMS (LDI-TOF, m/z): calculated $C_{44}H_{18}F_{12}N_4$: 830.13344, found: cluster of peaks at 830.13183 [M+].

5,10,15,20-tetrakis(2,3,6-trifluorophenyl)porphyrin

Following procedure C, to propionic acid (75 ml) was added pyrrole (1.81 ml, 1.75 g, 26.1 mmol) and 2,3,6-trifluorobenzaldehyde (1.78 ml, 2.54 g, 15.9 mmol). Upon work-up, a purple solid was obtained (0.20 g, 0.24mmol, 6%). Mp >300°C; IR (ATR): ν_{max} = 3313, 1616, 1517, 1448, 1353, 1270, 1184, 1062, 964, 791 cm^{-1}; UV-vis (DCM/MeOH) λ_{max}: 584, 508, 411 nm; ^1H NMR (500 MHz, CD_2Cl_2): δ_H = 9.01 (s, 8H, Ar *H*), 7.72-7.80 (m, 4H, Ar *H*), 7.40-7.46 (m, 4H, Ar *H*), -2.84 (s, 2H, N*H*) ppm; HRMS (LDI-TOF, m/z): calculated $C_{44}H_{18}F_{12}N_4$: 830.13344, found: cluster of peaks at 830.13316 [M+].

5,10,15,20-tetrakis(2,4,5-trifluorophenyl)porphyrin

Following procedure B, to propionic acid (75 ml) was added pyrrole (1.80 ml, 1.74 g, 25.9 mmol) and 2,4,5-trifluorobenzaldehyde (1.43 ml, 2.02 g, 12.6 mmol). Upon work-up, a purple solid was obtained (0.14 g, 0.17 mmol, 5%). Mp >300°C; IR (ATR): ν_{max} = = 3305, 1602, 1577, 1429, 1367, 1282, 1244, 1092, 983, 788 cm^{-1}; UV-vis (DCM/MeOH) λ_{max}: 587, 508, 410 nm; ^1H NMR (500 MHz, CD_2Cl_2): δ_H = 8.96 (s, 8H, Ar *H*), 8.03-8.10 (m, 4H, Ar *H*), 7.48-7.55 (m, 4H, Ar *H*), -2.92 (s, 2H, N*H*) ppm; HRMS (LDI-TOF, m/z): calculated $C_{44}H_{18}F_{12}N_4$: 830.13344, found: cluster of peaks at 830.13203 [M+].

5,10,15,20-tetrakis(2,4,6-trifluorophenyl)porphyrin[173]

Following procedure B, to propionic acid (75 ml) was added pyrrole (1.80 ml, 1.74 g, 25.9 mmol) and 2,4,6-trifluorobenzaldehyde (1.99 g, 12.4 mmol). Upon work-up, a purple solid was obtained (0.09 g, 0.11 mmol, 3%). Mp >300°C; IR (ATR): ν_{max} 3310, 1603, 1509, 1435, 1327, 1299, 1264, 1123, 1049, 969, 786 cm^{-1}; UV-vis (DCM/MeOH) λ_{max}: 586, 508, 412 nm; ^1H NMR (500 MHz, CD_2Cl_2): δ_H = 8.99 (s, 8H, Ar *H*), 7.77-7.88 (m, 8H, Ar *H*), -2.91 (s, 2H, N*H*) ppm; HRMS (LDI-TOF, m/z): calculated $C_{44}H_{18}F_{12}N_4$: 830.13344, found: cluster of peaks at 830.13380 [M+].

5,10,15,20-tetrakis(3,4,5-trifluorophenyl)porphyrin[174]

Following procedure B, to propionic acid (75 ml) was added pyrrole (1.65 ml, 1.60 g, 23.8 mmol) and 3,4,5-trifluorobenzaldehyde (1.54 ml, 2.18 g, 13.6 mmol). Upon work-up, a purple solid was obtained (0.39 g, 0.47 mmol, 14%). Mp >300°C; IR (ATR): ν_{max} = 3308, 1597, 1532, 1412, 1327, 1285, 1163, 1054, 975, 788cm^{-1}; UV-vis (DCM/MeOH) λ_{max}: 587, 510, 413 nm; ^1H NMR (500 MHz, CD_2Cl_2): δ_H = 8.95 (s, 8H, Ar *H*), 7.88-7.95 (m, 8H, Ar *H*), -3.00 (s, 2H, N*H*) ppm; HRMS (LDI-TOF, m/z): calculated $C_{44}H_{18}F_{12}N_4$: 830.13344, found: cluster of peaks at 830.13179 [M+].

8 Appendix

8.1 Additional characterisation of phthalocyanine ligands used in attempted MOF synthesis reactions

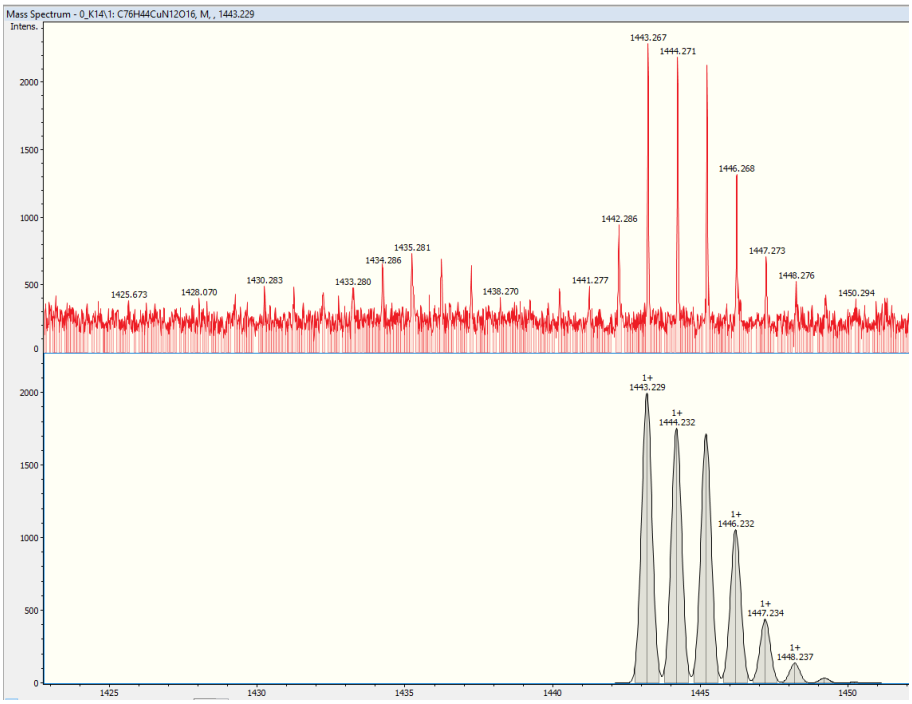

Figure 8.1: The LDI-MS spectrum of the ethyl-ester protected version of the Cu(II)TCIPc ligand.

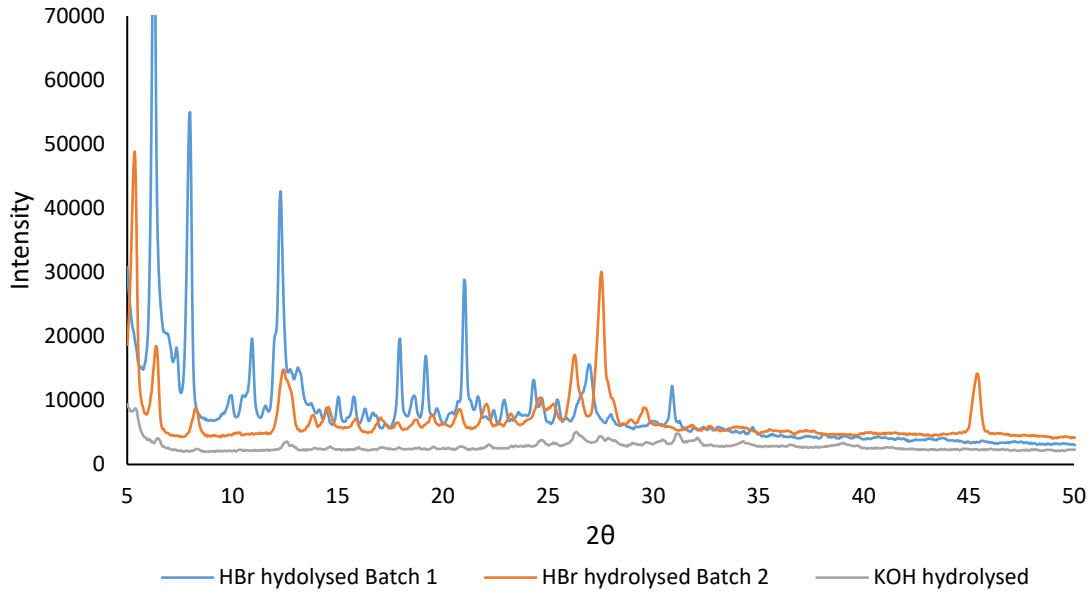

Figure 8.2: The powder XRD patterns of various synthesised Cu(II) OCPc samples.

8.2 Crystallographic data

Pc	TPP	Chemical Formula	Space Group	a (Å)	b (Å)	c (Å)	Phthalocyanine Curvature (degrees)	Metal to metal distance (Å)	Macrocycle to macrocycle distance (Å)
$(diPhO)_8PcCu$	CuTPP	$C_{128}H_{142}N_8O_8Cu$, $C_{44}H_{26}N_4Cu$	Cubic ($Pn\bar{3}n$)	37.8504	37.8504	37.8504	16.78	3.447	3.513
$(diPhO)_8PcCo$	CoTPP	$C_{128}H_{142}N_8O_8Co$, $C_{44}H_{26}N_4Co$	Cubic ($Pn\bar{3}n$)	37.9452	37.9452	37.9452	13.92	3.567	3.486
$(diPhO)_8PcCo$	CuTPP	$C_{128}H_{142}N_8O_8Co$, $C_{44}H_{26}N_4Cu$	Cubic ($Pn\bar{3}n$)	37.7840	37.7840	37.7840	16.32	3.384	3.385
$(diPhO)_8PcH_2$	ZnTPP	$C_{128}H_{144}N_8O_8$, $C_{44}H_{26}N_4Zn$	Cubic ($Pn\bar{3}n$)	37.8374	37.8374	37.8374	16.88	N/A	3.451
$(diPhO)_8PcH_2$	CuTPP	$C_{128}H_{144}N_8O_8$, $C_{44}H_{28}N_4Cu$	Monoclinic $P2_1/c$	21.4135	56.7632	19.6131	4.30	N/A	3.459
$(diPhO)_8PcH_2$	H_2TPP	$C_{128}H_{144}N_8O_8$, $C_{44}H_{28}N_4$	Cubic ($Pn\bar{3}n$)	37.7730	37.7730	37.7730	18.60	N/A	3.461
$(diPhO)_8PcH_2$	$(4Me)_4H_2TPP$	$C_{128}H_{144}N_8O_8$, $C_{48}H_{36}N_4$	Orthorhombic Pnma	20.2254	39.3105	20.5963	6.39	N/A	3.447
$(diPhO)_8PcH_2$	$(2F)_4H_2TPP$	$C1_{28}H_{144}N_8O_8$, $C_{44}H_{24}F_4N_4$	Cubic ($Pn\bar{3}n$)	37.7703	37.7703	37.7703	19.57	N/A	3.423
$(diPhO)_8PcH_2$	$(3F)_4H_2TPP$	$C1_{28}H_{144}N_8O_8$, $C_{44}H_{24}F_4N_4$	Cubic ($Pn\bar{3}n$)	38.0035	38.0035	38.0035	18.79	N/A	3.417
$(diPhO)_8PcH_2$	$(4F)_4H_2TPP$	$C1_{28}H_{144}N_8O_8$, $C_{44}H_{24}F_4N_4$	Cubic ($Pn\bar{3}n$)	38.1090	38.1090	38.1090	17.12	N/A	3.380
$(diPhO)_8PcH_2$	$(2,4F)_4H_2TPP$	$C1_{28}H_{144}N_8O_8$, $C_{44}H_{20}F_8N_4$	Cubic ($Pn\bar{3}n$)	38.1835	38.1835	38.1835	17.25	N/A	3.482
$(diPhO)_8PcH_2$	$(3,4F)_4H_2TPP$	$C1_{28}H_{144}N_8O_8$, $C_{44}H_{20}F_8N_4$	Tetragonal (I4mm)	28.9772	28.9772	11.0570	1.31	N/A	3.654
$diPhO_8PcH_2$	$(3,5F)_4H_2TPP$	$C1_{28}H_{144}N_8O_8$, $C_{44}H_{20}F_8N_4$	Cubic ($Pn\bar{3}n$)	37.7040	37.7040	37.7040	23.04	N/A	3.399
$diPhO_8PcH_2$	$(3,4,5F)_4H_2TPP$	$C1_{28}H_{144}N_8O_8$, $C_{44}H_{16}F_{12}N_4$	Tetragonal (I4mm)	29.0574	29.0574	11.0492	2.73	N/A	3.716

Table 8.1: The crystal structure data for the obtained structures.

8.3 Additional UV-vis spectra relevant to Pc: TPP aggregation

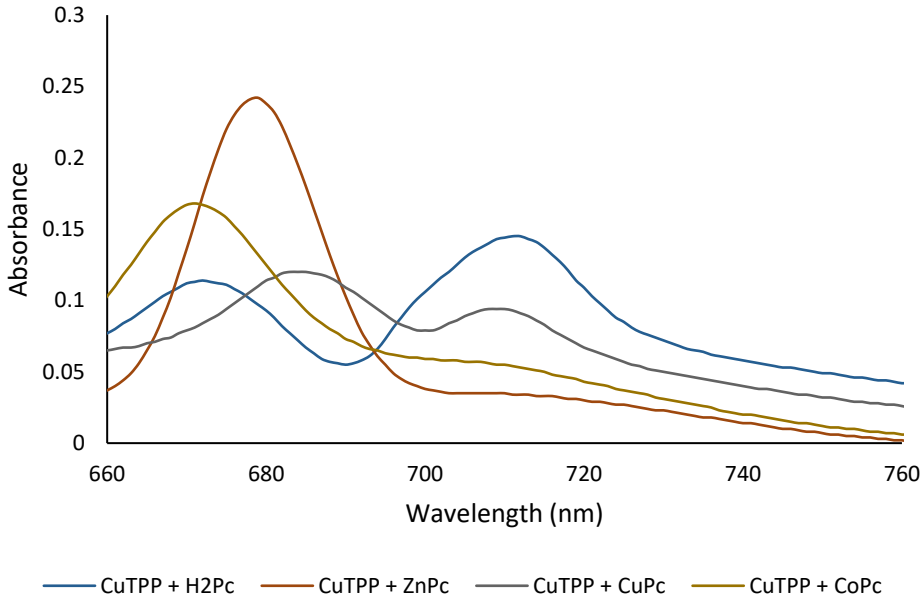

Figure 8.4: The UV-vis spectra of the metallated-Pc: CuTPP dimers

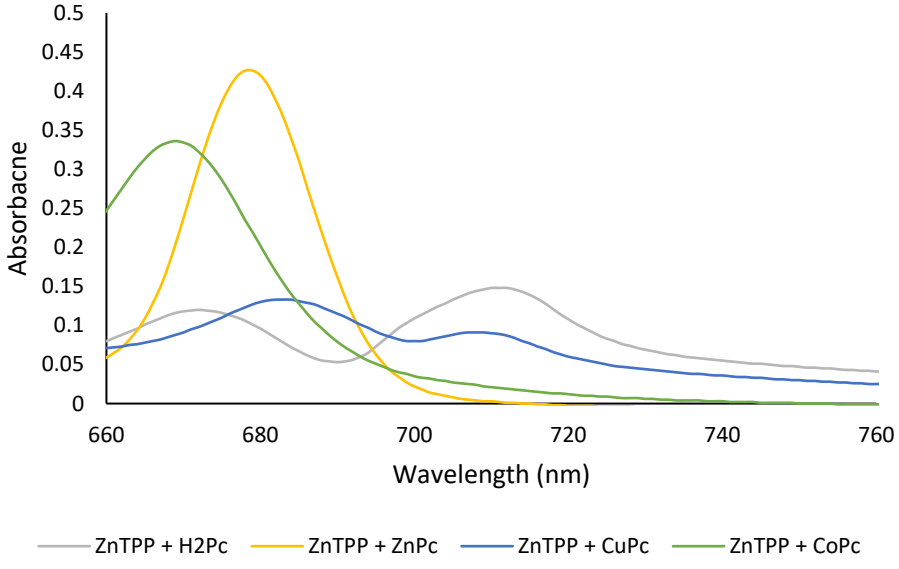

Figure 8.5: The UV-vis spectra of the metallated-Pc: ZnTPP dimers

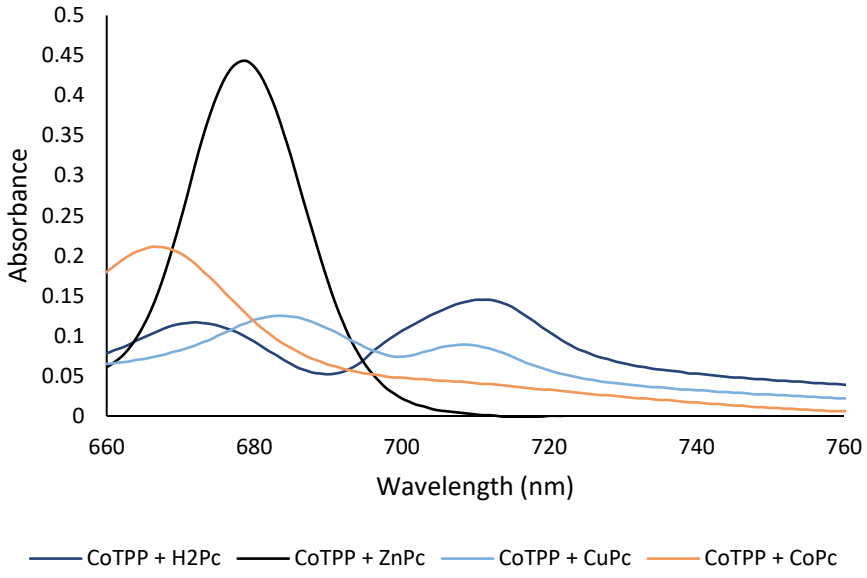

Figure 8.6: The UV-vis spectra of the metallated-Pc: CoTPP dimers

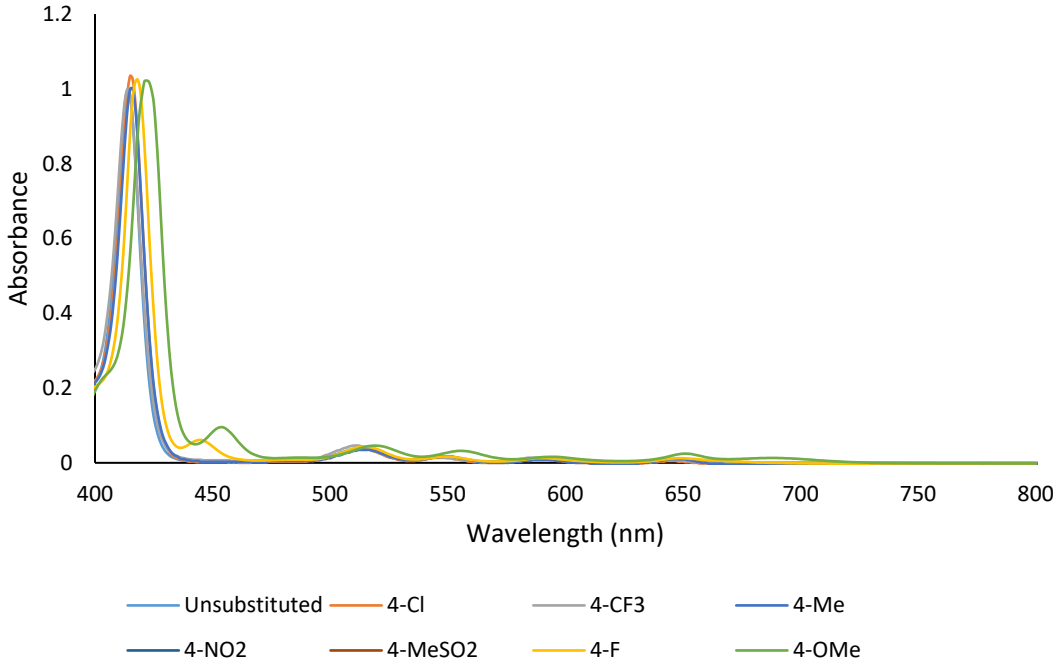

Figure 8.7: The UV-vis spectra of the synthesised *para*-substituted tetraphenylporphyrins

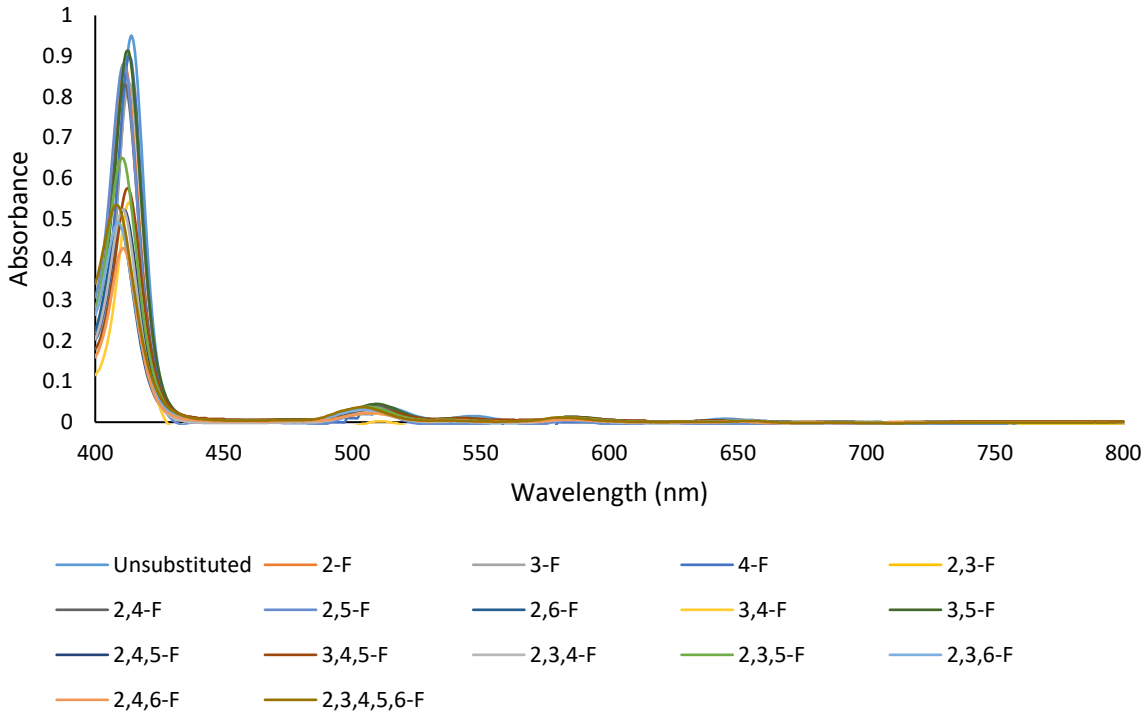

Figure 8.8: The UV-vis spectra of the synthesised fluorinated tetraphenylporphyrins

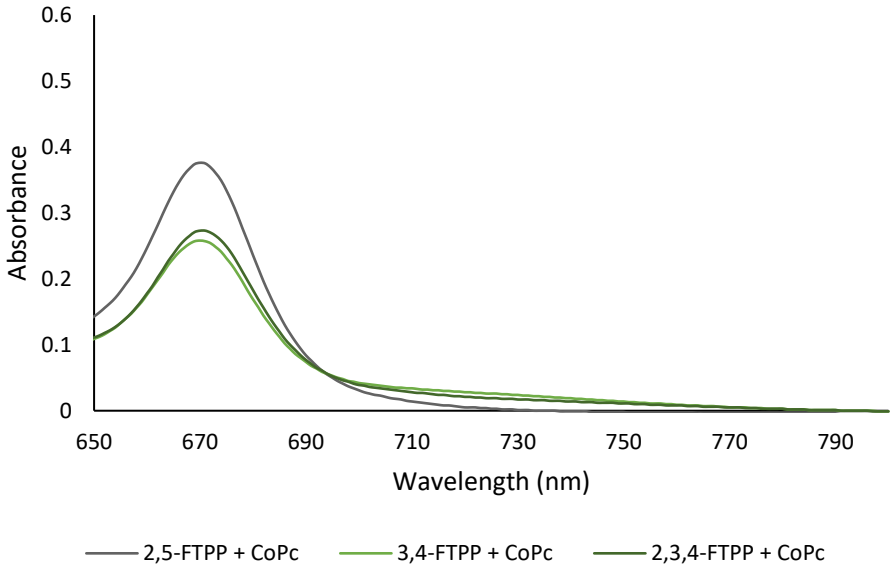

Figure 8.9: The UV-vis spectra of the CoPc: fluorinated TPP dimers

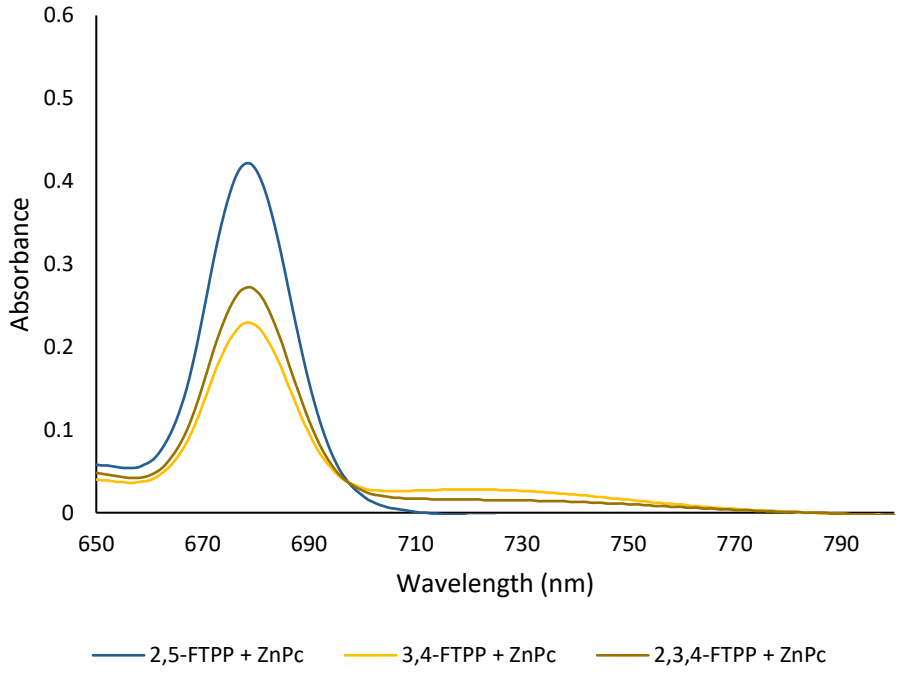

Figure 8.10: The UV-vis spectra of the ZnPc: fluorinated TPP dimers

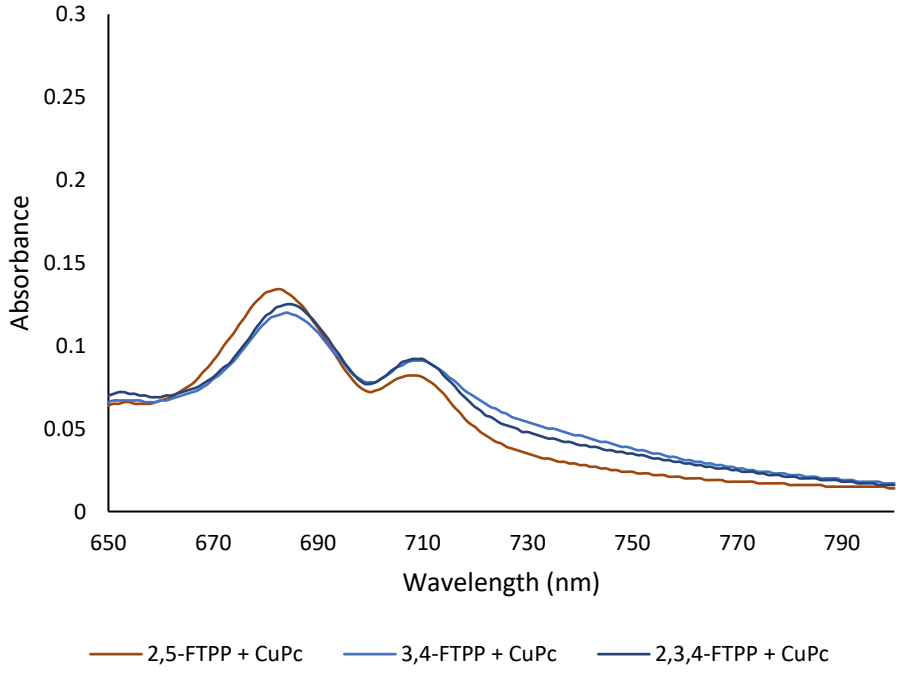

Figure 8.11: The UV-vis spectra of the CuPc: fluorinated TPP dimers

9 References

1. D. Hohnholz, S. Steinbrecher and M. Hanack, *Journal of Molecular Structure*, 2000, **521**, 231-237.
2. M. A. Rauf, S. Hisaindee, J. P. Graham and M. Nawaz, *Journal of Molecular Liquids*, 2012, **168**, 102-109.
3. Z. Cheng, S. Du, W. Guo, L. Gao, Z. Deng, N. Jiang, H. Guo, H. Tang and H. J. Gao, *Nano Research*, 2011, **4**, 523-530.
4. J. Mack and M. J. Stillman, *Coordination Chemistry Reviews*, 2001, **219**, 993-1032.
5. T. Shen, Z.-l. Yuan and H.-j. Xu, *Dyes and Pigments*, 1989, **11**, 77-80.
6. B. L. Wheeler, G. Nagasubramanian, A. J. Bard, L. A. Schechtman and M. E. Kenney, *Journal of the American Chemical Society*, 1984, **106**, 7404-7410.
7. H. Isago, *Optical Spectra of Phthalocyanines and Related Compounds*, National Intitute for Materials Science, Tsukuba, Japan, 2015.
8. J. R. Sommer, A. H. Shelton, A. Parthasarathy, I. Ghiviriga, J. R. Reynolds and K. S. Schanze, *Chemistry of Materials*, 2011, **23**, 5296-5304.
9. P. Zimcik, V. Novakova, K. Kopecky, M. Miletin, R. Z. Uslu Kobak, E. Svandrlikova, L. Váchová and K. Lang, *Inorganic Chemistry*, 2012, **51**, 4215-4223.
10. W. Keawsongsaeng, J. Gasiorowski, P. Denk, K. Oppelt, D. H. Apaydin, R. Rojanathanes, K. Hingerl, M. Scharber, N. S. Sariciftci and P. Thamyongkit, *Advanced Energy Materials*, 2016, **6**, 1600957.
11. S. V. Kudrevich and J. E. van Lier, *Coordination Chemistry Reviews*, 1996, **156**, 163-182.
12. G. de la Torre, P. Vázquez, F. Agulló-López and T. Torres, *Chemical Reviews*, 2004, **104**, 3723-3750.
13. C. G. Bezzu, M. Helliwell, J. E. Warren, D. R. Allan and N. B. McKeown, *Science*, 2010, **327**, 1627-1630.
14. S. Banfi, F. Montanari, S. Quici, S. V. Barkanova, O. L. Kaliya, V. N. Kopranenkov and E. A. Luk'yanets, *Tetrahedron Letters*, 1995, **36**, 2317-2320.
15. S.-I. Murahashi, X.-G. Zhou and N. Komiya, *Synlett*, 2003, **3**, 321-324.
16. B. Basu, S. Satapathy and A. K. Bhatnagar, *Catalysis Reviews*, 1993, **35**, 571-609.
17. S. M. Paradine and M. C. White, *Journal of the American Chemical Society*, 2012, **134**, 2036-2039.
18. P. Kluson, M. Drobek, T. Strasak, J. Krysa, M. Karaskova and J. Rakusan, *Journal of Molecular Catalysis A: Chemical*, 2007, **272**, 213-219.

19. D. Jančula, L. Bláhová, M. Karásková and B. Maršálek, *Water Science and Technology*, 2010, **62**, 273-278.
20. R. Raja and P. Ratnasamy, *Applied Catalysis a-General*, 1997, **158**, L7-L15.
21. M. A. Zanjanchi, A. Ebrahimian and M. Arvand, *Journal of Hazardous Materials*, 2010, **175**, 992-1000.
22. I. Langmuir, *Journal of the American Chemical Society*, 1918, **40**, 1361-1403.
23. S. Brunauer, P. H. Emmett and E. Teller, *Journal of the American Chemical Society*, 1938, **60**, 309-319.
24. T. Matthias, K. Katsumi, V. N. Alexander, P. O. James, R.-R. Francisco, R. Jean and S. W. S. Kenneth, *Pure and Applied Chemistry*, 2015, **87**, 1051-1069.
25. S.-Y. Ding and W. Wang, *Chemical Society Reviews*, 2013, **42**, 548-568.
26. M. H. Zeng, Q. X. Wang, Y. X. Tan, S. Hu, H. X. Zhao, L. S. Long and M. Kurmoo, *Journal of the American Chemical Society*, 2010, **132**, 2561-2563.
27. S. I. Zones and M. E. Davis, *Current Opinion in Solid State and Materials Science*, 1996, **1**, 107-117.
28. S. Marchesini, A. Regoutz, D. Payne and C. Petit, *Microporous and Mesoporous Materials*, 2017, **243**, 154-163.
29. M. A. Nejad, P. Umstätter and H. M. Urbassek, *Journal of Molecular Modeling*, 2020, **26**, 54.
30. S. J. Allen, V. Balasundaram, P. M. Armenante, L. Thom and D. Kafkewitz, *Journal of Chemical Technology & Biotechnology*, 1995, **64**, 261-267.
31. D. Yuan, W. Lu, D. Zhao and H.-C. Zhou, *Advanced Materials*, 2011, **23**, 3723-3725.
32. K. Cousins and R. Zhang, *Polymers*, 2019, **11**, 690-715.
33. J.-X. Jiang, C. Wang, A. Laybourn, T. Hasell, R. Clowes, Y. Z. Khimyak, J. Xiao, S. J. Higgins, D. J. Adams and A. I. Cooper, *Angewandte Chemie International Edition*, 2011, **50**, 1072-1075.
34. L. Chen, Y. Yang, Z. Guo and D. Jiang, *Advanced Materials*, 2011, **23**, 3149-3154.
35. P. M. Budd, B. S. Ghanem, S. Makhseed, N. B. Mckeown, K. J. Msayib and C. E. Tattershall, *Chemical Communications*, 2004, **40**, 230-231.
36. R. R. Tiwari, J. Jin, B. D. Freeman and D. R. Paul, *Journal of Membrane Science*, 2017, **537**, 362-371.
37. F. Marken, M. Carta and N. B. McKeown, *Analytical Chemistry*, 2021, **93**, 1213-1220.
38. B. S. Ghanem, N. B. Mckeown, P. M. Budd, J. D. Selbie and D. Fritsch, *Advanced Materials*, 2008, **20**, 2766-2771.
39. B. S. Ghanem, N. B. Mckeown, P. M. Budd, N. M. Al-Harbi, D. Fritsch, K. Heinrich, L. Starannikova, A. Tokarev and Y. Yampolskii, *Macromolecules*, 2009, **42**, 7881-7888.

40. M. Carta, R. Malpass-Evans, M. Croad, Y. Rogan, J. C. Jansen, P. Bernardo, F. Bazzarelli and N. B. Mckeown, *Science*, 2013, **339**, 303-307.
41. S. Venkatachalam, K. V. C. Rao and P. T. Manoharan, *Journal of Polymer Science Part B: Polymer Physics*, 1994, **32**, 37-52.
42. D. Wöhrle and B. Schulte, *Die Makromolekulare Chemie*, 1988, **189**, 1229-1238.
43. R. P. Kingsborough and T. M. Swager, *Angewandte Chemie International Edition*, 2000, **39**, 2897-2900.
44. N. B. Mckeown and P. M. Budd, *Chemical Communications*, 2002, **44**, 2780-2781.
45. H. J. Mackintosh, P. M. Budd and N. B. McKeown, *Journal of Materials Chemistry*, 2008, **18**, 573-578.
46. L. Cai, Y. Li, Y. Li, H. Wang, Y. Yu, Y. Liu and Q. Duan, *Journal of Hazardous Materials*, 2018, **348**, 47-55.
47. V. Ganesan and S. Yoon, *Catalysts*, 2020, **10**, 905.
48. H. H. Abdel-Razik, S. El-Sayed and A. Hassen, *Journal of Applied Polymer Science*, 2011, **121**, 3579-3589.
49. H. H. Abdel-Razik, B. H. Asghar and E. Kenawy, *Chinese Journal of Polymer Science*, 2013, **31**, 242-250.
50. A. P. Cote, A. I. Benin, N. W. Ockwig, M. O'Keeffe, A. J. Matzger and O. M. Yaghi, *Science*, 2005, **310**, 1166-1170.
51. F. J. Uribe-Romo, J. R. Hunt, H. Furukawa, C. Klo, M. O. Keeffe and O. M. Yaghi, *Journal of the American Chemical Society*, 2009, **131**, 4570-4571.
52. S. Y. Ding, J. Gao, Q. Wang, Y. Zhang, W. G. Song, C. Y. Su and W. Wang, *Journal of the American Chemical Society*, 2011, **133**, 19816-19822.
53. X. Han, Q. Xia, J. Huang, Y. Liu, C. Tan and Y. Cui, *Journal of the American Chemical Society*, 2017, **139**, 8693-8697.
54. X. Feng, L. Chen, Y. Dong and D. Jiang, *Chemical Communications*, 2011, **47**, 1979-1981.
55. G. Lin, H. Ding, R. Chen, Z. Peng, B. Wang and C. Wang, *Journal of the American Chemical Society*, 2017, **139**, 8705-8709.
56. S. Lin, C. S. Diercks, Y.-B. Zhang, N. Kornienko, E. M. Nichols, Y. Zhao, A. R. Paris, D. Kim, P. Yang, O. M. Yaghi and C. J. Chang, *Science*, 2015, **349**, 1208-1213.
57. E. L. Spitler and W. R. Dichtel, *Nature Chemistry*, 2010, **2**, 672-677.
58. H. Daglar and S. Keskin, *Coordination Chemistry Reviews*, 2020, **422**, 213470.
59. H. C. Zhou, J. R. Long and O. M. Yaghi, *Chemical Reviews*, 2012, **112**, 673-674.
60. O. M. Yaghi and H. Li, *Journal of the American Chemical Society*, 1995, **117**, 10401-10402.

61. H. Li, M. Eddaoudi, M. O'Keeffe and O. M. Yaghi, *Nature*, 1999, **402**, 276-279.
62. S. S.-Y. Chui, S. M.-F. Lo, J. P. H. Charmant, A. G. Orpen and I. D. Williams, *Science*, 1999, **283**, 1148-1150.
63. H. Furukawa, K. E. Cordova, M. O'Keeffe and O. M. Yaghi, *Science*, 2013, **341**, 974-987.
64. J. Lee, O. K. Farha, J. Roberts, K. A. Scheidt, S. T. Nguyen and J. T. Hupp, *Chemical Society Reviews*, 2009, **38**, 1450-1459.
65. M. E. Kosal, J.-H. Chou, S. R. Wilson and K. S. Suslick, *Nature Materials*, 2002, **1**, 118-121.
66. A. M. Shultz, O. K. Farha, J. T. Hupp and S. T. Nguyen, *Journal of the American Chemical Society*, 2009, **131**, 4204-4205.
67. X. L. Yang, M. H. Xie, C. Zou, Y. He, B. Chen, M. O'Keeffe and C. D. Wu, *Journal of the American Chemical Society*, 2012, **134**, 10638-10645.
68. X. S. Wang, L. Meng, Q. Cheng, C. Kim, L. Wojtas, M. Chrzanowski, Y. S. Chen, X. P. Zhang and S. Ma, *Journal of the American Chemical Society*, 2011, **133**, 16322-16325.
69. L. Meng, Q. Cheng, C. Kim, W. Y. Gao, L. Wojtas, Y. S. Chen, M. J. Zaworotko, X. P. Zhang and S. Ma, *Angewandte Chemie International Edition*, 2012, **51**, 10082-10085.
70. D. Feng, Z. Y. Gu, J. R. Li, H. L. Jiang, Z. Wei and H. C. Zhou, *Angewandte Chemie International Edition*, 2012, **51**, 10307-10310.
71. D. W. Feng, W.-C. Chung, Z. W. Wei, Z.-Y. Gu, H.-L. Jiang, Y.-P. Chen, D. J. Darensbourg and H.-C. Zhou, *Journal of the American Chemical Society*, 2013, **135**, 17105-17110.
72. S. De, T. Devic and A. Fateeva, *Dalton Transactions*, 2021, **50**, 1166-1188.
73. H. Nagatomi, N. Yanai, T. Yamada, K. Shiraishi and N. Kimizuka, *Chemistry – A European Journal*, 2018, **24**, 1806-1810.
74. H. Zhong, K. H. Ly, M. Wang, Y. Krupskaya, X. Han, J. Zhang, J. Zhang, V. Kataev, B. Büchner, I. M. Weidinger, S. Kaskel, P. Liu, M. Chen, R. Dong and X. Feng, *Angewandte Chemie International Edition*, 2019, **58**, 10677-10682.
75. F. Wang, Z. Liu, C. Yang, H. Zhong, G. Nam, P. Zhang, R. Dong, Y. Wu, J. Cho, J. Zhang and X. Feng, *Advanced Materials*, 2020, **32**, 1905361.
76. H. Jia, Y. Yao, J. Zhao, Y. Gao, Z. Luo and P. Du, *Journal of Materials Chemistry A*, 2018, **6**, 1188-1195.
77. R. Matheu, E. Gutierrez-Puebla, M. Á. Monge, C. S. Diercks, J. Kang, M. S. Prévot, X. Pei, N. Hanikel, B. Zhang, P. Yang and O. M. Yaghi, *Journal of the American Chemical Society*, 2019, **141**, 17081-17085.
78. P. Sozzani, S. Bracco, A. Comotti, L. Ferretti and R. Simonutti, *Angewandte Chemie International Edition*, 2005, **44**, 1816-1820.

79. M. Mastalerz and I. M. Oppel, *Angewandte Chemie International Edition*, 2012, **51**, 5252-5255.
80. M. E. Kosal and K. S. Suslick, *Journal of Solid State Chemistry* 2000, **152**, 87-98.
81. W. Yang, B. Li, H. Wang, O. Alduhaish, K. Alfooty, M. A. Zayed, P. Li, H. D. Arman and B. Chen, *Crystal Growth & Design*, 2015, **15**, 2000-2004.
82. N. B. Mckeown, S. Makhseed, K. J. Msayib, L.-L. Ooi, M. Helliwell and J. E. Warren, *Angewandte Chemie International Edition*, 2005, **44**, 7546-7549.
83. C. G. Bezzu, L. A. Burt, C. J. Mcmonagle, S. A. Moggach, B. M. Kariuki, D. R. Allan, M. Warren and N. B. Mckeown, *Nature Materials*, 2019, **18**, 740-745.
84. W. Morris, B. Volosskiy, S. Demir, F. Gándara, P. L. McGrier, H. Furukawa, D. Cascio, J. F. Stoddart and O. M. Yaghi, *Inorganic Chemistry*, 2012, **51**, 6443-6445.
85. D. Feng, H.-L. Jiang, Y.-P. Chen, Z.-Y. Gu, Z. Wei and H.-C. Zhou, *Inorganic Chemistry*, 2013, **52**, 12661-12667.
86. H.-L. Jiang, D. Feng, K. Wang, Z.-Y. Gu, Z. Wei, Y.-P. Chen and H.-C. Zhou, *Journal of the American Chemical Society*, 2013, **135**, 13934-13938.
87. O. K. Farha, A. M. Shultz, A. A. Sarjeant, S. T. Nguyen and J. T. Hupp, *Journal of the American Chemical Society*, 2011, **133**, 5652-5655.
88. P. M. Barron, C. A. Wray, C. Hu, Z. Guo and W. Choe, *Inorganic Chemistry*, 2010, **49**, 10217-10219.
89. K. Sakamoto and E. Ohno, *Progress in Organic Coatings*, 1997, **31**, 139 - 145.
90. C. Bailar, *Inorganic Chemistry*, 1972, **11**, 1578-1583.
91. D. Wöhrle, M. Eskes, K. Shigehara and A. Yamada, *Synthesis*, 1993, **1993**, 194-196.
92. G. Crucius, A. Lyubimtsev, M. Kramer, M. Hanack and T. Ziegler, *Synlett*, 2012, **23**, 2501-2503.
93. D. M. Opris, F. Nüesch, C. Löwe, M. Molberg and M. Nagel, *Chemistry of Materials*, 2008, **20**, 6889-6896.
94. M. Sainlos and B. Imperiali, *Nature Protocols*, 2007, **2**, 3219-3225.
95. F. Kazemi, A. R. Kiasat and B. Mombaini, *Synthetic Communications*, 2007, **37**, 3219-3223.
96. J. Cremers, S. Richert, D. V. Kondratuk, T. D. W. Claridge, C. R. Timmel and H. L. Anderson, *Chemical Science*, 2016, **7**, 6961-6968.
97. C. Bergami, M. P. Donzello, C. Ercolani, F. Monacelli, K. M. Kadish and C. Rizzoli, *Inorganic Chemistry*, 2005, **44**, 9852-9861.
98. E. Biemmi, S. Christian, N. Stock and T. Bein, *Microporous and Mesoporous Materials*, 2009, **117**, 111-117.

99. C. McKinstry, E. J. Cussen, A. J. Fletcher, S. V. Patwardhan and J. Sefcik, *Crystal Growth & Design*, 2013, **13**, 5481-5486.
100. R. Prabakaran, R. Kesavamoorthy, G. L. N. Reddy and F. P. Xavier, *Physica Status Solidi B*, 2002, **229**, 1175-1186.
101. J. Ren, N. M. Musyoka, H. W. Langmi, J. Walker, M. Mathe and S. Liao, *Polyhedron*, 2018, **153**, 205-212.
102. D. Saha, S. Deng and Z. Yang, *Journal of Porous Materials*, 2008, **16**, 141-149.
103. J. Yu, J. Park, A. Van Wyk, G. Rumbles and P. Deria, *Journal of the American Chemical Society*, 2018, **140**, 10488-10496.
104. N. Micali, F. Mallamace, M. Castriciano, A. Romeo and L. Monsú Scolaro, *Analytical Chemistry*, 2001, **73**, 4958-4963.
105. M. Eddaoudi, J. Kim, N. Rosi, D. Vodak, J. Wachter, M. O'Keeffe and O. M. Yaghi, *Science*, 2002, **295**, 469-472.
106. Y. Zhou, W. Yang, M. Qin and H. Zhao, *Applied Organometallic Chemistry*, 2016, **30**, 188-192.
107. Q. Yang, S. Vaesen, F. Ragon, A. D. Wiersum, D. Wu, A. Lago, T. Devic, C. Martineau, F. Taulelle, P. L. Llewellyn, H. Jobic, C. Zhong, C. Serre, G. De Weireld and G. Maurin, *Angewandte Chemie International Edition*, 2013, **52**, 10316-10320.
108. X. Huang, M. Hu, X. Zhao, C. Li, Z. Yuan, X. Liu, C. Cai, Y. Zhang, Y. Hu and Y. Chen, *Organic Letters*, 2019, **21**, 3382-3386.
109. M.-L. Wang, P. A. Vivekanand and M.-C. Yu, *Journal of the Taiwan Institute of Chemical Engineers*, 2012, **43**, 207-214.
110. J. Li, J. Xie, W. Zeng, X. Wei, B. Zhou, X. Zeng and S. Qin, *Transition Metal Chemistry*, 2004, **29**, 488-494.
111. H. Isago, C. C. Leznoff, M. F. Ryan, R. A. Metcalfe, R. Davids and A. B. P. Lever, *Bulletin of the Chemical Society of Japan*, 1998, **71**, 1039-1047.
112. R. Kudo, M. Sonobe, Y. Chino, Y. Kitazawa and M. Kimura, *Molecules*, 2020, **25**, 5552-5563.
113. M. S. Mindorff and D. E. Brodie, *Canadian Journal of Physics*, 1981, **59**, 249-254.
114. A. Garg, M. Almáši, D. Rattan Paul, E. Poonia, J. R. Luthra and A. Sharma, *Frontiers in Energy Research*, 2021, **8**, 340-346.
115. K. A. S. Usman, J. W. Maina, S. Seyedin, M. T. Conato, L. M. Payawan, L. F. Dumée and J. M. Razal, *NPG Asia Materials*, 2020, **12**, 58-76.
116. A. V. Dighe, R. Y. Nemade and M. R. Singh, *Processes*, 2019, **7**, 527-538.
117. C. Atzori, G. C. Shearer, L. Maschio, B. Civalleri, F. Bonino, C. Lamberti, S. Svelle, K. P. Lillerud and S. Bordiga, *The Journal of Physical Chemistry C*, 2017, **121**, 9312-9324.

118. R. S. Forgan, *Chemical Science*, 2020, **11**, 4546-4562.
119. V. N. Nemykin, S. V. Dudkin, F. Dumoulin, C. Hirel, A. Gürek, and V. Ahsen, *Arkivoc*, 2014, **2014**, 142-204.
120. J. Ren, D. E. C. Rogers, T. Segakweng, H. W. Langmi, B. C. North, M. Mathe and D. Bessarabov, *International Journal of Materials Research*, 2014, **105**, 89-93.
121. W. Xu, K. B. Thapa, Q. Ju, Z. Fang and W. Huang, *Coordination Chemistry Reviews*, 2018, **373**, 199-232.
122. A. Fateeva, P. A. Chater, C. P. Ireland, A. A. Tahir, Y. Z. Khimyak, P. V. Wiper, J. R. Darwent and M. J. Rosseinsky, *Angewandte Chemie International Edition*, 2012, **51**, 7440-7444.
123. A. Suchan, J. Nackiewicz, Z. Hnatejko, W. Waclawek and S. Lis, *Dyes and Pigments*, 2009, **80**, 239-244.
124. K. S. W. Sing, *Pure and Applied Chemistry*, 1985, **57**, 603-619.
125. N. Gibson, P. Kuchenbecker, K. Rasmussen, V. Hodoroaba and H. Rauscher, in *Characterization of Nanoparticles*, ed. V. Hodoroaba, W. E. S. Unger and A. G. Shard, Elsevier, Amsterdam, 2020, ch. 4.1, pp. 265-294.
126. Y.-C. Chiang, C.-Y. Yeh and C.-H. Weng, *Applied Sciences*, 2019, **9**, 1977-1992.
127. A. J. Howarth, A. W. Peters, N. A. Vermeulen, T. C. Wang, J. T. Hupp and O. K. Farha, *Chemistry of Materials*, 2017, **29**, 26-39.
128. J. L. Woodliffe, R. S. Ferrari, I. Ahmed and A. Laybourn, *Coordination Chemistry Reviews*, 2021, **428**, 213578.
129. J. B. DeCoste, G. W. Peterson, H. Jasuja, T. G. Glover, Y.-g. Huang and K. S. Walton, *Journal of Materials Chemistry A*, 2013, **1**, 5642-5650.
130. T. Loiseau, C. Serre, C. Huguenard, G. Fink, F. Taulelle, M. Henry, T. Bataille and G. Férey, *Chemistry – A European Journal*, 2004, **10**, 1373-1382.
131. E. A. Lawton, *The Journal of Physical Chemistry*, 1958, **62**, 384-384.
132. C. Healy, K. M. Patil, B. H. Wilson, L. Hermanspahn, N. C. Harvey-Reid, B. I. Howard, C. Kleinjan, J. Kolien, F. Payet, S. G. Telfer, P. E. Kruger and T. D. Bennett, *Coordination Chemistry Reviews*, 2020, **419**, 213388.
133. M. Hanack, G. Schmid and M. Sommerauer, *Angewandte Chemie International Edition*, 1993, **32**, 1422-1424.
134. J. K. Schnobrich, O. Lebel, K. A. Cychosz, A. Dailly, A. G. Wong-Foy and A. J. Matzger, *Journal of the American Chemical Society*, 2010, **132**, 13941-13948.
135. M. Zhang, W. Lu, J.-R. Li, M. Bosch, Y.-P. Chen, T.-F. Liu, Y. Liu and H.-C. Zhou, *Inorganic Chemistry Frontiers*, 2014, **1**, 159-162.

136. P. Gawrys, T. Marszalek, E. Bartnik, M. Kucinska, J. Ulanski and M. Zagorska, *Organic Letters*, 2011, **13**, 6090-6093.
137. Y. I. Belozerova, S. V. Efimova, A. B. Korzhenevskii and O. I. Koifman, *Russian Journal of General Chemistry*, 2009, **79**, 2678-2684.
138. M. P. Donzello, Z. Ou, D. Dini, M. Meneghetti, C. Ercolani and K. M. Kadish, *Inorganic Chemistry*, 2004, **43**, 8637-8648.
139. P. Moro, M. P. Donzello, C. Ercolani, F. Monacelli and G. Moretti, *Journal of Photochemistry and Photobiology A: Chemistry*, 2011, **220**, 77-83.
140. Y. Xiao, B. T. Low, S. S. Hosseini, T. S. Chung and D. R. Paul, *Progress in Polymer Science*, 2009, **34**, 561-580.
141. N. B. McKeown, *Journal of Materials Chemistry*, 2000, **10**, 1979-1995.
142. L. A. Bermejo, C. Alvarez, E. M. Maya, C. Garcia, J. G. de la Campa and A. E. Lozano, *Express Polymer Letters*, 2018, **12**, 479-489.
143. M. Carta, M. Croad, J. C. Jansen, P. Bernardo, G. Clarizia and N. B. McKeown, *Polymer Chemistry*, 2014, **5**, 5255-5261.
144. B. S. Ghanem, F. Alghunaimi, Y. Wang, G. Genduso and I. Pinnau, *ACS Omega*, 2018, **3**, 11874-11882.
145. M. Hashem, C. Grazia Bezzu, B. M. Kariuki and N. B. McKeown, *Polymer Chemistry*, 2011, **2**, 2190-2193.
146. M. Heuchel, D. Fritsch, P. M. Budd, N. B. McKeown and D. Hofmann, *Journal of Membrane Science*, 2008, **318**, 84-99.
147. S. Makhseed and J. Samuel, *Polymer*, 2015, **74**, 144-149.
148. V. S. P. K. Neti, J. Wang, S. Deng and L. Echegoyen, *Journal of Materials Chemistry A*, 2015, **3**, 10284-10288.
149. S. Inomata, S.-i. Matsuoka, S. Sakai, H. Tajima and T. Ishizone, *Macromolecules*, 2012, **45**, 4184-4195.
150. G. Kwag, E. Park and S. N. Lee, *Journal of Applied Polymer Science*, 2005, **96**, 1335-1340.
151. K. S. Suslick and B. R. Cook, *Journal of the Chemical Society, Chemical Communications*, 1987, **0**, 200-202.
152. J. Kim, J. Y. Jaung and H. Ahn, *Macromolecular Research*, 2008, **16**, 367-372.
153. J. Jaung, M. Matsuoka and K. Fukunishi, *Synthesis*, 1998, **1998**, 1347-1351.
154. Y. Yamada, N. Mihara, S. Shibano, K. Sugimoto and K. Tanaka, *Journal of the American Chemical Society*, 2013, **135**, 11505-11508.
155. A. V. Gusev and M. A. J. Rodgers, *The Journal of Physical Chemistry A*, 2002, **106**, 1985-1992.

156. A. D. Adler, F. R. Longo, J. D. Finarelli, J. Goldmacher, J. Assour and L. Korsakoff, *The Journal of Organic Chemistry*, 1967, **32**, 476-476.
157. J. Calvo-Castro, G. Morris, A. R. Kennedy and C. J. McHugh, *Crystal Growth & Design*, 2016, **16**, 5385-5393.
158. A. V. Ivanov, K. V. Kabanova, M. O. Breusova, I. V. Zhukov, L. G. Tomilova and N. S. Zefirov, *Russian Chemical Bulletin*, 2008, **57**, 1665-1670.
159. B. Tylleman, R. Gómez-Aspe, G. Gbabode, Y. H. Geerts and S. Sergeyev, *Tetrahedron*, 2008, **64**, 4155-4161.
160. J. F. Bunnett, M. M. Rauhut, D. Knutson and G. E. Bussell, *Journal of the American Chemical Society*, 1954, **76**, 5755-5761.
161. R. Dieing, G. Schmid, E. Witke, C. Feucht, M. Dreßen, J. Pohmer and M. Hanack, *Chemische Berichte*, 1995, **128**, 589-598.
162. B. O. Agboola and K. I. Ozoemena, *Physical Chemistry Chemical Physics*, 2008, **10**, 2399-2408.
163. N. Usol'tseva, V. Bykova, G. Ananjeva, A. Smirnova, G. Shaposhnikov, V. Maizlish, E. Kudrik and A. Shirokov, *Molecular Crystals and Liquid Crystals Science and Technology. Section A. Molecular Crystals and Liquid Crystals*, 2000, **352**, 45-57.
164. S. V. Kudrevich, M. G. Galpern and J. E. van Lier, *Synthesis*, 1994, **1994**, 779-781.
165. M. Cook, P. R. J. Gaffney, L. G. Peeva and A. G. Livingston, *Journal of Membrane Science*, 2018, **558**, 52-63.
166. B. S. Ghanem, N. B. McKeown, P. M. Budd and D. Fritsch, *Macromolecules*, 2008, **41**, 1640-1646.
167. V. B. Jigajinni, P. N. Preston, V. K. Shah, S. W. Simpson, I. Soutar and N. J. Stewart, *High Performance Polymers*, 1993, **5**, 239-257.
168. Y. Gao, J. G. Pan, Y. J. Huang, S. Y. Ding and M. L. Wang, *Journal of Porphyrins and Phthalocyanines*, 2015, **19**, 1251-1255.
169. B. H. Lee, M. B. Park and B. S. Yu, *Bioorganic & Medicinal Chemistry Letters*, 1998, **8**, 1467-1470.
170. B. H. Lee, C. Y. Lee and B. S. Yu, *Journal of the Korean Chemical Society*, 1998, **42**, 302-305.
171. J. Śniechowska, P. Paluch and M. J. Potrzebowski, *RSC Advances*, 2017, **7**, 24795-24805.
172. D. Cefalo, J. Bommer, A. Trajkovska-Broach, R. Blum, A. Ishak and S. McGinnis, Int. Pat. 2015/171507 A1, 2015.
173. M. Asaka and H. Fujii, *Journal of the American Chemical Society*, 2016, **138**, 8048-8051.
174. G. N. Lim, S. Hedström, K. A. Jung, P. A. D. Smith, V. S. Batista, F. D'Souza, A. van der Est and P. K. Poddutoori, *The Journal of Physical Chemistry C*, 2017, **121**, 14484-14497.